Investigation of Potential Applications of Surfactant-free Microemulsions – Solubilisation, Separation and Extraction Processes and Reaction Media

Dissertation

zur Erlangung des Grades
Doktor der Naturwissenschaften (Dr. rer. nat.)
der Naturwissenschaftlichen Fakultät
Chemie und Pharmazie
Universität Regensburg

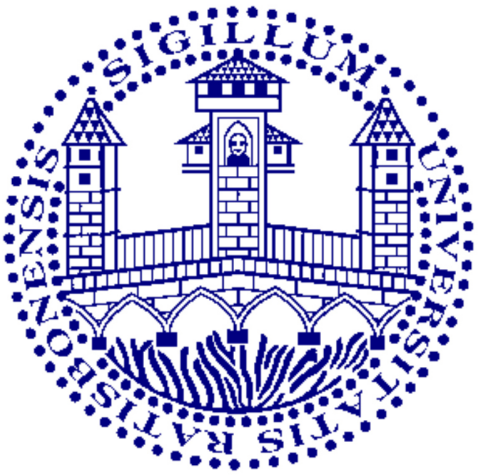

vorgelegt von
Sebastian Krickl
aus Spiegelhütte
September 2018

Die experimentellen Arbeiten für diese Dissertation wurden im Zeitraum von Oktober 2015 bis September 2018 an der Universität Regensburg am Lehrstuhl für physikalische und theoretische Chemie von Prof. Dr. Werner Kunz durchgeführt.

Datum der Abgabe: 28. September 2018

Datum des Promotionskolloquiums: 11. Dezember 2018

Die Arbeit wurde angeleitet von Prof. Dr. Werner Kunz.

Prüfungsausschuss:

Vorsitzender: **Prof. Dr. Frank-Michael Matysik**

1. Gutachter: **Prof. Dr. Werner Kunz**

2. Gutachter: **Prof. Dr. Thomas Zemb**

3. Gutachter: **Prof. Dr. Arno Pfitzner**

Acknowledgements

The achievements made in the course of this PhD thesis would not have been possible without the valuable aid and support of numerous people.

First of all, I would like to thank my supervisor Prof. Dr. Werner Kunz for giving me the opportunity to continue my research with this dissertation on a very fascinating and interesting topic. I was always very grateful for his tire-less commitment and support in terms of advices, discussions, new ideas and financial aspects.

In this context, special thanks goes to the *Verband der Chemischen Industrie* for giving me a well-paid fellowship for two years, enabling two research stays in France amongst other support. Many thanks belong to Dr. Stefanie Kiefer and Christine Lara for the uncomplicated administration of the provided funds.

I thank Prof. Dr. Thomas Zemb, Prof. Dr. Arno Pfitzner and Prof. Dr. Frank-Michael Matysik, who complete the examination board, for several productive collaborations established within the last years, leading to numerous publications.

I deeply thank Dr. Didier Touraud for being a sort of second mentor supporting me with countless discussions, ideas and advices. In addition, special thanks belongs to Dr. Thomas Buchecker and Dr. Pierre Bauduin regarding our pleasant collaborations resulting in many fruitful projects. I also want to thank Dr. Olivier Diat for numerous intensive discussions and advices regarding especially scattering experiments.

Furthermore, I would like to thank Prof. Dr. Burkhard König, Dr. Andreas Uwe Meyer, Dr. Andrea Beutner, Dr. Isabelle Grillo, Dr. Thomas Zinn, Dr. Klaus Schmid, Dr. Tobias Lopian Florian Buchecker, Maximilian Hahn, Nicole Heigl, Gasper Jost, Urška Mohorič, Robert Winkler, Lucija Jurko, Karolina Wolos, Jiaqi Hu, Usman Ali and Julia Märsch for several pleasant cooperations and support during the experimental work.

Cordial thanks belong to the permanent and former members of our institute, namely our perfectly organised secretaries Rosemarie Röhrl, Sonja Beutler and Bianca Frömel, Prof. Dr. Rainer Müller, Prof. Dr. Richard Buchner, Prof. Dr. Dominik Horinek, Prof. Dr. Hubert Motschmann, Dr. Roland Neueder, Dr. Peter Karageorgiev, Georg Berger, Hellmuth Schönsteiner, Franziska Wolf and Theresa Ferstl as well as to all other colleagues at the

Institute of Physical and Theoretical Chemistry for the pleasant working climate during the time I spent there.

In particular, I want to thank my office colleagues who accompanied me for the last years for an always cheerful and pleasant working atmosphere.

Further thanks belong to all members of the *ChemPharm Graduate School Regensburg* in which I was part as a member and speaker of the Department of Physical and Theoretical Chemistry.

Above all, my deepest thanks are reserved to my family and friends, with whom I spent some wonderful and relaxing moments apart from working life. I owe deepest gratitude to Beate, my parents, my sister and grandparents who always encourage me and give me strength to carry on in whatever respect. Thus, I want to dedicate this work in particular to my deceased mother in never-ending loving memory to her.

Thank you all very much!

Abstract

Within this dissertation, surfactant-free microemulsions (SFME) were investigated regarding potential applications as solvents for solubilisation, extraction, separation processes and chemical reactions. SFME studied in this work consist of a short-chain amphiphilic molecule (hydrotrope, *e.g.* a short-chain aliphatic alcohol) and two liquids, both of them being fully miscible with the hydrotrope but immiscible or only partially miscible with each other (*e.g.* water and a hydrophobic component). Dynamic light scattering, X-ray and neutron scattering as well as conductivity measurements were performed considering structural investigations of the used SFME.

General conclusions could be drawn for SFME formulation, regarding the choice of suitable hydrotropes for efficient solubilisation of different hydrophobic compounds in water. Based on this knowledge different applications of SFME were tested. Regarding separation and extraction processes, a surfactant-free alternative to classical microemulsion electrokinetic chromatography was developed, enabling for the first time its combined usage together with electrospray ionisation-mass spectrometry detection. In addition, two concepts were investigated particularly interesting for extraction purposes using SFME with cleavable constituents as well as (ultra)centrifugation techniques.

The second part of this thesis concentrates on the use of SFME as reaction media. A systematic study was performed providing an in-depth analysis of the structure-reactivity relationship between the kinetics of a model reaction and the mesoscale structuring of the reaction media. Furthermore, so-called reactivity “on water” was investigated in different SFME and surfactant-free emulsions as well as the enzyme activity of horse radish peroxidase in differently composed SFME. In addition, it was demonstrated that the use of mesoscale structured SFME has a decisive impact on the kinetic size control of growing polymers during polymerisation of methyl methacrylate used as model system.

Each study was carefully evaluated regarding the suitability of the used SFME for the desired application including proof of concept experiments, where necessary. It could be shown that subtle mesoscale structuring, meaning fluctuating ill-defined aggregation typically occurring in SFME, may have serious consequences on chemical reactivity, enzyme activity and polymer formation.

Zusammenfassung

Im Rahmen dieser Dissertation wurden tensidfreie Mikroemulsionen (TFME) hinsichtlich potentieller Anwendungen als Lösungsmittel für Solubilisierungs-, Extraktions-, Trennverfahren und chemische Reaktionen untersucht. Die in dieser Arbeit untersuchten TFME bestehen aus einem kurzkettigen Amphiphil (Hydrotrop, z.B. ein kurzkettiger aliphatischer Alkohol) und zwei Flüssigkeiten, die beide mit dem Hydrotrop komplett mischbar, miteinander jedoch nicht oder nur teilweise mischbar sind (z.B. Wasser und eine hydrophobe Komponente). Dynamische Licht-, Röntgen- und Neutronenstreuung, sowie Leitfähigkeits-messungen wurden zur Strukturaufklärung der verwendeten TFME durchgeführt.

Es konnten allgemeine Schlussfolgerungen für die Wahl geeigneter Hydrotrope zur TFME-Formulierung hergeleitet werden, die eine hohe Löslichkeit verschiedener hydrophober Verbindungen in Wasser erzielen. Aufbauend darauf wurden verschiedene Anwendungen von TFME untersucht. Zum einen konnte eine tensidfreie Variante zur klassischen mikroemulsionselektrokinetischen Chromatographie entwickelt werden, mit deren Hilfe es zum ersten Mal möglich ist, diese Technik mit der Elektrospray-Ionisations-Massenspektrometrie zu koppeln. Des Weiteren wurden zwei Konzepte basierend auf der Verwendung von TFME mit spaltbaren Komponenten und der (Ultra-)Zentrifugation von TFME untersucht, die von besonderem Interesse für Extraktionsverfahren sind.

Der zweite Teil dieser Arbeit beschäftigt sich mit der Verwendung von TFME als Reaktionsmedien. Dazu wurde eine systematische Studie erstellt, die den Zusammenhang zwischen der Struktur von TFME und der Kinetik einer darin ablaufenden chemischen Modelreaktion im Detail behandelt. Des Weiteren wurden sogenannte „on water-Reaktionen“ in verschiedenen TFME und tensidfreien Emulsionen, sowie die Enzymaktivität von Meerrettichperoxidase in TFME verschiedener Zusammensetzungen untersucht. Darüber hinaus konnte anhand der Polymerisation von Methylmethacrylat gezeigt werden, dass die mesoskopische Struktur von TFME einen entscheidenden Einfluss auf die kinetische Größenkontrolle von wachsenden Polymeren hat.

Jede einzelne Studie wurde sorgfältig auf die Tauglichkeit der TFME für die gewünschte Anwendung untersucht und gegebenenfalls mittels eines Proof of Concept bestätigt. Desweitern konnte gezeigt werden, dass die schwach ausgeprägte mesoskopische Strukturierung von TFME einen signifikanten Einfluss auf chemische Reaktionen, Enzymaktivitäten und Polymerisationen haben kann.

List of abbreviations

ABTS	2,2'-azino-bis(3-ethylbenzo thiazoline-6-sulphonic acid) diammonium salt
AIBN	2,2'-azodiisobutyronitrile
Ace	acetone
Ani	anisole
BA	benzyl alcohol
BGE	background electrolytes
CE	capillary electrophoresis
CDK	cyclohexanone dimethyl ketal
COSMO-RS	conductor-like screening model for realistic solvation
DLS	dynamic light scattering
DLVO	Derjaguin-Landau-Verwey-Overbeek
DMSO	dimethyl sulfoxide
DR-13	Disperse Red 13
EA	ethyl acetate
ESI	electrospray ionisation
EtOH	ethanol
GC	gas chromatography
H-bond	hydrogen bond
HDA	*trans*,*trans*-2,4-hexadienyl acetate
HLB	hydrophilic-lipophilic balance
HPLC	high-performance liquid chromatography
HRP	horseradish peroxidase
IS	internal standard
LLE	liquid-liquid equilibria
LOD	limit of detection
MD	molecular dynamics
MEEKC	microemulsion electrokinetic chromatography
MEKC	micellar electrokinetic chromatography
MMA	methyl methacrylate
MS	mass spectrometry
NBA	*n*-butanol
NMR	nuclear magnetic resonance
NPA	*n*-propanol
NPMI	*N*-(*n*-propyl)maleimide
OD	optical density
OZ	Ornstein-Zernike
PMMA	poly(methyl methacrylate)
PnP	1-propoxy-2-propanol
POM	polyoxometalate
PS	potassium persulphate
SANS	small-angle neutron scattering
SAXS	small-angle X-ray scattering
SBME	surfactant-based microemulsion
SDS	sodium dodecyl sulphate
SFE	surfactant-free emulsion
SFME	surfactant-free microemulsion
SF-MEEKC	surfactant-free microemulsion electrokinetic chromatography
SLD	scattering length density
SLS	static light scattering
SWAXS	small-and-wide-angle X-ray scattering
TBA	*tert*-butanol
TEC	triethyl citrate
THF	tetrahydrofuran
Toc	*α*-tocopherol
TOF	time-of-flight
Tol	toluene
UFME	ultraflexible microemulsion
UV	ultraviolet
VA	vanillic acid
Vis	visible

Table of contents

Chapter 1 General background

1.1. Introduction

1.1.1. Surfactant-based microemulsions and emulsions

Emulsions and microemulsions are versatile tools for manifold fields of application due to their fascinating features combining properties of very different types of solvents within tuneable unique systems.[1–3] Conventional surfactant-based microemulsions (SBME) usually consist of water, oil and a surfactant (+co-surfactant). Since water and the hydrophobic component (oil) are inherently not miscible, an amphiphile – meaning a chemical compound possessing both, hydrophilic and lipophilic properties (*e.g.* a surfactant) – needs be added to overcome this discrepancy of water and oil. Depending on the choice and composition of the constituents, different types of structured liquids can be formed with compartmented regions of water- and oil-rich domains (see Figure 1.1).[1]

Multi-phasic systems are formed, when an insufficient amount of surfactant is added for complete miscibility leading *e.g.* to well-known emulsions upon vigorous stirring of biphasic systems.

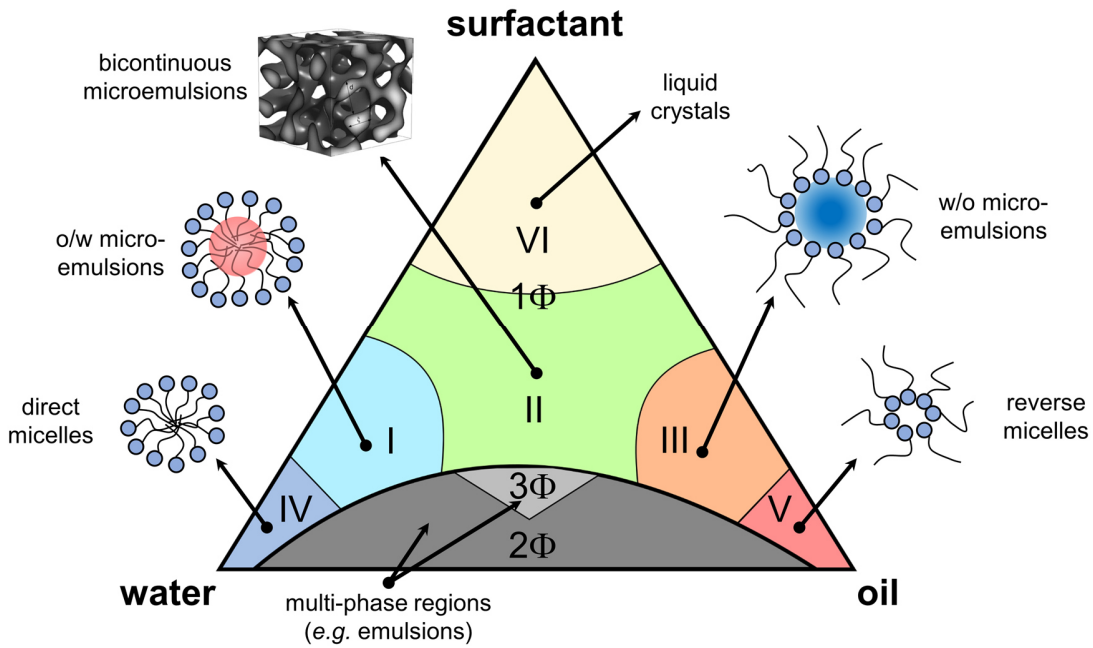

Figure 1.1: Schematic of a ternary phase diagram of water, surfactant and oil with different regions of structured solutions. 3D view of a bicontinuous structured microemulsion was reprinted from Mihailescu *et al*. with the permission of AIP Publishing.[4]

By doing so, emulsions can be formed with water- and oil-rich domains of a typical size range between 1 and 100 µm.[3] Such biphasic systems are kinetically stabilised by the surfactant (located at the water/oil interface) mainly due to the formation of a steric and/or electrostatic barrier preventing compartmented water- and oil-rich domains from coalescence. However, this repulsive interactions between formed aggregates is not sufficient for thermodynamic stability of the system, leading sooner or later to coalescence and thus macroscopic phase separation.[2,3]

A familiar, however different kind of solvent structuring can be found when enough surfactant (+co-surfactant) is added to obtain monophasic compositions. In such a case, mesoscale structured, homogenous, transparent liquids can be formed called microemulsions.[1] Such mixtures are – contrary to emulsions – thermodynamically stable solutions showing similar compartmentation of water- and oil-rich domains. Yet, the size range of formed domains is significantly lower compared to emulsions and typical characteristic length scales of 5-100 nm can be observed.[1–3] This is in the range of the so-called mesoscopic scale (the scale in between the microscopic, molecular and the macroscopic scale) and thus often shortly called mesoscale.

Microemulsions show different types of morphologies of the mesoscale compartmented domains,[1–3] similar to emulsions: in the water-rich region of a ternary phase diagram water, surfactant, oil (see region I in Figure 1.1), o/w microemulsions (oil droplets dispersed in an outer aqueous pseudo-phase) are formed in the presence of enough oil. Analogue to such kind of structures, also reverse aggregates occur for oil-rich ternary mixtures leading to w/o microemulsions (see III in Figure 1.1). In between, an extended region can be found with a bicontinuous microemulsion – a three-dimensional network of interpenetrating water-rich and oil-rich channels (see II in Figure 1.1). For every type of microemulsion, the surfactant is strongly accumulated at the interface between water and oil preventing both compartmented pseudo-phases from “coalescence”.[3] It has to be stressed that the above described phase-behaviour is restricted to a perfectly balanced, idealised system. This means that the surfactant must have an optimum hydrophilic-lipophilic balance (HLB) with no preferential solubility within one of the two pseudo-phases.[1] Furthermore, it is important (especially for the formation of bicontinuous microemulsions) that the surfactant-film, formed at the interface between oil and water, is flexible enough to be stable. For ionic surfactants, this is typically achieved by the addition of a co-surfactant (commonly linear aliphatic alcohols with C_4 to C_5).[1] Besides, also other mesoscale organised systems can be obtained. For mixtures with very low oil/water content, self-aggregation of surfactants dominates leading to the formation of

direct/inverse micelles (see IV and V in Figure 1.1). In addition, several types of liquid crystalline phases are described in literature for mixtures containing relatively high amounts of surfactants (see VI in Figure 1.1).[1–3] (It is worth noting that mesoscale structures shown in Figure 1.1. are idealised and do only partially reflect reality, since this static picture does not take into account dynamic processes as discussed later in this chapter.)

Since SBME are not in the centre of this work, the further focus will be pointed at surfactant-free systems, keeping in mind the relevant basics of microemulsions presented above. For a more thorough description of phase behaviour, structure and characteristics of surfactant-based systems, the reader is referred to additional literature.[1–3]

1.1.2. Surfactant-free microemulsions and emulsions

Unlike to SBME, which have been studied intensively for about 60-70 years now,[1] investigation of surfactant-free systems started at a later stage. Aside of rare pioneering studies of this topic in the 1970s and 1980s,[5–12] research has intensified in the field of binary and ternary structured solutions within the last ten years.[13-41] More thorough structural investigations of SFME have been made using light,[25] X-ray and neutron scattering techniques,[28,29,33,41] molecular dynamics (MD) simulations,[34–36] electron microscopy[24,30,31] and conductivity[24,40] measurements.

At the current state of research, surfactant-free microemulsions (SFME) can be defined as surfactant-free mesoscale structured ternary solvents consisting of a short chain amphiphilic molecule (hydrotrope) and two immiscible liquids (commonly water and a hydrophobic component) – with both of them being fully miscible with the hydrotrope. Consequently, the hydrotrope takes the role of the surfactant. Hydrotropes are molecules with a weak amphiphilic character, not distinct enough to classify them as surfactants, on the other hand strong enough to treat them separately from co-solvents.[42,43] This leads for example to aggregate formation of hydrotropes in aqueous solution, but not to the formation of micelles having several consequences for their phase behaviour in ternary mixtures as discussed later. Nonetheless, due to the weaker amphiphilic character of the hydrotrope compared to conventional surfactants, higher amounts of the hydrotrope have to be added to close the miscibility gap. Commonly, water and a hydrophobic component (oil) complete the ternary mixture to form SFME. However, also water-free SFME have been described in the literature.[23,44] Thus, the above mentioned definition is the most general one that can be stated at the moment. An example for a ternary system able to form SFME (meanwhile also one of the most investigated ones) is the system water/ethanol/1-octanol (shown in Figure 1.2).[25,28,29,33–36,39–41]

Due to the common term microemulsion, it appears evident that both systems – SBME and SFME – possess similar physicochemical properties. Indeed, there are various parallels, however, also many decisive distinctions between both kinds of mesoscale structured liquids. First, the parallels: as can be seen in Figure 1.2, the above mentioned ternary system composed of water, ethanol and 1-octanol possesses different regions of mesoscale structured liquids for different compositions of monophasic mixtures.[28,33] Similar to SBME different regions can be found with o/w microemulsions for water-rich compositions (also called pre-Ouzo region, see later in this section), w/o microemulsions for oil-rich compositions as well as bicontinuous structured liquids for mixtures in between.

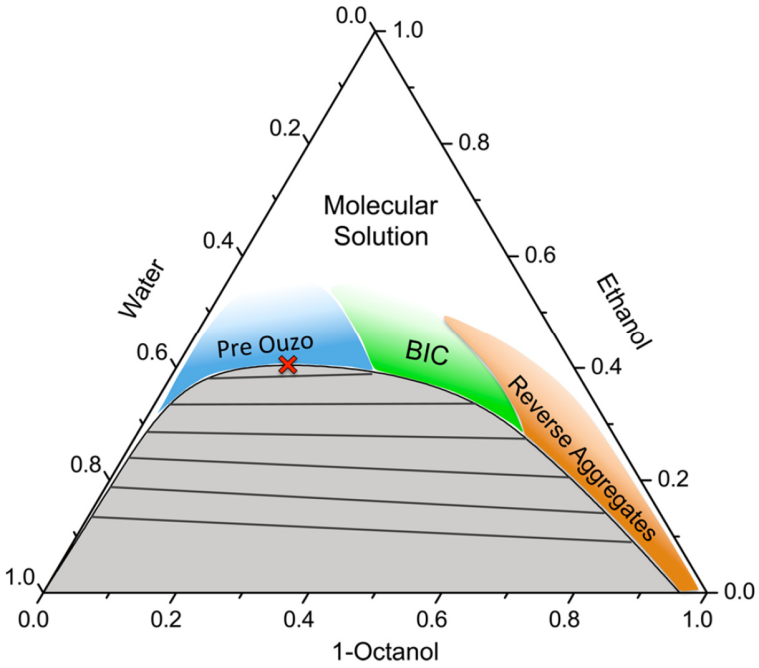

Figure 1.2: Ternary phase diagram of water, ethanol and 1-octanol given in weight fractions. Tie lines are marked as straight solid lines. The critical point is marked in red. Different regions of mesoscale structuring (o/w (Pre Ouzo), bicontinuous (BIC) and w/o (Reverse Aggregates)) are shown in blue, green and orange. This figure was reprinted from Lopian *et al*. with the permission of ACS.[28]

The morphology of these aggregates was revealed by numerous scattering experiments and MD simulations.[28,33–36,41] The latter can in addition provide a more detailed impression on the different kinds of mesoscale organised liquids (see Figure 1.3). For o/w SFME, spheroidal (at least rudimentarily) aggregates of 1-octanol are formed within an outer aqueous pseudo-phase. The number of aggregated molecules depends on the SFME composition and was found to be typically between 20 to a few hundreds of molecules.[28,36] Consequently, the formed aggregates create a cavity within the aqueous pseudo-phase. A similar behaviour is

discernible for w/o microemulsions. However, aggregates of water are less isolated and less defined compared to oil-rich aggregates. The bicontinuous region can be best described by two three-dimensional extended pseudo-phases of water and octanol-rich domains interpenetrating each other in a sponge-like structure.

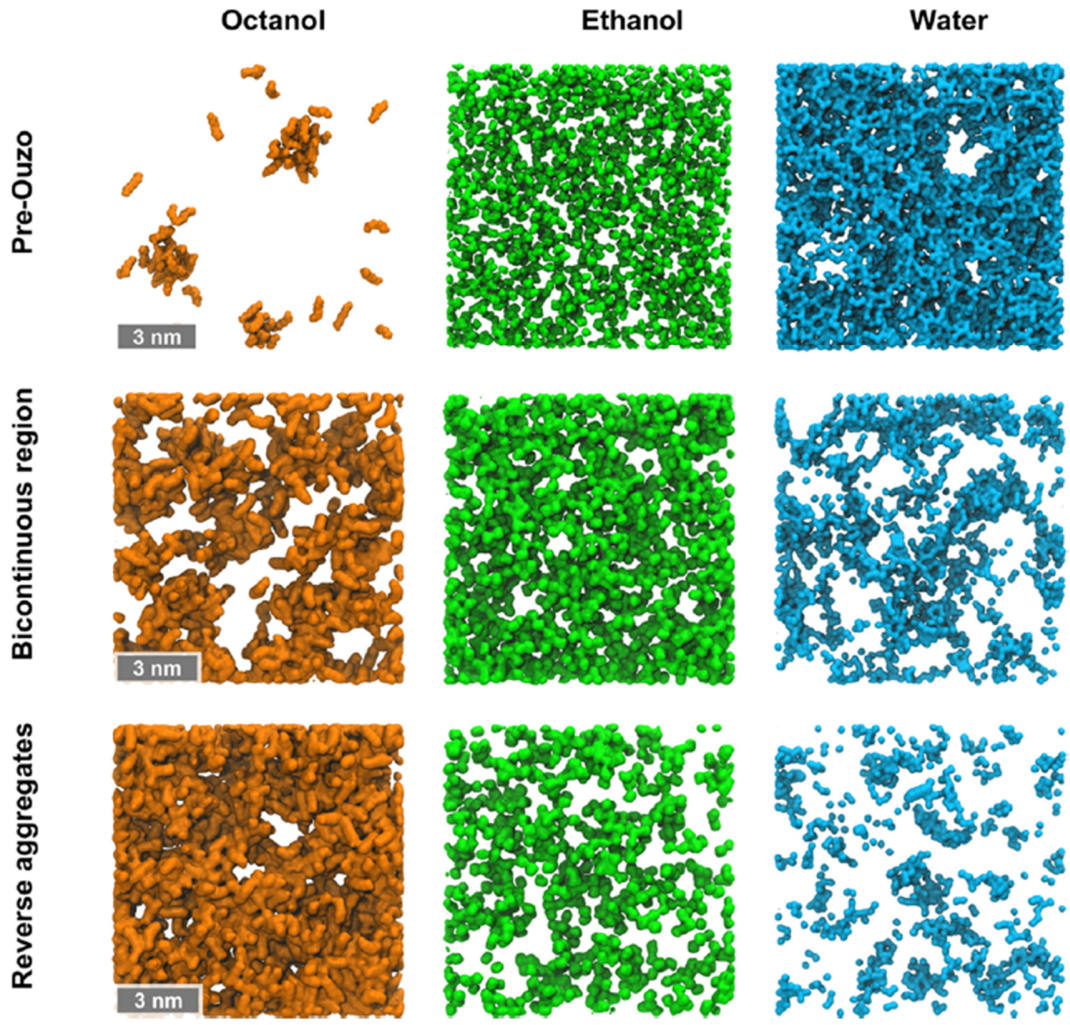

Figure 1.3: Snapshots of o/w (Pre Ouzo), bicontinuous (BIC) and w/o (Reverse Aggregates) SFME. Shown are slices of 2 nm thickness for each of the components in a surface representation. This figure was reprinted from Lopian *et al*. with the permission of ACS.[28]

The sizes of formed aggregates are typically in the range of a few nanometres up to ~ 100 nm in special cases.[24,39] Taking all these features into account, mesoscale structures of SFME are closely related to those of SBME, described earlier in this chapter. Nevertheless, also many significant differences can be drawn. Considering first the morphology of formed aggregates and pseudo-phases, it is evident that these are less defined compared to those

of SBME. Such aggregates have to be rather seen as more loose local accumulation of oil- and water-rich domains than distinct aggregates.

Although the picture of mesoscale structuring of SBME given in Figure 1.1 may be a too static and exaggerated one, SBME can be regarded by far more ordered compared to SFME. This point is indeed closely related to the dynamics of the system, meaning the fluctuation of the individual molecules in the microemulsions. It is a well-known fact that in micellar solutions and SBME, there is a dynamic exchange of surfactant molecules between the interface and the outer pseudo-phase as well as complete dissolution and reformation of swollen micelles (typically on the µs to ms time scale).[2] The same is true for fluctuating aggregates of SFME. The crucial difference, however, is the time scale at which dissolution and reformation of aggregates occurs. Yet, the average lifetime of SFME domains is presently not experimentally determined.[39] However, such processes are thought to happen on a time scale which is by a factor of at least 10^3 faster than for SBME. Thus, formed aggregates in SFME may be also regarded as highly-dynamic concentration fluctuations, explaining these ill-defined mesoscale structures. This fact is accompanied by a relatively low stability of formed aggregates of only a few k_BT. This was demonstrated by Zemb *et al*. who recently developed an extended Derjaguin–Landau–Verwey–Overbeek (DLVO) theory in order to provide a general explanation for the formation and thermodynamic stability of SFME.[39] This extended DLVO theory describes the subtle balance between free energy of hydration (hydration force between surfaces), van der Waals interactions (attractive dispersion forces) and mixing entropy (homogenous mixing of three components) leading to a minimum of the total free energy of SFME similar (although less pronounced) to conventional microemulsions and micellar solutions. Furthermore, it should be noted that such kinds of fluctuations have to be expressively separated from critical fluctuations occurring in close vicinity to the phase-separation border. Although mesoscale structuring of SFME are usually most pronounced near the critical point, the domains of SFME are largely extended into the monophasic regions, which would not be expected to occur for phenomena around a critical point.[25,39]

Another remarkable difference can be found regarding in particular the location of the hydrotrope. Whereas the surfactant has a pronounced tendency to accumulate at the interface between water- and oil-rich domains forming a more or less rigid interfacial film, the hydrotrope is distributed over both pseudo-phases with a less pronounced tendency to accumulate at the interface. So, the main difference to SBME is that the hydrotrope does not form a monolayer at the interface. This was elegantly proven by Diat *et al*. using combined neutron and X-ray scattering experiments together with contrast variation.[41] In addition, the curvature energy of

the interface is not significantly contributing to the system free energy. Thus, SFME are often labelled as ultraflexible microemulsions (UFME).[28,32,33] Although the expression UFME describes more precisely such dynamic systems regarding the physicochemical point of view, in this work, the term SFME is preferred, since it is commonly used in application-orientated studies.

In addition, the choice of the hydrotrope has a crucial effect on the formation of the SFME, as will be discussed in detail in this work. Thus, it has to be noted that for SFME as well as for SBME not all kinds of mesoscale structures (o/w, bicontinuous, w/o) can be observed for a given system and conditions. Furthermore, the structuring usually vanishes going to very high amounts of the hydrotrope, gradually forming a molecular dispersed solution.

Regarding the above mentioned features of SFME, it becomes evident that special care should be taken of the term “interface” when talking about SFME. Since formed aggregates are highly fluctuating and of no well-defined shape, no sharp interface can be defined. Thus, one may rather talk about an “interfacial domain”. In 2014, the working group of Dominik Horinek gave one of the first reasonable definitions for “the interface” between pseudo-phases of SFME.[36] Radial distribution functions were calculated for MD simulations of spheroidal aggregates of an o/w SFME composed of water, ethanol and octanol with varying aggregation numbers and different criteria were discussed by the authors for the definition of the interface. A self-consistent definition of the interface was given, taking either the crossing of octanol and water radial distribution function or the maximum of the ethanol radial distribution function. However, the whole interfacial domain may be set between the maximum of the octanol head group distribution and the crossing point between the ethanol and water distribution function (see Figure 1.4). This definition is an important result, which has always to be kept in mind talking about interfaces within SFME.

Aside of the formation of SFME, such kind of ternary mixtures commonly exhibit also other interesting features regarding the formation of emulsions in the two-phasic region. In 2003, Vitale and Katz were the first to study the effect occurring when water is added to the alcoholic beverage Ouzo.[45] By doing so, metastable liquid-liquid dispersions can be formed leading to remarkably stable emulsions – the “Ouzo-effect”.[45–48] The obtained emulsions were found to exhibit a high degree of dispersion with droplet diameters of a few µm. Furthermore, the main ingredients of these beverages fulfil the basic requirements for SFME and the effect could also be observed for many other SFME systems. Almost ten years later, when Klossek *et al*. started to investigate SFME in the monophasic region, the occurrence of mesoscale structures (SFME) extending widely into the monophasic region was thus called “pre-Ouzo effect”.[25] Vice

versa, one may also talk about surfactant-free emulsions (SFE), when the term “Ouzo effect” is used. Like SFME, SFE can be a useful tool for targeted usage in many kind of applications, due to their remarkable properties, simple composition and formation, as will be discussed in Section 1.3.

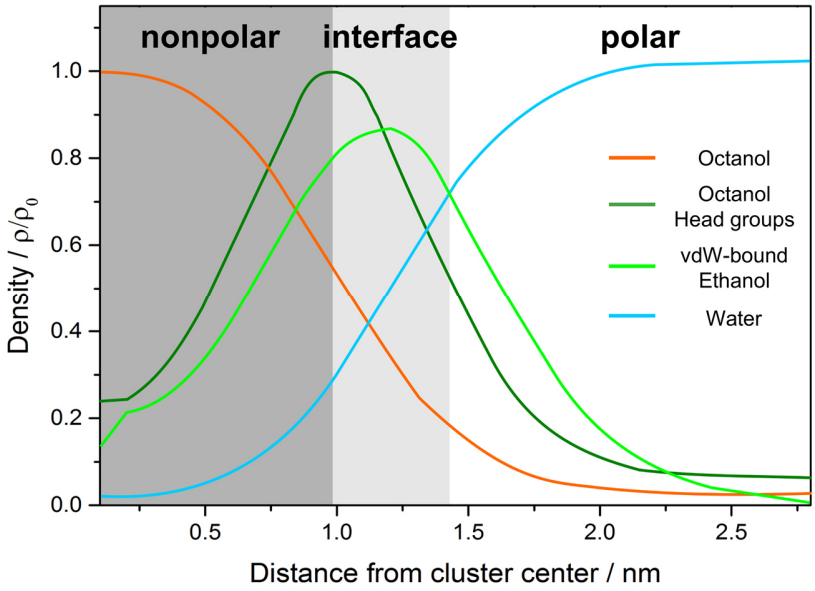

Figure 1.4: Radial distribution functions of water, octanol, octanol head group oxygens and bound ethanol as a function of the centre of mass of an octanol aggregate (*N*(octanol)=22). The Figure was redrawn from Schöttl *et al*.[36]

1.2. Characterisation of surfactant-free microemulsions

Characterisation of SFME remains a delicate issue, even when modern scattering and electron microscopy techniques are applied. Obviously, the biggest challenge is the highly fluctuating nature of such systems. Consequently, rather a set of different techniques than a single characterisation method has to be applied in order to gain reliable data on the investigated SFME. Such a set of investigation methods comprises light, X-ray and neutron scattering, MD simulations, electron microscopy and conductivity measurements, as mentioned before. However, it is evident that in practice this can hardly be done for every system of interest. Especially in this work, a balance between the structural investigation with moderate effort and the investigation of potential application had to be found. As a consequence of this compromise, dynamic light scattering (DLS) was mainly used as a rapid method to detect mesoscale structured solutions and to estimate the size of formed aggregates/domains. Where necessary, more sophisticated methods like small-and-wide-

angle X-ray or small-angle neutron scattering (SWAXS/SANS) experiments were conducted for a more thorough structural investigation of the used SFME. Furthermore, conductivity measurements were performed as supplementary measurements, in order to define regions of different types of mesoscale structuring (w/o, bicontinuous, o/w). For this reason, the two main methods used in this work – DLS and SWAXS – are described in more detail within this section. Additional information on conductivity measurements of SFME can be found in Section 2.4.1.2.

1.2.1. Dynamic light scattering

Dynamic light scattering provides a fast investigation technique to detect particles and mesoscale inhomogeneities in solutions.[49–55] Aside of the refractive index of the dispersed (pseudo-)phase and the viscosity of the dispersion medium, no additional information is necessary. The measurement principle (see Figure 1.5) is based on the light scattering of mostly monochromatic, coherent and vertically polarised laser light by smaller particles, macromolecules or aggregates and mesoscale inhomogeneities. Due to local variations of the refractive index in real media, both, destructive and predominantly constructive interference appears.

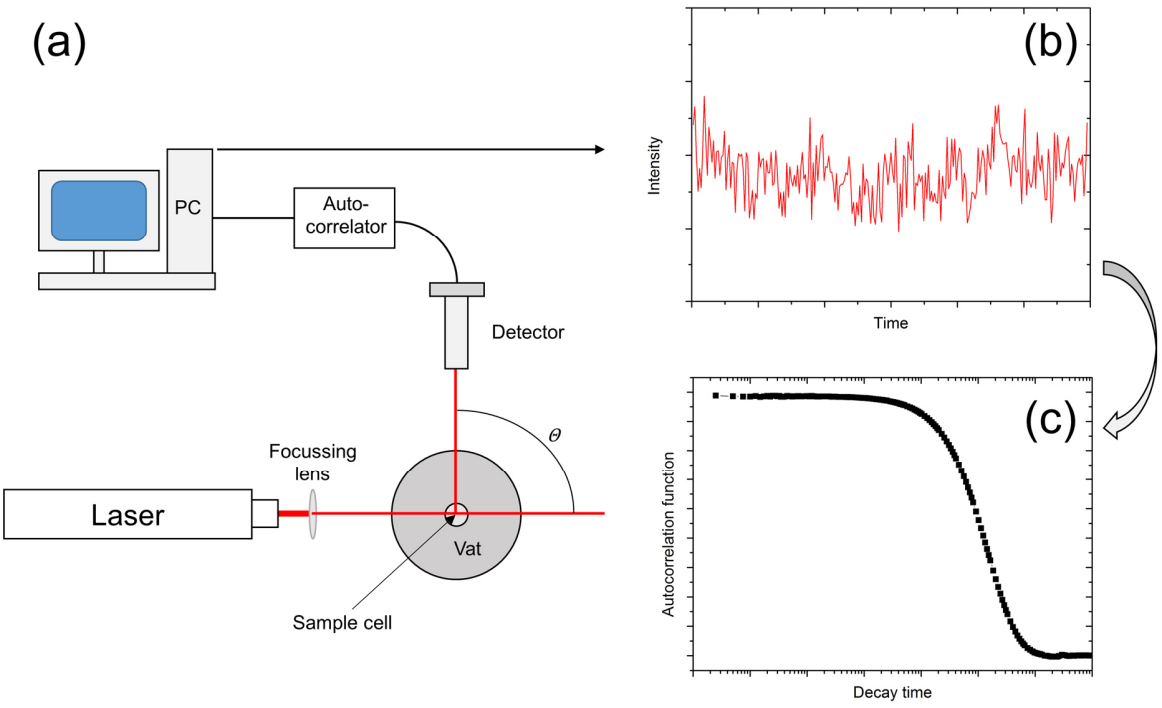

Figure 1.5: Schematic for the measurement principle of DLS including (a) the experimental setup, (b) the measured intensity over a certain time range and (c) the calculated autocorrelation function.

In real media, a significant difference between the refractive index of the dispersed phase and the dispersing media (contrast) is a fundamental prerequisite for experimentally observable light scattering. Scattered light is radiated in all directions with the scattering intensity being in direct proportion to the difference of the refractive indices. Due to the Brownian motion of moving aggregates, a fluctuation of the scattering intensity is observable. For a suitable analysis of the data, the resulting Doppler-shift-spectrum is used in its Fourier transformed form (autocorrelation function).[50]

The calculation of the autocorrelation function is based on the theory of noise. An analysis of the Doppler-shift-spectrum with common interferometric methods is very delicate, since the frequency shift (10 to several 1000 Hz) is very small compared to the frequency of the irradiated light (ca. 10^{14} Hz). Thus, the timely variations of the scattering intensity are analysed calculating the normalised autocorrelation function of intensity $g^{(2)}(\tau)$ by a Fourier transformation:[54]

$$g^{(2)}(\tau) = \frac{\langle I(t) \cdot I(t+\tau) \rangle}{\langle |I(t)| \rangle^2} \tag{1.1}$$

In Eq. (1.1), $I(t)$ and $I(t+\tau)$ are the intensities measured at an arbitrary time t and a time $t + \tau$ with τ as the so-called decay time. Information about the diffusion coefficient and hence information about the hydrodynamic radius of formed aggregates are finally accessible by the field correlation function $g^{(1)}(\tau)$. The measured normalised autocorrelation function of intensity $g^{(2)}(\tau) - 1$ is related to the normalised electric field correlation function $g^{(1)}(\tau)$ by the Siegert-relation:[50]

$$g^{(2)}(\tau) - 1 = \beta \left| g^{(1)}(\tau) \right|^2 + C \tag{1.2}$$

In Eq. (1.2), τ represents the decay time. C and β are fit parameters that correct minor baseline drifts and account for the deviation from ideal correlation (depending on the geometry and alignment of the laser beam in the light scattering setup). Assuming monodisperse spherical aggregates, $g^{(1)}(\tau)$ can be described by a single exponential decay:

$$g^{(1)}(\tau) = \exp(-\Gamma\tau) \tag{1.3}$$

Further, the decay rate Γ is defined as:

$$\Gamma = Dq^2 \tag{1.4}$$

with the translational diffusion coefficient D, and the scattering vector length $q = \pi n/\lambda \sin(\Theta/2)$ defined by the refractive index n, the wavelength of irradiated laser light λ and the scattering angle Θ. Assuming spherical geometry, the Stokes-Einstein equation relates the translational diffusion coefficient with the radius R of the aggregates:

$$D = \frac{\mathrm{k_B}T}{6\pi\eta R} \tag{1.5}$$

In Eq. (1.5), $\mathrm{k_B}$ represents Boltzmann's constant, T the temperature and η the dynamic viscosity of the dispersing medium.

Aside of a simple mono-exponential fitting procedure, cumulant analysis[49,50,54] of the scattering data can provide additional information using a polynomial function in the exponent:

$$\ln g^{(1)}(\tau) = \ln(B) + \sum_{n=1}^{\infty} K_n \frac{(-\tau)^n}{n!} \tag{1.6}$$

In a standard cumulant analysis procedure, polynomials up to $n \leq 3$ are used in order to avoid over-resolving of the data. The cumulants K_n are directly related to the moments of the distribution function. K_1 describes the intensity mean value, K_2 the width and K_3 the wryness of the distribution. Due to the experimental setup, the residual contribution of the background $\ln(B)$ has to be considered. Since $K_1 = \langle\Gamma\rangle$, hydrodynamic radii can be calculated as described above. Furthermore, the polydispersity index is given by the normalised second cumulant K_2/K_1^2, which can be used as a quality criterion for the size distribution.

Yet, the cumulant method is not suitable for the analysis of more complex (*e.g.* bimodal) systems. In such cases, distribution functions can be calculated with aid of the more complex constrained regularisation method based on CONTIN algorithm developed by Provencher.[56,57] However, droplet sizes inferred from DLS have to be considered carefully, as possible aggregates, which might be formed in SFME, are usually highly fluctuating systems and of no well-defined shapes. Thus, results obtained by DLS have to be often evaluated more qualitatively with regard to their decay rate and decay time. (As a rule of thumb, it can be assumed that the higher the correlation function is at short correlation times and the later it

drops down, the more time-stable and more pronounced is the mesoscale structuring of the solution). At this point it should be remarked that also static light scattering (SLS) is a useful method to investigate structuring of SFME.[25] However, DLS provides a much faster investigation technique and the gain of information additionally using SLS is rather little. For this reason, other static scattering techniques like X-ray or neutron scattering were used in this work for a more thorough investigation of the mesoscale structuring of the used SFME.

1.2.2. Small-and-wide-angle X-ray scattering

As discussed earlier in this section, the use of one single experimental method can be regarded as questionable and is generally not sufficient for complete structural investigation of SFME. In particular, measurements of artefacts have to be excluded. Thus, SWAXS was mostly used in this work as a second, more sophisticated investigation technique. Analogue to DLS, the scattering of X-rays by the sample is used to gain information on the investigated mixture.[58–61] A schematic for a typical X-ray scattering experiment is depicted in Figure 1.6.[62] In a typical setup, X-rays are generated, collimated and focused on the sample. Scattered X-rays are finally detected at a certain distance to the sample, depending on the angular range of interest: for wide-angle scattering, the detector is set to a smaller distance to the sample compared to small-angle scattering. Usually off-centre detection is used, meaning that the initial unscattered beam is not focused on the centre of the detector. This enables a larger *q*-range being observable.

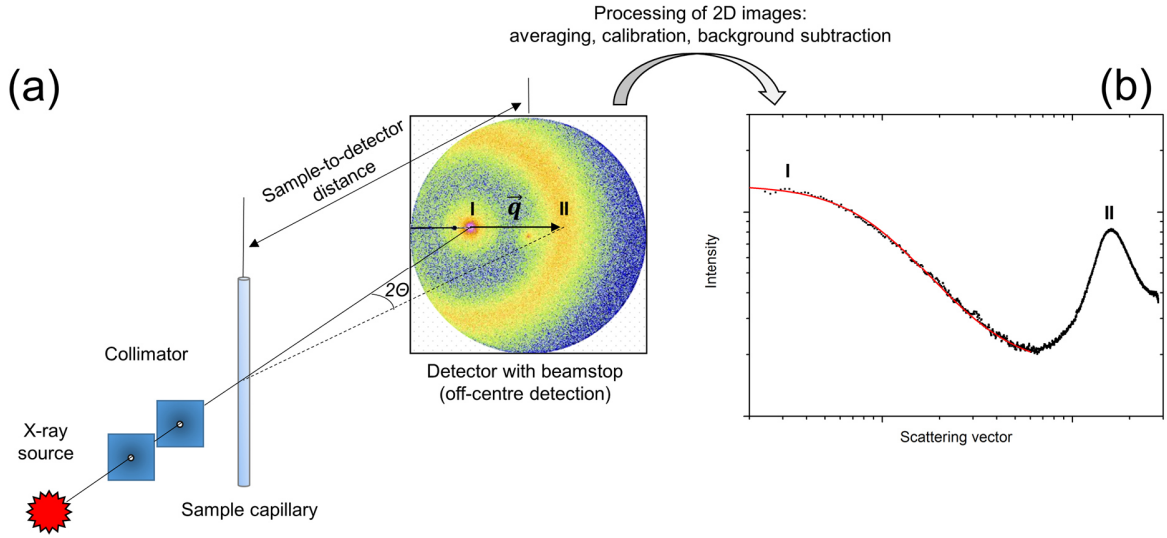

Figure 1.6: Schematic for the measurement principle of X-ray scattering including (a) the experimental setup and (b) transformation of obtained 2D images to 1D SWAXS-spectra.

With a common SWAXS equipment as used in this work, a *q*-range between 0.1 to 40 nm^{-1} can be covered. In addition, a beamstop has to be placed between sample and detector in order to avoid beam damage of the detector. After radial averaging, calibration and background subtraction, the processed 2D image is reduced to a 1D SWAXS spectra, ready for analysis.[62] The intensity of scattered X-ray radiation as a function of the scattering vector $I(q)$ for isotopically distributed scatterers can be defined as:[63]

$$I(q) = n \cdot \langle V^2 \rangle \cdot \langle \Delta SLD^2 \rangle \cdot P(q) \cdot S(q) \tag{1.7}$$

with the scattering vector $q = 4\pi/\lambda \sin(\Theta/2)$, the number density n and the average volume of scatterers V, the difference of the scattering length density ΔSLD, the form factor $P(q)$ and the structure factor $S(q)$. The difference of the scattering length density (SLD) can be often calculated or approximated and is based on the electron densities of the scatterers and the dispersion medium. The form factor takes into account the shape of a single scatterer (which is made of many atoms), whereas the structure factor considers an additional interference pattern due to interactions with neighbouring scatterers. In practice, different mathematical terms obtained from theoretical considerations are used for the form and structure factors.[58–61,64] Usually, there is more than one model to appropriately describe the experimental data. Thus, the used model has to be evaluated considering the fit quality as well as the physical meaning of the obtained parameters. Whereas in many cases more complex scattering patterns are observed, SWAXS-spectra of SFME are rather simple (see Figure 1.6b). Usually correlation peaks in the wide-angle range (high-*q* range, see Figure 1.6b, II) are observed corresponding to molecular interactions, *e.g.* pair correlations between aliphatic chains. In addition, an enhanced scattering intensity is observed in the low-*q* region (see Figure 1.6b, I). Such a scattering behaviour is typical for SFME and can be described by an Ornstein–Zernike (OZ) formalism. The simplest OZ expression appropriately describing such a scattering behaviour is given by:[32]

$$I(q) = \frac{I_0}{1 + \xi^2 q^2} \tag{1.8}$$

ξ is a correlation length in nm^{-1}; I_0 is the intensity for $q = 0$ and takes into account the scattering length density of the different species and volume fraction of each phase. Besides, there are more complex fitting procedures using *e.g.* OZ-type inverse quadratic functions.[28,29,32,33,39,41]

Nevertheless, it has to be mentioned that in-depth structural investigations of used SFME is not the key aspect of this dissertation and thus out of its scope.
Since X-ray scattering is a very familiar scattering technique to neutron scattering, the reader is referred to additional literature for further information on X-ray and neutron scattering.[58-62,64-66]

1.3. Applications of surfactant-free microemulsions and emulsions – State of the art

When talking about the application of SFME and SFE, one should first clarify the benefits and advantages of such systems compared to surfactant-based mixtures. Since SBME are already well established in many applications[1] (*e.g.* in cosmetics, pharmaceuticals, foods, for extraction and oil recovery and as reaction media), the question raises: "why to change a winning team?" The answer is rather simple: the main drawback of SBME is the use of the surfactant itself. Usually surfactants are foaming and have a strong tendency to adsorb at interfaces. This makes the recovery of surfactants subsequent to their application a very delicate and energy-consuming issue. Furthermore, most surfactants are often poorly biodegradable and (eco)toxic, making release to and accumulation in the environment a serious problem. SFME are in principal a reasonable alternative avoiding such consequences. Especially, when volatile hydrotropes like short-chain aliphatic alcohols are used or phase separation is induced upon water-addition, recovery of the individual components is significantly facilitated. Moreover, processes can be often improved, since hydrotropes are generally better biodegradable and often less foaming than conventional surfactants. For these reasons, SFME and SFE are getting more and more attention for well-established fields of applications commonly using surfactant-based mixtures.
First of all, SFME can be simply used as solvents due to their ability of making water and hydrophobic components miscible. In this context, the oil being dissolved can be either a part of the SFME as the third component or added to a SFME, resulting in a four-component system. The latter case is also closely related to the concept of facilitated hydrotropy.[26] This concept is based on the use of a co-solvent, which acts like a hydrotrope, and a further, more hydrophobic compound, acting as the facilitating hydrotrope. By doing so, the solubility of very hydrophobic compounds in aqueous solutions is often significantly enhanced compared to the use of a single hydrotrope. Having a second glance at this concept, it seems evident that such solvents usually fulfil the requirements of a SFME, in which a second more hydrophobic oil is

dissolved. For this reason, an emerging field of research is the usage of such systems as green solubilisation and extraction media using aqueous solutions instead of pure organic solvents. Recently, the working group of Ventosa *et al*. discovered nanostructured systems, composed of water, acetone and supercritical CO_2.[67,68] Such systems are of particular interest, since all used chemicals are either non-toxic or can be easily removed after extraction by pressure reduction, which can be an extreme benefit for extraction purposes in food and pharmaceutical industries. In addition, a more relevant example for laboratory purposes was presented by Breil *et al*.[69] In their work, they presented a green alternative for the well-known extraction technique developed by Bligh and Dyer.[70] In preference to ternary mixtures composed of water/methanol/chloroform, they proposed ternary (although unstructured) mixtures of water/ethanol/ethyl acetate showing comparable efficiency for the extraction and subsequent separation of sugar, lipids and proteins out of biological material.

One outstanding aspect concerning basic research is the use of SFME as reaction media. One of the first articles discussing this topic was published by Khmelnitsky *et al*. in 1987.[10] It could be shown that enzyme activity can be significantly improved in SFME composed of water, 2-propanol, *n*-hexane leading to comparable activities as observed for aqueous solution, but with a minimum amount of water.[10,71–75] Such results are a consequence of mesoscale structuring and would not be expected for molecular dispersive solutions. Especially, recent progresses in the understanding of SFME have raised the number of publications on this field.[76–78] Besides, interest in usage of SFME as reaction media for organic and inorganic reactions has also raised. More and more systematic studies appear, where targeted synthesis procedures are presented using SFME as reaction media and even nano-reactors for the templated synthesis of nanoparticles or nanocapsules.[79–83] Even more important is the fact that many reactions reported in literature may have been unconsciously conducted in mesoscale structured reaction media by a systematically screening of solvent compositions. Until now, many results cannot be explained neglecting solution structuring. Thus, the impact of mesoscale structuring on chemical reactions is likely to be by far more important than currently suggested.[84]

Besides, more practically relevant features of SFME have been investigated within the last years. For instance, it could be shown by Park *et al*. that the use of nanostructured fuels can help to improve the combustion properties of fuels, due to “nano-explosions” of suddenly evaporating water clusters.[44,85] Other interesting examples are the usage of SFME for fragrance tinctures and formulation of mosquito repellents.[86–88]

Apart from that, also biphasic systems like SFE and the Ouzo effect itself have been established for various applications.[46,89–93] Most relevant is the use of SFE for polymerisation of styrene, methyl methacrylate and other monomers. By doing so, polymer dispersions can be made with a comparable size control and quality as obtained by surfactant-based polymerisation techniques.[94–96]

The given list of applications has no claim to completeness and should rather give an overview on potential fields of applications. A more thorough literature survey is given in each section with more specific literature. However such studies demonstrate that the maximum potential of mesoscale structured liquids has by far not been exploited yet.

1.4. Aim of this work

Inspired by their fascinating features, the aim of this thesis (as the title already reveals) was to investigate novel potential applications of SFME. The first part of this dissertation (Chapters 2 and 3) covers the investigation of the general relationship between mesoscale structuring of SFME and solubilisation of hydrophobic components as part of the SFME itself. It is important to understand that the basic principles presented in these chapters are fundamental concepts applied throughout this work, since solubility of hydrophobic components in SFME, as well as structural aspects of SFME, are basic requirements for an appropriate SFME formulation and application. Thus, solubilisation of a hydrophobic component in binary mixtures water/hydrotrope is discussed in terms of pre-structuring of hydrotropes in water. In particular, different solubilisation mechanisms are presented, as well as general rules for SFME formulation concerning the choice of the hydrotrope with special regard to a given hydrophobic component. Whereas in Chapter 2, the influence of the aliphatic moiety of the hydrotrope is discussed, the focus of Chapter 3 lies on the hydrophilic head group. Analogue, different criteria are discussed for the choice of the hydrotrope for a given hydrophobic component to be dissolved in a ternary mixture with water. Furthermore, the formation of SFME was explored in order to find best combinations of hydrotropes and hydrophobic components that are beneficial for the formation of aqueous SFME.

Proceeding from the basic knowledge on mesoscale structuring of SFME and solubilisation, various other potential applications were investigated, which can be divided in two categories: separation and extraction processes and the usage as reaction media (see Figure 1.7).

In Chapter 4, the development and application of a new analytical separation technique is presented using SFME instead of SBME in order to couple microemulsion electrokinetic

chromatography (MEEKC) with UV and MS detection. Furthermore, two concepts were explored in Chapters 5 and 6 being potentially useful for extraction and subsequent separation processes, where the focus lies on the latter processing step. One of these concepts is based on SFME using cleavable constituents (hydrotrope and hydrophobic component). The other one is based on separation via centrifugation and ultracentrifugation.

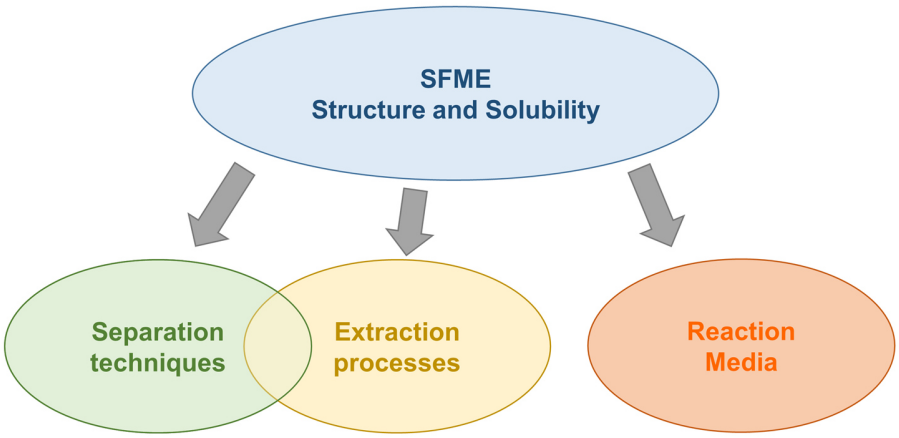

Figure 1.7: Schematic overview of linked fields of application of SFME as investigated within this thesis.

The last part of this dissertation is dedicated to investigations of SFME as reaction media. This issue was first addressed by a systematic study on the influence of mesoscale structuring on the kinetics of a model reaction. The basic knowledge on the structure-reactivity relationship was subsequently applied to different other types of reactions. In Chapter 8, reaction kinetics of a Diels–Alder reaction in SFME and SFE are discussed. In particular, the results are discussed in direct comparison to accelerated reaction rates found by Sharpless and co-workers, when performed on water (emulsion of reagents in pure water).[97] In the subsequent chapter, enzyme activity in SFME was investigated based on pioneering studies of Khmelnitsky *et al*.[10] This issue was treated with special regard to the relationship between SFME structuring and the enzyme activity. Moreover, parallels and distinctions to the enzyme activity in SBME published by Bauduin *et al*.[98] are thoroughly discussed. In the last chapter, a potentially industrially relevant study is presented comprising the development of a new polymerisation process. Analogue to classical microemulsion polymerisation, a surfactant-free version was established and tested for the polymerisation reaction of methyl methacrylate used as a model polymerisation reaction.

1.5. References

1 P. Kumar and K. L. Mittal, Handbook of microemulsion science and technology, Marcel Dekker, New York, 1999.

2 D. F. Evans and H. Wennerström, The colloidal domain: Where physics, chemistry, biology and technology meet, Wiley-VCH, New York, 2nd edn., 1999.

3 H.-D. Dörfler, Grenzflächen und kolloid-disperse Systeme, Springer, Berlin Heidelberg, 2002.

4 M. Mihailescu, M. Monkenbusch, H. Endo, J. Allgaier, G. Gompper, J. Stellbrink, D. Richter, B. Jakobs, T. Sottmann and B. Farago, *J. Chem. Phys*., **2001**, *115*, 9563–9577.

5 G. D. Smith, C. E. Donelan and R. E. Barden, *J. Colloid Interface Sci*., **1977**, *60*, 488–496.

6 B. A. Keiser, D. Varie, R. E. Barden and S. L. How, *J. Phys. Chem*., **1979**, *83*, 1276–1280.

7 N. F. Borys, S. L. Holt and R. E. Barden, *J. Colloid Interface Sci*., **1979**, *71*, 526–532.

8 G. Lund and S. L. Holt, *J. Am. Oil Chem. Soc*., **1980**, *57*, 264–267.

9 B. A. Keiser and S. L. Holt, *Inorg. Chem*., **1982**, *21*, 2323–2327.

10 Y. L. Khmelnitsky, I. N. Zharinova, I. V. Berezin, A. V. Levashov and K. Martinek, *Ann. N. Y. Acad. Sci.*, **1987**, *501*, 161–164.

11 T. M. Bender and R. Pecora, *J. Phys. Chem*., **1986**, *90*, 1700–1706.

12 G. W. Euliss and C. M. Sorensen, *J. Chem. Phys*., **1984**, *80*, 4767–4773.

13 D. Subramanian and M. A. Anisimov, *J. Phys. Chem. B*, **2011**, *115*, 9179–9183.

14 D. Subramanian and M. A. Anisimov, *Fluid Phase Equilib*., **2014**, *362*, 170–176.

15 H. Krienke, G. Ahn-Ercan and J. Barthel, *J. Mol. Liq*., **2004**, *109*, 115–124.

16 I. M. S. Lampreia, Â. F. S. Santos, C. M. Borges, M. S. C. S. Santos, M. L. C. J. Moita and J. C. R. Reis, *Phys. Chem. Chem. Phys*., **2016**, *18*, 17506–17516.

17 Z. Li, H. Cheng, J. Li, J. Hao, L. Zhang, B. Hammouda and C. C. Han, *J. Phys. Chem. B*, **2011**, *115*, 7887–7895.

18 R. Mhanna, R. Lefort, L. Noirez and D. Morineau, *J. Mol. Liq*., **2016**, *218*, 198–207.

19 K. Sadakane, H. Seto, H. Endo and M. Shibayama, *J. Phys. Soc. Japan*, **2007**, *76*, 4–6.

20 S. Schrödle, B. Fischer, H. Helm and R. Buchner, *J. Phys. Chem. A*, **2007**, *111*, 2043–2046.

21 S. Schrödle, G. Hefter and R. Buchner, *J. Phys. Chem. B*, **2007**, *111*, 5946–5955.

22 M. Sedlák and D. Rak, *J. Phys. Chem. B*, **2014**, *118*, 2726–2737.

23 V. Fischer, J. Marcus, D. Touraud, O. Diat and W. Kunz, *J. Colloid Interface Sci*., **2015**, *453*, 186–193.

24 W. Hou and J. Xu, *Curr. Opin. Colloid Interface Sci*., **2016**, *25*, 67–74.

25 M. L. Klossek, D. Touraud, T. Zemb and W. Kunz, *ChemPhysChem*, **2012**, *13*, 4116–4119.

26 M. L. Klossek, D. Touraud and W. Kunz, *Phys. Chem. Chem. Phys*., **2013**, *15*, 10971–10977.

27 Y. Liu, J. Xu, H. Deng, J. Song and W. Hou, *RSC Adv.*, **2018**, *8*, 1371-1377.

28 T. Lopian, S. Schöttl, S. Prevost, S. Pellet-Rostaing, D. Horinek, W. Kunz and T. Zemb, *ACS Cent. Sci*., **2016**, *2*, 467–475.

29 J. Marcus, D. Touraud, S. Prevost, O. Diat, T. Zemb and W. Kunz, *Phys. Chem. Chem. Phys*., **2015**, *17*, 32528–32538.

30 P. Ni and W.-G. Hou, *Chinese J. Chem.*, **2008**, *26*, 1335–1338.

31 P. Ni and W.-G. Hou, *Chinese J. Chem*., **2008**, *26*, 1985–1990.

32 S. Prevost, M. Gradzielski and T. Zemb, *Adv. Colloid Interface Sci*., **2017**, *247*, 374–396.

33 S. Prevost, T. Lopian, M. Pleines, O. Diat and T. Zemb, *J. Appl. Crystallogr*., **2016**, *49*, 2063–2072.

34 S. Schöttl, J. Marcus, O. Diat, D. Touraud, W. Kunz, T. Zemb and D. Horinek, *Chem. Sci.*, **2014**, *5*, 2949–2954.

35 S. Schöttl and D. Horinek, *Curr. Opin. Colloid Interface Sci.*, **2016**, *22*, 8–13.

36 S. Schöttl, D. Touraud, W. Kunz, T. Zemb and D. Horinek, *Colloids Surfaces A Physicochem. Eng. Asp.*, **2015**, *480*, 222–227.

37 F. Song, J. Xu and W. G. Hou, *Chinese Chem. Lett.*, **2010**, *21*, 880–883.

38 J. Xu, A. Yin, J. Zhao, D. Li and W. Hou, *J. Phys. Chem. B*, **2013**, *117*, 450–456.

39 T. Zemb, M. Klossek, T. Lopian, J. Marcus, S. Schöttl, D. Horinek, S. Prevost, D. Touraud, O. Diat, S. Marčelja and W. Kunz, *Proc. Natl. Acad. Sci. U.S.A.*, **2016**, *113*, 4260–4265.

40 P. Bošković, V. Sokol, T. Zemb, D. Touraud and W. Kunz, *J. Phys. Chem. B*, **2015**, *119*, 9933–9939.

41 O. Diat, M. L. Klossek, D. Touraud, B. Deme, I. Grillo, W. Kunz and T. Zemb, *J. Appl. Crystallogr.*, **2013**, *46*, 1665–1669.

42 W. Kunz, K. Holmberg and T. Zemb, *Curr. Opin. Colloid Interface Sci.*, **2016**, *22*, 99–107.

43 T. Zemb and W. Kunz, *Curr. Opin. Colloid Interface Sci.*, **2016**, *22*, 113–119.

44 D. Brock, T. Lopian, A. Khoshsima, P. Bauduin, O. Diat, D. Touraud and W. Kunz, *Colloids Interface Sci. Commun.*, **2016**, *14*, 1–3.

45 S. A. Vitale and J. L. Katz, *Langmuir*, **2003**, *19*, 4105–4110.

46 R. Botet, *J. Phys. Conf. Ser.*, **2012**, *352*, 012047 .

47 D. Carteau, I. Pianet, P. Brunerie, B. Guillemat and D. M. Bassani, *Langmuir*, **2007**, *23*, 3561–3565.

48 N. L. Sitnikova, R. Sprik, G. Wegdam and E. Eiser, *Langmuir*, **2005**, *21*, 7083–7089.

49 R. Pecora, *J. Nanoparticle Res.*, **2000**, *2*, 123–131.

50 L. Ogendal, Light Scattering Demystified Theory Pract., 2013, University of Copenhagen.

51 T. Nicolai, W. Brown and R. Johnsen, *Macromolecules*, **1989**, *22*, 2795–2801.

52 A. K. Jamting, J. Cullen, V. A. Coleman, M. Lawn, J. Herrmann, J. Miles and M. J. Ford, *Adv. Powder Technol*., **2011**, *22*, 290–293.

53 C. M. Hoo, N. Starostin, P. West and M. L. Mecartney, *J. Nanoparticle Res*., **2008**, *10*, 89–96.

54 P. A. Hassan, S. Rana and G. Verma, *Langmuir*, **2015**, *31*, 3–12.

55 L. M. Gugliotta, J. R. Vega and G. R. Meira, *J. Colloid Interface Sci*., **2000**, *228*, 14–17.

56 S. W. Provencher, *Comput. Phys. Commun*., **1982**, *27*, 229–242.

57 S. W. Provencher, *Comput. Phys. Commun*., **1982**, *27*, 213–227.

58 D. S. Sivia, Elementary Scattering Theory: For X-ray and Neutron Users, Oxford University Press, Oxford, 2011.

59 P. Lindner and T. Zemb, Eds., Neutrons, X-rays and Light: Scattering Methods Applied to Soft Condensed Matter, Elsevier Science, New York, 2002.

60 J. Guo, Ed., X-Ray in Nanoscience, Wiley-VCH, Weinheim, 2010.

61 L. A. Felgin and D. I. Svergun, Structure Analysis by Small-Angle X-ray and Neutron Scattering, Plenum Press, New York, 1987.

62 T. Li, A. J. Senesi and B. Lee, *Chem. Rev*., **2016**, *116*, 11128–11180.

63 B. Naskar, O. Diat, V. Nardello-Rataj and P. Bauduin, *J. Phys. Chem. C*, **2015**, *119*, 20985–20992.

64 R. Roe, Methods of X-Ray and Neutron Scattering in Polymer Science, Oxford University Press, New York, 2000.

65 C. D. Dewhurst, I. Grillo, D. Honecker, M. Bonnaud, M. Jacques, C. Amrouni, A. Perillo-Marcone, G. Manzin and R. Cubitt, *J. Appl. Crystallogr*., **2016**, *49*, 1–14.

66 H. Schnablegger and Y. Singh, The SAXS Guide, Anton-Paar, Graz, 2nd edn., 2011.

67 R. F. Hankel, P. E. Rojas, M. Cano-Sarabia, S. Sala, J. Veciana, A. Braeuer and N. Ventosa, *Chem. Commun*., **2014**, *50*, 8215–8218.

68 N. Grimaldi, P. E. Rojas, S. Stehle, A. Cordoba, R. Schweins, S. Sala, S. Luelsdorf, D. Piña, J. Veciana, J. Faraudo, A. Triolo, A. S. Braeuer and N. Ventosa, *ACS Nano*, **2017**, *11*, 10774–10784.

69 C. Breil, M. Abert Vian, T. Zemb, W. Kunz and F. Chemat, *Int. J. Mol. Sci*., **2017**, *18*.

70 E. G. Bligh and W. J. Dyer, *Can. J. Biochem. Physiol*., **1959**, *37*, 911–917.

71 K. Martinek, I. V. Berezin, Y. L. Khmelnitsky, N. L. Klyachko and A. V. Levashov, *Biocatal. Biotransformation*, **1987**, *1*, 9–15.

72 Y. L. Khmelnitsky, A. V. Levashov, N. L. Klyachko and K. Martinek, *Enzyme Microb. Technol.*, **1988**, *10*, 710–724.

73 Y. L. Khmelnitsky, A. Van Hoek, C. Veeger and A. J. W. G. Visser, *J. Phys. Chem.*, **1989**, *93*, 872–878.

74 Y. L. Khmelnitsky, A. K. Gladilin, I. N. Neverova, A. V. Levashov and K. Martinek, *Collect. Czech. Chem. Commun*., **1990**, *55*, 555–563.

75 E. N. Vulfson, G. Ahmed, I. Gill, I. A. Kozlov, P. W. Goodenough and B. A. Law, *Biotechnol. Lett.,* **1991**, *13*, 91–96.

76 M. Zoumpanioti, M. Karali, A. Xenakis and H. Stamatis, *Enzyme Microb. Technol*., **2006**, *39*, 531–539.

77 M. Zoumpanioti, H. Stamatis, V. Papadimitriou and A. Xenakis, *Colloids Surfaces B Biointerfaces*, **2006**, *47*, 1–9.

78 M. Zoumpanioti, E. Merianou, T. Karandreas, H. Stamatis and A. Xenakis, *Biotechnol. Lett.*, **2010**, *32*, 1457–1462.

79 J. Xu, H. Deng, J. Song, J. Zhao, L. Zhang and W. Hou, *J. Colloid Interface Sci*., **2017**, *505*, 816–823.

80 M. Jehannin, S. Charton, B. Corso, H. Möhwald, H. Riegler and T. Zemb, *Colloid Polym. Sci.*, **2017**, *295*, 1817–1826.

81 X. Yan, P. Alcouffe, G. Sudre, L. David, J. Bernard and F. Ganachaud, *Chem. Commun*., **2017**, *53*, 1401–1404.

82 Y. Zhao, J. Liu, Z. Chen, X. Zhu and M. Möller, Nat. Commun., **2018**, *9*, 1–9.

83 B. Sun, J. Chai, Z. Chai, X. Zhang, X. Cui and J. Lu, *J. Colloid Interface Sci.*, **2018**, *526*, 9–17.

84 L. O. Kononov, *RSC Adv.*, **2015**, *5*, 46718–46734.

85 J. W. Park, K. Y. Huh and K. H. Park, *Proc. Inst. Mech. Eng. Part D J. Automob. Eng.*, **2000**, *214*, 579–586.

86 J. Drapeau, M. Verdier, D. Touraud, U. Kröckel, M. Geier, A. Rose and W. Kunz, *Chem. Biodivers.*, **2009**, *6*, 934–947.

87 V. Tchakalova, T. Zemb and D. Benczedi, *Colloids Surfaces A Physicochem. Eng. Asp.*, **2014**, *460*, 414–421.

88 J. Marcus, M. L. Klossek, D. Touraud and W. Kunz, *Flavour Fragr. J.*, **2013**, *28*, 294–299.

89 Z. Lu, H. Xu, H. Zeng and X. Zhang, *Langmuir*, **2015**, *31*, 12120–12125.

90 S. J. Chiu, C. Y. Lin, H. C. Chou and T. M. Hu, *Langmuir*, **2016**, *32*, 211–220.

91 E. Aschenbrenner, K. Bley, K. Koynov, M. Makowski, M. Kappl, K. Landfester and C. K. Weiss, *Langmuir*, **2013**, *29*, 8845–8855.

92 J. Aubry, F. Ganachaud, J.-P. Cohen Addad and B. Cabane, *Langmuir*, **2009**, *25*, 1970–1979.

93 F. Ganachaud and J. L. Katz, *ChemPhysChem*, **2005**, *6*, 209–216.

94 C. G. Dobie and K. V. K. Boodhoo, *Chem. Eng. Process. Process Intensif.*, **2010**, *49*, 901–911.

95 S. T. Camli, F. Buyukserin, O. Balci and G. G. Budak, *J. Colloid Interface Sci.*, **2010**, *344*, 528–532.

96 K. Tauer, R. Deckwer, I. Kühn and C. Schellenberg, *Colloid Polym. Sci.*, **1999**, *277*, 607–626.

97 S. Narayan, J. Muldoon, M. G. Finn, V. V. Fokin, H. C. Kolb and K. B. Sharpless, *Angew. Chemie - Int. Ed.*, **2005**, *44*, 3275–3279.

98 P. Bauduin, D. Touraud, W. Kunz, M. P. Savelli, S. Pulvin and B. W. Ninham, *J. Colloid Interface Sci.*, **2005**, *292*, 244–254.

Chapter 2 The impact of the structuring of hydrotropes in water on the mesoscale solubilisation of a third hydrophobic component

2.1. Abstract and preface

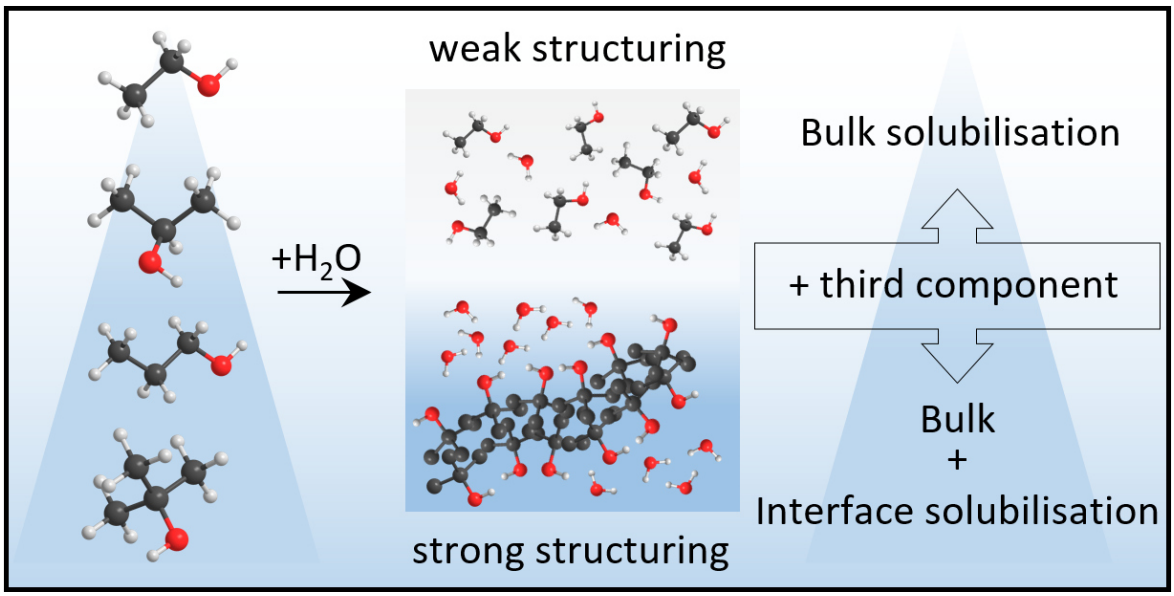

Figure 2.1: Graphical abstract schematically illustrating different mechanisms of the solubilisation of a hydrophobic component within mesoscale structured and non-structured binary mixtures of water and alcohol.

In the present contribution, the pre-structuring of binary mixtures of hydrotropes and H_2O is linked to the solubilisation of poorly water miscible compounds. We have chosen a series of short-chain alcohols as hydrotropes and benzyl alcohol, limonene and a hydrophobic azo-dye (Disperse Red 13) as organic compounds to be dissolved. A very weak pre-structuring is found for ethanol/H_2O and 2-propanol/H_2O mixtures. Pre-structuring is most developed for binary 1-propanol/H_2O and *tert*-butanol/H_2O mixtures and supports the bicontinuity model of alcohol-rich and water-rich domains as already postulated by Anisimov *et al.* Such a pre-structuring leads to a high solubilisation power for poorly water miscible components (limonene and Disperse Red, characterised by high octanol/water partition coefficients, log(*P*) values of 4.5 and 4.85), whereas a very weak pre-structuring leads to a high solubilisation power for slightly water miscible components (benzyl alcohol). This difference in solubilisation power can be linked to (i) the formation of mesoscale structures in the cases of ethanol and

2-propanol and (ii) the extension of pre-structures in the cases of 1-propanol and *tert*-butanol. Three different solubilisation mechanisms could be identified: bulk solubilisation, interface solubilisation and a combination of both (see Figure 2.1). These supramolecular structures in binary and ternary systems were investigated by small-and-wide-angle X-ray and neutron scattering, dynamic light scattering and conductivity measurements (in the presence of small amounts of salt).

This chapter has been published in *Physical Chemistry Chemical Physics* (T. Buchecker, S. Krickl, R. Winkler, I. Grillo, P. Bauduin, D. Touraud, A. Pfitzner and W. Kunz, *Phys. Chem. Chem. Phys.*, **2017**, *19*, 1806–1816.)
The authors T. Buchecker and S. Krickl contributed equally to the experimental work, analysis of the data and to the writing of the manuscript.

Contributions to the experimental work:

- Dynamic light scattering: S. Krickl
- Small-and-wide-angle X-ray scattering: T. Buchecker
- Conductivity measurements: S. Krickl, T. Buchecker and R. Winkler
- Ternary phase diagrams and optical density measurements: S. Krickl and R. Winkler
- Small-angle neutron scattering: T. Buchecker and I. Grillo

2.2. Introduction

Ternary systems comprising a short-chain amphiphilic molecule (hydrotrope) and two immiscible liquids, with both of them being fully miscible with the hydrotrope, are considered as powerful solubilisation media[1-3] and exhibit anomalies concerning enzymatic reactions[4,5] and vapour pressures.[6] The existence of well-defined mesoscale inhomogeneities in macroscopically transparent solutions was shown to be responsible for such unexpected behaviour. Such mesoscale inhomogeneities and compartmentation phenomena of oil-rich and water-rich domains are comparable to the micro-domains observed in water/oil/surfactant ternary systems (direct-, bicontinuous- and reverse-microemulsions) as shown using scattering techniques, molecular dynamics simulations (MD simulations) and conductivity measurements.[7-9] Only recently, Zemb *et al*. provided an extended Derjaguin–Landau–Verwey–Overbeek (DLVO) theory as a general explanation for the existence and thermodynamic stability of such surfactant-free microemulsions (SFME). This extended DLVO

theory describes the subtle balance between entropy, *i.e*. homogenous mixing of three components, and enthalpy, *i.e.* hydrophobic effects between two immiscible fluids causing micellar-like aggregation.[10]

Hydrotropes play a major role in the mesoscale solubilisation phenomenon of SFME. The concept of hydrotropy, defined by C. Neuberg in 1916,[11] outlines the capability of short-chain amphiphilic molecules to solubilise hydrophobic compounds in a hydrophilic solvent. In SFME showing the compartmentation of hydrophilic and hydrophobic domains, the hydrotrope accumulates mostly at the interface between water-rich and oil-rich domains as deduced from contrast variation experiments with small-angle neutron scattering (SANS) and MD simulations. The interface between the oil- and water-rich domains is usually considered as a kind of highly flexible film in dynamic exchange with the surrounding medium.[7,12]

When using hydrotropes, as in the case of SFME, the solubilisation of hydrophobic compounds in water is only significant at higher hydrotrope concentrations, typically above *c*(hydrotrope) > 0.2-0.5 M, which may be compared to surfactants for which solubilisation appears above the critical micellar concentration *c*(surfactant), which is typically > 10^{-5}-10^{-2} M. As a rule of thumb, the solubilisation by hydrotropes starts in the concentration range (*c* > 1 M), where the average distance between hydrotrope molecules becomes smaller or in the order of the molecular size (∼ 1 nm), encouraging molecular contact between hydrotrope molecules (cluster formation) and between the hydrotrope and the hydrophobic component to be dissolved.[13]

In contrast to surfactants, the amphiphilic character of hydrotropes is usually considered to be not enough pronounced to promote micellisation or self-aggregation of the hydrotrope itself in water.[13] Nevertheless, some hydrotropes, such as *tert*-butanol, are known to form clusters in water and thus produce heterogeneities in the sub-nanometre (molecular) or nanometre range.[14-17] Only recently, the group of Shimizu *et al.* developed an approach to describe hydrotropic solubilisation theoretically.[18-21] This approach derived from pure statistical thermodynamics uses the exact Kirkwood–Buff theory to describe the cooperative phenomena in hydrotropic solubilisation such as (i) the sudden onset of solubilisation of hydrophobic compounds in H_2O (commonly referred to as MHC) and (ii) solubility saturation of hydrophobic compounds at high hydrotrope concentrations. In a nutshell, they consider hydrotropic solubilisation to be the result of a subtle balance between solute–hydrotrope interaction and hydrotrope–hydrotrope interaction. In other studies the authors argued that strong hydrotrope–hydrotrope interactions resulting in a pre-structuring of the hydrotrope in

H_2O diminish the solubilisation efficiency of solutes.[22,23] As we will show here, things are even more complex.

Already a vast number of publications have focused on the microscopic inhomogeneities of short-chain alcohols in H_2O.[24-39] The microscopic structuring in these binary mixtures is mostly attributed to the hydrophobic hydration of non-polar aliphatic chains of alcohols and a highly dynamic network of hydrogen bonds between alcohols and H_2O.[15] Anomalies concerning permittivity, surface tension, self-diffusion coefficients, structuring, *etc*. are most pronounced for *tert*-butanol/H_2O mixtures as *tert*-butanol provides the largest aliphatic chain among fully water-miscible alcohols.[29-38,40,41]

The goal of this work is to link such molecular inhomogeneities in binary alcohol/H_2O mixtures to the mesoscale solubilisation of a third hydrophobic component, called ‘‘third component’’ hereafter. To establish this link, it is essential to understand the origin of the compartmentation of water- and oil-rich domains in the ternary systems. Three questions are essential in this context:

(i) Do the pre-structuring and microscopic inhomogeneities of the hydrotrope in the binary system alcohol/H_2O have an influence on the structuring of the ternary system?

(ii) Is the structuring in SFME caused by the hydrotrope or by a third, (more) hydrophobic component?

(iii) Does the mesoscale solubilisation mechanism of the third, hydrophobic component depend on its hydrophobicity?

Hence, it is necessary to understand the structuring of short-chain alcohols in water as a function of the increasing aliphatic moiety of the alcohol. We extend the pioneering studies by M. Anisimov and M. Sedlák on the mesoscale solubilisation of a third component in the pre-structured binary mixture *tert*-butanol/ H_2O[14,17,42] to the homologous series of alcohols and to other hydrophobic compounds. To this purpose, we investigate the structuring of ethanol (EtOH), 1-propanol (NPA), 2-propanol (IPA) and *tert*-butanol (TBA) in water using conductivity measurements and scattering techniques. The structuring in the binary alcohol/H_2O mixtures is related to its impact on the mesoscale solubilisation of a third hydrophobic component, *i.e.* benzyl alcohol, limonene and an azo dye, Disperse Red 13 (DR-13). As we will show, the observed differences in solubility are the consequence of different solubilisation mechanisms.

2.3. Experimental

2.3.1. Chemicals

Ethanol (EtOH, purity ≥ 99.8%), acetone (≥ 99.5%), 2-propanol (IPA, ≥ 99.8%), 1-pentanol (≥ 99%), (*R*)-(+)-limonene (97%, *ee*: 98%), dodecane (≥ 99%) and Disperse Red 13 (DR-13, dye content 95%) were purchased from Sigma-Aldrich (Steinheim, Germany). Sodium bromide (≥ 99.99%), 1-propanol (NPA, ≥ 99.5%), and benzyl alcohol (≥ 99%) were purchased from Merck (Darmstadt, Germany), and *tert*-butanol (TBA, ≥ 99%) from Carl Roth (Karlsruhe, Germany). Sodium dodecyl sulphate (SDS, ≥ 99%) was purchased from Applichem (Darmstadt, Germany). All chemicals were used without further purification. Aqueous solutions were prepared using deionised water with a resistivity of 18 MΩ cm.

2.3.2. Methods and techniques

2.3.2.1. Ternary phase diagrams

Phase diagrams were recorded using dynamic and static processes according to Clausse *et al.*[43] To this purpose, binary mixtures (each 3 g) were prepared in screw tubes of borosilicate glass. The third component was added gradually until a visible change in the phase behaviour occurred. Measurements were carried out at room temperature and phase transition was determined by the naked eye. Weight fractions were calculated from the mass of the individual components derived from precise weight measurements.

2.3.2.2. Dynamic light scattering

Dynamic light scattering (DLS) experiments were performed using a temperature controlled CGS-3 goniometer system from ALV (Langen, Germany) equipped with an ALV-7004/FAST Multiple Tau digital correlator and a vertically polarised 22 mW HeNe laser (wavelength λ = 632.8 nm). Before starting the measurements, all samples were filtered into dust-free cylindrical light scattering cells (10 mm outer diameter) using a 0.2 µm PTFE membrane filter. The sealed measurement cells could be directly placed into the measurement apparatus. Measurements were performed at a scattering angle of 90° after thermostatting to (25 ± 0.1) °C. Data points were collected for 300 s. Aggregates in SFME are usually highly fluctuating and have no well-defined shape. Hence, we renounced the calculations of the exact hydrodynamic radii. Instead, the DLS spectra were evaluated qualitatively with regard to their correlation coefficient and their lag time, and an estimate of the size of the microscopic inhomogeneities is provided. (As a rule of thumb, it was assumed that a higher intercept of

the correlation function for small lag times and larger lag times of the correlation function represent the more time-stable and more pronounced structuring in the solution.)

2.3.2.3. Small-and-wide-angle X-ray and neutron scattering

Small-and-wide-angle X-ray scattering (SWAXS) measurements were performed on a bench built by XENOCS using Mo radiation (λ = 0.071 nm). The scattered beam was recorded using a large online scanner detector (diameter: 345 mm, from MAR Research). A large *q*-range (0.2 to 40 nm^{-1}) was covered with an off-centre detection. Collimation was applied using a 12:∞ multilayer Xenocs mirror (for Mo radiation) coupled to two sets of scatterless FORVIS slits providing a 0.8 x 0.8 mm^2 X-ray beam at the sample position. Preanalysis of data was performed using FIT2D software. The scattered intensities are recorded versus the magnitude of the scattering vector $q = 4\pi/\lambda \sin(\Theta/2)$, where λ is the wavelength of incident radiation and Θ the scattering angle. 2 mm quartz capillaries were used as sample containers for the solutions. The usual corrections for background (empty cell and detector noise) subtractions and intensity normalisation using a high density polyethylene film as a standard were applied. Experimental resolution was $\Delta q/q$ = 0.05. Silver behenate in a sealed capillary was used as the scattering vector calibration standard. Measurements were performed at room temperature.

Small-angle neutron scattering (SANS) experiments were performed using a D33 instrument at the ILL, Grenoble, France.[44] The wavelength was set at 6 Å and two sample-to-detector distances 2 m and 5 m with collimation at 5.3 m for both configurations were used to cover a *q*-range from 0.08 to 0.47 $Å^{-1}$. A 7 x 10 mm^2 aperture was placed before the sample. The samples were filled in 1 mm thick Hellma cells and thermostatted at room temperature using a circulating water bath. The raw data were corrected for the electronic background and empty cells, and were normalised on the absolute scale using the attenuated direct beam to calculate the incident flux using the ILL Lamp software.[45]

The scattering intensity was plotted against the magnitude of *q*, and the curves were fitted with an Ornstein–Zernike (OZ) function (see Section 1.2.2, Eq. 1.8).[10] The full fitting of the spectra is beyond the scope of this paper.

2.3.2.4. Conductivity measurements

Conductivity measurements were carried out in a thermostatted measurement cell (25 ± 0.2 °C) under permanent stirring using a low-frequency WTW inoLab Cond 730 conductivity meter connected with a WTW TetraCon 325 electrode (Weilheim, Germany).

20 g of each sample (pure hydrotrope or hydrotrope/benzyl alcohol mixtures of different mass fractions) were filled in the measurement cell and successively diluted with pure water. Each sample contained in addition 0.2 wt% sodium bromide to ensure a sufficient amount of charge carriers, which did not noticeably affect the microstructure or the miscibility gap present in the phase diagram. In cases where sodium bromide did not dissolve completely, a small amount of water was added to the pure hydrotrope or hydrotrope/benzyl alcohol mixture before the measurement was started. In addition, conductivity measurements of a classical SDS-based microemulsion system were carried out for comparison. To this purpose, a mixture of SDS, 1-pentanol, dodecane and water was used as a starting solution with 9 wt% water, a $R_{SDS/PenOH}$ mass ratio of SDS to 1-pentanol of 1:2 and a $R_{O/TS}$ mass ratio of oil to total surfactant of 21:79. The conductivity curve was determined as described above.

2.3.2.5. UV-Vis measurements

The solubilisation of DR-13 in different hydrotrope/water mixtures was determined by optical density (OD) measurements via UV-Vis measurements. Saturated solutions of DR-13 in hydrotrope/water mixtures of different mass fractions were prepared. To this purpose, an excess of DR-13 was added to the mixtures. After equilibrating the solutions under intense stirring for seven days, excess dye was removed by filtration using a 0.2 µm PTFE membrane filter. OD measurements were carried out at λ = 525 nm in 10 mm path length cells using a Lambda 18 UV-Vis spectrometer from Perkin Elmer (Waltham, USA). Samples with absorbance higher than 1 were diluted with an appropriate amount of acetone before the measurement. The initial absorbance was calculated by using the respective dilution factor. In addition, a standard curve of DR-13 in acetone was measured to further calculate the amount of DR-13 dissolved by a given amount of hydrotrope.

2.4. Results and discussion

2.4.1. Binary mixtures

2.4.1.1. Scattering experiments

In order to get a first insight into the structuring of alcohol/water binary mixtures, DLS measurements were performed. Correlation functions obtained by DLS measurements are shown in Figure 2.2. EtOH and IPA do not show significant correlations over the whole miscibility range, whereas correlations exist in the NPA/water and TBA/water systems

indicating the presence of fluctuating structures. Correlation functions are most pronounced for concentrations ranging from 30 to 50 wt% in NPA and TBA. The decay in the autocorrelation function for TBA/H_2O mixtures appear at longer lag times, compared to the NPA/H_2O system. This indicates that the fluctuating structures are larger, with lower diffusion coefficients, in the TBA/water mixtures than in the NPA/water system. No correlation functions were measured for EtOH/H_2O and IPA/H_2O mixtures in the whole concentration range. Nevertheless, it is well known that in EtOH/H_2O mixtures cluster formation and inhomogeneous mixing are observed.[24-27] However, this type of structuring appearing at the small molecular scale would produce too fast fluctuations, *i.e.* with high diffusion coefficients, in EtOH/H_2O and IPA/H_2O systems to be detectable by DLS.

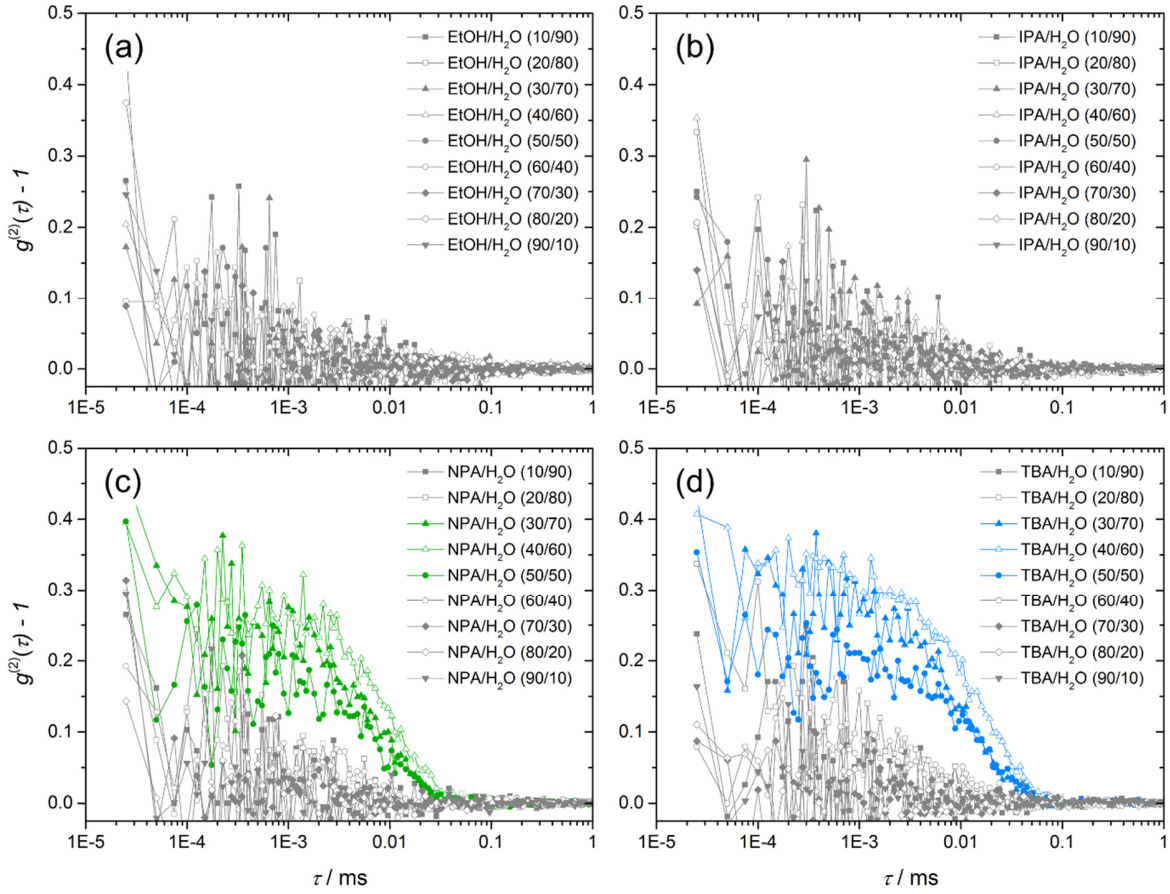

Figure 2.2: Self-correlation functions obtained by DLS measurements at 25 °C for the binary systems (a) EtOH/H_2O, (b) IPA/H_2O, (c) NPA/H_2O and (d) TBA/H_2O. The symbols refer to different mass ratios of alcohol to H_2O. Correlation functions indicating the presence of mesoscale structured solutions are highlighted in green and blue, respectively.

As the DLS auto-correlation functions are most pronounced for TBA/water mixtures, additional SWAXS and one particular SANS measurement were performed for this system, see Figure 2.3 and Figure A1.1 in Appendix A.1. Four features can be observed in SWAXS spectra, assigned to (i–iv). A correlation peak (i) is observed at 20 nm^{-1}, originating mainly from the O–O pair correlations in the H-bonding network of H_2O. This peak does not significantly shift in position and decreases in intensity as the amount of water decreases.

Another correlation peak (ii) is found at 10.5 nm^{-1}, corresponding to the pair correlations between aliphatic chains. This peak also does not undergo any shift in position and its intensity depends on the TBA concentration.

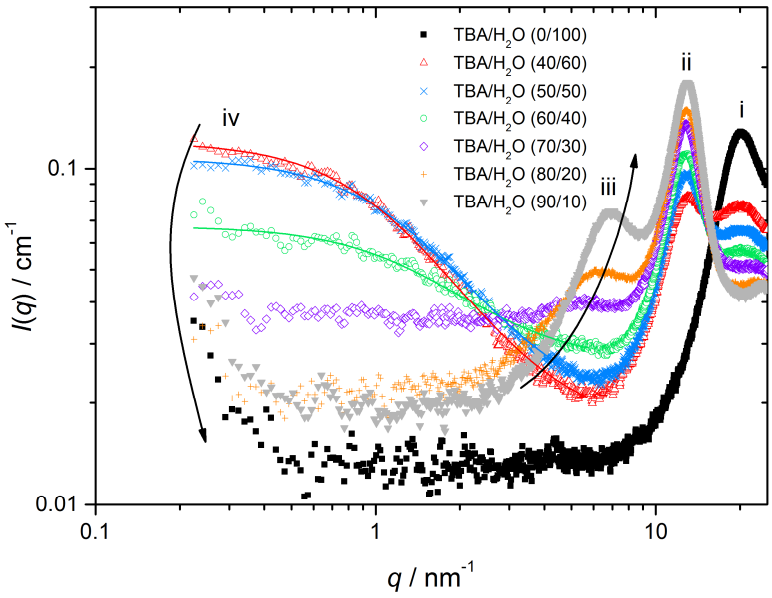

Figure 2.3: SWAXS spectra of the binary mixture TBA/H_2O. Symbols indicate the different mass ratios of TBA to H_2O. Points (i–iv) denote the different features found in the spectra.

For TBA concentrations above 70 wt%, a correlation peak (iii) emerges at 5-7 nm^{-1}, which corresponds to average distances between 0.9 and 1.3 nm. This peak can be attributed to the pair-correlations between hydroxyl groups of TBA as its intensity increases with the TBA content. The peak (iii) shifts to lower *q*-values with increasing water concentrations indicating a swelling of the H-bond network, formed by the TBA hydroxyl groups, by the addition of water. Furthermore (iv), a significant excess of scattering is observed in the low-*q* range ($q < 5$ nm^{-1}) for 40, 50 and 60 wt% of TBA with a maximum I_0 intensity for 40 wt%. It has been noticed that the low-*q* scattering is only observed in the absence of a correlation peak of the alcohol (–OH) groups (iii). The existence of low *q*-scattering in SWAXS experiments indicates the existence of a *meso*-structured system.[10,12] Curves exhibiting low *q*-scattering were fitted with

an OZ formalism to determine the correlation length of different compositions. Correlation lengths of 0.6 nm (60/40 TBA/H_2O), 0.7 nm (50/50 TBA/H_2O) and 0.8 nm (40/60 TBA/H_2O) were found. The scattered intensity is rather constant for $q < 1$ nm^{-1} indicating the presence of structures/inhomogeneities with a size of around 6 nm.

SANS measurements on one particular composition, *i.e.* 40/60 TBA/D_2O, confirm the results obtained by SWAXS, see Figure A1.1 (Appendix A.1). The existence of low scattering again indicates the presence of a structured system. Fitting the curve with an OZ fit yields a correlation length of 0.7 nm, which is approximately the same as that obtained for SWAXS for this composition (0.8 nm). The slight difference in the correlation lengths obtained from SWAXS and SANS can be ascribed to the different scattering contrasts of SWAXS and SANS. Therefore, SWAXS and SANS experiments support the results obtained by DLS: the existence of a structured system in the binary mixture TBA/H_2O with microscopic inhomogeneities in the order of 4-6 nm. The structuring is most pronounced between 30 and 50 wt% of TBA.

2.4.1.2. Conductivity measurements

To further investigate the structuring of the binary mixture alcohol/H_2O, conductivity measurements were performed. Conductivity measurements provide detailed information on the mobility of charge carriers and yield insight into the structuring of a system, for example, for surfactant-stabilised microemulsions.[43,46,47] Conductivity measurements in surfactant-stabilised microemulsions are a well-known and common method to distinguish between regions of o/w, w/o and bicontinuous microemulsions.[9,43] The results of conductivity measurements as a function of the alcohol/H_2O mass and mole fractions, respectively, are depicted in Figure 2.4a and b. All curves show a more or less pronounced increase for low water content. With increasing water content, a maximum is reached before the conductivity decreases again due to excessive dilution of the present charge carriers. The slope of increase in conductivity and sharpness of the maximum increase in the following order: TBA > NPA ≈ IPA > EtOH.

Conductivity was also measured for a classical SDS-based microemulsion, see Figure 2.4c.[43] Such systems show a flat rise at low water content, followed by a change in the slope passing over into a strong linear increase of conductivity (point T1 in Figure 2.4c) with increasing water content. After this linear increase, the slope of the curve starts to decrease again (point T2) and passes a maximum (point T3).

For structured solutions – as is the case for microemulsions – these changes in conductivity are explained by transitions between o/w, bicontinuous, and w/o microemulsions. A w/o microemulsion is present for low water content and causes low conductivity. With the increasing water content, percolation of water droplets is observed, causing the formation of conducting water channels by merging water droplets, which leads to a significant change in the slope (point T1). Further, point T2 marks the transition to an oil-rich bicontinuous microemulsion. A subsequent transition to a water-rich bicontinuous microemulsion is observed upon addition of H_2O. The maximum conductivity represents the presence of an extended water-rich bicontinuous phase (point T3). For very high water contents ($x > 0.9$), an o/w microemulsion is formed and dilution effects prevail, causing conductivities to decrease.

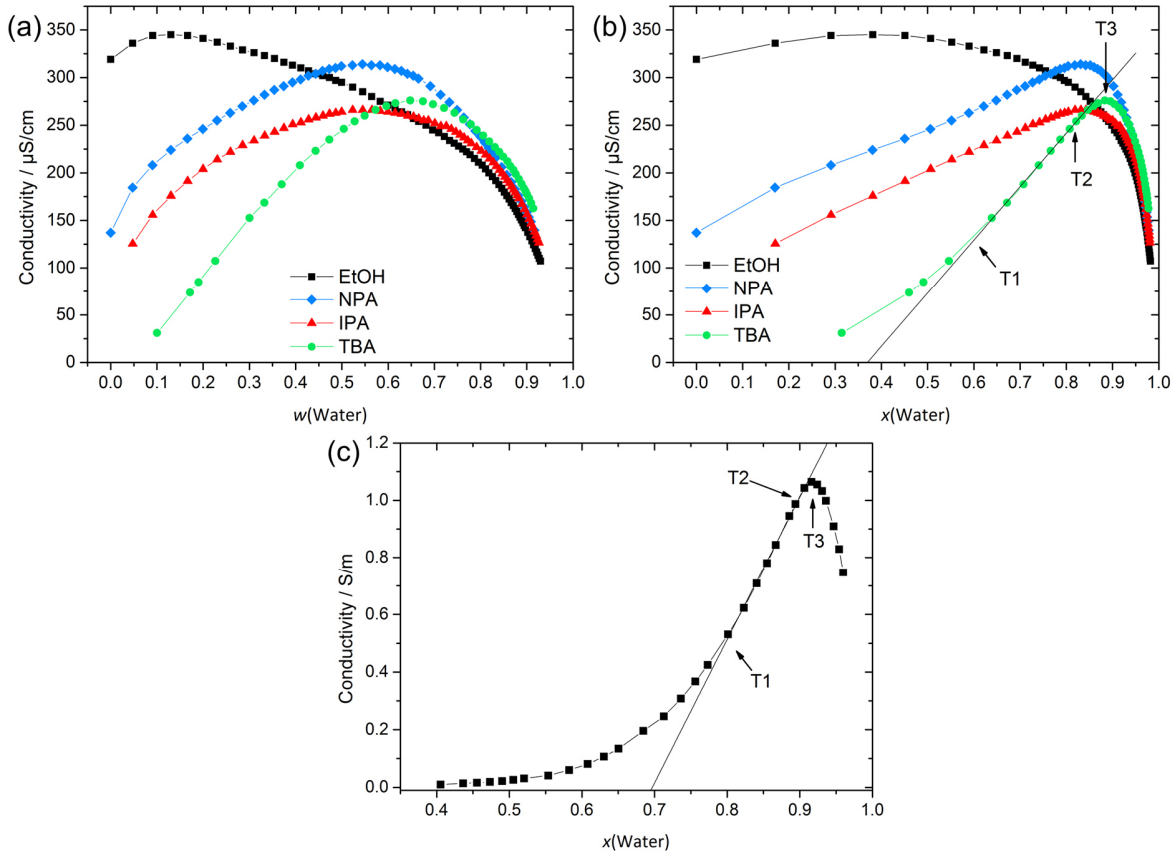

Figure 2.4: Conductivity measurements at 25 °C for binary mixtures of H_2O and EtOH/IPA/NPA/TBA plotted in (a) weight and (b) mole fractions of H_2O. In order to ensure measurable conductivities, 0.2 wt% of NaBr was dissolved in the pure alcohol phase for EtOH, NPA and IPA and in a 10 wt% (H_2O) mixture for the TBA binary system. (c) Conductivities measured at 25 °C for the system H_2O/SDS/1-pentanol/dodecane. Point T1 marks the point of transition to percolative behaviour of w/o microemulsions and points T2 and T3 mark the transitions from w/o to oil-rich and to water-rich bicontinuous microemulsions.

A comparison of the conductivity curve of this SDS-based system with the curves of TBA and NPA (Figure 2.4b and c) shows many similarities regarding the range of increase, the percolation behaviour and the decrease in conductivity for high water contents. The maximum conductivity for NPA/H_2O lies in a range of approximately 75-90 mol% water content and for TBA in a range of approximately 85-95 mol% water content. This maximum conductivity coincides with the highest correlation coefficients in DLS and the strongest signal in low-*q* of SWAXS. It is also well known for TBA/H_2O that the binary mixture displays two eutectics, one of them being located at 94 mol% H_2O, which also coincides with the range of maximum conductivity.[48] It was found that thermodynamic anomalies and inhomogeneous mixing are most pronounced for this composition even at temperatures above the deep eutectic temperature. The presence of a percolation point around 40 mol% H_2O in the case of TBA and a conductivity behaviour, see points T1–T3 in Figure 2.4b, similar to the SDS system lead to the conclusion that the structuring of TBA/H_2O is similar to the structuring of H_2O/SDS/1-pentanol/dodecane. Therefore, we propose the presence of a bicontinuity of water-rich and TBA-rich domains, as already suggested by the research group of Anisimov *et al.* for the ternary system H_2O/TBA/propylene oxide, based on MD simulations and the observation of mesoscale inhomogeneities.[42] However, conductivity measurements here suggest the formation of a bicontinuous phase already in the binary mixture TBA/H_2O. Apparently, this bicontinuous structuring behaviour is not only restricted to TBA, but is also observable for aqueous NPA mixtures, as suggested by DLS measurements, although to a much smaller extent.

The conductivity curve of EtOH differs strongly from the conductivity curves of IPA, NPA, TBA and SDS regarding the ranges of increase, decrease and the position of the maximum. The small conductivity increase for low water contents might be explained by an enhanced ion dissociation as well as a higher electrophoretic mobility in aqueous media. For the increasing water content, the conductivity decrease can be explained by the excessive dilution of charge carriers. Therefore, it is assumed that microscopic inhomogeneities in the case of EtOH are very weak and cannot be detected in detail by conductivity measurements.

The conductivity of IPA is in between the conductivities of EtOH and NPA indicating a progressive structuring with the increasing aliphatic chain length. Therefore, EtOH/H_2O is a good example of a weakly structured system and TBA/H_2O is a representative binary mixture of a system with pronounced structuring.

2.4.2. Ternary mixtures

2.4.2.1. Solubilisation power of the hydrotropes for benzyl alcohol, limonene and DR-13

As discussed in the preceding section, scattering and conductivity experiments of the binary mixtures reveal a trend of progressive structuring in the investigated series of fully water miscible alcohols: EtOH < IPA < NPA < TBA. In the next step, three different hydrophobic compounds were dissolved in alcohol/H_2O binary mixtures, *i.e.* benzyl alcohol, limonene and DR-13. The difference between these compounds is their miscibility with water. Benzyl alcohol is slightly miscible with H_2O. Limonene, as well as DR-13, are poorly water miscible compounds. The realms of solubility in the cases of benzyl alcohol and limonene are shown in the ternary phase diagrams in Figure 2.5a and b and the OD as a measure of the solubility of DR-13 in Figure 2.5c.[49,50] The solubilisation power of the alcohols in the case of benzyl alcohol decreases in the following order: EtOH > IPA > NPA ≈ TBA, while phase diagrams with NPA and TBA are very similar.

The solubilisation power of the alcohols in the case of limonene gradually increases in the following order: EtOH < IPA < NPA < TBA. Its miscibility with H_2O is very poor (less than in the case of benzyl alcohol) and therefore the two-phase region is larger than in the case of benzyl alcohol. The solubility of limonene in TBA/H_2O starts to increase significantly at x(TBA) = 10 mol% (see point T3 in Figure 2.5) and at x(TBA) > 40 mol% the miscibility gap is closed. Furthermore, and most importantly, the hydrotrope efficiency for the solubilisation of limonene is reversed compared to the solubilisation efficiency of the alcohols considered for benzyl alcohol.

In the case of the solubilisation of DR-13, the dissolved amount of DR-13 increases in the following order: EtOH ≪ IPA < NPA < TBA for the hydrotrope content x(hydrotrope) < 0.4. For the hydrotrope content x(hydrotrope) > 0.4 the situation is different. Note that in the case of the solubilisation of DR-13 in TBA/H_2O, the solubility starts to increase at point T3 (remember: maximum of the water-rich bicontinuous phase in TBA/H_2O). After point T3, the solubility of DR-13 increases linearly up to the point T1, where the slope of the solubility of DR-13 in TBA diminishes. All in all, the solubilisation power of the alcohols for DR-13 follows the same trend as for limonene. However, comparing the results of DR-13 solubilisation to the solubilisation of benzyl alcohol and limonene, there are huge differences regarding the absolute amounts of dissolved hydrophobic compound on the order of ≈ 10^6 mol.

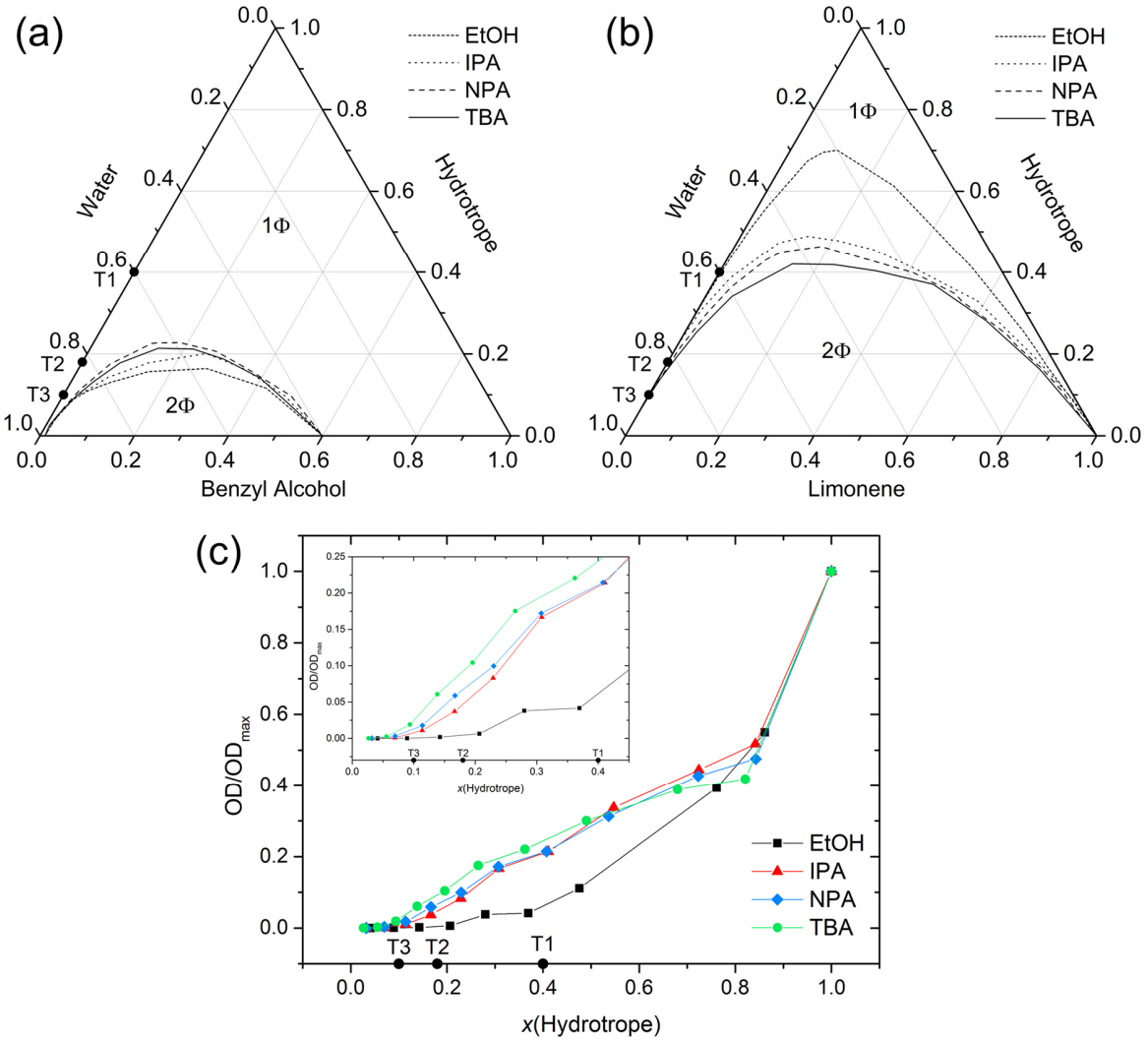

Figure 2.5: Ternary phase diagrams for the systems (a) H_2O/hydrotrope/benzyl alcohol and (b) H_2O/hydrotrope/limonene provided in mol%. (c) The results of the OD measurements of DR-13 in H_2O/hydrotrope mixtures given in mole fractions of hydrotrope. ODs obtained were divided by the OD value of the corresponding neat hydrotrope (OD_{max}). T1, T2 and T3 mark the transition points of the binary system TBA/H_2O in mole fractions as determined in Figure 2.4b.

2.4.2.2. Discussion of the solubilisation mechanisms in ternary systems

As for the binary systems, conductivity measurements were performed for several monophasic compositions of the ternary system H_2O/alcohol/benzyl alcohol, see Figure 2.6. In these experiments, alcohol/benzyl alcohol mixtures of different compositions, expressed here in mass percent of water, and in the presence of 0.2 wt% of NaBr were titrated with pure water. Conductivities for H_2O/EtOH/benzyl alcohol differ strongly from the conductivity curves obtained for H_2O/IPA/benzyl alcohol, H_2O/NPA/benzyl alcohol and H_2O/TBA/benzyl alcohol.

For systems containing NPA, IPA and TBA, the shapes of the curves do not significantly deviate for ternary systems H_2O/alcohol/benzyl alcohol from those of the binary system alcohol/H_2O. The decrease of the initial conductivity for $w(H_2O)$ = 0 only in the case of increasing EtOH/benzyl alcohol ratio can be explained by a higher charge mobility and enhanced ion dissociation.

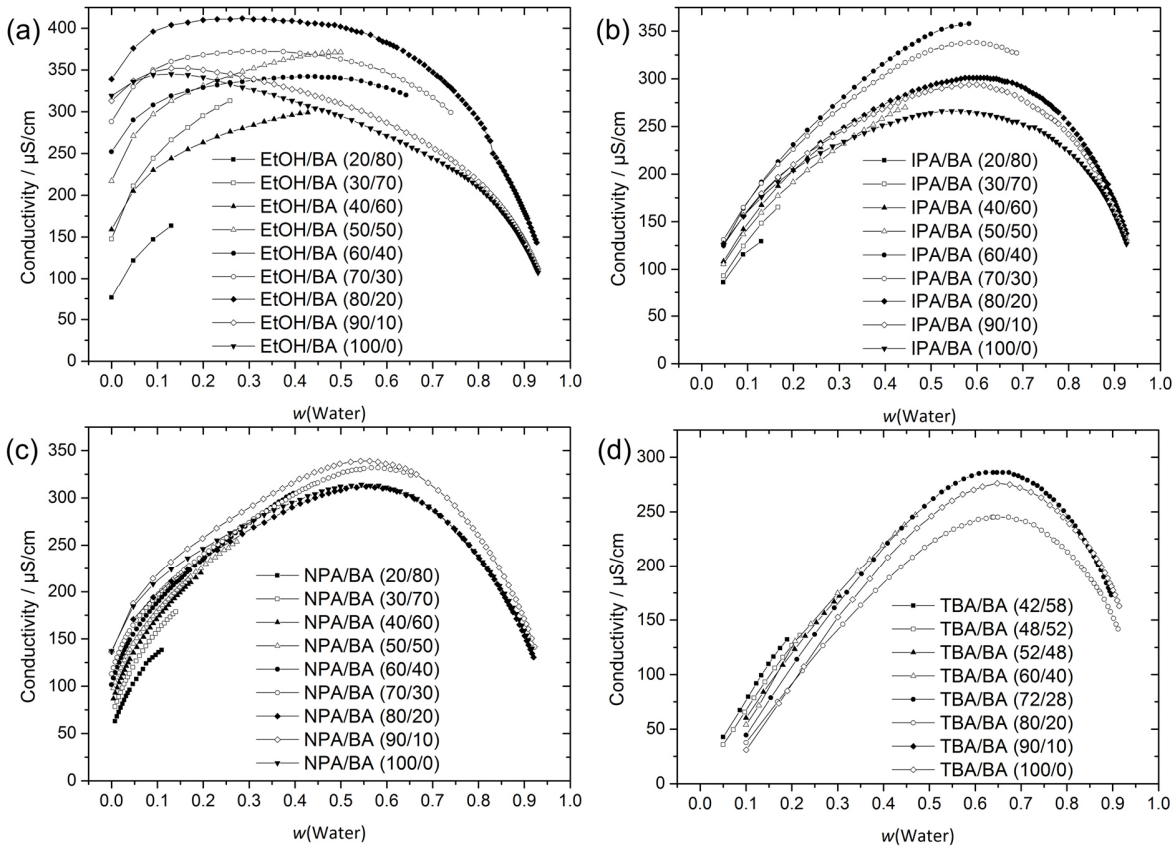

Figure 2.6: Conductivity measurements at 25 °C for ternary mixtures of H_2O/hydrotrope/benzyl alcohol plotted in weight fractions of H_2O. The measurements were performed by diluting a binary mixture hydrotrope/benzyl alcohol with H_2O. The symbols refer to different mass ratios of hydrotrope to benzyl alcohol (BA) in the binary starting mixture hydrotrope/benzyl alcohol before diluting with H_2O.

Taking into account the large difference in the solubilisation power of benzyl alcohol and limonene, different solubilisation mechanisms are proposed. For EtOH and IPA, no or very weak structuring is observed for their binary mixtures with H_2O. The addition of benzyl alcohol and limonene, respectively, induces the formation of a well-ordered system.[2,6] Hydrophobic hydration and agglomeration cause the hydrophobic compound to form clusters with accumulation of the hydrotrope mostly at the interface between the benzyl alcohol clusters and the water-rich domain. Consequently, the solubility of the hydrophobic compound is

enhanced with increasing hydrotrope concentration. This is in perfect agreement with the ideas forwarded recently.[22,23,51]

However, in contrast to weakly structured EtOH/H_2O and IPA/H_2O, the situation is completely different for binary, pre-structured TBA/H_2O and NPA/H_2O systems. As a bicontinuous structure is already given, the structure is not induced by the third component, but by the hydrotrope itself. Due to the formation of a bicontinuous system, an aliphatic-rich domain as well as a water-rich domain and a large area of interface are created.

In such a case of a pre-structured binary hydrotrope/water system, three possible solubilisation pathways are possible:

(i) solubilisation in the water-rich bulk phase (appears only for highly polar solutes which are not considered here),
(ii) solubilisation in the aliphatic-rich bulk phase and
(iii) solubilisation within the interfacial film between the aliphatic- and water-rich pseudo-bulk phases, see Figure 2.7.

The aliphatic-rich bulk-like pseudo-phase permits the incorporation of large amounts of hydrophobic components. This is confirmed by the solubilisation power of the hydrotropes in the case of limonene, where TBA shows the highest solubilisation power and EtOH the lowest solubilisation power. Further indications are conductivity measurements for ternary systems H_2O/alcohol/benzyl alcohol, where the absolute conductivity of NPA and TBA is maintained, indicating the retention of the pre-structures.

The SANS spectrum of one exemplary composition of a ternary mixture D_2O/TBA/benzyl alcohol (60/32/8 wt%) was compared to a SANS measurement of a binary TBA/H_2O mixture (40/60 wt%) to further support this fact, see Figure A1.1 (Appendix A.1). The substitution of TBA by benzyl alcohol leads to a large increase of the scattered intensity. Analysis of the correlation length of these curves (0.8 nm for the binary mixture and 2.1 nm for the ternary mixture) indicates an enlargement of the correlation length of the TBA/benzyl alcohol aliphatic-rich phase. This implies that benzyl alcohol and certainly also TBA are ‘‘driven’’ towards the aliphatic-rich continuum which is ‘‘blown up’’ and causes an increase of the correlation length. Therefore, the structure is reinforced by the addition of benzyl alcohol.

But in the case of benzyl alcohol, the situation is somehow different from the case of limonene, as it contains an alcohol functional group in addition to the aliphatic moiety. This leads us to the assumption that benzyl alcohol is not only dissolved within the aliphatic-rich continuum, due to its low water miscibility, but may also accumulate at the interfacial film, similar to a

co-surfactant. Another indicator is the fact that TBA provides the lowest solubilisation power for benzyl alcohol in the series EtOH, IPA and NPA. In EtOH/H_2O mixtures, benzyl alcohol induces the formation of mesoscale structures, whereas in the case of TBA/H_2O mixtures, it intercalates into the given pre-structure. As soon as the given pre-structure is completely ‘‘swollen up’’ and the interfacial film is saturated, further addition of benzyl alcohol causes the system to collapse and to form two phases.

In the case of the solubilisation of DR-13, the situation is again different from both the limonene and benzyl alcohol solubilisation processes, since DR-13 bears polar functional groups and an aromatic backbone much larger than that of benzyl alcohol. The solubilisation power of the hydrotropes in the case of DR-13 follows the same series as for limonene. However, a closer look at the amount of dissolved DR-13 per amount of the hydrotrope reveals a huge difference of the order of several orders of magnitude. Furthermore, DR-13 is assumed to be not capable of inducing micro-structuring, as the overall solubility in H_2O and H_2O/hydrotrope is too low. Therefore, the solubility in EtOH/H_2O is very low. However, as the solubility increases with progressive structuring of the H_2O/hydrotrope, we assume that the difference in solubility is based on a completely different solubilisation mechanism as compared to limonene. Instead of a bulk solubilisation within a hydrophobic mesoscale pseudo-phase, we suppose DR-13 to be mostly dissolved within the interfacial film of the two pseudo-bulk phases. This assumption is in good accordance with all results, because an interfacial film provides much less space than a bulky pseudo-phase for the solubilisation of DR-13. The solubility of DR-13 in TBA/H_2O mixtures starts to increase at point T3 representing the maximum of the water-rich bicontinuous phase, see Figure 2.4b and 2.5c. Beginning from T1 (representing the percolation threshold) the solubilisation power of TBA/H_2O diminishes compared to the region T3–T1. It is assumed that the interface of pre-structured binary alcohol/H_2O mixtures is rapidly saturated for low concentrations of DR-13. The further increase of the solubilisation of DR-13 for a higher TBA content (x(TBA) > 0.4) may be ascribed to bulk solubilisation due to saturation of the interface. Hence, DR-13 may preferentially solubilise at the interface in highly structured regimes of TBA 0.1 < x(TBA) < 0.4, passing over to a more bulk-like solubilisation mechanism for a higher TBA content. A more detailed analysis of the curve shapes clarifies these findings even better. A second-order differentiation of the fitted curves reveals huge differences in the solvent character of the hydrotrope (see Figure A1.2, Appendix A.1). In the case of EtOH, the curvature of the curve stays always positive over the whole miscibility range whereas there is a negative curvature in the case of TBA in the range of approximately 0.23 < x(TBA) < 0.6. This second order

differentiation shows that EtOH possesses a more co-solvent character, whereas TBA shows a hydrotropic behaviour when DR-13 is dissolved. The proposed interfacial solubilisation mechanism is further supported by the fact that DR-13 has a very poor solubility both in pure dodecane and pure water, for which both do not provide an interface at all. As a consequence, DR-13 is also scarcely soluble in poorly structured mixtures, such as EtOH/H_2O.

Solute	log(P)	Solubilisation mechanism	Solubilisation efficiency EtOH/H_2O IPA/H_2O NPA/H_2O TBA/H_2O
Benzyl alcohol 	1.1	bulk + interface	
DR-13 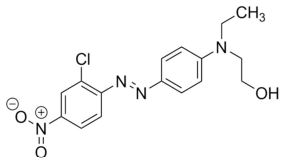	4.85	interface + (bulk)	
Limonene 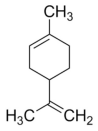	4.5	bulk	

Figure 2.7: Schematic overview of different solubilisation mechanisms and efficiencies of benzyl alcohol, DR-13 and limonene in binary water/alcohol mixtures. Octanol/water partition coefficients log(*P*) were taken from literature.[54–56]

2.5. Conclusion

We investigated the structuring of alcohol/H_2O binary mixtures, where the alcohol is miscible with H_2O in any proportion, *i.e.* EtOH, IPA, NPA and TBA. DLS, SWAXS, SANS and conductivity measurements revealed microscopic inhomogeneities in the cases of NPA/H_2O and TBA/H_2O. As in the case of micellar systems, we infer from conductivity measurements that these microscopic inhomogeneities are similar to direct or reverse micellar solutions (meaning organic aggregates in water or water aggregates in an organic pseudo-phase, respectively) and also, at some concentration ratios, to bicontinuous structuring with rapidly fluctuating water-rich and alcohol-rich domains in equilibrium. In the case of EtOH, no significant structuring could be detected by our methods. IPA marks the transition from a weakly structured system in the case of EtOH to structured systems in the cases of NPA and TBA.

It is found that this pre-structuring of a binary alcohol/H_2O system can be pivotal to the mesoscale solubilisation of a third component. In the cases of unstructured binary EtOH/H_2O and IPA/H_2O, a significant structuring is induced upon the addition of a third poorly water miscible component, *i.e.* limonene and benzyl alcohol. Until now, this solubilisation mechanism is considered to be dominant and fundamental in SFME, as is the case of the well-studied H_2O/EtOH/1-octanol system.[2,7,12,52,53] It was further argued that this structuring induced by the addition of the third, hydrophobic component, is crucial for a pronounced solubilisation power of the hydrotrope.[22,23,51] And indeed, the lower the pre-structuring in the binary hydrotrope/water mixture, the less hydrotrope is required to make benzyl alcohol water-miscible.

However, as we demonstrate here, hydrotropic solubilisation is more complicated. Firstly, it is just the other way around in the case of limonene: the more pronounced the pre-structuring in the binary hydrotrope/water mixture, the less hydrotrope is required to make the much more hydrophobic (compared to benzyl alcohol) limonene water-miscible. Secondly, the more pronounced the pre-structuring in the binary hydrotrope/water mixture, the lower is the minimum hydrotropic concentration (MHC) required to dissolve the dye DR-13, a very hydrophobic compound that is nevertheless nearly insoluble in both water and dodecane.

Two different solubilisation mechanisms can explain the hydrotropic solubilisation of very hydrophobic compounds:

(i) pseudo-bulk solubilisation of hydrophobic compounds in the aliphatic-rich moiety of pre-structured hydrotrope/water mixtures and

(ii) interface solubilisation of hydrophobic, but still slightly amphiphilic compounds in the interfacial film.

This leads to the conclusion that for solubilising a hydrophobic compound in an aqueous medium, the choice of the alcohol (hydrotrope) depends primarily on the nature of the hydrophobic substance. For more hydrophilic compounds bearing polar functional groups, short-chained alcohols are more favourable, which is in agreement with ref. 22, 23 and 51. In order to solubilise hydrophobic compounds without polar groups, structure-forming hydrotropes like TBA and NPA should be used instead.

At first glance, our conclusions may appear contradictory to recent statistical thermodynamic considerations of hydrotropy.[19-21] These state that the predominant driving forces for hydrotropic solubilisation are (i) solute induced interactions between the solute and hydrotrope molecules leading to a solute–hydrotrope association. In contrast, (ii) pre-structuring of

hydrotropes (hydrotrope–hydrotrope interactions) in water is considered to be rather obstructive for good solubilisation of the solute. Indeed, this holds true for solutes, which are able to interact with the hydrotrope due to the presence of polar functional groups, as is the case for benzyl alcohol. For this case, our results are in total agreement with the results obtained by thermodynamic calculations. However, the statistic thermodynamic studies by Shimizu *et al.* consider almost exclusively hydrotropes with polar functional groups, *e.g.* ester functional groups. Yet, for very hydrophobic substances (as is the case for limonene), the situation becomes subtler. In this case, the solute–hydrotrope interactions are expected to be weaker and no longer play the dominant role since there is no functional group to interact with the hydrotrope. Instead, it becomes more important that the highly hydrophobic solute molecules can intercalate into a significantly hydrophobic, aliphatic pseudo-phase (as is the case for TBA in H_2O), originated by the pre-structuring of the hydrotrope in water. For DR-13, we found a similar trend for its solubility as for the solubilisation of limonene, but based on a different solubilisation mechanism, due to its slightly amphiphilic character. Thus, the solubility depends on the chemical nature of both, the solute and the hydrotrope. Furthermore, we would like to emphasise that in addition to a different choice of solutes, the aforementioned studies by Shimizu *et al.* focused in most of the cases on completely different concentration ranges of the solute and hydrotrope. They considered a very low amount of solute in aqueous hydrotrope solutions. (This is important for the validity of Kirkwood–Buff theory used for statistical thermodynamic calculations in these studies.) Thus, our studies provide a more general and molecular-based model concept of hydrotrope solubilisation.

All in all, taking into account the different ways in which structuring can be induced and how they influence the involved solubilisation mechanisms, our picture of mesoscale solubilisation in ternary systems becomes more general and more complete now. Microscopic inhomogeneities and compartmentation phenomena in SFME can not only be induced by the addition of a third hydrophobic component to a H_2O/hydrotrope binary mixture, but can also have their origin in the pre-structuring of alcohol/ H_2O binary mixtures.

2.6. References

1 M. L. Klossek, D. Touraud, T. Zemb and W. Kunz, *ChemPhysChem*, **2012**, *13*, 4116–4119.

2 M. L. Klossek, D. Touraud and W. Kunz, *Phys. Chem. Chem. Phys.*, **2013**, *15*, 10971–10977.

3 V. Fischer, J. Marcus, D. Touraud, O. Diat and W. Kunz, *J. Colloid Interface Sci.*, **2015**, *453*, 186–193.

4 M. Zoumpanioti, H. Stamatis, V. Papadimitriou and A. Xenakis, *Colloids Surf. B*, **2006**, *47*, 1–9.

5 Y. L. Khmelnitsky, R. Hilhorst and C. Veeger, *Eur. J. Biochem.*, **1988**, *176*, 265–271.

6 J. Marcus, M. L. Klossek, D. Touraud and W. Kunz, *Flavour Fragrance J.*, **2013**, *28*, 294–299.

7 S. Schöttl, J. Marcus, O. Diat, D. Touraud, W. Kunz, T. Zemb and D. Horinek, *Chem. Sci.*, **2014**, *5*, 2949–2954.

8 P. Bošković, V. Sokol, T. Zemb, D. Touraud and W. Kunz, *J. Phys. Chem. B*, **2015**, *119*, 9933–9939.

9 Z. Li, X. Liu, Y. Lian, J. Xie, X. Gao and T. Chang, *World J. Eng.*, **2016**, *13*, 142–148.

10 T. Zemb, M. L. Klossek, T. Lopian, J. Marcus, S. Schöttl, D. Horinek, S. Prevost, D. Touraud, O. Diat, S. Marčelja and W. Kunz, *Proc. Natl. Acad. Sci. U. S. A.*, **2016**, *113*, 4260–4265.

11 C. Neuberg, *Biochem. Z.*, **1916**, *76*, 107–108.

12 O. Diat, M. L. Klossek, D. Touraud, B. Deme, I. Grillo, W. Kunz and T. Zemb, *J. Appl. Crystallogr.*, **2013**, *46*, 1665–1669.

13 P. Bauduin, A. Renoncourt, A. Kopf, D. Touraud and W. Kunz, *Langmuir*, **2005**, *21*, 6769–6775.

14 D. Subramanian and M. Anisimov, *J. Phys. Chem. B*, **2011**, *115*, 9179–9183.

15 D. Subramanian, C. T. Boughter, J. B. Klauda, B. Hammouda and M. Anisimov, *Faraday Discuss.*, **2013**, *167*, 217–238.

16 M. Sedlák, *J. Phys. Chem. B*, **2006**, *110*, 13976–13984.

17 M. Sedlák and D. Rak, *J. Phys. Chem. B*, **2014**, *118*, 2726–2737.

18 S. Shimizu and N. Matubayasi, *J. Phys. Chem. B*, **2014**, *118*, 10515–10524.

19 S. Shimizu and N. Matubayasi, *J. Phys. Chem. B*, **2014**, *118*, 3922–3930.

20 S. Shimizu and N. Matubayasi, *Phys. Chem. Chem. Phys.*, **2016**, *18*, 25621–25628.

21 T. W. J. Nicol, N. Matubayasi and S. Shimizu, *Phys. Chem. Chem. Phys.*, **2016**, *18*, 15205–15217.

22 J. J. Booth, S. Abbott and S. Shimizu, *J. Phys. Chem. B*, **2012**, *116*, 14915–14921.

23 J. J. Booth, M. Omar, S. Abbott and S. Shimizu, *Phys. Chem. Chem. Phys.*, **2015**, *17*, 8028–8037.

24 S. Dixit, J. Crain, W. C. K. Poon, J. L. Finney and A. K. Soper, *Nature*, **2002**, *416*, 829–832.

25 O. Gereben and L. Pusztai, *J. Phys. Chem. B*, **2015**, *119*, 3070–3084.

26 A. Ghoufi, F. Artzner and P. Malfreyt, *J. Phys. Chem. B*, **2016**, *120*, 793–802.

27 M. L. Tan, B. T. Miller, J. Te, J. R. Cendagorta, B. R. Brooks and T. Ichiye, *J. Chem. Phys.*, **2015**, *142*, 0645011.

28 L. Almásy, G. Jancsó and L. Cser, *Appl. Phys. A: Mater. Sci. Process.*, **2002**, *74*, 1376–1378.

29 K. Nishikawa, H. Hayashi and T. Iijima, *J. Phys. Chem.*, **1989**, *93*, 6559–6565.

30 D. T. Bowron, J. L. Finney and A. K. Soper, *J. Phys. Chem. B*, **1998**, *102*, 3551–3563.

31 K. Yoshida, T. Yamaguchi, A. Kovalenko and F. Hirata, *J. Phys. Chem. B*, **2002**, *106*, 5042–5049.

32 T. Fukasawa, Y. Tominaga and A. Wakisaka, *J. Phys. Chem. A*, **2004**, *108*, 59–63.

33 A. A. Bakulin, M. S. Pshenichnikov, H. J. Bakker and C. Petersen, *J. Phys. Chem. A*, **2011**, *115*, 1821–1829.

34 H. A. R. Gazi and R. Biswas, *J. Phys. Chem. A*, **2011**, *115*, 2447–2455.

35 B. Kezic and A. Perera, *J. Chem. Phys.*, **2012**, *137*, 0145011.

36 M. D. Hands and L. V. Slipchenko, *J. Phys. Chem. B*, **2012**, *116*, 2775–2786.

37 L. Comez, M. Paolantoni, L. Lupi, P. Sassi, S. Corezzi, A. Morresi and D. Fioretto, *J. Phys. Chem. B*, **2014**, *119*, 9236–9243.

38 D. Banik, A. Roy, N. Kundu and N. Sarkar, *J. Phys. Chem. B*, **2015**, *119*, 9905–9919.

39 S. K. Allison, J. P. Fox, R. Hargreaves and S. P. Bates, *Phys. Rev. B: Condens. Matter Mater. Phys.*, **2005**, *71*, 1–5.

40 P. G. Kusalik, A. P. Lyubartsev, D. L. Bergman and A. Laaksonen, *J. Phys. Chem. B*, **2000**, *104*, 9526–9532.

41 M. Tomsic, A. Jamnik, G. Fritz-Popovski, O. Glatter and L. Vladek, *J. Phys. Chem. B*, **2007**, *111*, 1738–1751.

42 D. Subramanian, J. B. Klauda, P. J. Collings and M. Anisimov, *J. Phys. Chem. B*, **2014**, *118*, 5994–6006.

43 M. Clausse, L. Nicolas-Morgantini, A. Zradba and D. Touraud, in Surfactant Science Series (Vol. 24) Microemulsion Systems, eds. H. L. Rosano and M. Clausse, Dekker, New York, 1987, p. 15.

44 C. D. Dewhurst, I. Grillo, D. Honecker, M. Bonnaud, M. Jacques, C. Amrouni, A. Perillo-Marcone, G. Manzin and R. Cubitt, *J. Appl. Crystallogr.*, **2016**, *49*, 1–14.

45 https://www.ill.eu/instruments-support/computing-for-science/cs-software/all-software/lamp/.

46 B. Lagourette, J. Peyrelasse, C. Boned and M. Clausse, *Nature*, **1979**, *281*, 60–62.

47 M. Clausse, J. Peyrelasse, J. Heil, C. Boned and B. Lagourette, *Nature*, **1981**, *293*, 636–638.

48 D. Subramanian and M. A. Anisimov, *Fluid Phase Equilib.*, **2014**, *362*, 170–176.

49 A. Arce, A. Marchiaro and A. Soto, *J. Solution Chem.*, **2004**, *33*, 561–569.

50 H. Li and K. Tamura, *Fluid Phase Equilib.*, **2008**, *263*, 223–230.

51 W. Kunz, K. Holmberg and T. Zemb, *Curr. Opin. Colloid Interface Sci.*, **2016**, *22*, 99–107.

52 J. Marcus, D. Touraud, S. Prevost, O. Diat, T. Zemb and W. Kunz, *Phys. Chem. Chem. Phys.*, **2015**, *17*, 32528–32538.

53 T. Lopian, S. Schöttl, S. Prevost, S. Pellet-Rostaing, D. Horinek, W. Kunz and T. Zemb, *ACS Cent. Sci.*, **2016**, *2*, 467–475.

54 L. O. Copolovici and Ü. Niinemets, *Chemosphere*, **2005**, *61*, 1390–1400.

55 Stephen B. Roscoe, Neal A. Rakow, Michael L. Husberg and Lester H. McIntosh, US Pat., 2005/0065062, **2005**.

56 G. G. Briggs, *J. Agric. Food Chem.*, **1981**, *29*, 1050–1059.

Chapter 3 The role of hydrogen bond donor and acceptor functionalities on the formation of surfactant-free microemulsions

3.1. Abstract and preface

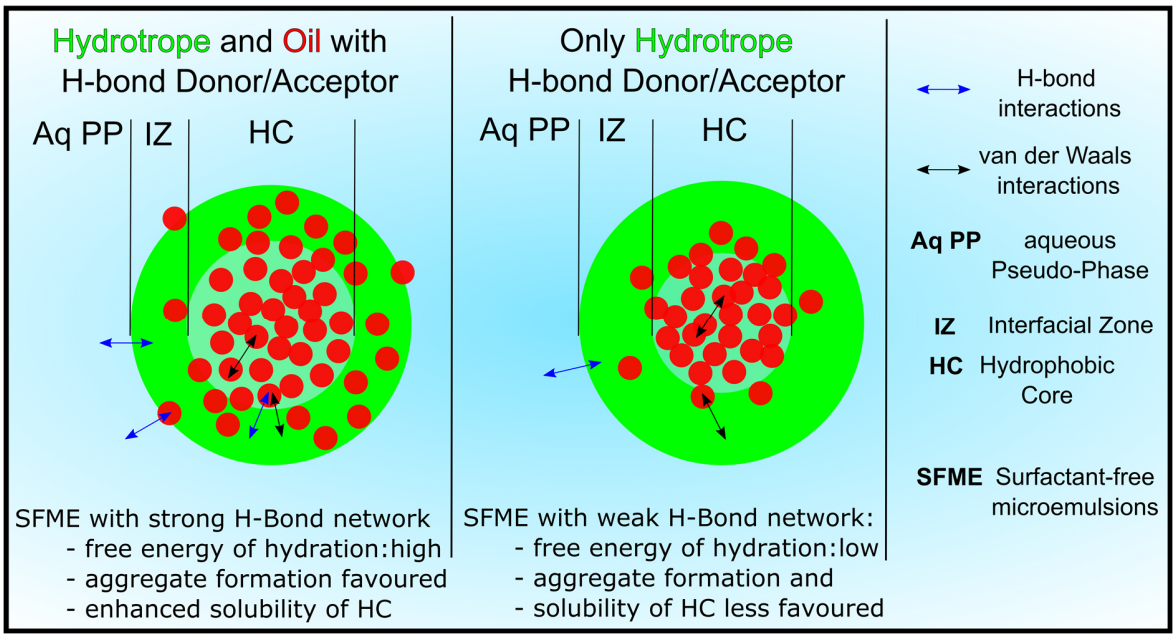

Figure 3.1: Graphical abstract schematically illustrating hydrogen bond and van der Waals interactions in SFME consisting of water/hydrotrope/hydrophobic component (oil). On the left: the hydrotrope and the oil have both, H-bond donor and acceptor functional groups. On the right: only the hydrotrope possesses an H-bond donor and acceptor functional group. Note that the hydrotrope is also present in the aqueous pseudo-phase, which is not indicated in the scheme.

The influence of hydrogen bond (H-bond) donor and acceptor functionalities on the formation of surfactant-free microemulsions (SFME) was investigated in ternary systems comprising water, hydrotrope and a hydrophobic component (see Figure 3.1). To this purpose, the miscibility of water, hydrotropes and hydrophobic components possessing different H-bond donor/acceptor groups was systematically investigated and mesoscopic structuring of monophasic compositions in these ternary mixtures was investigated using dynamic light scattering (DLS). The formation and size domain of aggregation of SFME was correlated with the solubility of the hydrophobic component within these systems. It was found that SFME consisting of hydrotropes and hydrophobic component, both providing an H-bond donor and an H-bond acceptor group (here: alcohol group), show most pronounced mesoscale

structuring accompanied by the best solubilisation efficiency with regard to the solubilisation of the hydrophobic component within these mixtures.

This chapter is part of a study considered for publication in *ACS Nano* (M. Hahn, S. Krickl, T. Buchecker, G. Jost, D. Touraud, P. Bauduin, A. Pfitzner, A. Klamt and W. Kunz, *ACS Nano*, **2018**, manuscript in preparation.)

Contributions to the experimental work:

- Dynamic light scattering: S. Krickl, G. Jost and T. Buchecker
- Phase diagrams: S. Krickl, G. Jost and T. Buchecker

3.2. Introduction

Surfactant-free microemulsions (SFME) are organised ternary solvents consisting of a short-chain amphiphilic molecule (hydrotrope) and two immiscible liquids – with both of them being fully miscible with the hydrotrope.[1–6] Mesoscopic organisation of such ternary systems into hydrophobic and hydrophilic domains is comparable to the mesoscopic organisation observed in water/oil/surfactant ternary systems (direct, bicontinuous and reverse microemulsions) as previously shown using scattering techniques, molecular dynamics simulations and conductivity measurements.[7–15] This unique mesoscopic structure offers a great variety of possible applications: SFME are powerful solubilisation media,[16,17] provide anomalies in enzymatic activity[18–20] and chemical reactivity when used as reaction media,[21,22] serve as nano-reactors for the templated synthesis of nanoparticles[23–25] and find several other application-orientated uses.[26–29] Zemb *et al.* recently developed an extended Derjaguin–Landau–Verwey–Overbeek (DLVO) theory in order to provide a general explanation for the formation and thermodynamic stability of SFME.[3] This extended DLVO theory describes the subtle balance between free energy of hydration (hydration force between surfaces), van der Waals interactions (attractive dispersion forces) and mixing entropy (homogenous mixing of three components) leading to a minimum of the total free energy of SFME similar (although less pronounced) to conventional microemulsions and micellar solutions. Nonetheless, there is still a lack of studies that systematically investigate the formation of SFME based on the molecular properties of the SFME constituents in order to provide more application-orientated rules to appropriately formulate SFME.[17] To this purpose, the present contribution focuses on the role of hydrogen bond (H-bond) donors/acceptors on the formation of SFME. In particular, hydrogen bonding between H_2O/hydrotrope/oil components has to be considered as the main

contribution to the free energy of hydration, and thus also for the stabilisation of mesoscale compartments (aside from van der Waals contributions). For these reasons, the goal of this work is to investigate the role of H-bond donor and acceptor functionalities of the hydrotrope and the oil on the occurrence of mesoscale inhomogeneities in aqueous SFME. The following questions are essential in this context:

(i) What is the general role of hydrogen bonding on the formation of SFME?

(ii) Is the presence of hydrotropes/oil components possessing H-bond donors and/or acceptors essential for the formation mesoscale inhomogeneities?

(iii) Which combination basically provides most pronounced mesoscale structures?

(iv) What is the effect of formed mesoscale structures on the solubility of the hydrophobic component within the ternary mixture?

To address all these questions, the formation of SFME in ternary solutions (water/hydrotrope/oil) was investigated by systematically changing the H-bond acceptor/donor functional groups of the hydrotrope and the oil component. To this purpose, ethanol (EtOH, H-Bond donor and acceptor), acetone (Ace, H-bond acceptor) and tetrahydrofuran (THF, H-bond acceptor) were selected as hydrotropes. Benzyl alcohol (BA, H-Bond donor and acceptor), anisole (Ani, H-bond acceptor) and toluene (Tol, no H-Bond donor/acceptor functional group) were chosen as the hydrophobic components, see Figure 3.2. Ternary phase diagrams were recorded to determine the monophasic regions, where SFME formation can occur in principal.

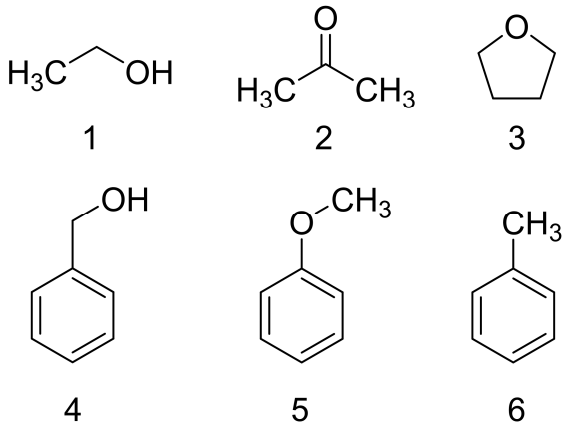

Figure 3.2: Chemical structures of (1) ethanol, (2) acetone, (3) tetrahydrofuran, (4) benzyl alcohol, (5) anisole and (6) toluene. Benzyl alcohol is hydrogen bond donor and acceptor, anisole is hydrogen bond acceptor and toluene is neither a hydrogen bond donor nor acceptor.

Dynamic light scattering (DLS) was used to detect and quantify the size of mesoscale inhomogeneities for the different ternary systems. Based on these measurements, conclusions were drawn on the best combination of H-Bond donor/acceptor functionalities of the hydrotrope and the hydrophobic component for preferably pronounced mesoscale structured SFME. Finally, the solubilisation efficiency of the hydrophobic component in the resulting ternary mixture was correlated with the presence/absence of mesoscale structuring.

3.3. Experimental

3.3.1. Chemicals

Ethanol (EtOH, ≥ 99.8%) and (*R*)-(+)-limonene (97%, ee: 98%) were obtained from Sigma-Aldrich (Steinheim, Germany). Benzyl alcohol (BA, ≥ 99%), anisole (Ani, ≥ 99%) and acetonitrile (≥ 99.5%) were purchased from Merck (Darmstadt, Germany). Toluene (Tol, ≥ 99.99%) and tetrahydrofuran (THF, ≥ 99.5 %) were purchased from Fischer Scientific (Loughborough, UK) and acetone (Ace, 100%) from VWR Chemicals (Fontenay-sois-Bois, France). All chemicals were used without further purification. Aqueous solutions were prepared using deionised water with a resistivity of 18 MΩ cm.

3.3.2. Ternary phase diagrams

Phase diagrams were recorded at 25 °C using a dynamic and static process according to Clausse *et al*. (see Section 2.3.2.1).[30]

3.3.3. Dynamic light scattering

DLS experiments were performed as described in Section 2.3.2.2. Six points were selected for DLS measurements in every ternary system and marked with letters from *a* to *f*. Selected points were always 5 mol% above the maximum of the phase separation border in their respective ternary phase diagrams thereby providing the same molar percentage of hydrotrope. Points from *a* to *f* correspond to different compositions with 0, 5, 10, 15, 20 and 25 mol% of hydrophobic component (see for example, Appendix A.2, Figure A2.1).

Aggregates in SFME are usually highly fluctuating and of no well-defined shape. Thus, normalised intensity autocorrelation functions $g^{(2)}(\tau) - 1$ were first evaluated qualitatively with regard to their y-intercept and decay time τ. As a rule of thumb, it was assumed that a higher intercept of the correlation function for small decay times and larger decay times of the correlation function represent the more time-stable and more pronounced structuring of the

SFME. In addition, a more thorough analysis of the data was done assuming SFME with approximately spherical geometry of pure oil-rich aggregates dispersed in an outer pseudo-phase composed of water/hydrotrope. To this purpose, cumulant analysis was applied in order to provide a rough estimation for the size domains of formed aggregates (see Section 1.2.1).[31,32]

3.4. Results

3.4.1. Ternary phase diagrams

Ternary phase diagrams of H_2O, hydrotrope (EtOH, Ace, THF) and the hydrophobic component (BA, Ani, Tol) are depicted in Figure 3.3. The realms of miscibility of the ternary systems increase from Tol < Ani < BA independent of the used hydrotrope. BA, possessing an H-Bond acceptor and donor functional group, is better soluble in all binary H_2O/hydrotrope mixtures than Ani, which is solely an H-Bond acceptor. Tol is neither an H-Bond donor nor acceptor and was found to have the lowest solubility in all three systems.

Furthermore, ternary mixtures containing EtOH as an H-Bond donor and acceptor show the smallest miscibility gap for all hydrophobic components compared to Ace and THF being only H-bond acceptors. Consequently, regarding the efficiency of the used hydrotropes to solubilise the hydrophobic components in aqueous solution following order can be found: EtOH > Ace > THF.

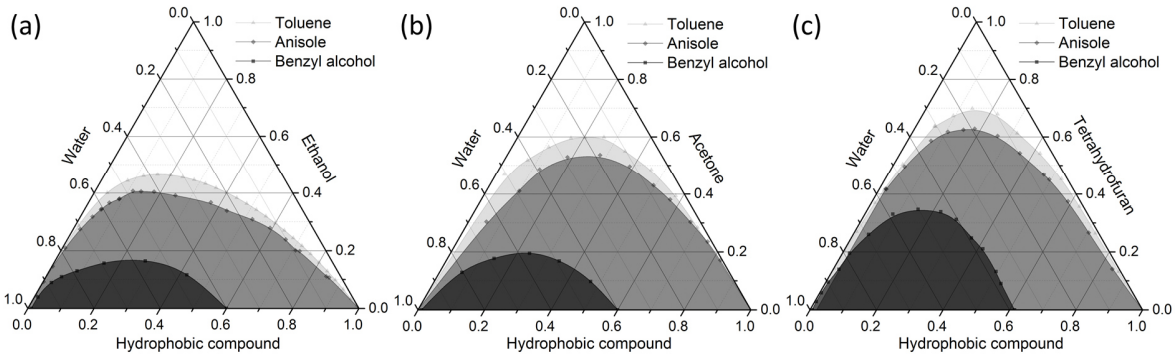

Figure 3.3: Ternary phase diagrams of (a) H_2O/EtOH/hydrophobic component, (b) H_2O/Ace/hydrophobic component and (c) H_2O/THF/hydrophobic component at 25 °C provided in mole fractions. Dark grey, grey and light grey areas represent biphasic realms of the ternary systems with BA, Ani and Tol, respectively.

3.4.2. Dynamic light scattering

DLS experiments were performed to investigate the occurrence and size domain of mesoscale inhomogeneities in the ternary mixtures depicted in Figure 3.3. Correlation functions obtained by DLS are shown in Figure 3.4. Binary mixtures of H_2O/EtOH do not show any correlation functions indicating a molecular distributed binary solvent mixture as forwarded recently.[17] Upon the addition of (5, 10, 15, 20 and 25 mol%) BA, Ani or Tol to H_2O/EtOH a gradual formation of well-defined correlation functions with an increasing shift to higher decay times is observed (Figure 3.4a-c). However, for higher BA concentrations (x(BA) > 0.15), correlation functions decrease again. A similar, yet less pronounced trend is observed for ternary mixtures of H_2O/Ace/BA and H_2O/THF/BA (Figure 3.4d and 3.4g). Such correlation functions are typical for ill-defined SFME caused by mesoscopic compartmentation of aliphatic- and water-rich pseudo-phases.[1,16,17] Overall, correlation functions and decay times decrease in the order EtOH > Ace > THF for a constant hydrophobic component and decrease in the order BA > Ani ≥ Tol for a constant hydrotrope. Note that significant correlation functions are only observed for ternary compositions where either the hydrotrope (EtOH) or the hydrophobic component (BA) possesses both, an H-bond donor and acceptor. For ternary systems containing Ace/THF in combination with Ani/Tol no correlation could be observed at all, indicating the absence of mesoscale structured solutions.

For a more quantitative analysis and interpretation of the correlation functions (Figure 3.4a-d, g), hydrodynamic radii were calculated as a measure of the size domain of the hydrophobic compartments by assuming a spherical geometry of oil-rich aggregates dispersed in H_2O/hydrotrope mixtures (see Figure 3.5). For ternary systems containing EtOH as a hydrotrope, hydrodynamic radii r_H of the hydrophobic compartments increase upon the addition of the hydrophobic component. Upon addition of BA, a maximum of the hydrodynamic radius appears for x(BA) = 0,15 (r_H = 1.7 nm). For Ani and Tol hydrodynamic radii of mesoscale inhomogeneities reach a constant value after steadily increasing (r_H = 0.8 nm for Ani and 0.6 nm for Tol). Note that with decreasing hydrodynamic radii, a reduced solubility of the hydrophobic component was observed within the ternary mixtures H_2O/EtOH/hydrophobic component by going from BA to Ani and Tol. A similar result was found for ternary mixtures containing Ace and THF. Yet, mesoscale structuring is completely lost by going from BA to Ani/Tol for mixtures containing Ace/THF as a hydrotrope, which is not case for EtOH containing mixtures.

A second trend is observable for H_2O/hydrotrope/BA mixtures concerning the effect of the hydrotropes on the size domain of mesoscale structures of the SFME: correlation functions are most pronounced for ternary mixtures containing EtOH as a hydrotrope followed by Ace and THF as hydrotropes, see Figure 3.4a,d,g. Hydrodynamic radii calculated from correlation functions of ternary systems containing EtOH as a hydrotrope are larger compared to ternary systems containing Ace and THF as a hydrotrope, see Figure 3.5b. Note that a decreasing size domain of mesoscale inhomogeneities in H_2O/Ace/BA and H_2O/THF/BA is again accompanied by a lower solubility of BA.

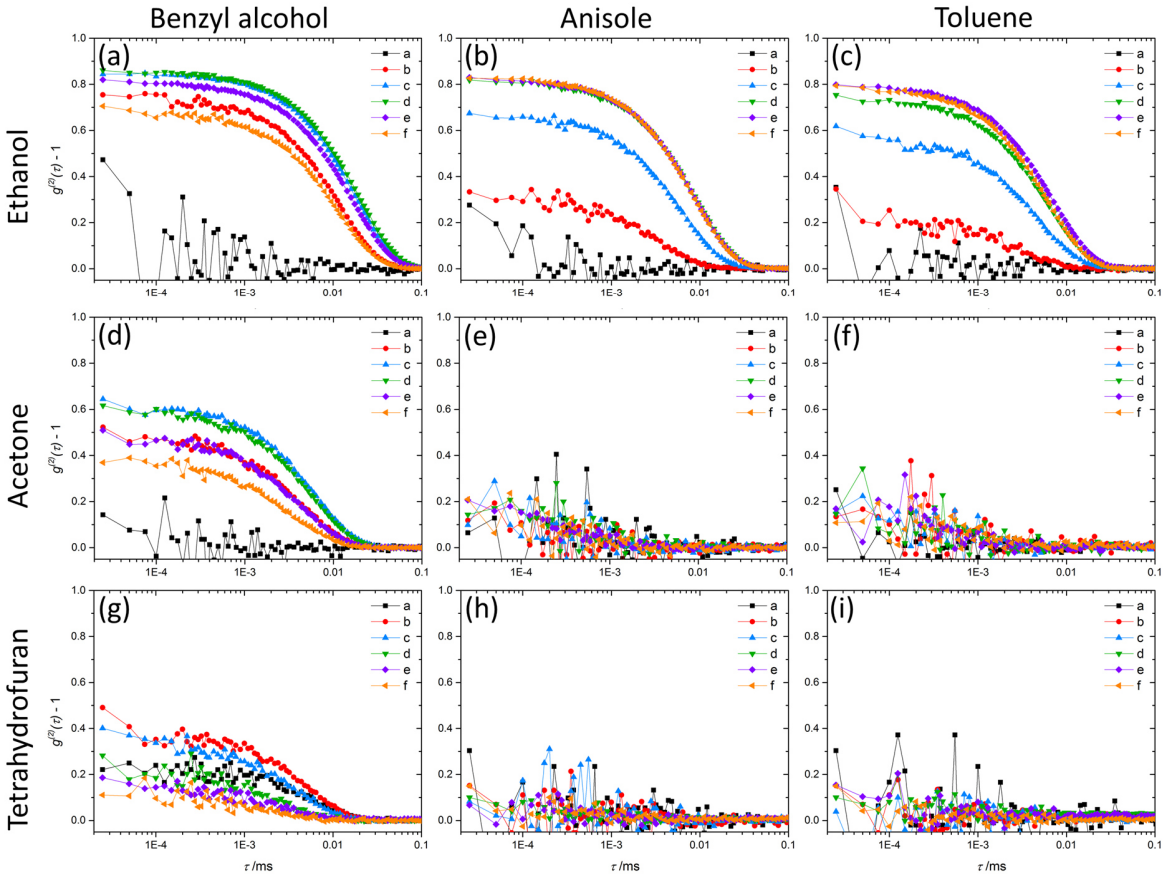

Figure 3.4: Normalised intensity autocorrelation functions obtained by DLS measurements for ternary mixtures (a) H_2O/EtOH/BA, (b) H_2O/EtOH/Ani, (c) H_2O/EtOH/Tol, (d) H_2O/Ace/BA, (e) H_2O/Ace/Ani, (f) H_2O/Ace/Tol, (g) H_2O/THF/BA, (h) H_2O/THF/Ani and (i) H_2O/THF/Tol at 25 °C.

It is worth noting that the trend of hydrodynamic radii as a function of increasing *x*(BA) for EtOH and Ace is similar (maximum r_H = 1.7 nm at *x*(BA) = 0.15 for EtOH and r_H = 1.1 nm *x*(BA) = 0,10 for Ace), whereas largest hydrodynamic radii for H_2O/THF/BA are obtained for *x*(BA) = 0 and decrease upon the addition of BA. Note that DLS measurements on binary mixtures H_2O/THF already show mesoscale compartmentation of hydrophobic and hydrophilic

components. This pre-structuring of H_2O/THF gets more and more destroyed upon the addition of a third hydrophobic component, as forwarded recently resulting in less pronounced correlation functions.[17]

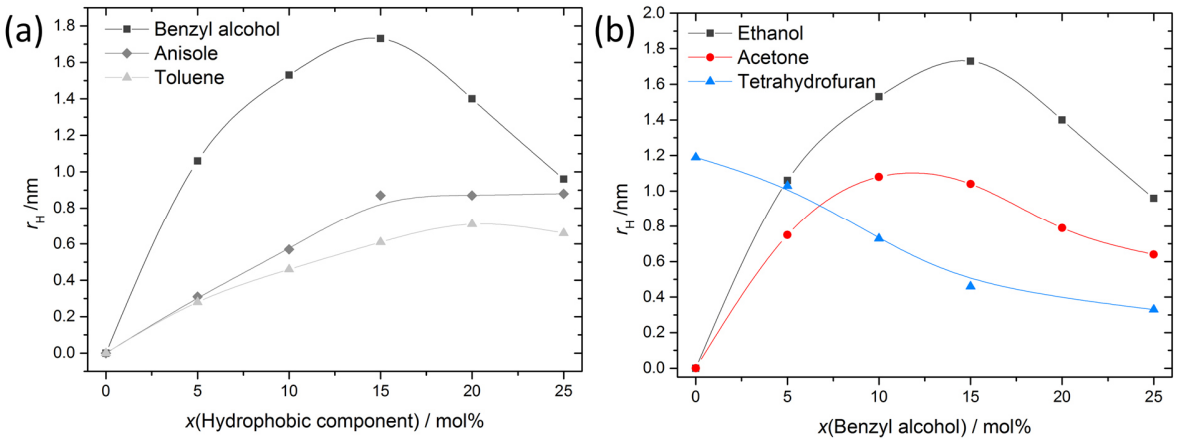

Figure 3.5: Hydrodynamic radii r_H obtained from DLS measurements for (a) ternary solutions containing H_2O/EtOH/hydrophobic component (hydrophobic component = BA, Ani, Tol) (b) ternary solutions containing H_2O/hydrotrope/BA (hydrotrope = EtOH, Ace, THF).

3.5. Discussion

3.5.1. Influence of H-bond donor/acceptor functional groups on the formation of SFME

Altogether, results obtained from solubility and DLS experiments suggest a correlation between the presence of H-bond donor/acceptor functional groups of the hydrotrope/hydrophobic component and the formation of mesoscale structured ternary mixtures with water (SFME). At least three cases should be distinguished: (i) the hydrotrope bears an H-bond donor and acceptor, (ii) the hydrophobic component possesses an H-bond donor and acceptor (in this study: OH-groups), (iii) only H-bond acceptors are involved.

Regarding case (i), mesoscale structuring in these kind of ternary systems is favoured, independent of whether the hydrophobic component possesses an H-Bond acceptor/donor or not. However, the size domains of aggregation strongly depend on the acceptor/donor properties of the hydrophobic component. If the hydrophobic component possesses an OH-group (BA), more extended mesoscale structuring is observed. Replacing this OH-group by a group that can only act as H-bond acceptor (Ani), the size of formed mesoscale structures

decreases significantly and decreases even further upon replacement by a non-functionalized (aliphatic) group (Tol).

In case (ii), in which the hydrophobic component contains an H-bond donor and acceptor functionality (BA), mesoscale structuring can still be found, even if the hydrotrope is only an H-bond acceptor (*e.g.* Ace, THF). In this case, strength and extent of structuring should primarily scale with the strength of the acceptor properties of the hydrotrope. However, it has to be noted that due to the reduced possibility of H-Bond interactions of the hydrotrope, other contributions like Dipole-Dipole and van der Waals interactions may gain more and more importance.

Furthermore, the findings suggest that in case (iii), in which only H-bond acceptors are involved (aside from water neither the hydrotrope nor the hydrophobic component is an H-bond donor), the formation of mesoscale structured solutions is not favoured. However, in literature SFME are reported for such a case. For instance, Ventosa and co-workers reported well-structured SFME composed of water, Ace (or acetonitrile) and CO_2 in the supercritical state.[33,34] This fact may be explained by several effects, since the supercritical state can have a significant influence on the chemical properties, *e.g.* enhanced keto-enol tautomerism or enhanced H-bond donor/acceptor strength. To this purpose, a ternary system was additionally investigated composed of acetonitrile/acetone/limonene, where no H-bond formation is basically possible (see Appendix A.2, Figure A2.2 for the ternary phase diagram and DLS data). It could be shown that even in such an H-bonding-free system, mesoscale structuring could be detected. This leads to the conclusion that even strong Dipole-Dipole and van der Waals interactions may be sufficient for the occurrence of SFME. At this point, it has to be stressed that this study has no claim to completeness. It has to be admitted that structured systems may exist, where mesoscale structuring occurs due to more specific interactions. Furthermore, the role of van der Waals interactions on the formation of SFME was not treated into detail in this study. Observations and conclusions made in this study should rather provide a basis for the prediction of systems which are basically favoured to form SFME than to give absolutely essential prerequisites for SFME formation.

3.5.2. Correlation between solubility of the hydrophobic component and mesoscale structuring of SFME

As mentioned above, results presented in this study show a second interesting feature concerning the relationship between the occurrence and extent of mesoscale structures and the solubility of the hydrophobic component. It was found that mesoscale structuring favours

the solubility of hydrophobic components in H_2O/hydrotrope mixtures. Size domains of formed SFME cohere with an enhanced solubility of the hydrophobic component, *cf.* ternary systems water/EtOH/hydrophobic component (Figure 3.3a and 3.5a): an increasing size of mesoscale compartmentations is generally accompanied by a higher solubility of the hydrophobic component. A similar trend is observed with regard to phase diagrams of H_2O/Ace/(BA/Ani/Tol) and H_2O/THF/(BA/Ani/Tol). SFME composed of water, Ace/THF and BA show a strongly enhanced solubility of BA, which again scales with the size domain of the compartmentations whereas all ternary mixtures with Ani/Tol (unstructured) have a similar, relatively large miscibility gap. Yet, no quantitative conclusion on the correlation between the size of formed aggregates and the amount of dissolved oil can be drawn. Furthermore, not all systems with low miscibility gaps must show mesoscale compartmentation and not all systems with a high miscibility gap have to be unstructured. Nevertheless, it can be stated that mesoscale structuring was found to be beneficial for an enhanced solubility of the hydrophobic component in the corresponding ternary mixture.

3.6. Conclusion

This study focused on the systematic investigation of the role of H-Bond donor/acceptor functionalities of the hydrotrope and the oil component on the formation of aqueous SFME. To this purpose, several ternary systems composed of water, EtOH/Ace/THF as hydrotropes and BA/Ani/Tol as the hydrophobic component were investigated by solubilisation experiments and DLS. It was found that different combinations of acceptor/donor functional groups of both, hydrotrope and oil, play a major role on the occurrence of these mesoscopic structured liquids as well as on the size domain of formed aggregates. Most pronounced structuring was observed for systems, where the hydrotrope as well as the hydrophobic component bear an H-bond acceptor and donor functional group.

Structuring gets less pronounced (i) by successively changing the functional groups of the oil to groups, which have exclusively acceptor properties or to non-functionalized (aliphatic) groups. The size of mesoscale aggregates formed in the corresponding SFME decreases, accompanied by a restricted solubility of the hydrophobic component.

A similar trend was observed upon changing (ii) the functional group of the hydrotrope from donor/acceptor functional groups to groups that can solely act as H-bond acceptors. Analogously, size domains of the aliphatic-rich compartments decrease as well as the solubility of the oil in the corresponding SFME. For ternary mixtures, without any H-bond donor

functionalities of the hydrotrope/hydrophobic component, no mesoscale structuring was found. Although one may not exclude the existence of structured ternary systems with hydrotropes/hydrophobic components that exclusively bear H-bond acceptors, this study revealed that such systems are in principal not favoured for the formation of SFME.

Taking all these aspects into consideration, one may conclude that the presence of hydrotropes/hydrophobic components possessing H-bond donor/acceptor groups is beneficial for a well-organised and extended SFME resulting in an enhanced solubility of the hydrophobic component within such systems. Consequently, results presented in this study contribute to a deeper understanding of SFME formation and give a general basis to appropriately select hydrotropes and/or hydrophobic components for a targeted formulation of well-organised SFME.

3.7. References

1 M. L. Klossek, D. Touraud, T. Zemb and W. Kunz, *ChemPhysChem*, **2012**, *13*, 4116–4119.

2 V. Fischer, J. Marcus, D. Touraud, O. Diat and W. Kunz, *J. Colloid Interface Sci.*, **2015**, *453*, 186–193.

3 T. Zemb, M. L. Klossek, T. Lopian, J. Marcus, S. Schöttl, D. Horinek, S. Prevost, D. Touraud, O. Diat, S. Marčelja and W. Kunz, *Proc. Natl. Acad. Sci. U. S. A.*, **2016**, *113*, 4260–4265.

4 P. Ni and W.-G. Hou, *Chinese J. Chem.*, **2008**, *26*, 1985–1990.

5 J. Xu, A. Yin, J. Zhao, D. Li and W. Hou, *J. Phys. Chem. B*, **2013**, *117*, 450–456.

6 S. Prevost, M. Gradzielski and T. Zemb, *Adv. Colloid Interface Sci.*, **2017**, *247*, 374–396.

7 S. Prevost, T. Lopian, M. Pleines, O. Diat and T. Zemb, *J. Appl. Crystallogr.*, **2016**, *49*, 2063–2072.

8 T. Lopian, S. Schöttl, S. Prevost, S. Pellet-Rostaing, D. Horinek, W. Kunz and T. Zemb, *ACS Cent. Sci.*, **2016**, *2*, 467–475.

9 O. Diat, M. L. Klossek, D. Touraud, B. Deme, I. Grillo, W. Kunz and T. Zemb, *J. Appl. Crystallogr.*, **2013**, *46*, 1665–1669.

10 J. Marcus, D. Touraud, S. Prevost, O. Diat, T. Zemb and W. Kunz, *Phys. Chem. Chem. Phys.*, **2015**, *17*, 32528–32538.

11 S. Schöttl, J. Marcus, O. Diat, D. Touraud, W. Kunz, T. Zemb and D. Horinek, *Chem. Sci.*, **2014**, *5*, 2949–2954.

12 S. Schöttl and D. Horinek, *Curr. Opin. Colloid Interface Sci.*, **2016**, *22*, 8–13.

13 S. Schöttl, D. Touraud, W. Kunz, T. Zemb and D. Horinek, *Colloids Surfaces A Physicochem. Eng. Asp.*, **2015**, *480*, 222–227.

14 W. Hou and J. Xu, *Curr. Opin. Colloid Interface Sci.*, **2016**, *25*, 67–74.

15 P. Bošković, V. Sokol, T. Zemb, D. Touraud and W. Kunz, *J. Phys. Chem. B*, **2015**, *119*, 9933–9939.

16 M. L. Klossek, D. Touraud and W. Kunz, *Phys. Chem. Chem. Phys.*, **2013**, *15*, 10971–10977.

17 T. Buchecker, S. Krickl, R. Winkler, I. Grillo, P. Bauduin, D. Touraud, A. Pfitzner and W. Kunz, *Phys. Chem. Chem. Phys.*, **2017**, *19*, 1806–1816.

18 Y. L. Khmelnitsky, I. N. Zharinova, I. V. Berezin, A. V. Levashov and K. Martinek, *Ann. N. Y. Acad. Sci.*, **1987**, *501*, 161–164.

19 M. Zoumpanioti, H. Stamatis, V. Papadimitriou and A. Xenakis, *Colloids Surfaces B Biointerfaces*, **2006**, *47*, 1–9.

20 S. Krickl, D. Touraud, P. Bauduin, T. Zinn and W. Kunz, *J. Colloid Interface Sci.*, **2018**, *516*, 466–475.

21 L. O. Kononov, *RSC Adv.*, **2015**, *5*, 46718–46734.

22 S. Krickl, T. Buchecker, A. U. Meyer, I. Grillo, D. Touraud, P. Bauduin, B. König, A. Pfitzner and W. Kunz, *Phys. Chem. Chem. Phys.*, **2017**, *19*, 23773–23780.

23 B. Sun, J. Chai, Z. Chai, X. Zhang, X. Cui and J. Lu, *J. Colloid Interface Sci.*, **2018**, *526*, 9–17.

24 J. Xu, H. Deng, J. Song, J. Zhao, L. Zhang and W. Hou, *J. Colloid Interface Sci*., **2017**, *505*, 816–823.

25 Y. Zhao, J. Liu, Z. Chen, X. Zhu and M. Möller, *Nat. Commun*., **2018**, *9*, 1–9.

26 D. Brock, T. Lopian, A. Khoshsima, P. Bauduin, O. Diat, D. Touraud and W. Kunz, *Colloids Interface Sci. Commun*., **2016**, *14*, 1–3.

27 J. Marcus, M. L. Klossek, D. Touraud and W. Kunz, *Flavour Fragr. J*., **2013**, *28*, 294–299.

28 J. Marcus, M. Müller, J. Nistler, D. Touraud and W. Kunz, *Colloids Surfaces A Physicochem. Eng. Asp.*, **2014**, *458*, 3–9.

29 V. Tchakalova, T. Zemb and D. Benczedi, *Colloids Surfaces A Physicochem. Eng. Asp.*, **2014**, *460*, 414–421.

30 M. Clausse, L. Nicolas-Morgantini, A. Zradba and D. Touraud, in Surfactant Science Series (Vol. 24) Microemulsion Systems, eds. H. L. Rosano and M. Clausse, Dekker, New York, 1987, p. 15.

31 T. Nicolai, W. Brown and R. Johnsen, *Macromolecules*, **1989**, *22*, 2795–2801.

32 R. Pecora, *J. Nanoparticle Res.*, **2000**, *2*, 123–131.

33 R. F. Hankel, P. E. Rojas, M. Cano-Sarabia, S. Sala, J. Veciana, A. Braeuer and N. Ventosa, *Chem. Commun.*, **2014**, *50*, 8215–8218.

34 N. Grimaldi, P. E. Rojas, S. Stehle, A. Cordoba, R. Schweins, S. Sala, S. Luelsdorf, D. Piña, J. Veciana, J. Faraudo, A. Triolo, A. S. Braeuer and N. Ventosa, *ACS Nano*, **2017**, *11*, 10774–10784.

Chapter 4 Surfactant-free microemulsion electrokinetic chromatography (SF-MEEKC) with UV and MS detection – a novel approach for the separation and ESI-MS detection of neutral compounds

4.1. Abstract and preface

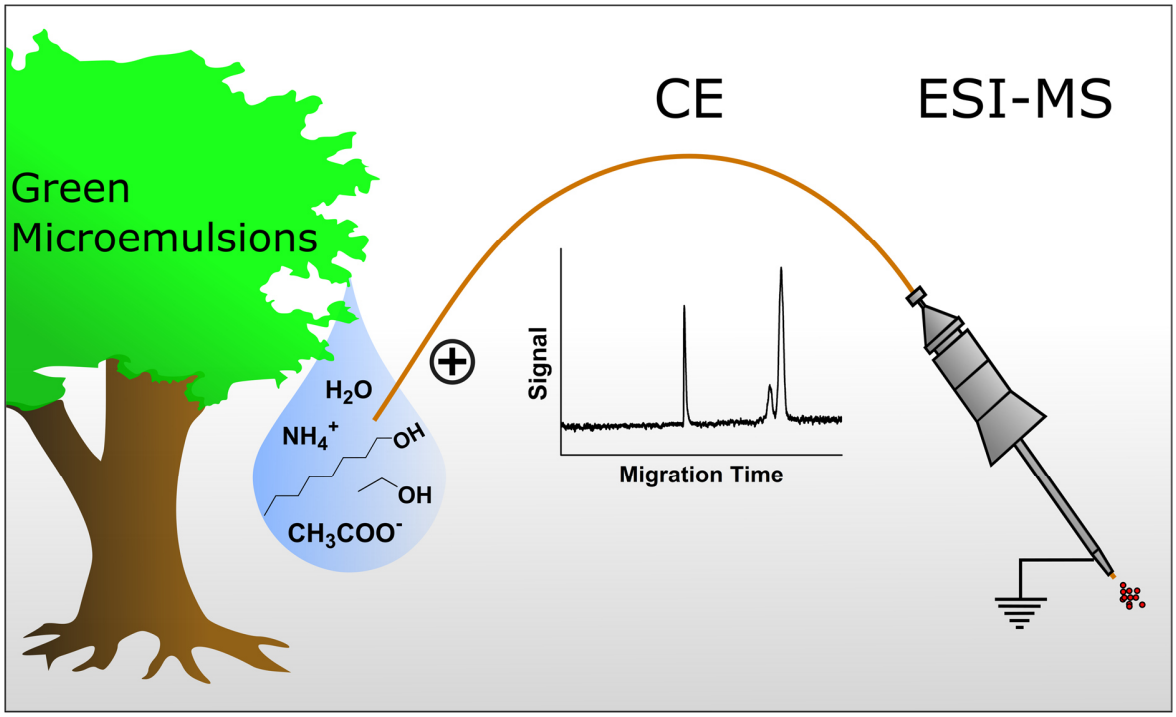

Figure 4.1: Graphical abstract schematically illustrating the principle of surfactant-free microemulsion electrokinetic chromatography (SF-MEEKC) using green, surfactant-free microemulsions.

Microemulsion electrokinetic chromatography (MEEKC) is a powerful tool to separate neutral species based on differences in their hydrophobic and hydrophilic properties. However, as a major drawback the conventionally used SDS-based microemulsions are not compatible with electrospray ionisation mass spectrometry (ESI-MS). In this work, a surfactant-free microemulsion (SFME) consisting of water, ethanol, and 1-octanol is used for surfactant-free microemulsion electrokinetic chromatography (SF-MEEKC, see Figure 4.1). Ammonium acetate was added to the SFME enabling electrophoretic separations. The stability of SFME containing ammonium acetate was investigated using small-angle X-ray scattering (SAXS)

and dynamic light scattering (DLS). A method for the separation of a model system of hydrophobic and hydrophilic neutral vitamins, namely the vitamins B_2 and D_3, and the cationic vitamin B_1 was developed using UV/VIS detection. The influence of the ammonium acetate concentration on the separation performance was studied in detail. The method was characterised concerning reproducibility of migration times and peak areas and concerning the linearity of the calibration data. Furthermore, SF-MEEKC was coupled to ESI-MS investigating the compatibility between SFME and the ESI process. The signal intensities of ESI-MS measurements of the model analytes were comparable for SFME and aqueous systems. Finally, the vitamin D_3 content of a drug treating vitamin D_3 deficiency was determined by SF-MEEKC coupled to ESI-MS using 25-hydroxycholecalciferol as an internal standard.

This chapter has been published in *Analytical and Bioanalytical Chemistry* (U. Mohorič, A. Beutner, S. Krickl, D. Touraud, W. Kunz and F.-M. Matysik, *Anal. Bioanal. Chem.*, **2016**, *408*, 8681–8689.)
The authors S. Krickl and A. Beutner contributed equally to this work.

Contributions to the experimental work:

- Dynamic light scattering: S. Krickl
- Small-angle X-ray scattering: T. Lopian and S. Krickl
- Electrokinetic chromatography with UV and MS detection: U. Mohorič and A. Beutner

4.2. Introduction

Capillary electrophoresis (CE) is a well-established analytical technique for the separation of charged analytes. There are special modes of CE that enable also the separation of neutral compounds using micellar solutions as background electrolytes (BGE). The corresponding technique is termed micellar electrokinetic chromatography (MEKC).[1] In addition, microemulsion electrokinetic chromatography (MEEKC) is another CE separation method that typically uses a BGE consisting of an oil-in-water microemulsion to separate charged and neutral analytes based on electrophoresis and partition chromatography. Charged analytes migrate according to their size and charge whereas neutral analytes can be separated based on their hydrophobic and hydrophilic properties due to different interactions with microemulsion oil droplets.[2,3] The thermodynamically stable and transparent microemulsions

are typically composed of oil, water, surfactant, and co-surfactant forming nanometre-sized stable oil droplets in aqueous buffer.[3] Sodium dodecyl sulphate (SDS) is the most commonly used surfactant in MEEKC leading to negatively charged oil droplets, where the concentration of SDS determines the charge-to-size ratio of the droplet. This ratio affects the electrophoretic mobility and the migration time of the analytes that interact with the charged microemulsion droplets.[3] Apart from SDS, a microemulsion based on sodium *bis*(2-ethylhexyl) sulfosuccinate was used for MEEKC to determine natural and synthetic estrogens simultaneously by Lucangioli and co-workers.[4] MEEKC has been applied, furthermore, to several model mixtures such as steroids,[5] preservatives in pharmaceutical products[6,7] and foods,[8] amino acid derivatives,[9] as well as neutral products.[10]

Furthermore, the comparison between micellar and microemulsion electrokinetic chromatography for the determination of water- and fat-soluble vitamins has been done by Terabe and Matsubara.[11] It was found that the separation efficiency is higher using MEEKC as the composition of the microemulsion droplets leads to a higher solubility of hydrophobic molecules compared to the micellar structures. MEEKC has also been used as a suitable tool for lipophilicity determination of acidic, neutral, and basic compounds.[12]

MEEKC is most commonly coupled to UV/VIS detectors.[13,14] As many organic compounds show UV absorbance, it is a useful technique for pharmaceutical applications. However, UV/VIS detection has a major drawback due to its relatively low sensitivity and selectivity[15] as a consequence of the short optical path length of the capillary detection window.[13,14] Coupling to alternative detection techniques has been described such as laser-induced fluorescence detection,[9] electrochemical detection,[16] and inductively coupled plasma mass spectrometry.[17]

MS detection has major advantages compared to conventional UV detection due to its high selectivity, low detection limits, and versatility.[18,19] However, MEEKC with typically used SDS-based microemulsions has major limitations when it comes to the hyphenation to electrospray ionisation mass spectrometry (ESI-MS), the most powerful detector in combination with separation techniques, due to the non-volatile properties of SDS.[19]

A new generation of surfactant-free microemulsions (SFME) has been recently studied by Klossek *et al*.[20] Although such SFME were already observed and introduced by Barden and co-workers in the 1970s,[21] it took a long time to characterise such systems and to understand the origin of their structuring. To get detailed insight into these structures, static and dynamic light scattering (DLS), as well as small-angle X-ray scattering (SAXS) and neutron scattering have been applied.[20,22,23]

SFME basically consist of three components. Component A (usually water), which is completely mixable with a component B (usually a hydrotrope, like ethanol), but poorly miscible with the hydrophobic component C (*e.g.*, 1-octanol), that in turn, is fully miscible with component B. In such systems, fine and remarkably time-stable emulsions can be formed in the two-phasic region, *e.g.*, by adding a sufficient amount of water to a mixture of ethanol and 1-octanol. This phenomenon is known as the Ouzo effect.[24] But what is more and of particular interest here, scattering experiments and molecular dynamics simulations revealed that in such systems well-defined aggregates on a nanometre scale can occur already in the monophasic region (near the phase separation border, but still far away from critical fluctuations).[22,25] This observation was called the "pre-Ouzo" effect.[20] Ternary mixtures in this pre-Ouzo region are thermodynamically stable, transparent, homogenous solutions, just as classical microemulsions. The aggregates inside are also similar to structures in conventional surfactant-based microemulsions and consist of a highly fluctuating oil-rich core in an outer aqueous pseudo-phase. The hydrotrope is distributed over both pseudo-phases, accumulating at the interface of the oil-rich domain. Furthermore, the thermodynamic stability of these aggregates could recently be explained and even predicted theoretically by an extended Derjaguin–Landau–Verwey–Overbeek (DLVO) theory.[26] Even bicontinuous or reverse aggregates can be formed, depending on the components and compositions. For these reasons, SFME provide a promising alternative to surfactant-based microemulsions for several applications.[27-29]

In this work, the use of this new generation of SFME containing water, ethanol, and 1-octanol for SF-MEEKC is described for the first time. Ammonium acetate was added as electrolyte. The stability of the BGE was investigated using SAXS and DLS. A method for the separation of a model system consisting of hydrophobic and hydrophilic neutral vitamins with SF-MEEKC coupled to UV/VIS detection was developed and optimised. Furthermore, compatibility between the SF-MEEKC and the ESI process was investigated. Finally, the method was applied to a real sample, namely the quantification of vitamin D_3 in a drug treating vitamin D_3 deficiency using an internal standard.

4.3. Experimental

4.3.1. Chemicals and materials

4.3.1.1. Chemicals

Ethanol was purchased from Sigma-Aldrich (Steinheim, Germany, ≥ 99.8%). Ammonium acetate (≥ 96.0%), 1-octanol (≥ 99.0%), sodium hydroxide solution, formic acid, and 2-propanol were purchased from Merck (Darmstadt, Germany). All chemicals were used without further purification. Water was purified using a Milli-Q System (Millipore, Bedford, MA, USA). The vitamins B_1, B_2, and D_3 were obtained from Sigma-Aldrich (MO, USA) as well as 25-hydroxycholecalciferol, which was used as an internal standard in SF-MEEKC-MS experiments. The vitamins were stored at 4 °C and kept in the dark to avoid decomposition.

4.3.1.2. Buffer and sample preparation

SFME were prepared by weighing water, ethanol, and 1-octanol in the following proportions: 37.5% water, 43.75% ethanol, and 18.75% 1-octanol (weight fraction). Ammonium acetate was used to prepare the BGE in different concentrations (mmol kg^{-1} of SFME). The order of addition was found to be irrelevant for the formation of the SFME, as it could be expected for a thermodynamically stable system. All solutions were filtered through 0.45 µm PTFE Rotilabo® syringe filters (Carl Roth, Karlsruhe, Germany). The amount of ammonium acetate was varied (50, 100, 150, 200, and 250 mmol kg^{-1}) to study its effect on the separation performance and is therefore specified further in the experiments.

Standard stock solutions of each vitamin were prepared daily by weighing certain amounts of each vitamin and dissolving them in the SFME. The final concentrations of standard stock solution for vitamin B_1 and vitamin D_3 were 10 and 0.085 mg mL^{-1} for vitamin B_2. Samples were prepared daily by diluting the stock solutions appropriately with BGE and filtering them through 0.45 µm syringe filters before use.

4.3.1.3. Capillary preparation

Fused silica capillaries were obtained from Polymicro Technologies (Phoenix, AZ, USA). The capillaries (outer diameter (OD) = 360 µm, inner diameter (ID) = 50 µm) were cut properly (total and effective lengths are specified further in the experiments) and the ends were polished with polishing paper (grid size 12 and 30 µm) to create a smooth surface. For CE-UV/VIS experiments a detection window (5-10 mm) was made by removing the polyimide coating with a microtorch. For CE-ESI-MS experiments, the polyimide coating was removed

from the MS side end of the capillary. Before use, the capillaries were flushed for 15 min with 0.1 M NaOH solution, 15 min with Milli-Q water, and 30 min with BGE. For CE-UV/VIS experiments, the capillary was additionally flushed with BGE for 5 min between the experiments to ensure reproducibility of migration times. After the experiments, the capillaries were flushed with water for storage. All solutions used for flushing were filtered through 0.45 µm filters before use.

4.3.2. Experiments

4.3.2.1. Dynamic light scattering

Dynamic light scattering (DLS) experiments were performed as described in Section 2.3.2.2.

4.3.2.2. Small-angle X-ray scattering

SAXS measurements were performed as described in Section 2.3.2.3. In order to determine the correlation length and the radii of the aggregates, an Ornstein–Zernike (OZ) formalism was used for data fitting in the low-*q*-range (0.275-4 nm^{-1}).

The OZ function (see Section 1.2.2) can be linked to the radius of gyration R_G of the aggregates by

$$I(q) = \frac{I_0}{1 + \xi^2 q^2} = \frac{I_0}{1 + \frac{R_G^2 q^2}{3}} \tag{2.1}$$

where ξ is the correlation length and I_0 the intensity for q = 0.[30,31] The scattering vector q is given by

$$q = \frac{4\pi}{\lambda} \sin\frac{\Theta}{2} \tag{2.2}$$

with Θ being the scattering angle. The average spherical radius R_S of the aggregates can be finally estimated as follows:

$$R_G^2 = \frac{3}{5} R_S^2 \tag{2.3}$$

Hence, the following correlation between correlation length and the spherical radius of the aggregates is valid:

$$R_S = \sqrt{5}\xi \approx 2.24 \cdot \xi \tag{2.4}$$

4.3.2.3. SF-MEEKC-UV/VIS

A laboratory built device consisting of a modified autosampler additionally equipped with a polished syringe needle electrode at the capillary inlet and a 30 kV high-voltage source (ISEG GmbH, Dresden, Germany) was used for all experiments. Control of the CE device was performed using a software developed by the Electronic workshop of the University of Regensburg.

For UV/VIS experiments, a second electrode made of a platinum wire was introduced to the system. A Bischoff Lambda 1010 UV/VIS system was used as detector. The wavelength of 272.0 nm was set for all experiments. Data acquisition was performed using a LabVIEW-based software written by a member of the working group. Injection was performed hydrodynamically by gravity flow. Ensuring equal injection conditions, the difference in height between inlet and outlet vial was kept constant at 10 cm for all experiments.

The performance of the SF-MEEKC-UV/VIS setup was investigated concerning selectivity, linearity, limit of detection (LOD), and reproducibility. If not stated differently, a sample containing 500 µg mL^{-1} of the vitamins B_1 and D_3 and 77 µg mL^{-1} of vitamin B_2 was used. First, the resolution of the neutral species was optimised varying the concentration of ammonium acetate in the BGE (50, 100, 150, 200, and 250 mmol kg^{-1}). The reproducibility (n = 9) of the migration times and the peak areas was further investigated using a BGE containing 150 mmol kg^{-1} ammonium acetate.

A set of five standard solutions was measured three times, respectively, examining the linearity of the calibration curve. The concentrations of the samples were between 100 and 1000 µg mL^{-1} for vitamin B_1 and between 250 and 1250 µg mL^{-1} for vitamin D_3. For vitamin B_2, four standard solutions with different concentrations ranging from 65 to 80 µg mL^{-1} were measured.

4.3.2.4. SF-MEEKC-ESI-MS

The ESI-MS system consisted of a Bruker micrOTOF (Bruker Daltonics, Bremen, Germany) time-of-flight mass spectrometer (TOF-MS), equipped with an orthogonal ESI source for coupling with capillary electrophoresis. In detail, a coaxial sheath liquid electrospray ionisation interface (Agilent,Waldbronn, Germany) was used. The Bruker software micrOTOF control version 2.3 was used for data acquisition. For optimal ESI conditions, positioning of the tip of the capillary inside the interface was controlled by a microscope camera. Sheath liquid (water/ 2-propanol/formic acid, 49.9/49.9/0.2, *v*/*v*/*v*) was introduced by a syringe pump (KD Scientific, Holliston, MA, USA) with a flow rate of 0.48 mL h^{-1}. Analysis was carried out in positive ion

mode. The electrospray voltage was -4 kV (grounded sprayer tip), and other parameters were set as follows: end plate offset, -500 V; dry gas (N_2) flow, 4.0 L/min; dry gas temperature, 190 °C; capillary exit, 75 V; skimmer 1, 25.3 V; hexapole 1, 23 V; hexapole RF, 65 Vpp; Skimmer 2, 23 V; lens 1 transfer, 49 µs; lens 1 prepulse storage, 5 µs; mass-to-charge (*m*/*z*) ratio, 22-550; spectra acquisition rate, 3 Hz. The mass traces of the analyte model mixture were selected as follows: vitamin B_1, m/z 265.15; vitamin B_2, *m*/*z* 377.19; vitamin D_3, *m*/*z* 385.39, and 25- hydroxycholecalciferol, *m*/*z* 401.40.

The SF-MEEKC system was coupled to ESI-TOF-MS validating the compatibility of SFME with ESI by comparing the LOD of vitamins B_1 and B_2 using SF-MEEKC to a conventional aqueous CE method using 0.1 M acetic acid as BGE. Finally, SF-MEEKC-ESI-TOF-MS was applied for the quantification of vitamin D_3 in a drug treating vitamin D_3 deficiency using 25-hydroxycholecalciferol as an internal standard (IS).

The commercial drug formulation (Vitamin D_3 Hevert 4000 IE, Hevert-Arzneimittel GmbH & Co. KG, Nussbaum) for treating vitamin D_3 deficiency was bought in a local pharmacy in Regensburg (Germany). Samples were stored in their original packets at room temperature until the analysis was carried out. Drug tablets were finely powdered and one tablet corresponding to 0.1 mg of vitamin D_3 was dissolved together with the internal standard in a total volume of 1 mL of the SFME. The solution was vortexed for 5 min, then centrifuged for 10 min at 3500 RPM × g. The supernatant was collected and filtered through a 0.45 µm syringe filter. 520 µL of supernatant was taken and filled up to the total volume of 1 mL for further analysis.

4.4. Results and discussion

4.4.1. Composition and structural investigations of the surfactant-free microemulsion

The SFME chosen for application in SF-MEEKC is composed of water, ethanol, and 1-octanol. Figure 4.2 shows the ternary phase diagram water/ethanol/1-octanol at room temperature, with *α* indicating the exact composition of the surfactant-free microemulsion in weight fractions used for SF-MEEKC. For sakes of clarity, the two-phasic region was redrawn from data given by Klossek *et al.*[20] The mixture of 37.5% water, 43.75% ethanol, and 18.75% 1-octanol (*w*/*w*/*w*) (solution *α*) was chosen, since recent publications revealed the presence of aggregates of well-characterised shape at this composition.[20,22,23,25]

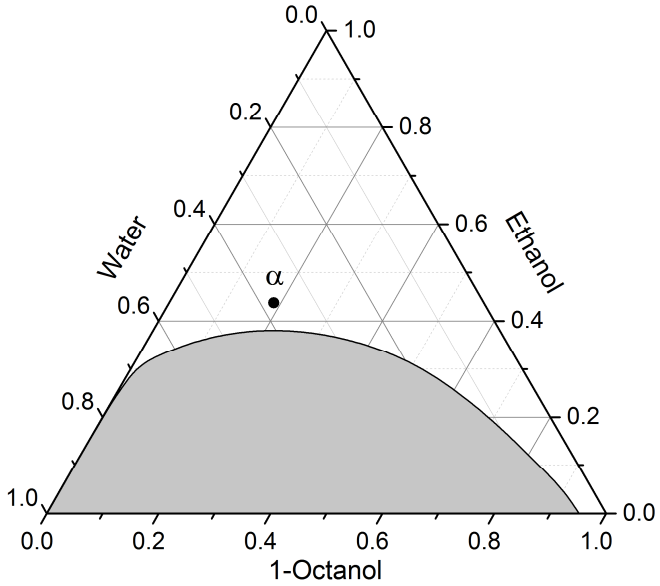

Figure 4.2: Ternary phase diagram in weight fractions of the system water/ ethanol/1-octanol at 25 °C. The two phasic region (shaded) was redrawn by data of Klossek *et al*.[20] The macroscopically homogeneous, one-phase region is given in white. The point *α* corresponds to the surfactant-free microemulsion used for SF-MEEKC consisting of 37.5% water, 43.75% ethanol, and 18.75% 1-octanol (*w*/*w*/*w*).

To be applicable in electrophoresis, ammonium acetate was added in order to establish a well-defined conductivity and in expectation of charging the interface between the two pseudo-phases by ion adsorption. In addition, ammonium acetate has the advantage to be compatible with ESI-MS detection. To exclude unwanted effects on the structuring within the SFME, the influence of the added salt on the structuring of the ternary mixture was investigated by DLS and SAXS measurements. The results of the light scattering experiments are shown in Figure 4.3. Correlation functions for 0-250 mmol kg^{-1} are not significantly altered. However, correlation functions start to break down at 500 mmol kg^{-1} of added salt. For 1000 and 1500 mmol kg^{-1}, there are already significant deviations compared to the correlation functions corresponding to samples with lower ammonium acetate concentrations. This means that structures, present in the initial ternary solution *α*, are maintained over a certain concentration range of ammonium acetate and progressively vanish after adding more than 500 mmol kg^{-1} of the salt. To make an independent check of the occurrence of pre-Ouzo aggregates and in order to further analyse the influence of the added salt, SAXS measurements were performed (see Figure A3.1, Appendix A.3).

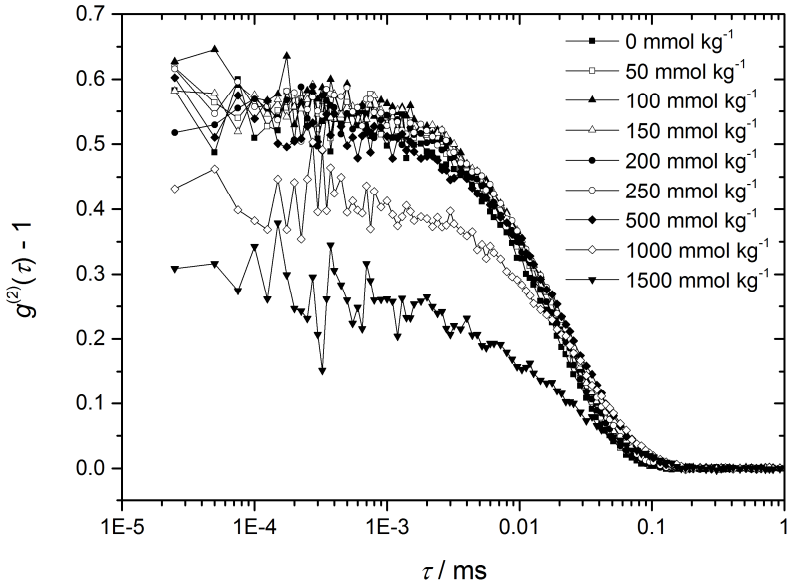

Figure 4.3: Time-dependent self-correlation functions obtained by DLS at 25 °C. The symbols correspond to the different molalities of added ammonium acetate in the SFME consisting of 37.5% water, 43.75% ethanol, and 18.75% 1-octanol (*w*/*w*/*w*).

SAXS measurements for 0, 50, 100, 150, 200, and 250 mmol kg^{-1} showed a significant low-*q* scattering accompanied by successively enhanced I_0 values for increasing amounts of ammonium acetate. Radii calculated with the OZ equation were in the range between 1.9 and 2.3 nm, increasing with increasing amount of ammonium acetate (see Table A3.1, Appendix A.3). Addition of the analytes as described in Section 4.3.1.2 did not show a notable influence on the radius and on the structuring of the SFME. Further, the scattering results lead to the assumption that the polarisable ions, ammonium, and/or acetate are accumulating at the interface between the two pseudo-phases. The order of separation of the analytes (see Section 4.4.2) leads to the conclusion that acetate has a higher affinity towards the interface between the water- and octanol-rich domains than the ammonium ions. Consequently, the hydrophobic octanol-rich aggregates can be assumed to be charged negatively overall, which allows successful application in SF-MEEKC. In addition, ammonium acetate may have salted out ethanol towards the interface or into the octanol-rich aggregates, which would also explain the increasing radii of these objects.[23]

4.4.2. SF-MEEKC-UV/VIS

4.4.2.1. Chemical properties of the model analytes

The structures of the analytes are depicted in Figure 4.4. The separation in SF-MEEKC is based on the electrophoretic and partitioning behaviour of the analytes. The migration order of neutral compounds is therefore determined by their hydrophobicity, indicating that compounds which are more soluble in the oil phase will migrate differently than the ones that partition more into the aqueous phase.[33,34]

4.4.2.2. Optimizing of SF-MEEKC-UV regarding electrolyte concentration

Figure 4.5 shows SF-MEEKC-UV separations of the model analytes using varying concentrations of ammonium acetate. Vitamin B_1 migrates first as it is positively charged. Neutral fat-soluble species are mostly partitioning into the oil droplets, whereas the neutral hydrophilic species reside mainly in the aqueous phase.[33] The neutral and water-soluble vitamin B_2 migrates before the neutral, fat-soluble vitamin D_3. This indicates that the oil droplets are negatively charged and thus the migration time of the fat-soluble vitamin D_3 is retained. The IS 25-hydroxycholecalciferol is co-migrating with vitamin D_3 as it has the same molecular structure apart from an additional hydroxyl group.

The concentration of ammonium acetate in SFME was varied between 50 and 250 mmol kg^{-1}. The conditioning of the capillary after changing the BGE was done by flushing 5 min with 0.1 M NaOH, 5 min with water, and 30 min with the new BGE. Some changes in the absolute migration times can occur depending on details of the conditioning protocol. However, the separation performance and the precision of repetitive measurements with the same BGE were quite good as specified later in this section.

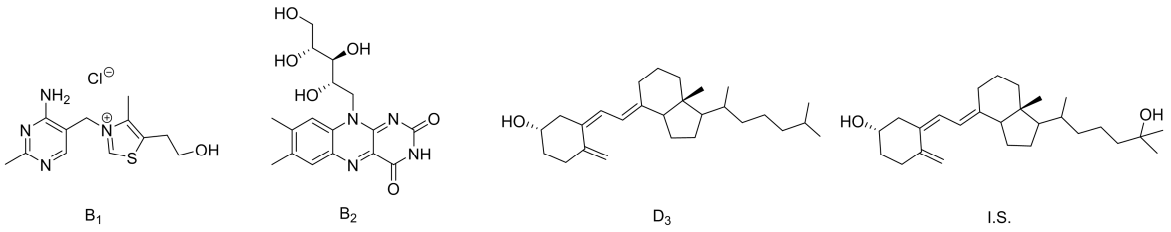

Figure 4.4: Molecular structures of the model mixture and the internal standard: thiamine hydrochloride (vitamin B_1, pK_{a1} = 4.8, pK_{a2} = 9.2),[32] riboflavin (vitamin B_2, pK_{a1} = 1.9, pK_{a2}= 10.2),[32] cholecalciferol (vitamin D_3), and 25-hydroxycholecalciferol (IS).

When the microemulsion containing 50 mmol kg^{-1} ammonium acetate was used as BGE in SF-MEEKC, the signals of the vitamins B_2 and D_3 were not completely separated. The resolution of the signals for the two neutral species improved with higher concentrations of ammonium acetate added to the mixture. Baseline separation of signals of vitamins B_2 and D_3 was first achieved using 150 mmol kg^{-1} ammonium acetate. The resolution of signals of vitamins B_2 and D_3 was in fact best when SFME with a content of 200 mmol and 250 mmol kg^{-1} ammonium acetate were used as BGE. However, due to higher concentrations of ammonium acetate in SFME, rather high electrophoretic currents (≥ 90 µA) were generated, when applying high voltages (larger than 20.5 kV) leading to a breakdown of electrophoretic current during separation. Therefore, a maximal separation voltage of 19 kV was applicable. However, when applying lower separation voltages, much longer migration times of analytes were observed. Therefore, a compromise between resolution and migration time was made and the SFME containing 150 mmol kg^{-1} and applying a separation voltage of 22.5 kV was chosen as the best compromise for separation of the vitamins B_1, B_2, and D_3.

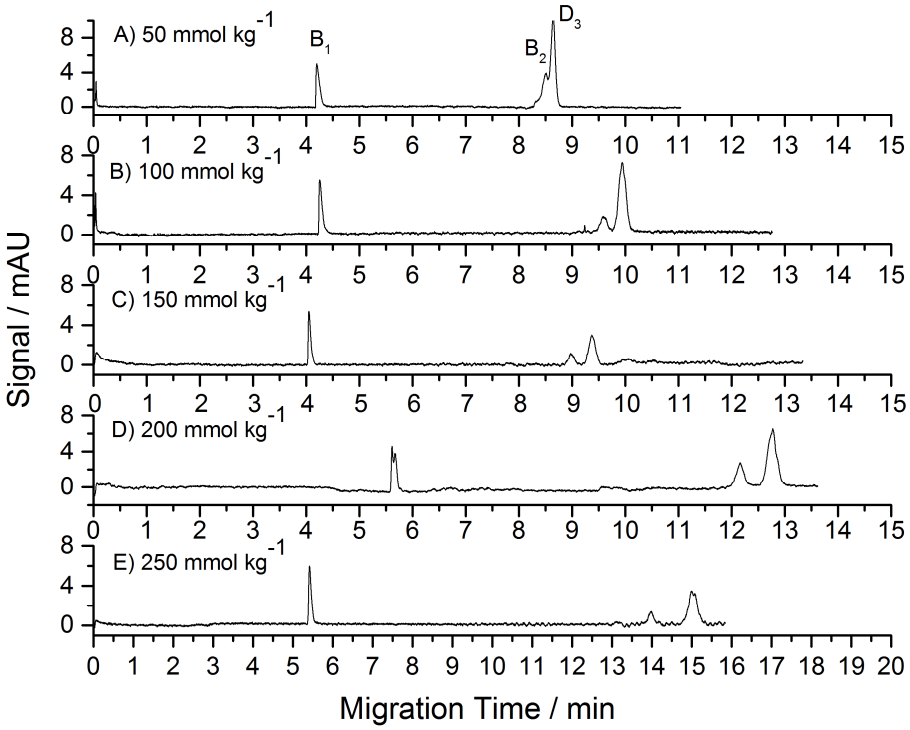

Figure 4.5: SF-MEEKC-UV separation of vitamin B_1 (0.50 mg mL^{-1}), B_2 (0.077 mg mL^{-1}), and D_3 (0.50 mg mL^{-1}) using the following concentrations of ammonium acetate in SFME.
A) 50 mmol kg^{-1}, separation voltage 22.5 kV. B) 100 mmol kg^{-1}, separation voltage 22.5 kV. C) 150 mmol kg^{-1}, separation voltage 22.5 kV. D) 200 mmol kg^{-1}, separation voltage 20.5 kV. E) 250 mmol kg^{-1}, separation voltage 20.5 kV. Capillary: total length 31 cm × 50 µm I.D. (effective length 21 cm). Hydrodynamic injection with a height difference of 10 cm for 30 s. UV detection was set at 272 nm.

Using this protocol, the reproducibility of the migration times and of the peak areas of the different vitamins was characterised by relative standard deviations ranging between 2.3 and 3.5% and between 8.6 and 12%, respectively (conditions as in Figure 4.5c, n = 9). Further analytical characteristics are specified in Table 4.1. Analytical characteristics in the concentration range from 100 to 1000 µg mL^{-1} for vitamin B_1, from 65 to 80 µg mL^{-1} for vitamin B_2, and from 25 to 1250 µg mL^{-1} for vitamin D_3, with triplicate injection at each concentration level were determined by SF-MEEKC-UV. The relatively small range of concentrations of vitamin B_2 was due to its low solubility. The linearity was evaluated by plotting peak areas versus concentrations of analytes. The corresponding calibration parameters of the three analytes are summarised in Table 4.1. Due to its low solubility, quantification of B_2 is limited.

Table 4.1: Analytical characteristics for SF-MEEKC determinations of the vitamins B_1, B_2, and D_3 with UV (MS) detection.

Vitamin	Concentration range for calibration[a] (UV) / µg mL^{-1}	R^2[b]	LOD (UV) / µg mL^{-1}	LOD (MS) / µg mL^{-1}
B_1	100-1000	0.9998	7.5	0.5
B_2	65-80	0.9755	51.0	7.5
D_3	250-1250	0.9881	12.5	2.9

[a]Three data points with three replicate injections at each concentration level (N = 3). [b]The LOD corresponds to a signal-to-noise ratio of three.

4.4.3. SF-MEEKC-ESI-TOF-MS

4.4.3.1. Investigation of the ESI compatibility of the SFME

Ensuring compatibility of the SFME with ESI, the LODs of the vitamins were compared using SF-MEEKC and a conventional aqueous CE method with 0.1 M acetic acid as BGE. The LODs of the SF-MEEKC-ESI-TOF-MS were determined to be 0.53 µg mL^{-1} for vitamin B_1, 7.54 µg mL^{-1} for vitamin B_2, and 2.89 µg mL^{-1} for vitamin D_3 (Table 4.1). The LODs of vitamins B_1 and B_2 for aqueous CE were determined to be 0.63 and 12.5 µg mL^{-1}, respectively. Vitamin D_3 is not soluble in water and thus the LOD could not be determined with conventional aqueous CE. Comparing the LODs of CE and SF-MEEKC, it can be stated that the SFME are compatible with ESI as the LODs are in the same range. An exact comparison is limited as the injection conditions are different for both methods due to different viscosities of the media.

4.4.3.2. Application of the proposed SF-MEEKC-ESI-TOF-MS method

The potential of the developed method is demonstrated by quantifying vitamin D_3 in a commercial drug formulation. The content of vitamin D_3 in the commercial sample formulation was declared to be 100 µg. The UV/VIS detector was not suitable for the quantification of vitamin D_3 due to problems with matrix effects and limited selectivity compared to MS. In real sample analysis, the noise level of SFMEEKC- ESI-TOF-MS measurements was also higher than in case of standard solutions. Due to the more complex sample preparation protocol and to improve the precision of results, SF-MEEKC-ESI-TOF-MS measurements were performed using 25-hydroxycholecalciferol as an internal standard. Five different concentration levels (from 120 to 200 µM for 25-hydroxycholecalciferol and from 90 to 150 µM for vitamin D_3) with triplicate injections were investigated. Different concentrations of standard solutions of vitamin D_3 and IS were chosen to obtain similar MS intensities for both species and to investigate the response factor in this concentration range. Figure 4.6 shows exemplarily results for real sample analysis by SF-MEEKC-ESI-TOF-MS.

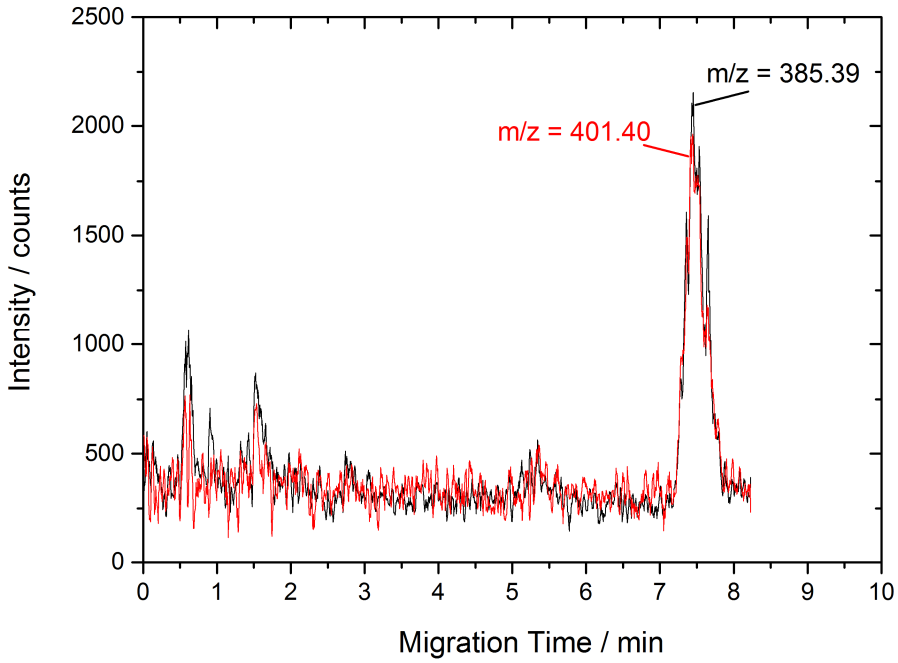

Figure 4.6: Extracted ion electropherogram for SF-MEEKC-ESI-TOF-MS determination of the vitamin D_3 in a commercial sample (*m*/*z* = 385.39, black line) using 25-hydroxycholecalciferol (*m*/*z* = 401.40, red line) as an internal standard. Microemulsion composition: 37.5% of water, 43.75% of ethanol, 18.75% of 1-octanol (*w*/*w*/*w*), and 150 mmol kg^{-1} ammonium acetate. Capillary: total length 30 cm × 50 µm I.D. (effective length 21.5 cm); applied voltage 16 kV, hydrodynamic injection for 10 s.

The migration times of vitamin D_3 and 25-hydroxycholecalciferol are equal indicating that the latter one is well suited as an IS. The response ratio (D_3/IS) was found to be independent of the concentration of vitamin D_3 and of IS in the studied range. The results of real sample analysis are summarised in Table 4.2. The contents of vitamin D_3 determined in the individual drug samples ranged between 95 and 113 µg, which is in good agreement to the declared mass of 100 µg.

Table 4.2. Determination of vitamin D_3 in a commercial drug formulation (vitamin D_3, 400 IE) by SF-MEEKC-ESI-TOF-MS using 25-hydroxycholecalciferol as internal standard.

Sample no.	Declared amount of D_3 / µg	Found content of D_3 / µg	RSD (n = 3) / %
1	100	95	4
2	100	105	5
3	100	113	10.5

4.5. Conclusion

For the first time, we demonstrated the use of SFME for electrokinetic chromatography. In the so-called pre-Ouzo region, aggregate formation in the water/ethanol/1-octanol microemulsion is occurring spontaneously with no additional surfactant present in the mixture. DLS and SAXS measurements proved that the addition of ammonium acetate in the chosen concentration range was not altering aggregate formation in the SFME. SF-MEEKC allowed the separation of neutral species in the studied model mixture of vitamins. The compatibility of SF-MEEKC with ESI-MS could be demonstrated. Comparable sensitivity as in aqueous CE-ESI-MS was found. Finally, the practical applicability of SF-MEEKC-ESI-MS was demonstrated determining the content of vitamin D_3 in a commercial drug.

4.6. References

1 S. Terabe, K. Otsuka, K. Ichikawa, A. Tsuchiya and T. Ando, *Anal. Chem.*, **1984**, *56*, 111–113.

2 K. D. Altria, P. E. Mahuzier and B. J. Clark, *Electrophoresis*, **2003**, *24*, 315–324.

3 U. Pyell, ed. Electrokinetic chromatography: theory, instrumentation and applications. John Wiley & Sons; 2006.

4 V. Tripodi, S. Flor, A. Carlucci and S. Lucangioli, *Electrophoresis*, **2006**, *27*, 4431–4438.

5 L. Vomastova, I. Mikšik and Z. Deyl, *J. Chromatogr. B Biomed. Sci. Appl.*, **1996**, *681*,107–113.

6 P. E. Mahuzier, K. D. Altria and B. J. Clark, *J. Chromatogr. A*, **2001**, *924*, 465–470.

7 H. Y. Huang, Y. C. Lai, C. W. Chiu and J. M. Yeh, *J. Chromatogr. A*, **2003**, *993*,153–164.

8 H. Hsi-Ya, C. Chia-Ling, C. Chen-Wen and Y. Jui-Ming, *Food Chem.*, **2005**, *89*, 315–322.

9 J. Xie, J. Zhang, H. Liu, J. Liu, J. Tian, X. Chen and Z. Hu, *Biomed. Chromatogr.*, **2004**, *18*, 600–607.

10 T. Javor, W. Buchberger and I. Tanzcos, *Microchim. Acta.*, **2000**, *135*, 45–53.

11 S. Terabe, N. Matsubara, Y. Ishihama and Y. Okada, *J. Chromatogr. A*, **1992**, *608*, 23–29.

12 X. Subirats, H. P. Yuan, V. Chaves, N. Marzal and M. Roses, *Electrophoresis*, **2016**, *37*, 2010–2016.

13 A. J. Zemann, *Trends Anal. Chem.*, **2001**, *20*, 346–354.

14 L. A. Gennaro, O. Salas-Solano and S. Ma, *Anal. Biochem.*, **2006**, *355*, 249–258.

15 J. A. Olivares, N. T. Nguyen, C. R. Yonker and R. D. Smith, *Anal. Chem.*, **1987**, *59*, 1230–1232.

16 L. S. Yu, X. Q. Xu, L. Huang, J. M. Ling and G. N. Chen, *Electrophoresis*, **2008**, *29*, 726–733.

17 A. K. Bytzek, M. R. Reithofer, M. Galanski, M. Groessl, B. K. Keppler and C. G. Hartinger, *Electrophoresis*, **2010**, *31*, 1144–1150.

18 E. Hoffmann, and V. Stroobant, Mass spectrometry. Principles and applications. John Wiley & Sons; 2007.

19 F.-M. Matysik, C. Neusüss and M. Pelzing, *Analyst.*, **2008**, *133*, 1764–1766.

20 M. L. Klossek, D. Touraud, T. Zemb and W. Kunz, *ChemPhysChem*, **2012**, *13*, 4116–4119.

21 G. D. Smith, C. E. Donelan and R. E. Barden, *J. Colloid Interface Sci*., **1977**, *60*, 488–496.

22 O. Diat, M. L. Klossek, D. Touraud, B. Deme, I. Grillo, W. Kunz and T. Zemb, *J. Appl. Crystallogr.*, **2013**, *46*, 1665–1669..

23 J. Marcus, D. Touraud, S. Prevost, O. Diat, T. Zemb and W. Kunz, *Phys. Chem. Chem. Phys.*, **2015**, *17*, 32528–32538.

24 S. A. Vitale and J. L. Katz, *Langmuir*, **2003**, *19*, 4105–4110.

25. S. Schöttl, J. Marcus, O. Diat, D. Touraud, W. Kunz, T. Zemb and D. Horinek, *Chem. Sci.*, **2014**, *5*, 2949–2954.

26 T. Zemb, M. L. Klossek, T. Lopian, J. Marcus, S. Schöttl, D. Horinek, S. Prevost, D. Touraud, O. Diat, S. Marčelja and W. Kunz, *Proc. Natl. Acad. Sci. U. S. A*., **2016**, *113*, 4260–4265.

27 V. Fischer, J. Marcus, D. Touraud, O. Diat and W. Kunz, *J. Colloid Interface Sci.*, **2015**, *453*, 186–193.

28 R.F. Hankel, P. E. Rojas, M. Cano-Sarabia, S. Sala, J. Veciana, A. Braeuer and N. Ventosa, *Chem. Commun.*, **2014**, *50*, 8215–8218.

29 M. Zoumpanioti, M. Karali, A. Xenakis and H. Stamatis, *Enzym. Microb. Technol.*, **2006**, *39*, 531–539.

30 K. L. Gawrys, G. A. Blankenship and P. K. Kilpatrick, *Langmuir*, **2006**, *22*, 4487–4497.

31. T. Lopian, S. Schöttl, S. Prevost, S. Pellet-Rostaing, D. Horinek, W. Kunz and T. Zemb, *ACS Cent. Sci*., **2016**, *2*, 467–475.

32. K. Callmer and L. Davies, *Chromatographia*, **1974**, *7*, 644–50.

33. R. L. Boso, M. S. Bellini, I. Miksik, Z. Deyl, *J. Chromatogr. A*, **1995**, *709*, 11–9.

34. K. D. Altria, *J. Chromatogr. A*, **2000**, *892*, 171–86.

Chapter 5 Surfactant-free microemulsions with cleavable constituents

5.1. Abstract and preface

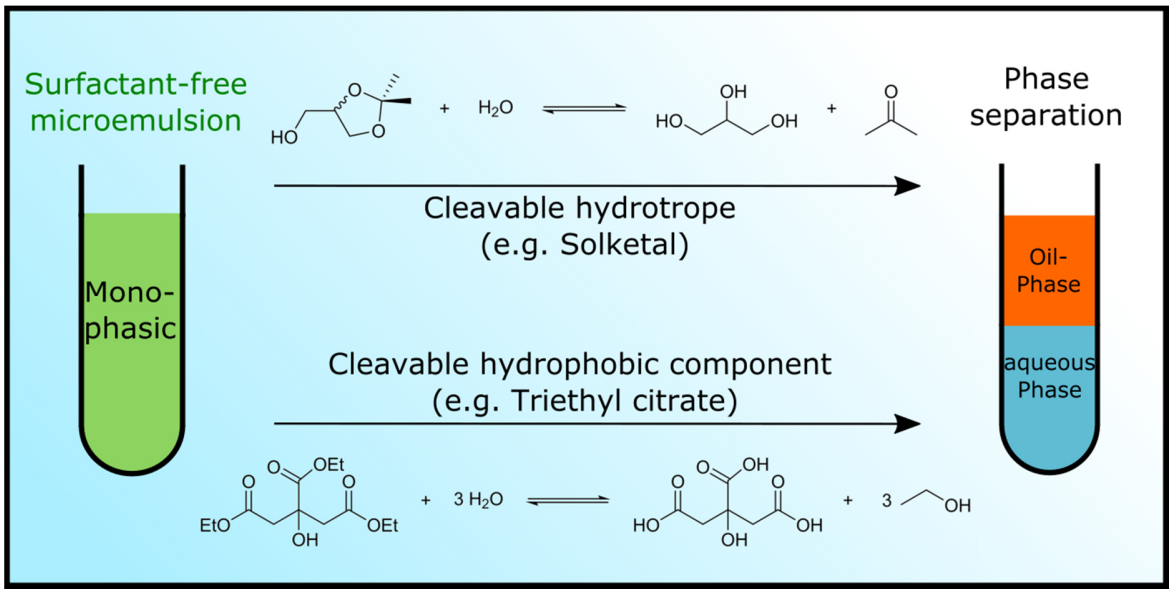

Figure 5.1: Graphical abstract schematically illustrating phase separation of SFME using cleavable hydrotropes/hydrophobic components.

Surfactant-free microemulsions (SFME) comprising a cleavable hydrotrope/hydrophobic component were investigated regarding potential applications for green, microemulsion-mediated extraction processes (see Figure 5.1). To this purpose, dynamic light scattering (DLS) experiments were performed for ternary systems consisting of water/(2,2-dimethyl-1,3-dioxolan-4-yl)methanol (Solketal)/oleic acid and water/ethanol/triethyl citrate (TEC) in order to detect mesoscopic structured compositions. Further, kinetic measurements were performed for the acid-catalysed hydrolysis of Solketal (cleavable hydrotrope) and base-catalysed hydrolysis of TEC (cleavable hydrophobic component) at different temperatures/different pH of the aqueous pseudo-phase. As proof of concept, *α*-tocopherol and vanillic acid were dissolved in the ternary mixtures as extractable surrogates in order to simulate an extraction and separation process. It was found that well-structured SFME can be obtained for both systems, which basically allows microemulsion-mediated extraction. Moderate changes of temperature and/or pH, leads to rapid hydrolysis of Solketal and TEC within a few hours. Finally, it could be shown that upon hydrolysis of Solketal/TEC, separation of the used

surrogate solutes from the hydrolysed products is facilitated and quantitative separation could be achieved.

This chapter has been published in *Journal of Molecular Liquids* (S. Krickl, L. Jurko, K. Wolos, D. Touraud and W. Kunz, *J. Mol. Liq*., **2018**, *271*, 112–117.).

Contributions to the experimental work:

- Dynamic light scattering: S. Krickl and L. Jurko
- Ternary phase diagrams: S. Krickl and L. Jurko
- Kinetic measurements: S. Krickl, K. Wolos and L. Jurko
- Proof of concept: S. Krickl, K. Wolos

5.2. Introduction

Surfactant-mediated extraction is a versatile tool for the extraction of natural compounds and metal ions for analytical and industrial processes.[1–3] In this technique, profit is often taken of the formation of supramolecularly structured solutions (*e.g.* micelles or microemulsions) to extract and dissolve organic/ionic compounds.[4] First, the formation of a micellar solution/microemulsion takes place (direct/reverse), leading to a compartmentation of hydrophilic and hydrophobic pseudo-phases. Upon extraction, the desired products can be dissolved in the corresponding pseudo-phase, depending on the nature of the extracted compounds. Surfactant-mediated extraction comprises plenty of advantages compared to conventional solvent extraction: low amounts of surfactants are needed, compared to the amount of organic solvents used in conventional solvent extraction, the solvent properties can be tuned using different surfactants and the resulting mixtures are usually non-volatile and non-flammable.[3,4] Yet, subsequent to the extraction process, the extracted compounds have to be separated from the surfactant solution, which can be a very delicate issue. Several techniques are known to do so (*e.g.* the use of thermo-, salt-, pH-sensitive or photo-switchable surfactants).[4,5]

Aside of solely changing the environmental conditions of the surfactant, also the use of chemical processing methods are used comprising *e.g.* the use of cleavable surfactants.[6–15] Such molecules are amphiphiles with a weak linkage commonly, but not always, between the hydrophobic tail and the polar headgroup.[11] Prerequisite for their application is that the surfactant is stable under given conditions for the intended process. Afterwards, the surfactant

properties get destroyed upon controlled cleavage of the surfactant at the designated labile bonds inducing phase separation. The mechanism by which cleavage occurs can be of different origin, including for instance acid/alkaline hydrolysis[15], UV/visible light irradiation[10,13], heat decomposition[9], oxidation[10] or enzyme-catalysed degradation[11]. Using such methods can be desirable, especially regarding environmental aspects, since the cleavable surfactant itself, as well as the resulting surfactant fragments, are often better biodegradable.[8]

In this context, also surfactant-free emulsions and microemulsions (SFE/SFME) gain more and more attention for several applications, *e.g.* for extraction, solubilisation, separation techniques as well as for chemical processing.[16–23] Such systems usually contain a hydrotrope taking the role of the surfactant. Depending on the composition (water/hydrotrope/oil) SFME can be obtained with different types of mesoscale structuring (direct, bicontinuous, inverse).[24-30] By doing so, processes can be often improved, since hydrotropes are generally better biodegradable and often less foaming than conventional surfactants.

For these reasons, we present a study in which both concepts are unified, using cleavable SFME for greener extraction processes. This approach combines the use of SFME containing predominantly biodegradable, low-toxic hydrotropes or oil components for micelle-like/microemulsion-mediated extractions. By doing so, (i) the advantages of microemulsion-mediated extraction techniques can be exploited and in a second step (ii) the ingredients of the extraction medium (SFME) are decomposed, leading to even better biodegradable, less toxic (preferably food-approved) decomposition products. Due to the cleavage of either the hydrotrope and or the oil, extraction products can be obtained in relatively high degree of purity or solubilised within a pure oil phase (remaining from the initial SFME).

Thus, in the present study we investigated (2,2-dimethyl-1,3-dioxolan-4-yl)methanol (Solketal) as a cleavable hydrotrope and triethyl citrate (TEC) as representative for a cleavable oil phase (see Figure 5.2). Dynamic light scattering (DLS) was performed in order to find compositions with microemulsion-like properties in ternary systems composed of water/Solketal/oleic acid and water/ethanol/TEC. Furthermore, kinetics of the acid-catalysed hydrolysis of Solketal and base-catalysed hydrolysis of TEC were measured at different temperatures and/or different pH of the aqueous pseudo-phase. As a consequence of the formed hydrophilic decomposition products (glycerol, acetone and citrate, ethanol), it can be expected that separation of hydrophobic solutes from the SFME residues is significantly facilitated due to different solubilities of solute and residue in water. Thus, as a proof of concept, hydrolysis of the hydrotrope/oil phase was performed in the presence of hydrophobic components *α*-tocopherol

(Toc) and vanillic acid (VA) used as surrogates to investigate separation procedures of solute and SFME residue after a hypothetic extraction process (see Figure 5.2).

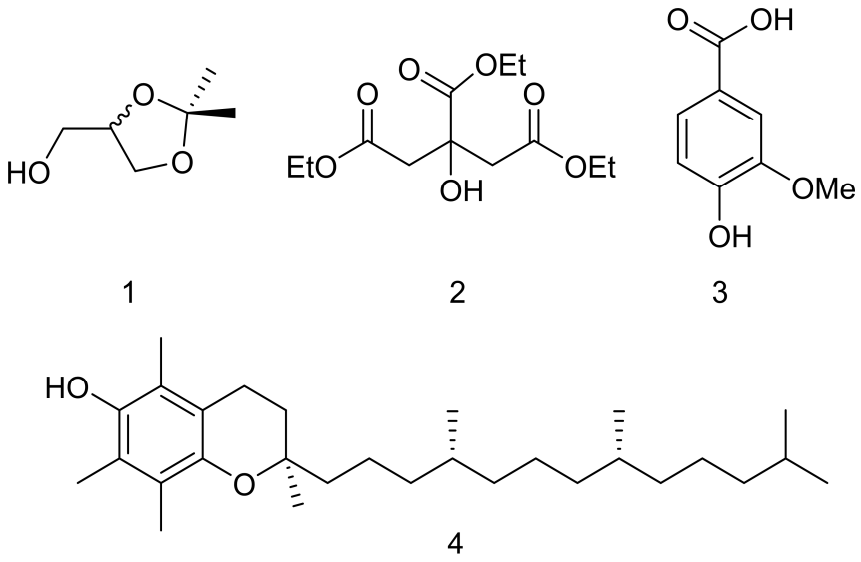

Figure 5.2: Chemical structures of Solketal (1), TEC (2), VA (3) and Toc (4).

5.3. Experimental

5.3.1. Chemicals

Ethanol (EtOH, purity ≥ 99.8%), triethyl citrate (TEC, ≥ 98%), glycerol triacetate (Triacetin, ≥ 99%), oleic acid (≥ 90%), acetone (≥ 99.5%), vanillic acid (VA, ≥ 97%), *α*-tocopherol (Toc, ≥ 96%) and 1-pentanol (≥ 99%) were purchased from Sigma-Aldrich (Steinheim, Germany). Sodium hydroxide (pellets, ≥ 98.5%), hydrochloric acid (aq, 37%) were obtained from VWR Chemicals (Fontenay-sous-Bois, France) and (2,2-dimethyl-1,3-dioxolan-4-yl)methanol) (Solketal) from Syntharo Fine Chemicals (Troisdorf, Germany). Methanol (≥ 99.9%) in gradient grade for liquid chromatography was purchased from Merck (Darmstadt, Germany). Deuterium oxide (99.9 atom% deuterated) and dimethyl sulfoxide-d6 (DMSO, 99.5 atom% deuterated) were purchased from Deutero GmbH (Kastellaun, Germany).
All chemicals were used without further purification. Aqueous solutions were prepared using deionised water with a resistivity of 18 MΩ cm.

5.3.2. Methods and techniques

5.3.2.1. Ternary phase diagrams

Phase diagrams were recorded at 25 °C using a dynamic and static process according to Clausse *et al*. (see Section 2.3.2.1).[31]

5.3.2.2. Dynamic light scattering

Dynamic light scattering (DLS) experiments were performed as described in Section 2.3.2.2.

5.3.2.3. Kinetic measurements of the hydrolysis reactions

Kinetic measurements of the hydrolysis of Solketal and TEC were performed for binary mixtures of water/Solketal, pure TEC and ternary mixtures of water/ethanol/TEC. Hydrolysis of Solketal was carried out at different temperatures (40 and 60 °C) and pH of the added water (pH = 2 and 3) under reduced pressure (300 mbar). Adjustment of the pH was performed using hydrochloric acid and pH was measured using a commercial glass electrode (VWR, pH 1000L). Hydrolysis of TEC was performed under alkaline conditions at different temperatures (25 and 40 °C). To this purpose, 5 M NaOH solution was added to the ternary mixture/pure TEC with n(NaOH)/n(TEC) = 3:1. Conversion of Solketal and TEC was determined using ^{1}H-NMR spectroscopy (Bruker Avance 300 MHz NMR spectrometer) in DMSO (Solketal mixtures) and D_2O (TEC mixtures), respectively.

5.3.2.4. Proof of concept: solubilisation and separation of surrogate solutes

Toc was solubilised in oleic acid (*w*(Toc) =10 wt%). The resulting mixture was used to prepare a SFME consisting of 27.5 wt% water, 62.5 wt% Solketal and 10 wt% of oleic acid/Toc mixture. Hydrolysis of Solketal was performed at 60 °C and 300 mbar. After phase separation and complete conversion, samples were taken from both, the upper oil-phase and the lower aqueous phase. Subsequently, the Toc content of both phases was measured using high-performance liquid chromatography (HPLC). HPLC measurements were performed using a Waters 717plus autosampler, a Waters 2487 Dual λ UV/Vis detector and a C18 reverse phase HPLC column. The UV/Vis detector was set to a detection wavelength of 295 nm. All measurements were conducted at a temperature of 25 °C. Samples were measured for 14 min. HPLC-samples were prepared by dissolving 200 mg of each sample in 3 g of 1-pentanol. Methanol was degassed for 10 min in an ultrasonic bath at the beginning of each measurement and used as the mobile phase.

For SFME composed of water, ethanol and TEC, VA was used as surrogate solute. To this purpose, 4.75 wt% of VA was dissolved in a mixture of 55 wt% water, 25 wt% ethanol and 20 wt% TEC. 5 M NaOH solution was added to the mixture with n(NaOH)/n(TEC) = 3:1. The resulting mixture was stirred for 3 h at 25 °C. Subsequently, water and ethanol was removed at 40 °C and 30 mbar and the remaining solid was dried at 60 °C. The residue was neutralised with conc. HCl and preferably low amounts of 2 M HCl were added to obtain a fine suspension. In order to separate the non-soluble VA from the readily soluble hydrolysed ester residue, the resulting suspension was filtered using a glass frit and the filter cake was dried at 60 °C. Afterwards, the filtered VA and the washing solution were measured via ^{1}H-NMR spectroscopy (Bruker Avance 300 MHz NMR spectrometer).

5.4. Results and discussion

5.4.1. Structural investigation of the used SFME

Ternary phase diagrams of water/Solketal/oleic acid and water/ethanol/TEC are shown in Figure 5.3. Regarding ternary mixtures of water/Solketal/oleic acid, a large two-phasic region can be seen, particularly at the water-rich side. Above 60 wt% of Solketal, the miscibility gap is closed and solely monophasic mixtures are obtained.

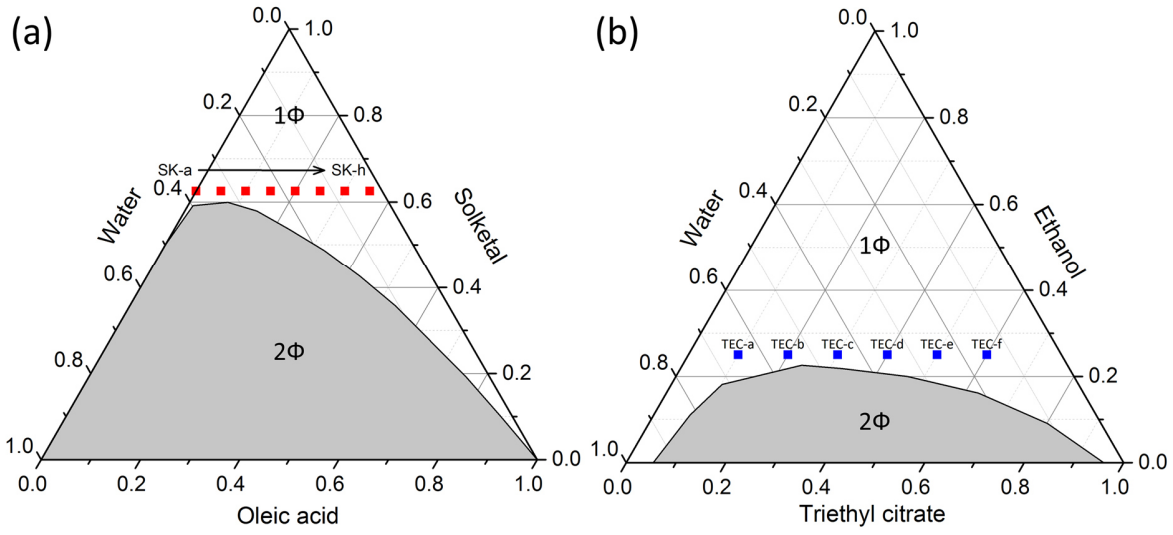

Figure 5.3: Ternary phase diagrams for the systems (a) water/Solketal/oleic acid and (b) water/ethanol/TEC at 25 °C, provided in weight fractions. The mono- and two-phasic areas are represented as white and grey areas, respectively. Symbols denote the different compositions measured with DLS.

For ternary mixtures consisting of water/ethanol/TEC, the two-phase region was found to be smaller, with a more symmetric shape. A slight solubility of water in TEC (4 wt%) and TEC in water (5 wt%) was found and miscibility gap closes above 23 wt% of ethanol. In addition, samples SK-a to SK-h and TEC-a to TEC-f (see Figure 5.3) were investigated using DLS in order to detect mesoscopically structured compositions of the ternary mixtures. Samples were chosen with a constant weight fraction of hydrotrope (Solketal/ethanol), 2.5 wt% above the miscibility gap.

Results obtained by DLS are shown in Figure 5.4. For mixtures containing Solketal, the binary mixture of water/Solketal (sample SK-a) show an ill-defined correlation function decreasing very rapidly (decay time τ < 0.01 ms). Adding oleic acid leads to a tremendous increase of the autocorrelation function with a significant shift to larger decay times (sample SK-b, decay time τ up to 1 ms). A further increase of the amount of oleic acid causes the correlation function to decrease, accompanied with a shift to smaller decay times until finally near binary mixtures Solketal/oleic acid no correlation can be observed at all (SK-h). DLS measurements of ternary mixtures composed of water/ethanol/TEC show a similar result: again, increasing amounts of TEC first lead to more defined correlation functions with higher decay times with a maximum for *w*(TEC) = 0.3 (TEC-c), before decreasing at larger amounts of TEC (*w*(TEC) > 0.3).

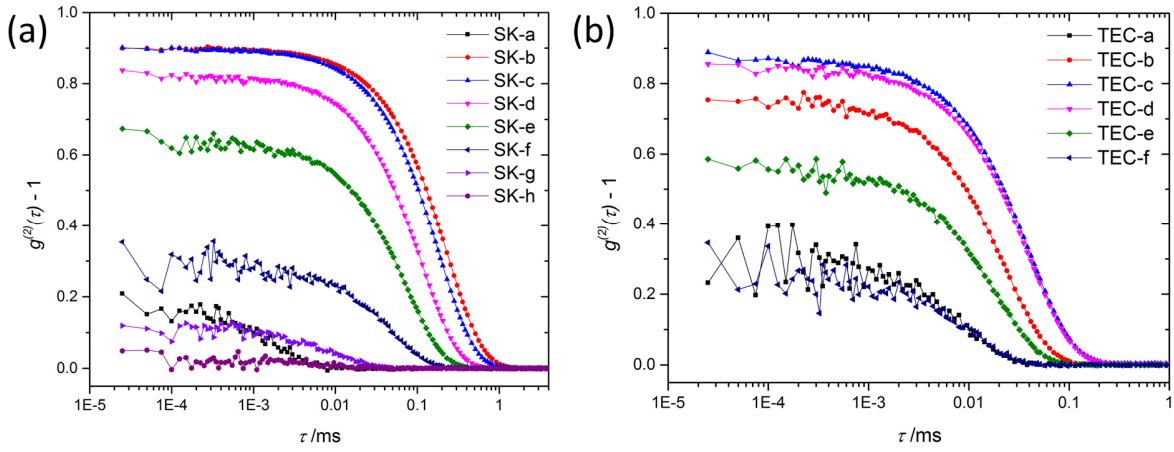

Figure 5.4: Normalised autocorrelation functions of intensity obtained by DLS measurements at 25 °C for the ternary systems (a) water/Solketal/oleic acid and (b) water/ethanol/TEC. The symbols refer to the specific compositions, which are indicated in Figure 5.3.

Results obtained by DLS indicate the presence of large monophasic areas with well-defined mesoscopic structured solutions in the range of 1 to 12 nm (see Figure A4.1, Appendix A.4). This size domains are typical of SFME and structural changes from direct to bicontinuous and

inverse microemulsions can be expected, as reported previously for similar ternary mixtures.[22] Consequently, such structured solutions allow the application for microemulsion-mediated extraction techniques with preferably high water-contents, leading to enhanced solubility of possible solutes gained by extraction. In the case of SFME, this effect is similar to the concept of facilitated hydrotropy.[21]

5.4.2. Kinetic measurements of Solketal and triethyl citrate cleavage

In order to appropriately separate potential solutes from the SFME, we make use of a new principle: using cleavable hydrotropes/oil components like Solketal/TEC. To this purpose, kinetic measurements of the acid-catalysed hydrolysis of Solketal and the base-catalysed hydrolysis of TEC were made (see Figure 5.5). In order to quantitatively run these reactions, hydrolysis products have to be removed from the equilibrium. In case of Solketal cleavage, this was achieved by the removal of acetone under reduced pressure. In case of TEC hydrolysis, removal of ethanol is more difficult and energy-consuming. For this reason, reactions were performed under alkaline conditions, in order to irreversibly deprotonate the formed citric acid to citrate. By doing so, the formed citrate is deactivated for the backward reaction to TEC and the equilibrium is shifted to the product side. It should be mentioned that also other techniques can be used to effectively cleave the used components, *e.g*. enzyme-catalysed reactions. The used methods are rather a selection of common hydrolysis reactions easy to perform.

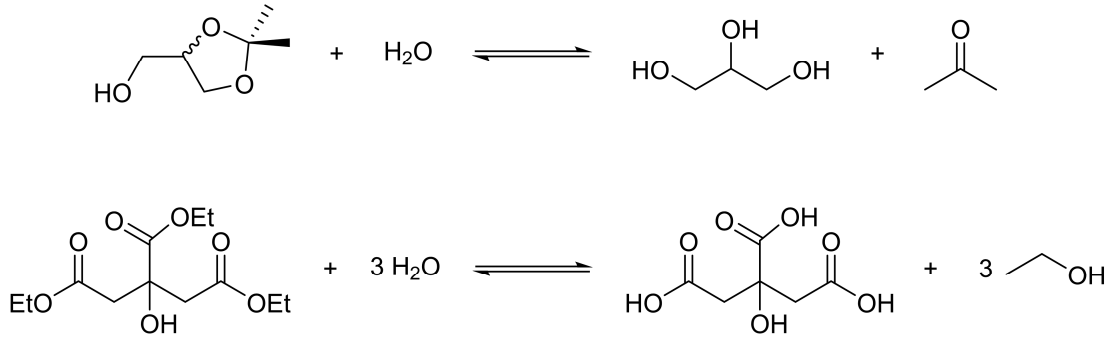

Figure 5.5: Chemical equilibria of Solketal hydrolysis (formation) to glycerol and acetone and TEC hydrolysis (formation) to citric acid and ethanol.

Kinetics of Solketal hydrolysis in binary water/Solketal mixtures (see point SK-a, Figure 5.3a) at different temperatures and pH of the used water are shown in Figure 5.6a. Moderate yields are obtained at 40 °C and pH 3 with time to completion of approximately 12 h. Increasing either the temperature to 60 °C or lowering the pH to 2 effectively accelerates the reaction, resulting in full conversion in less than 4h.

It is worth noting that pressure reduction to 150 mbar did not noticeably affect the reaction kinetics. No kinetics were measured for ternary systems composed of water/Solketal/oleic acid, due to the fact that such mixtures inevitably turn into a biphasic mixture upon Solketal cleavage. This leads to difficulties for the reproducibility of these measurements, since other factors like stirring rate can play a major role.

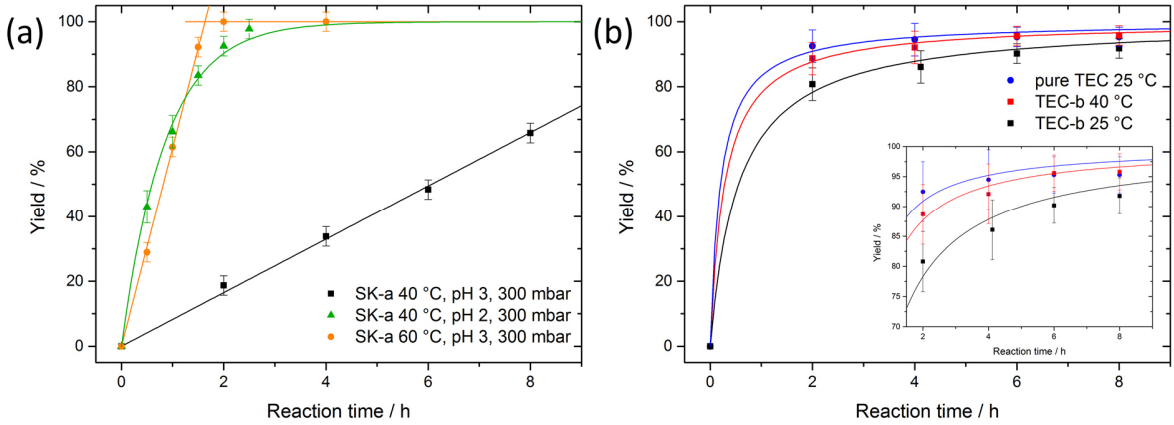

Figure 5.6: Reaction kinetics of (a) water Solketal mixtures (sample SK-a, see also Figure 5.3a) and (b) pure TEC and water/ethanol/TEC mixtures (sample TEC-b, see also Figure 5.3b) at different temperature, pressure and pH of the aqueous pseudo-phase.

In Figure 5.6b, results of the kinetic measurements of the TEC hydrolysis are presented. All reactions were performed with equal proportion of hydroxide to ester bonds. Best results were obtained adding sodium hydroxide solution to pure TEC at 25 °C with > 90% ester bonds cleaved after only 2 h of stirring. In addition, reaction kinetics were measured for a ternary mixture composed of water/ethanol/TEC as a representative for a SFME (see point TEC-b, Figure 5.3b). At 25 °C, about 80% and at 40 °C about 88% of the ester bonds are cleaved within 2 h. For all three measurements, the residual mixture of citrate and monoethyl citrate was found to be readily water soluble (solubility > 50 wt% in water).

As a result, (i) Solketal was found to be usable as cleavable hydrotrope. It has an adequate stability at ambient conditions, high enough for extraction purposes and can be easily and effectively cleaved upon moderate change of temperature and pH. For this reason, Solketal provides a good opportunity for a low to non-toxic cleavable hydrotrope, resulting in the even less toxic (food approved) and eco-friendly glycerol as decomposition product. Sole drawback is the release of acetone, which has to be removed from the mixture. Yet, due to its high volatility, acetone can be separated without considerable effort. Obviously, acetone could be used directly, instead of Solketal, since the removal of acetone is an ineluctable step during the procedure. However, acetone has to be added in similar amounts than Solketal (62 wt%

for acetone and 60 wt% for Solketal, see Appendix A.4, Figure A4.2a for phase diagrams) in order to reach complete miscibility between water and oleic acid. In other words, using Solketal instead of acetone reduces the effective amount of acetone in the solution by 58% with respect to the mole fraction. This is a significant advantage regarding toxicity, volatility and flammability of the resulting mixtures. Besides, acetone was found to form less structured SFME compared to Solketal containing SFME (see Appendix A.4, Figure A4.2b).

In addition, (ii) kinetic measurements showed that TEC is an appropriate choice for a cleavable oil pseudo-phase. High conversion of TEC during the base-catalysed hydrolysis is achieved within a few hours at moderate temperatures (25-40 °C), resulting in ethanol and citrate. All components used within this system are either non-toxic or food approved. Except of ethanol, none of them is flammable and SFME can be formed with high water contents. Furthermore, pure TEC can also be used for extraction processes. SFME residues are readily water-soluble and possible hydrophobic solutes can be easily separated due to their poor water-solubility.

5.4.3. Separation of surrogate solutes from SFME residues

As a proof of concept, the hydrolysis of the hydrotrope/oil phase in the presence of a hydrophobic component (Toc and VA) was investigated for two representative SFME compositions (SK-c and TEC-b, see Figure 5.3) in order to simulate separation processes after an hypothetic extraction process.

For ternary systems containing water/Solketal/oleic acid, Toc was dissolved within the ternary mixture and Solketal cleavage was performed at 60 °C at a pH of 3. It was found that the amount of oleic acid used in the mixture is already sufficient to lower the pH to the desired value (see Appendix A.4, Figure A4.3). During cleavage of Solketal, the solution turned into a biphasic mixture, due to glycerol formation. Furthermore, it was found that oleic acid is not soluble in water/glycerol mixtures (except for trace amounts). Thus, oleic acid separated from the resulting water/glycerol mixture forming a second pure oil phase upon full conversion of Solketal and removal of acetone. Subsequently, the Toc content of both phases was analysed. It was found that Toc quantitatively partitioned to the oil-phase and no Toc could be detected in the aqueous phase (see Appendix A.4, Figure A4.4). So the results show that hydrophobic solutes can be quantitatively separated from the residual water/glycerol mixture. Depending on whether an additional oil pseudo-phase (in this case oleic acid) is used or not, solutes can either form a separate phase or are dissolved within the pure oil phase. In case of oleic acid,

the resulting mixture could be for instance used in order to subsequently formulate self-emulsifying mixtures.

For VA dissolved in SFME composed of water/ethanol/TEC, 3 h at 25 °C with n(NaOH)/n(TEC) = 3:1 was found to be sufficient to quantitatively separate VA from the residual citrate/monoethyl citrate. It has to be mentioned that the solubility of VA strongly depends on the pH of the water it is to be dissolved in. Consequently, remaining TEC residues had to be removed washing at low pH (2 M HCl solution). Since the TEC residue is highly water-soluble (even under acidic conditions), VA was dissolved in the washing solution in significantly low amounts in order to perform quantitative separation. Consequently, no citrate/monoethyl citrate residues were found in the separated VA and only trace amounts of VA were detected in the washing solution, which were too low to quantify via ^{1}H-NMR spectroscopy (see Appendix A.4 Figure A4.5). At the same time, this shows that the yield of the separation process strongly depends on the water solubility of the solute, increasing with decreasing water solubility.

Furthermore, the performed experiments also reveal the limiting factors of the two systems for usage as extraction media. Beside of the solubility within the corresponding SFME, possible solutes have to be stable under the given conditions essential for effective hydrolysis of Solketal and TEC, meaning pH and temperature. For SFME using Solketal as cleavable hydrotrope, the components have to be stable at 40-60 °C at a pH of 2-3, for several hours. For TEC containing SFME, solutes have to be stable at 25 °C under alkaline conditions. However, it is worth noting that chemical strain can be reduced to a certain amount by the experimental approach. Adding for example sodium hydroxide dropwise to mixtures of water/ethanol/TEC can avoid high pH values, since the readily formed citric acid reacts rapidly with the hydroxide ions, leading to the formation of the weaker base sodium citrate. Furthermore, milder and more selective ways for targeted hydrolysis can be used like enzyme-catalysed decomposition of the SFME.

5.5. Conclusion

In the present contribution, we investigated cleavable SFME consisting of water/Solketal/oleic acid and water/ethanol/TEC suitable for microemulsion-mediated extraction processes. It was found that both systems show extended areas in the monophasic region with well-structured SFME in the size domain between 1 and 12 nm. Kinetic measurements of the acid-catalysed hydrolysis of Solketal (cleavable hydrotrope) and base-catalysed hydrolysis of TEC (cleavable

oil) showed rapid conversion upon pH and/or temperature changes. Furthermore, surrogate solutes were dissolved within the SFME in order to give a proof of concept for the facilitated and quantitative separation of these solutes from the hydrolysed products.

Results showed that cleavable SFME present an attractive alternative to cleavable surfactants. Almost all chemicals used in this system (including also the decomposition products) are either non-toxic or food approved. Furthermore, all mixtures are largely composed of eco-friendly, low-volatile and non-flammable components. Moreover, it has to be stressed that the principle of cleavable SFME can be also adopted to other classes of hydrotrope and oil compounds like short-chain triglycerides (*e.g*. Triacetin, see Appendix A.4, Figure A4.6 and A4.7). Thus, a great variety of compounds can be used to form such systems. For these reasons, such SFME could be of great interest for food and pharmaceutical applications representing non-toxic and eco-friendly solvents for extraction processes.

5.6. References

1 C. D. Stalikas, *TrAC - Trends Anal. Chem*., **2002**, *21*, 343– 355.

2 H. Tani, T. Kamidate and H. Watanabe, *J. Chromatogr. A*, **1997**, *780*, 229–241.

3 A. D. Gadhave and J. T. Waghmare, *IJRET Int. J. Res. Eng. Technol*., **2014**, *3*, 147–158.

4 A. Ballesteros-Gómez, M. D. Sicilia and S. Rubio, *Anal. Chim. Acta*, **2010**, *677*, 108–130.

5 P. Brown, C. P. Butts and J. Eastoe, *Soft Matter*, **2013**, *9*, 2365–2374.

6 D. A. Jaeger, Y. M. Sayed and A. K. Dutta, *Tetrahedron Lett*., **1990**, *31*, 449–450.

7 D. A. Jaeger, *Supramol. Chem*., **1995**, *5*, 27–30.

8 D. Lundberg, M. Stjerndahl and K. Holmberg, in Adv. Polym. Sci., ed. R. Narayanan, Springer Berlin Heidelberg, Berlin, Heidelberg, 2008, vol. 218, pp. 57–82.

9 J. R. McElhanon, T. Zifer, S. R. Kline, D. R. Wheeler, D. A. Loy, G. M. Jamison, T. M. Long, K. Rahimian and B. A. Simmons, *Langmuir*, **2005**, *21*, 3259–3266.

10 A. M. Amat, A. Arques, M. A. Miranda, R. Vincente and S. Seguí, *Environ. Eng. Sci*., **2007**, *24*, 790–794.

11 A. Tehrani-Bagha and K. Holmberg, *Curr. Opin. Colloid Interface Sci*., **2007**, *12*, 81–91.

12 D. A. Jaeger, J. Jamrozik, T. G. Golich, M. W. Clennan and J. Mohebalian, *J. Am. Chem. Soc.*, **1989**, *111*, 3001–3006.

13 H. Sakai, S. Aikawa, W. Matsuda, T. Ohmori, Y. Fukukita, Y. Tezuka, A. Matsumura, K. Torigoe, K. Tsuchiya, K. Arimitsu, K. Sakamoto, K. Sakai and M. Abe, *J. Colloid Interface Sci.*, **2012**, *376*, 160–164.

14 M. Karlberg, M. Stjerndahl, D. Lundberg and L. Piculell, *Langmuir*, **2005**, *21*, 9756–9763.

15 P. Hellberg, K. Bergström and K. Holmberg, *J. Surfactants Deterg*., **2000**, *3*, 81–91.

16 R. F. Hankel, P. E. Rojas, M. Cano-Sarabia, S. Sala, J. Veciana, A. Braeuer and N. Ventosa, *Chem. Commun*., **2014**, *50*, 8215–8218.

17 N. Grimaldi, P. E. Rojas, S. Stehle, A. Cordoba, R. Schweins, S. Sala, S. Luelsdorf, D. Piña, J. Veciana, J. Faraudo, A. Triolo, A. S. Braeuer and N. Ventosa, *ACS Nano*, **2017**, *11*, 10774–10784.

18 S. Krickl, D. Touraud, P. Bauduin, T. Zinn and W. Kunz, *J. Colloid Interface Sci*., **2018**, *516*, 466–475.

19 U. Mohorič, A. Beutner, S. Krickl, D. Touraud, W. Kunz and F. M. Matysik, *Anal. Bioanal. Chem*., **2016**, *408*, 8681–8689.

20 J. Xu, H. Deng, J. Song, J. Zhao, L. Zhang and W. Hou, *J. Colloid Interface Sci*., **2017**, *505*, 816–823.

21 M. L. Klossek, D. Touraud and W. Kunz, *Phys. Chem. Chem. Phys*., **2013**, *15*, 10971–10977.

22 T. Buchecker, S. Krickl, R. Winkler, I. Grillo, P. Bauduin, D. Touraud, A. Pfitzner and W. Kunz, *Phys. Chem. Chem. Phys*., **2017**, *19*, 1806–1816.

23 L. O. Kononov, *RSC Adv*., **2015**, *5*, 46718–46734.

24 T. Lopian, S. Schöttl, S. Prevost, S. Pellet-Rostaing, D. Horinek, W. Kunz and T. Zemb, *ACS Cent. Sci*., **2016**, *2*, 467–475.

25 S. Schöttl and D. Horinek, *Curr. Opin. Colloid Interface Sci*., **2016**, *22*, 8–13.

26 T. Zemb, M. L. Klossek, T. Lopian, J. Marcus, S. Schöttl, D. Horinek, S. Prevost, D. Touraud, O. Diat, S. Marčelja and W. Kunz, *Proc. Natl. Acad. Sci. U. S. A*., **2016**, *113*, 4260–4265.

27 S. Prevost, T. Lopian, M. Pleines, O. Diat and T. Zemb, *J. Appl. Crystallogr*., **2016**, *49*, 2063–2072.

28 W. Hou and J. Xu, Curr. Opin. *Colloid Interface Sci*., **2016**, *25*, 67–74.

29 P. Ni and W.-G. Hou, *Chinese J. Chem*., **2008**, *26*, 1985–1990.

30 J. Xu, A. Yin, J. Zhao, D. Li and W. Hou, *J. Phys. Chem. B*, **2013**, *117*, 450–456.

31 M. Clausse, L. Nicolas-Morgantini, A. Zradba and D. Touraud, in Surfactant Science Series (Vol. 24) Microemulsion Systems, eds. H. L. Rosano and M. Clausse, Dekker, New York, 1987, p. 15.

Chapter 6 Surfactant-free microemulsion supported extraction and separation – precise density data for (pseudo-)phase separation using (ultra)centrifugation techniques

6.1. Abstract and preface

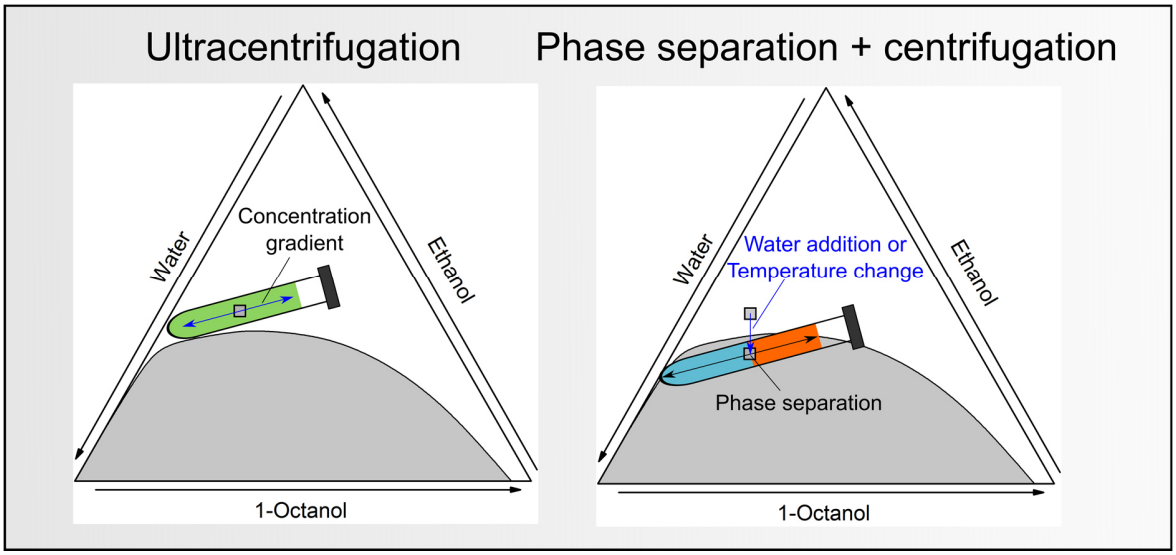

Figure 6.1: Graphical abstract schematically illustrating (pseudo-)phase separation of SFME using (ultra)centrifugation techniques.

For separation techniques using ultracentrifugation of surfactant-free microemulsions and centrifugation of biphasic mixtures of the corresponding systems (see Figure 6.1), precise knowledge of density and molar volumes are of great importance. For this reason, densities of surfactant-free microemulsions composed of water/ethanol/1-octanol, water/ethanol-d6/ 1-octanol and water/1-propoxy-2-propanol/ethyl acetate were measured at 20 °C with high precision and high experimental point density of the measured samples. Molar volumes were calculated and all data sets were carefully analysed in order to determine empirical hypersurfaces allowing rapid calculations of density and molar volume for these ternary mixtures.

This work was done in collaboration with Prof. Helmut Cölfen from the University of Konstanz and Prof. Thomas Zemb from the ICSM Marcoule.

Contributions to the experimental work:

- Density measurements: Jiaqi Hu and S. Krickl
- Data analysis: S. Krickl

6.2. Introduction

Facilitated hydrotropy is a powerful tool for efficient solubilisation of hydrophobic components in aqueous solutions.[1–5] The concept of facilitated hydrotropy is based on the use of a co-solvent, which acts like a hydrotrope, and a further more hydrophobic compound, acting as the facilitating hydrotrope. By doing so, solubility of very hydrophobic compounds is often significantly enhanced compared to the use of a single hydrotrope. Most likely, this effect may have its origin in aggregate formation.[2,4] Having a second glance at this concept, it seems evident that such mixtures usually fulfil the requirements of so-called surfactant-free microemulsions (SFME).[6–9] Such ternary systems usually consist of a hydrophilic liquid (commonly water), which is fully miscible with a hydrophilic hydrotrope that is again fully miscible with a water-insoluble oil component. In cases of solubilisation of an even more hydrophobic component in such systems, the initial oil component of the SFME plays the role of the second, more hydrophobic hydrotrope. Thus, regarding extraction processes, one may also talk about microemulsion-mediated or supported extraction. The great advantage of this surfactant-free method towards conventional microemulsion-mediated extraction obviously is the absence of surfactants. Contrary to surfactants, hydrotropes are generally cheaper, better bio-degradable, less foaming and easier to separate from the solution after usage.[10]

In order to separate extracted solutes from the extraction medium, phase separation is usually induced first, resulting in a water-rich and an oil-rich phase. In cases of SFME, this can be easily achieved by crossing the phase separation border. This can be done for instance by the addition of water or by slightly changing the temperature combined with centrifugation at moderate conditions in order to accelerate phase separation due to a density difference of both phases (see Figure 6.2a).[11–13] By doing so, hydrophobic solutes are already pre-concentrated in the oil-rich phase. Afterwards, compounds of both phases can be separated with less effort using different separation techniques like for instance distillation. However, recent approaches on new separation processes of SFME are currently developed at the University of Konstanz. Based on pioneering works of Barden and Miller[14,15] and suggested by T. Zemb, the working group around Helmut Cölfen wants to introduce a continuous separation process using ultracentrifugation of homogenous, monophasic

solutions, composed of the well-known SFME water/ethanol/1-octanol (see Figure 6.2b). By doing so, a concentration gradient is formed within the solution, basically allowing continuous separation within a one-phase mixture. Reasons for this astonishing phenomenon are not fully understood, yet. Nevertheless, such concepts are interesting processes for efficient separation of SFME, allowing easy recovery of SFME constituents and separation from hypothetically extracted solutes. However, both concepts need precise knowledge of density and partial molar volumes of the used SFME.

Whereas density is an important key parameter for macroscopic phase separation using conventional centrifugation, partial molar volumes are essential for the investigation of SFME-separation via ultracentrifugation. Yet, data on density and partial molar volumes of ternary mixtures are mostly rare or suffer from insufficient accuracy.[16] For these reasons, this study presents precise data on densities and partial molar volumes of different ternary systems, which are of great interest for potential applications and for the understanding of SFME-ultracentrifugation processes. All in all, three ternary mixtures were investigated: water/ethanol/1-octanol and the more thermosensitive ternary mixtures water/1-propoxy-2-propanol (PnP)/ethyl acetate (EA)[17,18] as well as ternary mixtures composed of water/ethanol-d6/1-octanol. Whereas the first two systems are of particular interest for applications, the latter is more important for the theoretical explanation and understanding of the ultracentrifugation-induced separation process.[19,20]

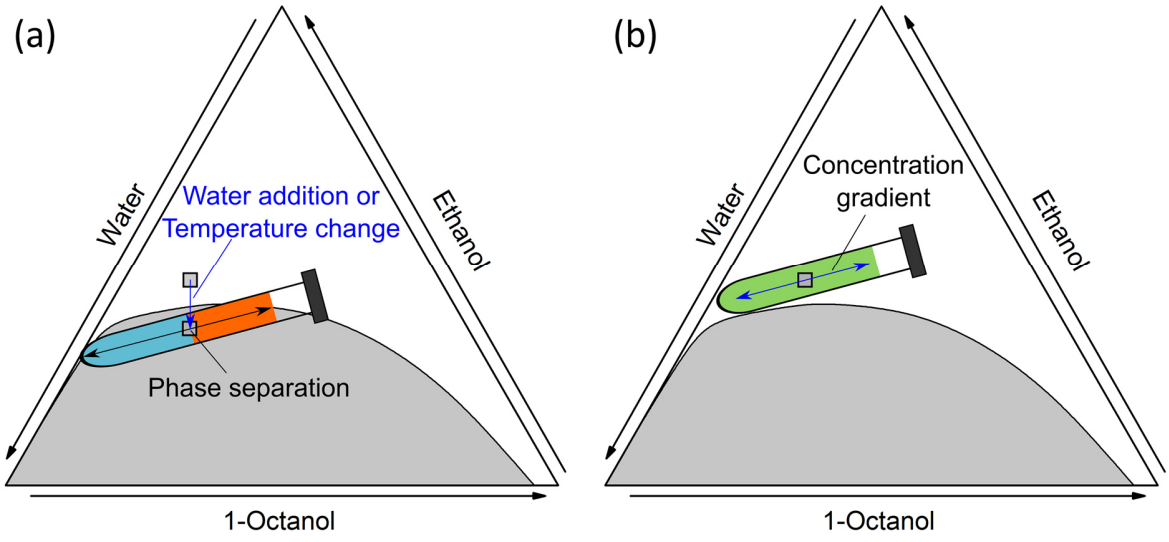

Figure 6.2: Schematic illustration of (a) conventional phase-separation using centrifugation and (b) formation of concentration gradients in SFME induced by ultracentrifugation.

6.3. Experimental

6.3.1. Chemicals

Ethanol (> 99.8%), ethyl acetate (EA, > 99.8%) and 1-propoxy-2-propanol (PnP, 99%) were purchased from Sigma-Aldrich (Steinheim, Germany). 1-Octanol (> 99.0%) was obtained from Merck (Darmstadt, Germany). Ethanol-d6 (99.00 atom% deuterated, water content < 0.3 %) was purchased from Eurisotop (Saint-Aubin, France). All chemicals were used without further purification. Aqueous solutions were prepared using deionised water with a resistivity of 18 MΩ cm.

6.3.2. Methods and techniques

6.3.2.1. Ternary phase diagrams

Phase diagrams were recorded at (20 ± 0.1) °C using a dynamic and static process according to Clausse *et al*. (see Section 2.3.2.1).[21]

6.3.2.2. Determination of the critical point

Critical points were defined as the sample composition at the phase separation border, where both phases have equal volume. In order to determine the critical point, ternary mixtures near the phase separation border (each 3 g) were prepared in closable, volume-scaled tubes of borosilicate glass at (20 ± 0.1) °C and water was added dropwise until phase transition occurred. After complete phase separation the volume ratio between water- and oil-rich phases was determined by the naked eye.

6.3.2.3. Density measurements

Solution densities ρ were determined with a vibrating tube density meter (DMA 5000 M, Anton Paar, Austria) at (20 ± 0.005) °C with a nominal precision of $\pm 5 \cdot 10^{-6}$ g cm^{-3}. Calibration was performed using air and pure water at 20 °C. At the beginning and at the end of each day, calibration was checked using pure water and between each measurement against air (allowed deviation: $\pm 5 \cdot 10^{-5}$ g cm^{-3}).

6.3.2.4. Calculation of molar and partial molar volumes

Molar volumes V_m were calculated as follows:

$$V_\mathrm{m} = \frac{V}{\sum_{i=1}^{3} n_i} = \frac{V}{\sum_{i=1}^{3} \frac{w_i \rho V}{\mathrm{M}_i}} \tag{6.1}$$

with w_i being the weight fraction of component i, the molar mass M_i of component i and the density ρ of the mixture.

Partial molar volumes were finally calculated with the first order derivative of the molar volumes:

$$V_{\mathrm{m}}^{\mathrm{P}} = \left(\frac{\partial V}{\partial n_i}\right)_{p,T,n_{j\neq i}} = \left(\frac{\partial V_{\mathrm{m}}}{\partial x_i}\right)_{p,T,x_{j\neq i}} \tag{6.2}$$

6.4. Results and discussion

For the sake of clarity, exclusively results of the ternary system water/ethanol/1-octanol will be presented in this section. Relevant results for ternary systems consisting of water/ethanol-d6/1-octanol and water/PnP/EA can be found in Appendix A.5 (see Table A5.1, A5.3, A5.4).

6.4.1. Ternary phase diagrams and sample compositions

Ternary phase diagrams including compositions of the chosen samples for water, ethanol, 1-octanol are shown in Figure 6.3. Samples were chosen in intervals of 5 wt% (see Figure 6.3, black points) and 1 wt% (blue points) around the critical point (orange point). In addition, measurements were performed near to and for binary mixtures of water and ethanol (see Figure 6.3, green and red points). Consequently, a high point density for the complete monophasic region was ensured.

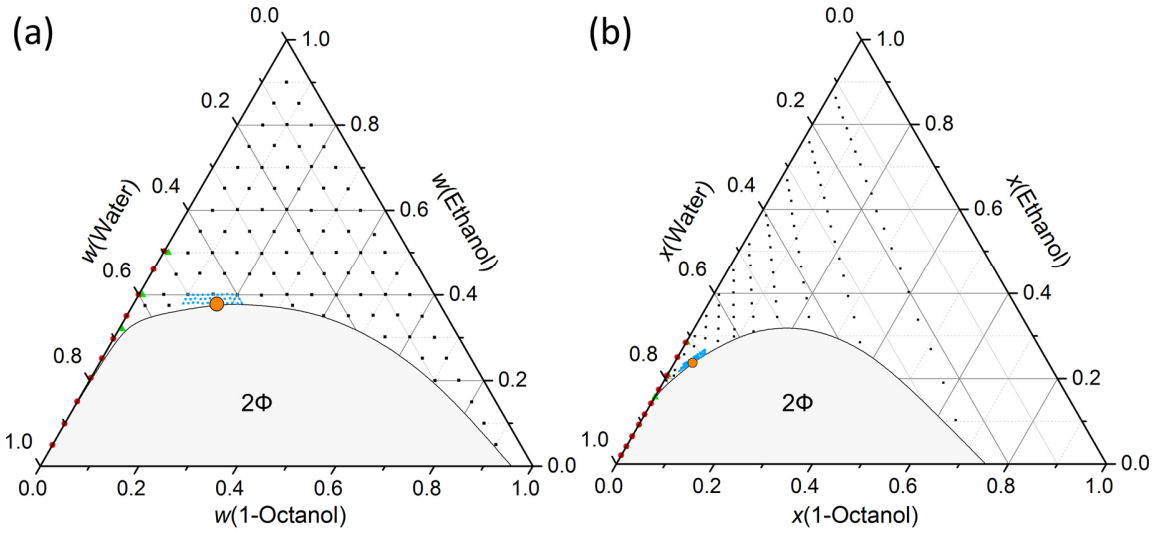

Figure 6.3: Ternary phase diagrams for the systems water/ethanol/1-octanol at 20 °C provided in (a) weight fractions and (b) mole fractions. The mono- and two-phasic areas are represented as white and grey areas, respectively. Symbols denote the different compositions chosen for density measurements. The critical point is marked in orange.

6.4.2. Density and molar volume hypersurfaces

Ternary contour diagrams for the density measurements of water, ethanol, 1-octanol are shown in Figure 6.4. It can be seen that there is a significant difference of the densities between the water- and 1-octanol-rich phases, which can be used for the formation of a concentration gradient upon ultracentrifugation. Furthermore, slight changes in temperature or the addition of water to homogeneous mixtures in the pre-Ouzo region can cause phase separation. The resulting phases are in equilibrium and density differences of $\Delta\rho \approx 0.1$ g cm^{-3} are easily achieved resulting in a facilitated separation upon centrifugation at moderate g-factors. Results of the molar volumes of ternary mixtures are shown in Figure 6.5. Molar volumes as a function of the mole fraction of each component behave linearly and no anomalies were observed.

In order to empirically describe the data, hypersurfaces were fitted to the experimental data. Fit-functions and corresponding fit parameters for density data of water/ethanol/1-octanol are summarised in Table A5.1, Appendix A.5. Fit functions were chosen as simple as possible with preferably high correlation coefficients and best results for data fitting at the edge of the fit range (see Figure 6.6a).

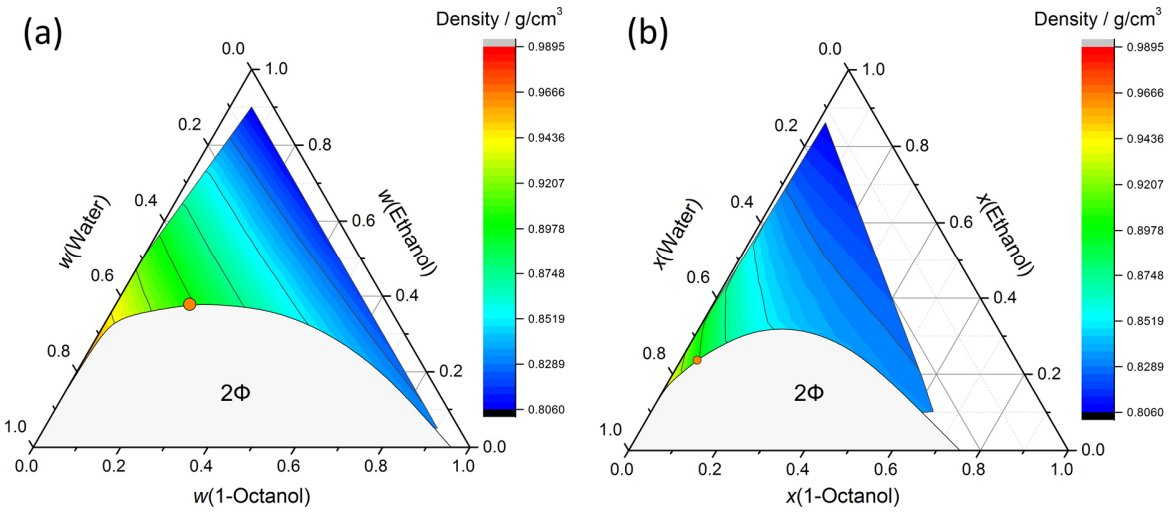

Figure 6.4: Ternary contour diagrams for density measurements at 20 °C of water/ethanol/1-octanol ternary mixtures provided in (a) weight and (b) mole fractions.

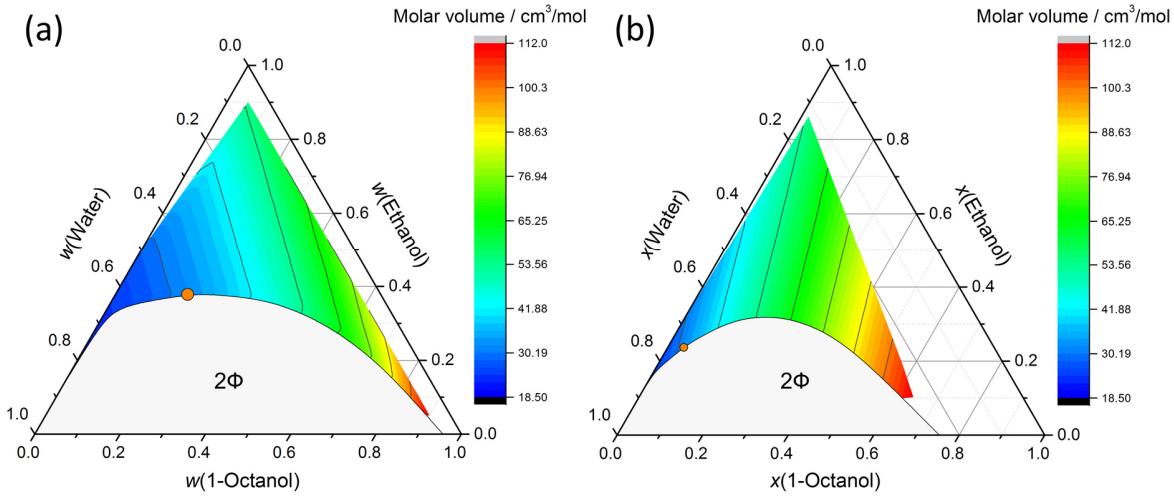

Figure 6.5: Ternary contour diagrams for calculated molar volumes at 20 °C of water/ethanol/1-octanol ternary mixtures provided in (a) weight and (b) mole fractions.

The same procedure was done for the calculated molar volumes in order to obtain partial molar volumes (see Figure 6.6b and Appendix A.5, Table A5.2). Hypersurfaces of the molar volumes can be simply described by a plane. Consequently, partial molar Volumes V_m^P were found to be ±141.24 cm^3 mol^{-1} for 1-octanol/water (*x*(ethanol) = const.), ±100.758 cm^3 mol^{-1} for ethanol/1-octanol (*x*(water) = const.) and ±40.482 cm^3 mol^{-1} for water/ethanol (*x*(1-octanol) = const.).

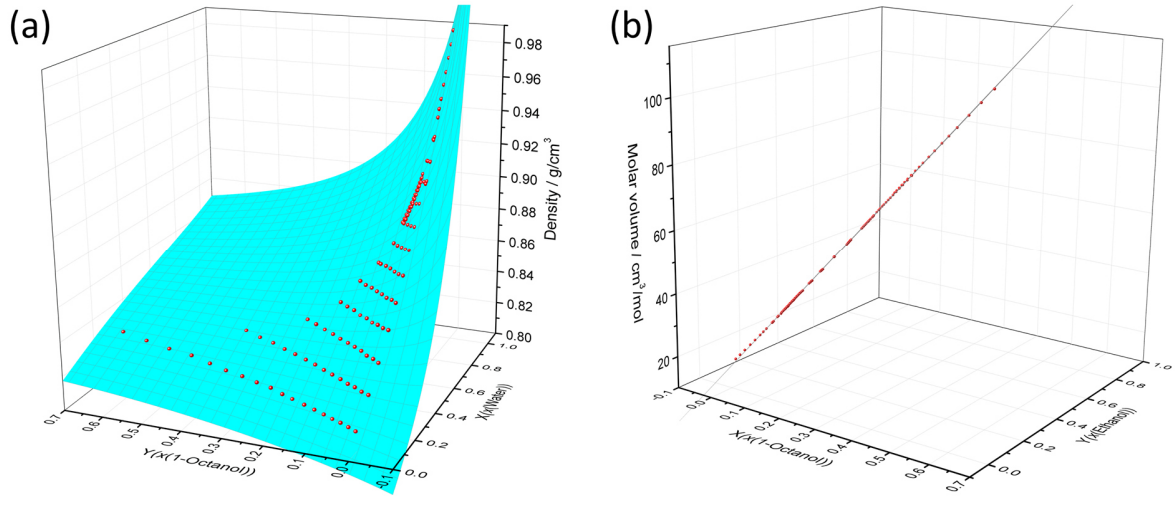

Figure 6.6: Selected hypersurfaces empirically describing densities (a) and calculated molar volumes (b) of ternary mixtures composed of water/ethanol/1-octanol at 20 °C. Note that in (b) the view is perpendicular to the normal of the plane.

6.5. Conclusion

Data on density and molar volumes for three ternary mixtures water/ethanol/1-octanol, water/ethanol-d6/1-octanol and water/1-propoxy-2-propanol/ethyl acetate were collected and carefully analysed. Due to the high point density of the measured samples and accuracy of the measurements, the obtained hypersurfaces can be described with high precision using relatively simple empirical fit functions. Thus, data for density and molar volumes can now be calculated easily for any ternary composition of each system. Consequently, such data sets are of great value for future centrifugation and ultracentrifugation experiments enabling potential applications of SFME for extraction and separation techniques.

6.6. References

1 P. Simamora, J. M. Alvarez and S. H. Yalkowsky, *Int. J. Pharm.*, **2001**, *213*, 25–29.

2 M. Durand, A. Stoppa, V. Molinier, D. Touraud and J. M. Aubry, *J. Solution Chem.*, **2012**, *41*, 555–565.

3 W. Kunz, K. Holmberg and T. Zemb, *Curr. Opin. Colloid Interface Sci.*, **2016**, *22*, 99–107.

4 M. L. Klossek, D. Touraud and W. Kunz, *Phys. Chem. Chem. Phys.*, **2013**, *15*, 10971–10977.

5 T. Buchecker, S. Krickl, R. Winkler, I. Grillo, P. Bauduin, D. Touraud, A. Pfitzner and W. Kunz, *Phys. Chem. Chem. Phys.*, **2017**, *19*, 1806–1816.

6 S. Prevost, T. Lopian, M. Pleines, O. Diat and T. Zemb, *J. Appl. Crystallogr.*, **2016**, *49*, 2063–2072.

7 T. Zemb, M. Klossek, T. Lopian, J. Marcus, S. Schöttl, D. Horinek, S. Prevost, D. Touraud, O. Diat, S. Marčelja and W. Kunz, *Proc. Natl. Acad. Sci. U. S. A.*, **2016**, *113*, 4260–4265.

8 M. L. Klossek, D. Touraud, T. Zemb and W. Kunz, *ChemPhysChem*, **2012**, *13*, 4116–4119.

9 S. Schöttl and D. Horinek, *Curr. Opin. Colloid Interface Sci.*, **2016**, *22*, 8–13.

10 R. Lebeuf, E. Illous, C. Dussenne, V. Molinier, E. Da Silva, M. Lemaire and J. M. Aubry, *ACS Sustain. Chem. Eng.*, **2016**, *4*, 4815–4823.

11 K. L. Planken and H. Cölfen, *Nanoscale*, **2010**, *2*, 1849–1869.

12 H. Cölfen, Ed., Analytical Ultracentrifugation V, Springer, Berlin, 1999.

13 D. F. Evans and H. Wennerström, The colloidal domain: Where physics, chemistry, biology and technology meet, Wiley-VCH, New York, 2nd edn., 1999.

14 J. F. Jeng and C. A. Miller, *Colloids and Surfaces*, **1987**, *28*, 271–288.

15 G. D. Smith, C. E. Donelan and R. E. Barden, *J. Colloid Interface Sci.*, **1977**, *60*, 488–496.

16 A. Arce, A. Blanco, A. Soto and I. Vidal, *J. Chem. Eng. Data*, **1993**, *38*, 336–340.

17 K. Lunkenheimer, S. Schrödle and W. Kunz, *Prog. Colloid Polym. Sci.*, **2004**, *126*, 14–20.

18 P. Bauduin, L. Wattebled, S. Schrödle, D. Touraud and W. Kunz, *J. Mol. Liq.*, **2004**, *115*, 23–28.

19 R. Piazza, S. Buzzaccaro, E. Secchi and A. Parola, *Phys. Biol.*, **2013**, *10*, 045005.

20 K. Ishikawa, M. Behrens, S. Eriksson, D. Topgaard, U. Olsson and H. Wennerström, *J. Phys. Chem. B*, **2016**, *120*, 6074–6079.

21 M. Clausse, L. Nicolas-Morgantini, A. Zradba and D. Touraud, in Surfactant Science Series (Vol. 24) Microemulsion Systems, eds. H. L. Rosano and M. Clausse, Dekker, New York, 1987, p. 15.

Chapter 7 A systematic study of the influence of mesoscale structuring on the kinetics of a chemical reaction

7.1. Preface and abstract

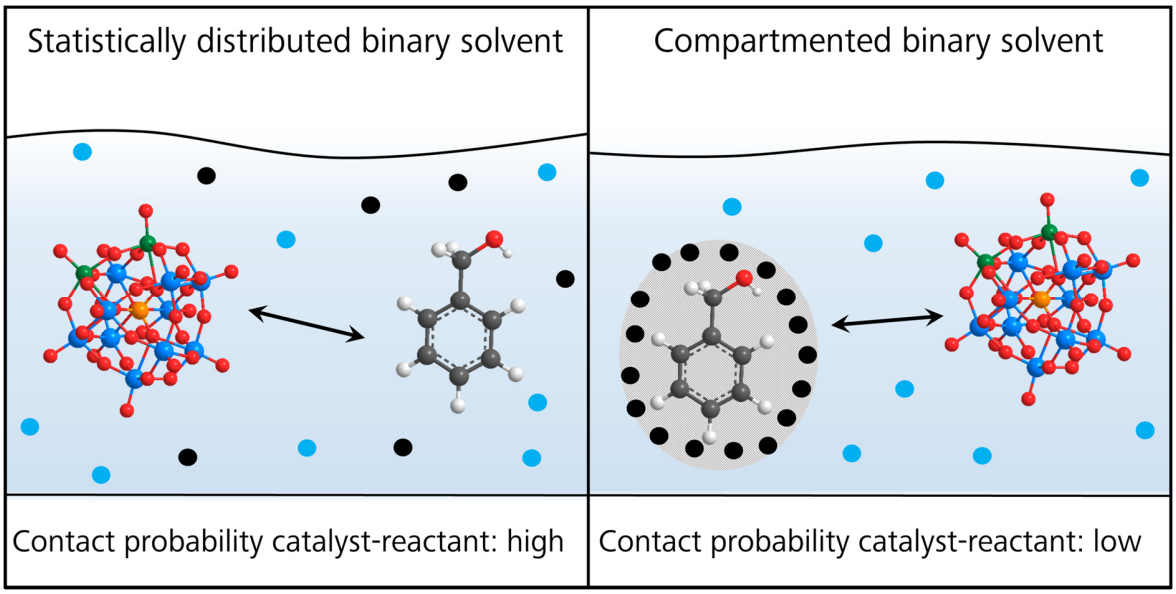

Figure 7.1: Graphical abstract schematically illustrating different effects of non-structured and mesoscale structured solutions on the contact probability of catalyst and reagent.

In this contribution, we (i) link the mesoscopic structuring of the binary structured solvent mixture H_2O/*tert*-butanol (TBA) to the kinetics and the efficacy of the oxidation of benzyl alcohol (BA) to the corresponding aldehyde catalysed by $H_5PMo_{10}V_2O_{40}$. We also compare the catalytic efficacy of this reaction in the mesoscopically structured solvent H_2O/TBA to an unstructured (or very weakly structured) solvent H_2O/ethanol (EtOH). In this context, we (ii) also give a methodological outline on how to study systematically the catalytic efficacy of chemical reactions as a function of the mesoscale structuring of a binary solvent. We demonstrate that the obtained yields of benzyl aldehyde depend on the type of mesoscopic structuring of the binary solvent H_2O/TBA. An elevated catalytic performance of at least 100% is found for unstructured binary mixtures H_2O/TBA compared to compartmented binary mixtures H_2O/TBA. We conclude that compartmentation of both the organic substrate and the

catalyst in TBA and water-rich micro-phases seems to be unfavourable for the catalytic efficacy (see Figure 7.1).

This chapter has been published in *Physical Chemistry Chemical Physics* (S. Krickl, T. Buchecker, A. U. Meyer, I. Grillo, D. Touraud, P. Bauduin, B. König, A. Pfitzner and W. Kunz, *Phys. Chem. Chem. Phys.*, **2017**, *19*, 23773–23780.)
The authors S. Krickl and T. Buchecker contributed equally to the experimental work, analysis of the data and to the writing of the manuscript.

Contributions to the experimental work:

- Dynamic light scattering: S. Krickl
- Small-angle X-ray scattering: T. Buchecker
- Small-angle neutron scattering: T. Buchecker and I. Grillo
- Conductivity measurements: S. Krickl and T. Buchecker
- Ternary phase diagram: S. Krickl
- Chemical reactions and GC analysis: A. U. Meyer, S. Krickl and T. Buchecker
- Synthesis and characterisation of the $H_5PMo_{10}V_2O_{40}$ catalyst: T. Buchecker

7.2. Introduction

The focus in synthesis and catalysis is often on the understanding of the reaction mechanism of isolated, *i.e.* molecularly dissolved, reacting molecules. In practice, such a situation can only be realised in gas phase reactions. However, most reactions are carried out in solutions using a neat one-component solvent or a mixture of solvents.[1] It is well known that a change of the solvent and the solvent–solute structure leads to large differences in yields and in stereoselectivity of the desired products.[2–4] Up to now, a common method to find the best solvent that leads to preferably high yields and/or the desired stereoselectivity is to screen the reaction in several solvents/solvent mixtures. It is evident that solvent screening inevitably requires considerable and time-consuming efforts. The obtained yields are then usually discussed merely in terms of solvent and solute polarity or polarizability or other molecular parameters. However, mesoscopic organisation is often neglected in the context of chemical reactions, but solvent-structuring effects may play an important role in chemical reactivity.
Yet, the origin of solvent induced effects on reactivity of organic compounds is not trivial and comprises plenty of different aspects, like hydration, solvation and hydrophobic effects,[5–7]

oligomer formation,[4,8] as well as transport properties like diffusion[9,10] and viscosity.[11] Another important point is certainly the formation of mesoscale inhomogeneities or surfactant-free microemulsions (SFME) in the case of binary and ternary solvent mixtures, respectively. In recent studies and reviews, it is claimed that chemical reactivity in solutions is not (solely) related to the molecular nature of the solvent, but may also depend on the mesoscopic structuring of the system (solvents + reagents). Slight changes in this subtle solvent organisation may lead to very different reactivity patterns.[2,3]

Recent studies in the field of mesoscale structuring of liquid binary and ternary mixtures unveiled new aspects for the understanding of spontaneous self-assembly and weak interactions in structured liquids.[12–20] Even in macroscopically homogeneous binary mixtures (*e.g.* H_2O/TBA), it was found that compartmentation into hydrophilic and hydrophobic domains can be present with significant consequences for several thermodynamic properties, like vapour pressure, apparent molar volume, viscosity or solubilisation power.[21–23] It should be stressed that these interesting features allow new applications in research and industry.[21,24-26]

Nevertheless, studies on the impact of these mesoscale structuring on reactivity are still rare. Although first investigations on structure–reactivity relationships in SFME go back to the late 1980s, when Khmelnitsky *et al.* investigated enzymatic reactions in SFME, few researchers continued in this field, mostly due to lacking experimental access to structural information on the microemulsion systems. In these pioneering studies, large differences in the enzymatic activity were found, depending on the composition of the ternary reaction medium consisting of water/2-propanol/*n*-hexane, and the different enzymatic activities were related to the presence of mesoscale inhomogeneities in the SFME.[27–31] Besides, there is only a small number of studies focussing on the influence of the solvent-, solvent–solute- or solute-structuring on the chemical reactivity patterns.[2–4,6,7,32–35]

Regarding these studies, it sounds reasonable that compartmentation phenomena (such as the mesoscale separation of substrates or of catalyst and substrate) should have a strong impact on chemical reactivity. Consequently, considering all this, in-depth studies of the structure–reactivity relationship between solvent structuring and chemical reactions are essential for a future ‘‘tailor-made’’ experimental design in chemical and biochemical synthesis.

In the present contribution, we (i) show, with the help of one exemplary reaction, the impact of the mesoscale structuring on the chemical reactivity. For this purpose, we chose the visible light-mediated oxidation of benzyl alcohol (BA), with atmospheric oxygen as terminal oxidising agent and with a photocatalytic active polyoxometalate $H_5PMo_{10}V_2O_{40}$ (POM), as a simple

model reaction (Figure 7.2). Within this context, we also provide (ii) a general approach for the investigation of such mesoscale inhomogeneities of binary solvent mixtures and their influence on the chemical reactivity.

The reaction provides several advantages: both, the light-mediated reaction and all structural investigations are performed at ambient conditions and in the presence of the catalyst. The reaction is only triggered upon irradiation with blue LED light. Oxygen is used as a cheap terminal oxidising agent to reoxidise the catalyst and to close the catalytic cycle. Furthermore, oxygen is supposed to have a negligible influence on the solution structure. Two different solvent systems are investigated: binary H_2O/TBA and H_2O/EtOH mixtures. H_2O/TBA is selected, because different regimes of mesoscale structuring can be found similar to surfactant containing solutions (*i.e.* solutions showing inhomogeneities in concentration in the supramolecular range). Depending on the H_2O/TBA ratio unstructured regimes, direct structuring (TBA clusters at low TBA concentration), bicontinuous structuring (for moderate TBA concentrations) and reverse structuring of H_2O in TBA (for high TBA concentrations) are supposed.[23] The type of mesoscale structuring in binary mixtures H_2O/TBA is then correlated with the yield of the oxidation product, *i.e*. benzaldehyde. H_2O/EtOH is chosen as a not (or very weak) structured solvent mixture generally observed for all H_2O/EtOH ratios (molecular solution).

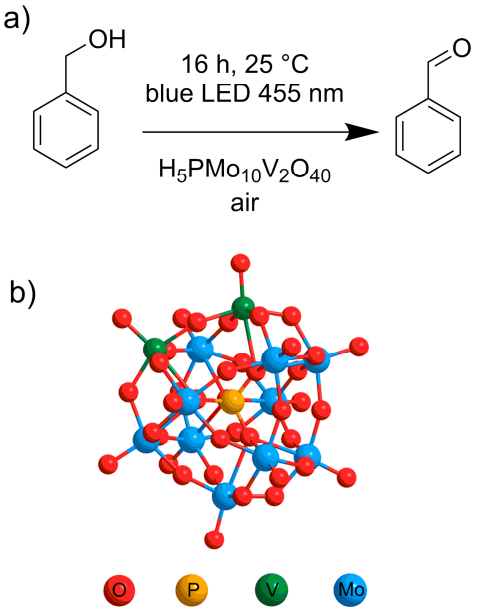

Figure 7.2: (a) Catalytic oxidation reaction of benzyl alcohol (BA) to the corresponding aldehyde with the given parameters: 25 °C, 16 h, molecular oxygen as a sacrificial oxidising agent and a blue LED (455 nm, 1.2 W) to trigger the reaction. (b) Structure of the catalyst: *α*-Keggin type polyoxometalate $PMo_{10}V_2O_{40}^{5-}$ (POM) anion.

7.3. Experimental

7.3.1. Chemicals

Sodium bromide (≥ 99.99%), sodium sulphite (95%) and benzyl alcohol (BA, ≥ 99%) were purchased from Merck (Darmstadt, Germany) and *tert*-butanol (TBA, ≥ 99%) from Carl Roth (Karlsruhe, Germany). Ethanol (EtOH, ≥ 99.8%), $NaVO_3$ (99.9%), Na_2MoO_4 (≥ 99.5%), $Na_2HPO_4 \cdot H_2O$ (≥ 98.5%), benzaldehyde (≥ 99.5%) and cyclohexanone dimethyl ketal (CDK, 99%) were purchased from Sigma-Aldrich (Steinheim, Germany). All chemicals were used without further purification. Aqueous solutions were prepared using deionised water with a resistivity of 18 MΩ cm.

7.3.2. Synthesis and characterisation of the catalyst

The catalyst, $H_5PMo_{10}V_2O_{40}$ (POM), was synthesised according to a literature procedure given by Tsigdinos *et al*.[36] and dried under vacuum. The product was characterised by IR (characteristic bands of POM: 1052 cm^{-1} (P–O bond), 954 cm^{-1} (terminal M–O), and 877 and 731 cm^{-1} (edge and corner bridging M–O–M)), ^{31}P-NMR (-3.11, -3.29, -3.38, -3.56), ICP-AES (ratio of P:Mo:V (calcd.) found: (1)1.0:(10)9.9:(2)2.0), TGA (8 H_2O), PXRD and compared to literature.[36,37] UV-Vis measurements were carried out at λ = 455 nm in 1 mm path length cells (Hellma 110-QS) using a Lambda 18 UV-Vis spectrometer from Perkin Elmer (Waltham, USA) to determine the molar extinction coefficient of $H_5PMo_{10}V_2O_{40}$ at 455 nm as applied for the catalytic reactions (ε(455 nm) = $1.2 \cdot 10^5$ L·dm mol^{-1}).

7.3.3. Methods

7.3.3.1. Small-angle neutron scattering

Small-angle neutron scattering (SANS) experiments and data analysis were performed as described in Section 2.3.2.3.[38,39] Full fitting of the spectra is out of the scope of this paper.

7.3.3.2. Dynamic light scattering

Dynamic light scattering (DLS) experiments were performed as described in Section 2.3.2.2.

7.3.3.3. Conductivity measurements

Conductivity measurements were carried out in a thermostatted measurement cell (25 ± 0.2 °C) under permanent stirring using a low-frequency WTW inoLab Cond 730 conductivity meter connected with a WTW TetraCon 325 electrode (Weilheim, Germany).

20 g of alcohol (EtOH/TBA) was filled in the measurement cell and successively diluted with pure water. Each sample contained in addition 0.1 wt% sodium bromide to ensure a sufficient amount of charge carriers, which did not noticeably affect the microstructure or the miscibility gap present in the phase diagram. In case of TBA (where sodium bromide did not dissolve completely), a small amount of water was added before the measurement was started.

7.3.3.4. Oxygen solubility measurements

Measurements of the dissolved oxygen in binary mixtures of H_2O/EtOH and H_2O/TBA were carried out at (23 ± 0.2) °C using a TPS Aqua-D oxygen-meter connected with a TPS ED1 electrode (Brisbane, Australia). A two-point-calibration was performed against air and against a solution of 2 g sodium sulphite in 100 mL water. No corrections were made for the ambient air pressure. Samples (each 10 g) were stirred overnight in closed vials for ideal mixing and equilibration. By doing so, it was ensured that conditions for sample preparation were close to those of the reactivity measurements. Measurements themselves were performed without stirring and values were taken after an equilibration time of 30 min to ensure constant and reproducible results. Note that solutions are not necessarily saturated with oxygen, since conditions of sample preparation were adjusted to those of the reactivity experiments.

7.3.3.5. Oxidation reactions and GC analysis

Oxidation reactions were performed at 25 °C for monophasic compositions of the ternary system in the presence of 2 mM of $H_5PMo_{10}V_2O_{40}$. Glass vials suited for temperature-controllable blocks were used as sample containers and filled to a height of 1 cm (2 mL). This ensures light absorption of the catalyst to an efficacy of 92%. Samples were irradiated with blue LEDs (λ = 455 nm, 1.12 W) for 16 h, atmospheric oxygen was used as a sacrificial agent to complete the catalytic cycle. To this purpose, two needles were inserted into the septum-sealed vials to ensure the presence of enough oxygen. The amount of benzyl aldehyde was determined by GC measurements with CDK as internal standard. All oxidation reactions were performed for the following conditions:

(i) sample + catalyst + irradiation,
(ii) sample + catalyst without irradiation,
(iii) sample without catalyst + irradiation,
(iv) sample without catalyst and without irradiation.

Only in case (i), detectable yields of benzyl aldehyde were obtained. Hence, it is ensured that BA and POM do not undergo a reaction during all structural investigations.

7.4. Results and discussion

7.4.1. Determination of the optimum reaction conditions and experimental design

In order to relate the catalytic efficacy of a reaction to its mesoscopic structuring different experimental designs are possible: (i) constant mole fractions of BA in a given solvent mixture or (ii) constant molar concentrations of BA in given solvent mixtures. The molar ratio of BA/catalyst has to remain constant (here 50:1) for both to obtain comparable results between the different reaction mixtures.

Constant (i) mole fractions provide the advantage of an equal ratio of BA molecules to solvent molecules. Nevertheless, due to a strong difference in the molar volumes of H_2O, TBA and BA, the molar concentration of BA increases with increasing H_2O mole fraction (and decreasing TBA mole fraction). Therefore, a constant mole fraction of BA has the ‘‘disadvantage’’ of a different molar concentration of BA. This, on the other hand, leads to an increasing catalyst concentration to keep the same BA/catalyst ratio of 50:1. Since the adsorption of the incident LED light (according to Beer-Lambert law) is strongly dependent on the concentration of the photocatalyst, solely highly dilute photocatalyst solutions ensure absorption below 99% of the incident light. Hence, only in the dilute region where Beer–Lambert’s law is applicable (usually around 100 mM up to 8 mM, strongly depending on the absorption coefficient of the catalyst, the thickness of the reaction solution, *etc.*), catalyst concentrations lead to reliable results for reactivity measurements. At higher concentrations, not all $H_5PMo_{10}V_2O_{40}$ catalysts are activated by irradiation, which affects the catalytic efficiency significantly.

In contrast to constant mole fractions of BA, constant concentrations of BA (ii) provide the ‘‘disadvantage’’ of a different molar fraction of BA. Nevertheless, constant concentrations of BA are practically most feasible since the catalyst concentration is kept constant due to a constant BA/catalyst ratio. Hence, the photo-catalyst concentration can be adjusted according to the Beer–Lambert law leading to 90-99% absorption of the incident LED light (c(POM) = 2 mM) with a constant BA/POM ratio (in our case 50:1, *i.e.* c(BA) = 100 mM) for each solvent composition. Such low BA concentrations change the composition of the ternary system only marginally, *cf.* ternary phase diagram Figure 7.3a. It was shown recently that such low BA concentrations enhance the structuring of H_2O/TBA solutions, but do not change the type of structuring of the binary mixture H_2O/TBA.[23] Statistical contact between the catalyst

and BA should only be a function of the inherent mesoscopic structuring of the binary solvent H_2O/alcohol.

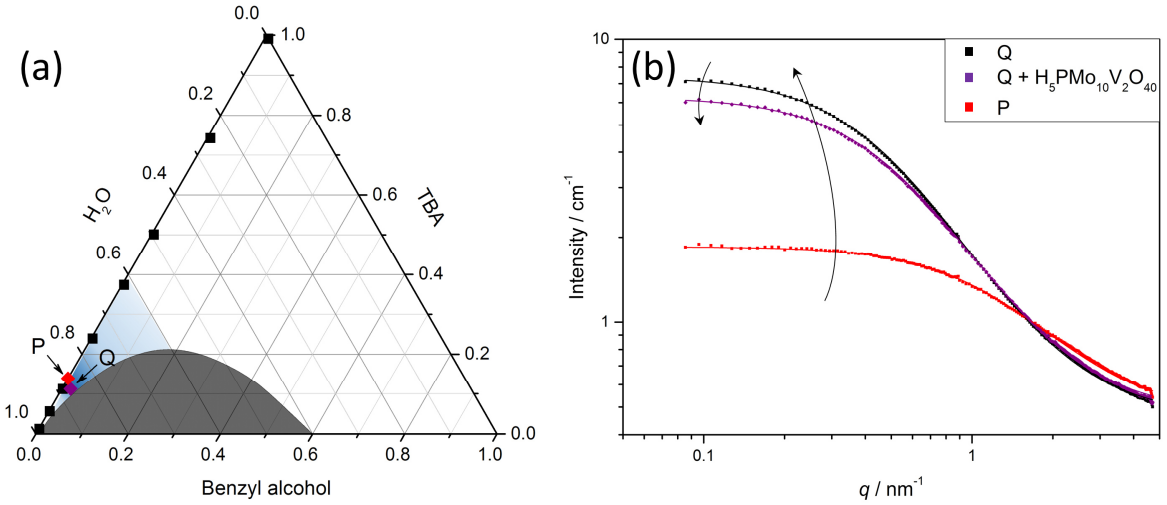

Figure 7.3: Ternary phase diagram of H_2O/TBA/BA at 25 °C provided in mole fractions. The most pronounced structured region of the binary solvent H_2O/TBA is indicated in blue. The black squares in (a) represent the ternary composition of the reaction mixtures. (b) Small-angle neutron scattering (SANS) patterns of two compositions at 25 °C indicated in (a), *i.e.* compositions P (D_2O/TBA 0.86/0.14) and Q (D_2O/TBA/BA 0.87/0.11/0.02). For composition Q, the catalyst, $c(H_5PMo_{10}V_2O_{40})$ = 2 mM, was added (the same concentration as applied for the catalytic reactions).

7.4.2. Influence of the catalyst and its location within the ternary system H_2O/TBA/BA

Next, the location of the catalyst in the reaction mixture and its influence on the structuring of the solution was investigated. In case of no (or very weakly structured) H_2O/EtOH mixtures, a homogenous distribution is assumed. For structured mixtures of H_2O/TBA with an inherent interface, the location of the catalyst is important for the catalytic process. For an effective catalysis, the catalyst as well as the organic substrate should be located at a surface/interface to enhance the contact probability of the catalyst and the organic substrate. Here, a polyoxometalate, *i.e.* $H_5PMo_{10}V_2O_{40}$ (POM), was chosen as a suitable catalyst as it (i) is highly water soluble, (ii) can be applied as photocatalyst and as (iii) similar polyoxometalates were recently shown to exhibit a strong propensity to adsorb at neutral soft interfaces covered with electrically neutral functional groups.[40,41] The catalyst was localised in the ternary structured liquid H_2O/TBA/BA by scattering experiments, see Figure 7.3b. In contrast to recent experiments, small-angle X-ray scattering (SAXS) could not be used as a technique to investigate the influence of additives on mesoscale structured liquids. POMs provide a strong scattering signal in SAXS due to their high scattering length density superimposing the

scattering signal of the mesoscale structured liquid. Hence, SANS was chosen, as the scattering contrast between the POM and the solvent and solute is different (see also Appendix A.6, Table A6.1). Solutions of POMs in D_2O provide a constant (low) scattering signal in SANS over the whole *q*-range, as it has a scattering length density close to D_2O and therefore does not produce a significant contrast. Therefore, SANS reflects only the change in the mesoscale structuring of H_2O/TBA/BA upon the addition of POM.

Two different compositions (provided in mole fractions) were chosen, *i.e.* point P (D_2O/TBA 0.86/0.14) and Q (D2O/TBA/BA 0.87/0.11/0.02), *cf.* Figure 7.3a. The binary composition P exhibits strong pre-structuring in the binary system H_2O/TBA, which has been previously investigated by SAXS and DLS experiments. Note that the difference between P and Q is only the substitution of TBA by BA. For composition Q, POM was added to ensure a concentration of $c(H_5PMo_{10}V_2O_{40})$ = 2 mM as used in reaction mixtures.

The binary mixture D_2O/TBA provides a strong scattering signal indicating the presence of a structured binary liquid.[23] The substitution of TBA by BA leads to a strong increase of the scattered intensity. The addition of the POM catalyst to the ternary mixture leads to a decrease in the scattered intensity. As the POM does not produce a contrast, the decrease in the scattered intensity is only due to a change in the mesoscale structure of the TBA-rich pseudo-phase. To obtain qualitative information a correlation length of the nano-domains was obtained from the fitting of the SANS spectra using the OZ formalism. The correlation length increases from 0.8 nm for the binary D_2O/TBA mixture (Sample P) up to 2.1 nm for the ternary D_2O/TBA/BA mixture (Sample Q). The correlation length of Q decreases from 2.1 to 1.9 nm in the presence of the POM catalyst.

The increase in the scattered intensity from the binary D_2O/TBA to the ternary D_2O/TBA/BA mixture indicates a strengthening of the structuring and swelling of the aliphatic (or TBA/BA) rich pseudo-phase. The decrease in the scattered intensity and thus the decreasing correlation length of composition Q in the presence of the POM suggest an adsorption of the catalyst at the interface between the TBA-rich and the water-rich bulk phases and therefore a charging of the interface. The compressibility of the system decreases resulting in a decreasing scattered intensity. The decrease in the correlation length is also a consequence of the lower compressibility of the system: due to repulsive interactions between the domains, smaller aggregates are formed.[16] In an additional experiment, see Figure A6.1 (Appendix A.6), the propensity of POM to adsorb at neutral soft interfaces covered with polar functional groups was also confirmed.[40] The adsorption of POM at the surface of non-ionic micelle was indeed proved using SAXS.

From SANS and SAXS experiments, we conclude that hydrophilic POMs (fivefold negative charge) should mostly be solubilised in the water-rich pseudo-phase (rather than in the aliphatic-rich pseudo-phase) with a tendency to adsorb at the interface of the ternary structured liquid H_2O/TBA/BA.

7.4.3. Reactivity measurements

After clarifying the reaction conditions with a constant BA concentration and a constant $H_5PMo_{10}V_2O_{40}$ concentration, catalytic reactions were performed as a function of the H_2O/alcohol solvent ratio at constant BA concentration of 100 mM and 2 mM of POM. Remember that in case of H_2O/TBA, the type of mesoscopic structuring depends on the molar ratios (similar to a micellar system as indicated by the conductivity curves of binary solutions H_2O/alcohol), see Figure 7.4a: for low water contents no structuring, for increasing water content a reverse structuring (water droplets in oil) is observed followed by a percolation threshold around $x(H_2O) \approx 0.6$ leading to a bicontinuous structuring. For high water contents around $x(H_2O) \approx 0.9$, a direct structuring is proposed followed by an unstructured region for very high water contents $x(H_2O) > 0.95$.[23] Note that reaction conditions (16 h and 25 °C) were chosen to prevent full conversion.

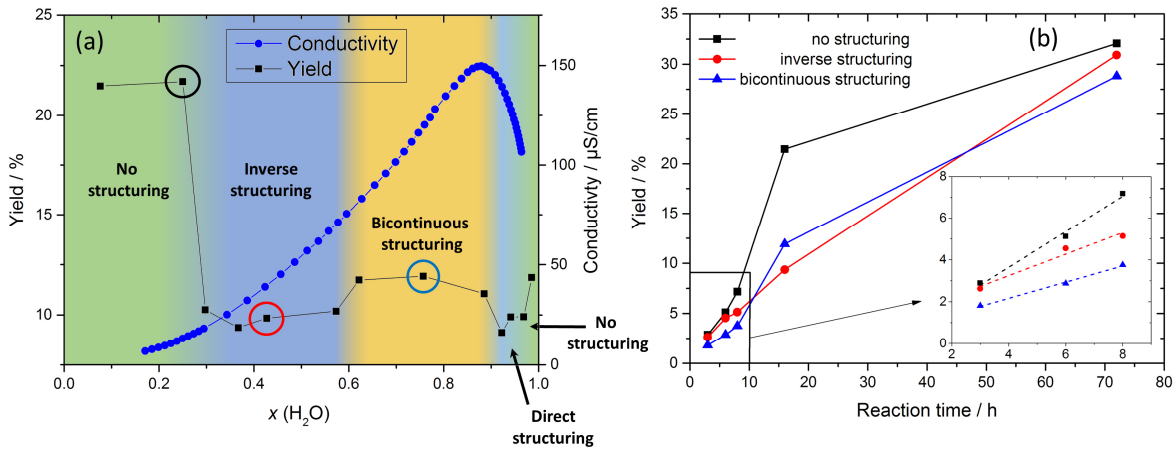

Figure 7.4: (a) Yields of the reaction product, benzyl aldehyde, after 16 h determined by GC-FID with internal standard (black squares), and conductivity measurements for the binary system H_2O/TBA at 25 °C (blue squares). The amount of water of the binary H_2O/alcohol mixture is given in mole fractions of water $x(H_2O)$. Regions of different morphologies of water/TBA (derived from the conductivity curve) are represented by different colours. (b) Yield of benzyl aldehyde as a function of time for a representative unstructured mixture H_2O/TBA ($x(H_2O) = 0.25$), an inversely structured mixture H_2O/TBA ($x(H_2O) = 0.37$) and a bicontinuously structured mixture H_2O/TBA ($x(H_2O) = 0.76$), as indicated by circles in (a). The inset shows linear fits (dotted lines) for the initial conversion for 3 h ≤ t ≤ 8 h.

Relatively high yields (up to 22%) of benzyl aldehyde are observed for the unstructured region at low water content, see Figure 7.4a. In the region where mesoscale inhomogeneities of H_2O/TBA mixtures are found, the yield of benzyl aldehyde decreases to 9-12% for identical reaction times and conditions. Hence, the yield correlates with the formation and presence of mesoscale inhomogeneities. For low water content ($x(H_2O) < 0.3$), the binary mixture H_2O/TBA can be considered as an ideal solvent mixture, *i.e.* a molecular solution, with a distinct contact probability of POMs and BA. There, the yield of benzyl aldehyde doubles compared to structured regions. When the binary mixture H_2O/TBA starts to form mesoscale structures, the reactivity suddenly decreases. This observation may be the result of the different solubility of POMs and BA in the two pseudo-phases.

Since the hydrophilic POMs are mainly dissolved in the water-rich pseudo-phase with a certain affinity to adsorb at interfaces, contact with the hydrophobic BA (mostly solubilised in the TBA-rich pseudo-phase) is reduced. In other words, the solvent compartmentation leads to a different local environment of the reactants, due to their different hydrophilicity/hydrophobicity. The different partition of catalyst and substrate causes a reduced statistical contact of both the catalyst and the substrate and a decrease in the yield of benzyl aldehyde. Accordingly, in case of higher water contents from $x(H_2O) \geq 0.3$, the hydrated POM catalyst and the surrounding water molecules may also be considered as a clathrate-like structure. Such clathrate-like structures are known to change the activity coefficients of water and the POM catalyst. Hence, in this particular case, a change of the mesoscale structure is also associated with a change in water and POM activity due to the formation of a POM/H_2O clathrate-like structure. For very high water contents $x(H_2O) > 0.95$, the absence of mesoscale structure again leads to slightly elevated yields. The difference in absolute yields in the water-rich and TBA-rich unstructured regimes, respectively, may be the consequence of a lower O_2 solubility in the water-rich unstructured regime compared to the TBA-rich unstructured regime, see Figure A6.2 (Appendix A.6) (remember that O_2 is the terminal oxidant and completes the catalytic cycle).

Within the structured region, *i.e.* $0.3 < x(H_2O) < 0.95$, the bicontinuous structuring provides a slightly higher yield compared to the direct and reverse structuring of H_2O and TBA suggesting that the extent of interface might have a subtle influence on the obtained yield. However, the slight differences in yield between 9-12% are not significant enough to draw a clear conclusion.

To further investigate the correlation between the mesoscale structuring of the solvent and the chemical reactivity, additional experiments were performed. (i) Initial reaction rates were

measured for an unstructured, inversely and bicontinuously structured H_2O/TBA mixture and (ii) the reaction was carried out for 72 h instead of 16 h. As can be seen by the kinetics experiments, see Figure 7.4b, initial reaction rates (obtained by linear fitting of data from 3 h ≤ t ≤ 8 h) found for structured H_2O/TBA mixtures (0.48 mmol $(L \cdot h)^{-1}$ for bicontinuous and 0.51 mmol $(L \cdot h)^{-1}$ for inverse structuring), are significantly lower than the one measured for the unstructured H_2O/TBA mixture (0.85 mmol $(L \cdot h)^{-1}$). The corresponding H_2O/TBA solvent compositions are indicated with circles in Figure 7.4a and described in the caption. However, after 72 h, differences of the yield of benzyl aldehyde become less significant and almost constant, see Figure A6.3 (Appendix A.6). Hence, with increasing reaction time, the correlation between solvent structure and yield becomes more and more blurred until the solvent structure does no longer influence the yield.

Consequently, the influence of solvent structuring should be considered as a kinetic effect on the initial period of the conversion. If solvent structuring is present, compartmentation of the reactants within the solvent pseudo-phases can retard the chemical reaction. However, with increasing reaction time these compartmentations do no longer play a major role. This can be mainly attributed to the highly fluctuating nature of such mesoscale structures, which do not allow a complete suppression of the reaction. Thus, reaction yields converge with time to a nearly constant value, irrespective of the solvent structuring. It should be mentioned that the presence of solvent compartmentation remains unchanged irrespective of the benzyl aldehyde concentration as shown with DLS experiments, see Figure A6.4 (Appendix A.6).

In addition, control experiments were performed (i) to compare the reactivity of BA in a mesoscopically structured solvent H_2O/TBA to a mesoscopically unstructured solvent H_2O/EtOH, (ii) to exclude side effects of different oxygen solubility in the H_2O/alcohol mixtures and (iii) to investigate the repeatability of all the experiments.

In case of the unstructured binary solvent H_2O/EtOH, 6-10% of benzyl aldehyde are obtained, see Figure A6.5 (Appendix A.6). The yield slightly decreases with an almost linear dependence with increasing H_2O content. The linear decrease of the benzaldehyde yield with increasing H_2O content may result from different O_2 solubilities in H_2O and EtOH (see Figure A6.2, Appendix A.6). As no (or at least very weak) mesoscopic structuring is present in H_2O/EtOH mixtures, structure induced reactivity changes can be neglected in this case and no steep changes in the yields of benzyl aldehyde are observed by changing the solvent composition.

Furthermore, oxygen solubility measurements (measured for conditions close to those of the reaction) revealed that the oxygen solubility is higher in the alcohol-rich mixtures than in water

(see Figure A6.2, Appendix A.6). Although these findings partly explain the higher initial reactivity in the TBA-rich regions, no direct correlation between oxygen solubility and reactivity or oxygen solubility and mesoscale structuring can be derived. It has to be noted that also the location of oxygen within the mesoscale structured solvents should play a major role for the reactivity, since it reoxidises the catalyst. As the solubility of oxygen increases with increasing alcohol content we can expect that the repartition of O_2 may also be inhomogeneous within the two pseudo-domains. Consequently, an analogous compartmentation effect of O_2 and the POM catalyst is expected, having strong consequences on the reoxidation of the catalyst. At this point, we also want to emphasise that the reoxidation of the POM catalyst by O_2 is not the rate determining step. A depletion in oxygen would be indicated by a deeply black coloured solution of POMs (the well-known heteropoly blue species of reduced POMs with additionally incorporated electrons). However, all reaction mixtures were yellowish during all the reactions performed in this study. Hence, it can be ascertained that all reaction mixtures are saturated with oxygen over the whole period.[42]

Effects of viscosity[22,43] on the other hand can be neglected for both systems, since there is no correlation between viscosity and reactivity for neither the H_2O/TBA nor the H_2O/EtOH mixtures (see Figure A6.6, Appendix A.6).

As a last point, the repeatability of the reactions was probed. To this purpose, the reactions at t = 72 h were performed three times under the same conditions for every binary solvent composition H_2O/TBA. The standard deviation of the obtained yields were calculated for each solvent composition. We found standard deviations for the absolute yield ranging from ±0.7% to ±3.9% (average value of the standard deviation ±1.9%) after 72 h, see Figure A6.3 (Appendix A.6). We expect the standard deviation at 16 hours to be similar to the standard deviations found for 72 hours. Therefore, we assume an average value of the standard deviation of the yields after 16 hours to be at maximum ±4% (absolute yield percent), which is small enough not to question our conclusions.

7.5. Conclusion

We present a systematic study of the influence of mesoscale structuring on a simple model photocatalytic oxidation reaction. We linked the mesoscopic structuring of the binary structured solvent H_2O/TBA to the catalytic efficacy and to the reaction kinetics of the photo-oxidation of BA to the corresponding aldehyde with $H_5PMo_{10}V_2O_{40}$ as catalyst. We also compared the catalytic efficacy of this reaction in the mesoscopically structured solvent

H_2O/TBA to the mesoscopically unstructured (or very weakly structured) solvent H_2O/EtOH. SANS and conductivity measurements unveil that the addition of BA and the catalyst, $H_5PMo_{10}V_2O_{40}$, do not significantly affect the mesoscale structuring of such structured systems. Furthermore, SANS studies suggest that the POM catalyst adsorbs at the interface of the structured system.

Reactivity measurements showed that in case of the binary structured solvent H_2O/TBA, the initial formation of benzyl aldehyde strongly depends on the mesoscopic structuring of the binary solvent H_2O/TBA. In H_2O/TBA mixtures, mesoscale structuration was found to be unfavourable for the photochemical reactivity, compared to unstructured molecular solutions. We conclude that compartmentation of both the organic substrate and the catalyst are unfavourable for the catalytic efficacy. These observations are further reflected by initial rate constant measurements for an unstructured, an inversely structured and a bicontinuously structured mixture H_2O/TBA. However, we further showed that the correlation between solvent structure and reaction rates are even more complex. The correlation of solvent structure and yield must be considered as a kinetic effect, which may change with increasing reaction times, where yields equalise over the whole miscibility range of H_2O/TBA. We explain this observation by the highly fluctuating nature of the mesoscale solvent structures.

In case of the unstructured (or very weakly structured) binary solvent H_2O/EtOH, a linear increase of the yield of benzyl aldehyde is observed for increasing EtOH/H_2O ratios. This linear increase is explained by a higher O_2 solubility in alcohol-rich media.

In summary, we demonstrated that the chemical reactivity in solutions is not solely correlated to the molecular properties of the solvent, but that mesoscale structuring of the solvent plays a major role. Consequently, we suggest reconsidering the general approach of solvent selection for chemical reactions. Mesoscale structuring in solvent mixtures affects the kinetics of chemical reactions and should be considered for optimizing reaction times and reaction conditions.

7.6. References

1 M. B. Smith and J. March, March's Advanced Organic Chemistry: Reactions, Mechanisms, and Structure, John Wiley & Sons, Inc., Hoboken, New Jersey, 7th edn, 2013.

2 L. O. Kononov, *RSC Adv.*, **2015**, *5*, 46718–46734.

3 G. Cainelli, P. Galletti and D. Giacomini, *Chem. Soc. Rev.*, **2009**, *38*, 990–1001.

4 L. O. Kononov, Advances in Chemistry Research, Nova Science Publishers, Inc., Hauppauge, New York, 2013, vol. 18, pp. 143–177.

5 Y. L. Khmelnitsky, A. V. Levashov, N. L. Klyachko and K. Martinek, *Enzyme Microb. Technol*., **1988**, *10*, 710–724.

6 R. Breslow, *Acc. Chem. Res*., **1991**, *24*, 159–164.

7 S. Otto and J. B. F. N. Engberts, *Org. Biomol. Chem*., **2003**, *1*, 2809–2820.

8 J. N. Israelachvili, Intermolecular and Surface Forces, Elsevier, Inc., Amsterdam, 3rd edn, 2011.

9 D. F. Calef and J. M. Deutch, *Annu. Rev. Phys. Chem.*, **1983**, *34*, 493–524.

10 D. S. Achilias, Macromol. *Theory Simul.*, **2007**, *16*, 319–347.

11 W. Adam and A. V. Trofimov, *Acc. Chem. Res.*, **2003**, *36*, 571–579.

12 O. Diat, M. L. Klossek, D. Touraud, B. Deme, I. Grillo, W. Kunz and T. Zemb, *J. Appl. Crystallogr.*, **2013**, *46*, 1665–1669.

13 V. Fischer, J. Marcus, D. Touraud, O. Diat and W. Kunz, *J. Colloid Interface Sci.*, **2015**, *453*, 186–193.

14 M. L. Klossek, D. Touraud, T. Zemb and W. Kunz, *ChemPhysChem*, **2012**, *13*, 4116–4119.

15 T. Lopian, S. Schöttl, S. Prevost, S. Pellet-Rostaing, D. Horinek, W. Kunz and T. Zemb, *ACS Cent. Sci*., **2016**, *2*, 467–475.

16 J. Marcus, D. Touraud, S. Prevost, O. Diat, T. Zemb and W. Kunz, *Phys. Chem. Chem. Phys.*, **2015**, *17*, 32528–32538.

17 S. Schöttl, J. Marcus, O. Diat, D. Touraud, W. Kunz, T. Zemb and D. Horinek, *Chem. Sci.*, **2014**, *5*, 2949–2954.

18 T. Zemb, M. L. Klossek, T. Lopian, J. Marcus, S. Schöttl, D. Horinek, S. Prevost, D. Touraud, O. Diat, S. Marčelja and W. Kunz, *Proc. Natl. Acad. Sci. U. S. A*., **2016**, *113*, 4260–4265.

19 D. Subramanian and M. A. Anisimov, *Fluid Phase Equilib.*, **2014**, *362*, 170–176.

20 M. Sedlák and D. Rak, *J. Phys. Chem. B*, **2014**, *118*, 2726–2737.

21 J. Marcus, M. L. Klossek, D. Touraud and W. Kunz, *Flavour Fragrance J.*, **2013**, *28*, 294–299.

22 P. K. Kipkemboi and A. J. Easteal, *Can. J. Chem.*, **1994**, *72*, 1937–1945.

23 T. Buchecker, S. Krickl, R. Winkler, I. Grillo, P. Bauduin, D. Touraud, A. Pfitzner and W. Kunz, *Phys. Chem. Chem. Phys.*, **2017**, *19*, 1806–1816.

24 R. F. Hankel, P. E. Rojas,M. Cano-Sarabia, S. Sala, J. Veciana, A. Braeuer and N. Ventosa, *Chem. Commun.*, **2014**, *50*, 8215–8218.

25 U. Mohorič, A. Beutner, S. Krickl, D. Touraud, W. Kunz and F.-M. Matysik, *Anal. Bioanal. Chem.*, **2016**, *408*, 8681–8689.

26 V. Tchakalova, T. Zemb and D. Benczédi, *Colloids Surf. A*, **2014**, *460*, 414–421.

27 Y. L. Khmelnitsky, R. Hilhorst and C. Veeger, *Eur. J. Biochem.*, **1988**, *176*, 265–271.

28 Y. L. Khmelnitsky, A. K. Gladilin, I. N. Neverova, A. V. Levashov and K. Martinek, *Collect. Czech. Chem. Commun.*, **1990**, *55*, 555–563.

29 Y. L. Khmelnitsky, I. N. Zharinova, I. V. Berezin, A. V. Levashov and K. Martinek, *Ann. N. Y. Acad. Sci.*, **1987**, *501*, 161–164.

30 Y. L. Khmelnitsky, A. Van Hoek, C. Veeger and A. J. W. G. Visser, *J. Phys. Chem.*, **1989**, *93*, 872–878.

31 M. Zoumpanioti, H. Stamatis, V. Papadimitriou and A. Xenakis, *Colloids Surf. B*, **2006**, *47*, 1–9.

32 O. A.Kazantsev,D. S. Baruta, K. V. Shirshin, A. P. Sivokhin and D. M. Kamorin, *Russ. J. Phys. Chem. A*, **2010**, *84*, 2071–2076.

33 O. A. Kazantsev, A. P. Sivokhin, D. S. Baruta, K. V. Shirshin, D. M. Kamorin and A. I. Kvashennikov, *Polym. Sci. Ser. D*, **2011**, *4*, 284–288.

34 G. B. Manelis, G. V. Lagodzinskaya, A. I. Kazakov, A. V. Chernyak, N. G. Yunda and L. S. Kurochkina, *Russ. Chem. Bull.*, **2013**, *62*, 994–1002.

35 R. P. Tiger, M. A. Levina, S. G. Entelis and M. A. Andreev, *Kinet. Catal*., **2002**, *43*, 662–666.

36 G. A. Tsigdinos and C. J. Hallada, *Inorg. Chem*., **1968**, *7*, 437–441.

37 D. Barats-Damatov, L. J. W. Shimon, Y. Feldman, T. Bendikov and R. Neumann, *Inorg. Chem*., **2015**, *54*, 628–634.

38 C. D. Dewhurst, I. Grillo, D. Honecker, M. Bonnaud, M. Jacques, C. Amrouni, A. Perillo-Marcone, G. Manzin and R. Cubitt, *J. Appl. Crystallogr*., **2016**, *49*, 1–14.

39 https://www.ill.eu/instruments-support/computing-for-science/cs-software/all-software/lamp/.

40 B. Naskar, O. Diat, V. Nardello-Rataj and P. Bauduin, *J. Phys. Chem. C*, **2015**, *119*, 20985–20992.

41 T. Buchecker, X. LeGoff, B. Naskar, A. Pfitzner, O. Diat and P. Bauduin, *Chem. – Eur. J*., **2017**, *23*, 8434–8442.

42 M. T. Pope and A. Müller, *Angew. Chem., Int. Ed. Engl*., **1991**, *30*, 34–48.

43 I. S. Khattab, F. Bandarkar, M. A. A. Fakhree and A. Jouyban, *Korean J. Chem. Eng*., **2012**, *29*, 812–817.

Chapter 8 Diels–Alder reactions accelerated "on water" – SFME versus SFE

8.1. Preface and abstract

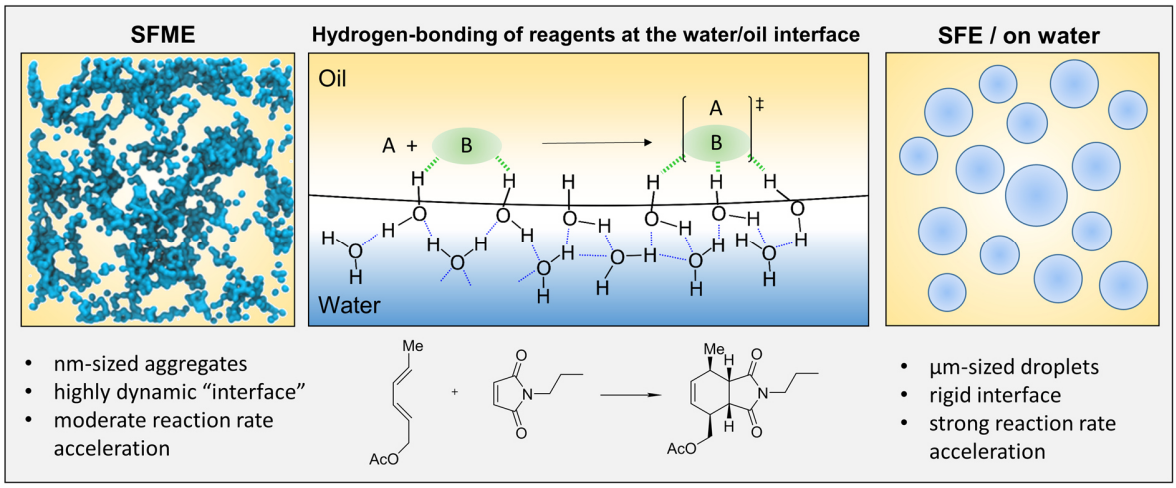

Figure 8.1: Graphical abstract showing the proposed mechanism responsible for reaction rate accelerations of Diels–Alder cycloadditions on water, in SFME and in SFE.

Kinetics of the Diels–Alder cycloaddition of *trans*,*trans*-2,4-hexadienyl acetate (HDA) and *N*-(*n*-propyl)maleimide (NPMI) were investigated in different solvents. To this purpose, different surfactant-free microemulsions and emulsions (SFME/SFE) were formed with water, HDA and NPMI (each 1 mol L^{-1} in the final mixtures) and a water-miscible aliphatic alcohol (methanol, MeOH, ethanol, EtOH, *n*-propanol, NPA and *tert*-butanol, TBA). COSMO-RS calculations were used to determine liquid-liquid equilibria (LLE) of the pseudo-ternary phase diagrams and mesoscale structuring of SFME was investigated using dynamic light scattering (DLS). It was found that reactions are most accelerated when performed in SFE. Moreover, LLE play a major role for efficient acceleration of the reaction. Consequently, the presence of a macroscopic interface to an aqueous solution was found to have a decisive influence on the reaction kinetics (see Figure 8.1).

Contributions to the experimental work:

- Dynamic light scattering experiments and measurement of reaction kinetics: S. Krickl
- COSMO-RS calculations: M. Hahn

8.2. Introduction

In water, *in the presence of water*, *on water*? Such terms can be found in an almost exponentially increasing number of articles dealing with organic reactions in aqueous media.[1-29] It has been known for a long time that the addition of water to reacting organic compounds can have significant effects on an organic reaction, *i.e.* reaction rate acceleration and/or enhanced stereoselectivity.[1,2,13,23,24] However, the group of Sharpless was one of the first who presented a systematic investigation into these phenomena in 2005.[7] They found tremendous rate acceleration (of factors up to 100 and higher) for a great variety of reactions performed *on water*, including for instance Diels–Alder reactions, 1,3-dipolar cycloadditions and Claisen rearrangements.[7,23] In this context, the term *on water* means that the reaction is performed in an emulsion between water and the organic reagents, which are not miscible with each other, resulting in two emulsified macroscopic phases upon stirring. In contrast, reactions *in water* are related to reactions in a homogenous solution of the reagents in water used as a solvent in its classical meaning. On the other hand, the term *in the presence of water* is ambiguous. However, usually it is an equivalent term for reactions performed on water.[11] A typical example for a Diels–Alder reaction accelerated on water performed by the working group of Sharpless is presented in Figure 8.2.[7,23] They investigated the cycloaddition of *trans*,*trans*-2,4-hexadienyl acetate (HDA) and *N*-(*n*-propyl)maleimide (NPMI) in different solvents and on water. A substantial rate acceleration could be observed in aqueous dispersion (emulsion) over homogeneous solution. Furthermore, the reaction rate was found to be higher in a protic solvent such as methanol than in non-protic solvents such as acetonitrile and toluene (see Table 8.1).[7,10]

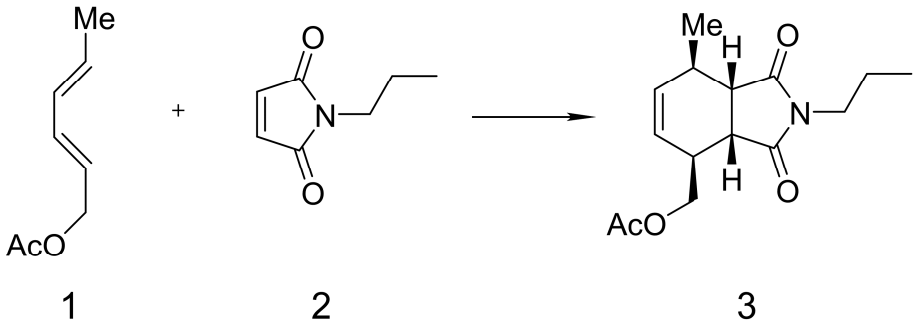

Figure 8.2: Typical Diels–Alder reaction accelerated on water of *trans*, *trans*-2,4-hexadienyl acetate (1) and *N*-(*n*-propyl)maleimide (2) as investigated by Sharpless *et al*.[7]

Table 8.1: Comparison of the Diels–Alder reaction of HDA and NPMI performed in different organic solvents and on water.[7]

Solvent	Concentration mol L^{-1}	Time to completion h	Yield %
toluene	1	144	79
acetonitrile	1	>144	43[a]
methanol	1	48	82
neat	3.69[b]	10	82
on water	3.69[b]	8	81

a: Yield after chromatographic purification. Other yields are of crude products, which were > 95% pure by ^{1}H-NMR spectroscopy. b: Calculated from the measured density of a 1:1 mixture of HDA and NPMI.

Yet, the reasons for the acceleration of such reactions in or on water are not fully understood. It is suggested that hydrogen bonding and hydrophobic effects may both be important for the observed rate acceleration.[10] Nevertheless, one has to distinguish several effects, which may occur simultaneously and have a competitive or mutually enhancing impact on reactivity in aqueous solution. Considering homogenous reactions in water, three effects are likely to prevail, according to Butler *et al.*[24]:

(i) the Breslow hydrophobic effect

(ii) hydrogen-bonding effects

(iii) polarity effects

The Breslow hydrophobic effect (i) describes aggregation of organic solutes, caused by hydrophobic interactions between the organic molecules minimizing energetically less favoured contact with water molecules (see Figure 8.3a).[5,14,21,23,24,27] This effect is considered to be always positive for rate acceleration of organic reactions. Yet, considerations on hydrophobic effects in these studies are rather restricted to the point of view of organic chemistry. For a more thorough, physicochemical approach to this issue, the reader is referred to the work of A. Ben-Naim.[30,31] Hydrogen-bonding effects (ii) on the other hand are caused by hydrogen bond donor and acceptor interactions directly influencing the energetic levels of the highest occupied molecular orbital (HOMO) and the lowest unoccupied molecular orbital (LUMO) and thus the HOMO-LUMO gap of the transition state.[24] Such interactions may add to or oppose the hydrophobic effect. The same is true for the polarity effect (iii). This effect is usually explained by the polarity of the solvent, the initial and the transition state. Water is a highly polar solvent, thus reactions with transition states more polar than the initial states will be sped up in water and slowed down when the transition states are less polar than the initial states.[24] Yet, it remains unclear if water is able to influence the polarity of the transition state

by itself or not. Such effects can be expected to take place not only in homogenous reactions in water. In fact, they may always occur for reactions in and also on water, since there is always a slight solubility of water in the organic reagents.

Moreover – for reactions on water – one has to take also effects into account, which may only take place and/or are enhanced at a given interface between the reagents and water. Most important in this context may be the trans-phase hydrogen-bonding effect described by Jung and Marcus in 2007.[14,24] Regarding two macroscopic phases with a common large interface, some water molecules have a free OH-group directed at the oil-boundary (see Figure 8.3b). In contrast, small hydrophobic aggregates formed due to hydrophobic effects can be fully enclosed by hydration water clusters with lateral H-bonds along the molecular boundary. Consequently, such protons can provide catalytic sites strongly affecting the transition state and/or induce a pre-orientation of the reagents at the interface. Beattie *et al*. went even a step further, stating an acid-catalysis mechanism facilitated by strong adsorption of the hydroxide ion by-product at the water-oil interface.[20] However, a full proton transfer remains questionable.

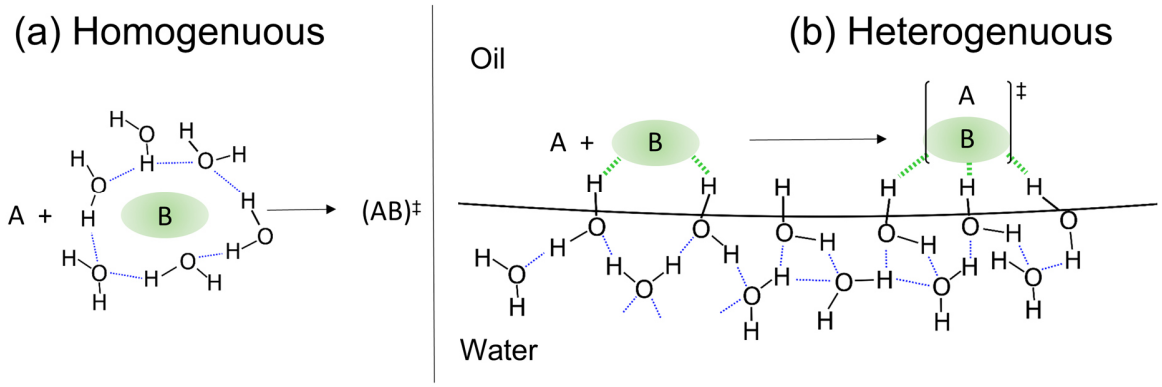

Figure 8.3: Summarizing scheme showing different H-bond networks occurring in (a) heterogenous and (b) homogenous solutions of water and hydrophobic reagents (redrawn from Jung *et al*.[14]).

Although many studies exist on the understanding of the mechanism of on water reactions, all aspects of the mechanisms and effects occurring for reactions performed on water have not been fully understood yet. Nevertheless, since the presence of a water/oil interface was undoubtedly found to be greatly beneficial for the rate enhancement of several Diels–Alder reactions, an increase of the surface area of such an interface should be helpful for further enhancing the reaction kinetics. Indeed, the way of homogenisation has a tremendous influence on the reaction rate in the expected way.[20] In other words, a high degree of dispersion has to be achieved for high reaction rates. Regarding the mesoscopic

compartmentation of water- and oil-rich domains in surfactant-free microemulsions (SFME), it seems evident that such kind of structured liquids could tremendously increase the surface area of the water/oil interface without considerable effort.[32] Thus, the question raises, if SFME could be used as efficient reaction media for on-water reactions in homogenous solutions. To this purpose, the reaction kinetics of the Diels–Alder cycloaddition of HDA and NPMI were investigated in different SFME and surfactant-free emulsions (SFE) composed of 1 mol L^{-1} of each reagent in water/alcohol mixtures.

8.3. Experimental

8.3.1. Chemicals

Ethanol (EtOH, ≥ 99.8%), *tert*-butanol (TBA, ≥ 99.7%), *trans*,*trans*-2,4-hexadienyl acetate (HDA, 97%) and chloroform-d (99.8 atom% deuterated) were purchased from Sigma-Aldrich (Steinheim, Germany). Methanol (MeOH, ≥ 99.9%) and *n*-propanol (NPA, ≥ 99.5%) were obtained from Merck (Darmstadt, Germany) and *N*-(*n*-propyl)maleimide (NPMI, 94%) from Alfa Aesar (Heysham, UK).

8.3.2. Methods and techniques

8.3.2.1. COSMO-RS calculations of liquid-liquid phase equilibria

Experimental determination of phase diagrams and liquid-liquid phase equilibria (LLE) was not possible, due to the ongoing reaction of HDA and NPMI after mixing. Thus, LLE were calculated with the aid of COSMO-RS (conductor-like screening model for realistic solvation) based calculations using COSMOtherm software. LLE calculations for the evaluated pseudo-ternary systems were performed on FINE level with a TZVPD basis set.

8.3.2.2. Dynamic light scattering

Dynamic light scattering (DLS) experiments were performed as described in Section 2.3.2.2.

8.3.2.3. Measurement of reaction kinetics

Reactions were performed at room temperature in 10 mL round-bottom flasks under permanent stirring (constant stirring rate of 800 rpm for all solutions). To this purpose, 0.5 g of an equimolar mixture of HDA and NPMI was diluted with solvent (alcohol, water or alcohol/water mixtures) resulting in a total concentration of each, HDA and NPMI, of 1 mol L^{-1}.

Samples were taken after 2, 4, 6 and 8 hours and the yield of the reaction was determined using ^{1}H-NMR spectrometry (Bruker Avance 300MHz NMR spectrometer) in $CDCl_3$. Residual water, which did not mix with $CDCl_3$ was removed prior to the measurement using a benchtop centrifuge. Reaction rate constants k were obtained by fitting the data with a second order kinetics model: $y(t) = 1 - 1/(1 + kt)$ with $y(t)$ being the yield expressed as molar ratio of product to starting material. All rate constants k were finally normalised as k/k_{pure} to the reaction rate constant k_{pure} obtained from the reaction of the pure reagents (HDA +NPMI).

8.4. Results and discussion

8.4.1. Ternary phase diagrams and structural investigation

Since tie lines and even ternary phase diagrams of the pseudo-ternary systems water/alcohol/reagents (HDA and NPMI) could not be determined, due to rapid reaction of the reagents, COSMO-RS calculations were performed instead. Results of the calculations are depicted in Figure 8.4 together with the sample compositions used for the reaction kinetic measurements of the Diels–Alder reaction between HDA and NPMI. It can be easily seen that all phase diagrams show a similar miscibility gap closing at an alcohol content of around 50 wt%. The largest monophasic areas are observed for pseudo-ternary mixtures containing EtOH and TBA, the smallest for MeOH and NPA. However, differences are not very significant. More pronounced distinctions can be found regarding the slope of the tie lines. Mixtures with MeOH and EtOH tend to demix to an almost pure reagent-rich phase and an aqueous solution of the alcohol containing minor amounts of reagents. The critical point was found to be at the water-poor side of the phase diagram. For mixtures containing NPA and TBA, the slopes of the tie lines are significantly different.The critical point was found to be at the water-rich side and demixing tends to the formation of relatively pure aqueous phase and a mixture of alcohol and the reagents. For very low water contents (*w*(water) < 0.2), differences between the tie lines for all calculated phase diagrams vanish more and more, leading to similar slopes of the tie lines for all ternary mixtures, independent of the used alcohol.

In addition, DLS experiments were performed for three mixtures containing water, HDA/NPMI (molar ratio 1:1) and alcohol (EtOH, NPA and TBA), see Figure 8.5. All samples contained 1 mol L^{-1} of each reagent and the ratio of alcohol to water was kept constant at 80/20 (*w*/*w*). It has to be noted that an equivalent mixture with MeOH was found to be biphasic and was

consequently not measured. Results obtained by DLS show a successively increasing correlation function going from EtOH to NPA and TBA with a shift to higher decay times. This indicates the presence of SFME for all three mixtures, with increasing size domains of compartmentations in the order: EtOH < NPA < TBA. This result is evident, since HDA and NPMI are extremely hydrophobic components and consequently a more amphiphilic hydrotrope is needed to form well-structured SFME (as discussed in Chapters 2 and 3).

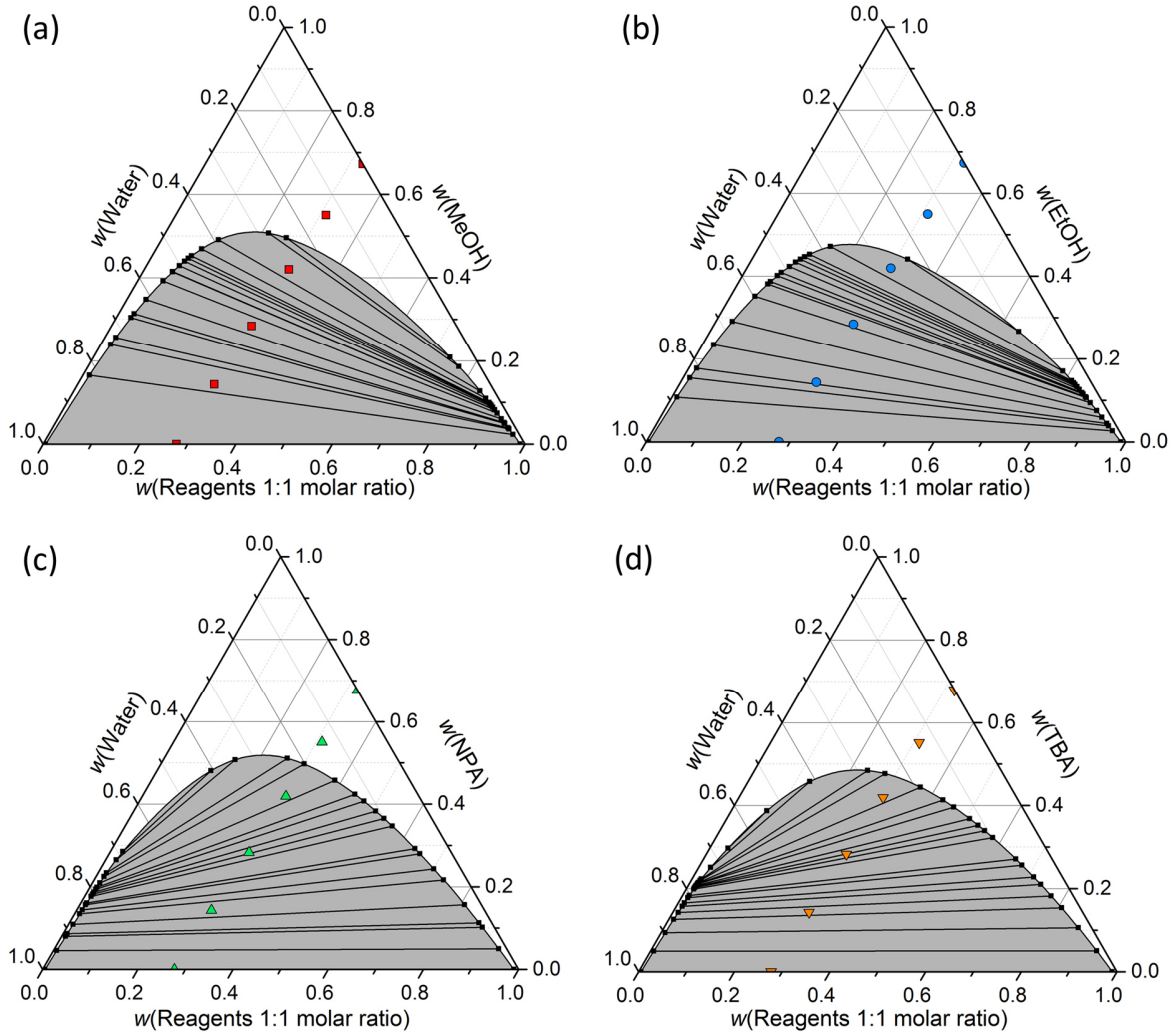

Figure 8.4: Ternary phase diagrams of (a) water/MeOH/reagents, (b) water/EtOH/reagents, (c) water/NPA/reagents and (d) water/TBA/reagents at 25 °C with corresponding tie lines (black solid lines and squares) calculated with COSMO-RS. Coloured symbols denote the sample compositions chosen for the investigation of reaction kinetics with ratios of water/alcohol of 0/100, 20/80, 40/60, 80/20 and 100/0 (*w*/*w*). Mono- and biphasic areas are represented as white and grey areas, respectively.

However, it is worth noting none of the obtained correlation functions can be described by a single-exponential decay, indicating a more complex structuring than usually observed for SFME. Unfortunately, DLS cannot provide detailed information on these findings. Nevertheless, the most important fact is that mesoscale structured liquids can be formed for such pseudo-ternary compositions, creating large interface areas between water- and oil-rich compartments, which can in principle enhance rate acceleration of the Diels–Alder cycloaddition of HDA and NPMI, as discussed before.

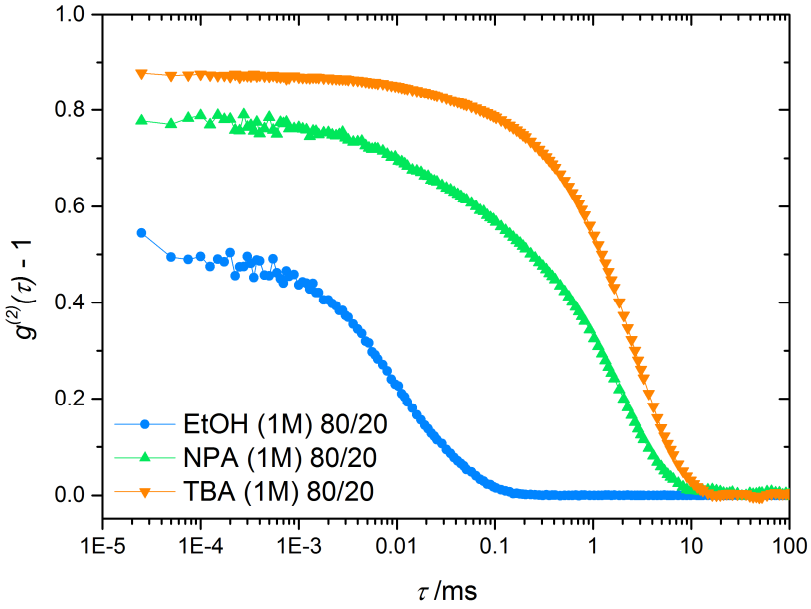

Figure 8.5: Normalised autocorrelation functions of intensity obtained by DLS measurements at 25°C for the pseudo-ternary mixtures of 1 mol L^{-1} HDA and NPMI in alcohol/water mixtures with EtOH, NPA and TBA. Numbers represent the weight fractions of the alcohol/water (solvent) given in percentage.

8.4.2. Kinetic measurements and correlation of reactivity and solution structure

Normalised reaction rate constants k/k_{pure} for the Diels–Alder reactions of HDA and NPMI for different solvent compositions are shown in Figure 8.6. It can be seen that reaction rates increase for all alcohols with increasing water content. Maxima were found for all pseudo-ternary mixtures in the biphasic region (Ouzo region or surfactant-free emulsions, SFE). The reaction “on water” leads to an acceleration of approximately 40% compared to the reaction of the pure components, which is in good accordance with results reported by the working group of Sharpless.[7] It was found that EtOH/MeOH containing mixtures and NPA/TBA containing mixtures lead to similar reaction rates with EtOH/MeOH > NPA ≥ TBA. For monophasic compositions, best results were found for EtOH containing mixtures

(w_{water}(solvent) = 0.2) leading to similar reactivity as obtained for the pure components (however, concentrations of the reagents were only 1 mol L^{-1} compared to 3.69 mol L^{-1} for the pure components).

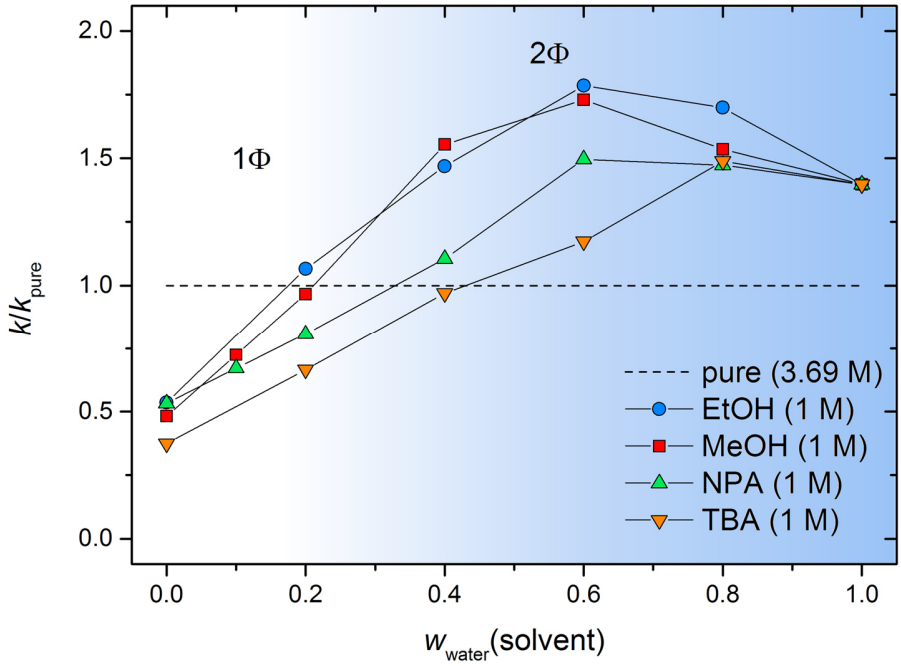

Figure 8.6: Normalised reaction rate constants k/k_{pure} for the Diels–Alder reaction of HDA and NPMI as a function of the water content of the added water/alcohol mixture (solvent), see also Figure 8.4. Reactions were performed at room temperature. Symbols denote the different reaction rate constants for different alcohols used in the added water/alcohol mixture. The dashed horizontal line is a visual guide line illustrating the reaction rate of the pure components. White and blue areas represent the monophasic and biphasic compositions, respectively. All mixtures were found to be biphasic or at least turn into a biphasic mixture during the reaction for a water content w_{water}(solvent) ≥ 0.4. For mixtures containing MeOH, the biphasic region already starts at w_{water}(solvent) ≥ 0.2.

It can be easily seen that macroscopic phase separation is essential for a major improvement of the reaction velocity. The occurrence of maxima may be explained by the formation of a finer dispersion (SFE) compared to reaction mixtures “on water”. In other words, a compromise between high water-content and high degree of dispersion has to be found for optimum reaction conditions. Differences in reaction rates found between the four alcohols can be explained by the slope of the tie lines in the pseudo-ternary phase diagram. For EtOH and MeOH containing reaction mixtures, phase separation leads always to the formation of an aqueous and almost pure reagent-rich phase (high concentration of the reagents). On the other hand, NPA and TBA based reaction mixtures rather separate in a reagent-rich phase, which is much more diluted with NPA and TBA, resulting in decreasing reaction rates. In addition, NPA and TBA have a more amphiphilic character. Consequently, it is more likely that

NPA and TBA have a stronger tendency to accumulate at the interface water/oil. Thus, the contact to free OH-groups of water molecules located in the aqueous phase is reduced. However, for a high water content (w_{water}(solvent) > 0.8), similar slopes of the tie-lines were calculated explaining that differences of reaction rates between the reaction mixtures are less pronounced, independently of the used alcohol. This separation behaviour may be also reflected in the monophasic region for the different pseudo-phases typically found for SFME, which could analogously explain differences of the reaction rates in the monophasic region.
However, several other considerations may explain why the used SFME are not able to accelerate the reaction rate in a comparable efficiency as biphasic mixtures do. (i) Aggregates formed in SFME composed of water/alcohol/reagents are probably too fluctuating in order to efficiently accelerate the reaction. In other words, reorientation of available free OH-groups of water molecules is too fast for efficient stabilisation of the transition state, as shown in Figure 8.3b. Furthermore (ii), it is likely that the water content available in the aqueous pseudo-phase is too low for a substantial increase of the reaction rates in the investigated SFME (over 70 wt% of the solvent is alcohol). (iii) The alcohol creates a barrier between water- and oil-rich domains. Consequently, contact to free OH-groups of water molecules located in the aqueous phase is reduced, as explained above.

8.5. Conclusion and outlook

Results presented in this study show that the presence of a macroscopic rigid interface between an aqueous and a preferentially pure reagent-rich phase is a basic prerequisite for efficient reaction rate acceleration of on-water reactions. This was achieved forming SFE containing water, alcohol and the reagents with an adequate ratio of water/alcohol in order to provide enough free water at the interface with preferably high degree of dispersion of the emulsion. Consequently, the amount of water molecules at the interface able to interact with the reagents was maximised. Besides, the slopes of the tie lines were found to be an important parameter for the reaction kinetics in biphasic reaction media, which are favoured for demixing that results in a relatively pure reagent-rich phase. The findings support recently proposed considerations by Jung and Marcus on catalysis occurring when reactions are performed on water.[14] In other words, free OH-Groups can interact at a macroscopic interface (water/reagents) with the reacting molecules or transition state and/or induce a pre-orientation of the reagents. These interactions are seemingly favoured at a macroscopic interface compared to highly dynamic interfaces between aqueous and hydrophobic pseudo-phases

typically occurring in SFME. Furthermore, it is likely that due to the relatively high amount of hydrotrope needed to form the SFME, the interface gets blocked by the amphiphile. This suggestion is further supported by the fact that reactions were found to be less accelerated in the presence of hydrotropes with a more pronounced amphiphillic character (TBA/NPA vs. EtOH/MeOH). Furthermore, findings presented in this work are in good accordance with early studies on this topic, in which SFME were already tested as reaction media for catalysis of Diels–Alder reactions.[2,33] However, a systematic study as presented in this work has not been done before.

Based on the results presented in this study, there are various other experiments worth to take into consideration. Since a large, rigid interface with available free OH-groups obviously favours reaction kinetics, reactions of the pure reagents in the presence of silica-nanoparticles may be of particular interest. Silica nanoparticles generally provide free OH-groups at their surface and the use of nanoparticles provides a large surface area when suspended in the pure reagents (see Figure 8.7). Thus, significant rate acceleration may be the consequence. First studies on this topic performed by Weinstein *et al.* already support this assumption.[34] Even modified silica particles with hydrophobic surfaces could be used as a sort of control experiment. In this context, kinetic experiments could be of interest, comparing reactions on water and on water plus a surface active component, which blocks the interface.

Furthermore, reactions in the presence of extremely polar solvents, like *N*-methylformamide could clarify, if exclusively H-Bond interactions are responsible for the unique reactivity on water. Moreover, also more complex reaction media like SBME, ionic liquids or salt containing solvents may provide new insights to this issue, as some studies already demonstrated.[25,26,29,35,36] All in all, such experiments are considered to contribute to a deeper understanding of chemical reactivity in and on water.

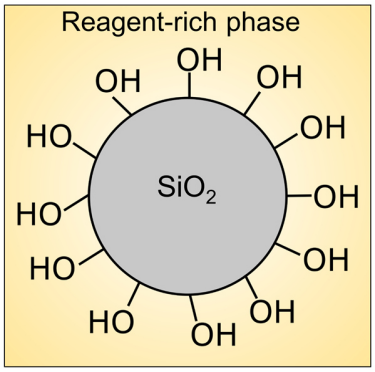

Figure 8.7: Schematic representation of the interface of a silica nanoparticle suspended in hydrophobic reagents.

8.6. References

1 D. C. Rideout and R. Breslow, *J. Am. Chem. Soc.*, **1980**, *102*, 7816–7817.

2 R. Breslow, U. Maitra and D. Rideout, *Tetrahedron Lett.*, **1983**, *24*, 1901–1904.

3 J. B. F. N. Engberts, *Pure Appl. Chem.*, **1995**, *67*, 823–828.

4 T. Rispens and J. B. F. N. Engberts, *Org. Lett.*, **2001**, *3*, 941–943.

5 S. Otto and J. B. F. N. Engberts, *Org. Biomol. Chem.*, **2003**, *1*, 2809–2820.

6 R. Breslow, *Acc. Chem. Res.*, **2004**, *37*, 471–478.

7 S. Narayan, J. Muldoon, M. G. Finn, V. V. Fokin, H. C. Kolb and K. B. *Sharpless, Angew. Chemie - Int. Ed.*, **2005**, 44, 3275–3279.

8 J. E. Klijn and J. B. F. N. Engberts, *Nature*, **2005**, *435*, 746–747.

9 S. Tiwari and A. Kumar, *Angew. Chemie*, **2006**, *118*, 4942–4943.

10 C.-J. Li and L. Chen, *Chem. Soc. Rev.*, **2006**, *35*, 68–82.

11 Y. Hayashi, *Angew. Chemie - Int. Ed.*, **2006**, *45*, 8103–8104.

12 S. Narayan, V. V. Fokin and K. B. Sharpless, in Organic Reactions in Water: Principles, Strategies and Applications, ed. U. M. Lindström, Blackwell Publishing, 2007, pp. 350–365.

13 R. Breslow and U. Maitra, *Tetrahedron Lett.*, **1984**, *25*, 1239–1240.

14 Y. Jung and R. A. Marcus, *J. Am. Chem. Soc.*, **2007**, *129*, 5492–5502.

15 N. Windmon and V. Dragojlovic, *Green Chem. Lett. Rev.*, **2008**, *1*, 155–163.

16 S. Minakata and M. Komatsu, *Chem. Rev.*, **2009**, *109*, 711–724.

17 M. Gruttadauria, F. Giacalone and R. Noto, *Adv. Synth. Catal.*, **2009**, *351*, 33–57.

18 L. L. Thomas, J. Tirado-Rives and W. L. Jorgensen, *J. Am. Chem. Soc.*, **2010**, *132*, 3097–3104.

19 M.-O. Simon and C.-J. Li, *Chem. Soc. Rev.*, **2012**, *41*, 1415–1427.

20 J. K. Beattie, C. S. P. McErlean and C. B. W. Phippen, *Chem. - A Eur. J.*, **2010**, *16*, 8972–8974.

21 M. B. Gawande, V. D. B. Bonifácio, R. Luque, P. S. Branco and R. S. Varma, *Chem. Soc. Rev.*, **2013**, *42*, 5522–5551.

22 K. Karhan, R. Z. Khaliullin and T. D. Kühne, *J. Chem. Phys.*, **2014**, *141*.

23 A. Chanda and V. V. Fokin, *Chem. Rev.*, **2009**, *109*, 725–748.

24 R. N. Butler and A. G. Coyne, *Chem Rev.*, **2010**, *110*, 6302–6337.

25 P. A. Grieco, J. J. Nunes and M. D. Gaul, *J. Am. Chem. Soc.*, **1990**, *112*, 4595–4596.

26 R. Breslow and C. J. Rizzo, *J. Am. Chem. Soc.*, **1991**, *113*, 4340–4341.

27 R. Breslow, *Acc. Chem. Res.*, **1991**, *24*, 159–164.

28 U. Pindur, G. Lutz and C. Otto, *Chem. Rev.*, **1993**, *93*, 741–761.

29 C. K. Pai and M. B. Smith, *J. Org. Chem.*, **1995**, *60*, 3731–3735.

30 A. Ben-Naim, Hydrophobic interactions, Plenum Press, New York, 1980.

31 A. Ben-Naim, *J. Chem. Phys.*, **1989**, *90*, 7412–7425.

32 T. Lopian, S. Schöttl, S. Prevost, S. Pellet-Rostaing, D. Horinek, W. Kunz and T. Zemb, *ACS Cent. Sci.*, **2016**, *2*, 467–475.

33 A. Gonzalez and S. L. Holt, *J. Org. Chem.*, **1982**, *47*, 3186–3188.

34 R. D. Weinstein, A. R. Renslo, R. L. Danheiser and J. W. Tester, *J. Phys. Chem. B*, **1999**, *103*, 2878–2887.

35 J. B. F. N. Engberts, E. Fernandez, L. Garcia-Rio and J. R. Leis, *J. Org. Chem.*, **2006**, *71*, 4111–4117.

36 H. Lü, X. An, J. Yu and X. Song, *J. Phys. Org. Chem.*, **2012**, *25*, 1210–1216.

Chapter 9 Enzyme activity of horseradish peroxidase in surfactant-free microemulsions

9.1. Preface and abstract

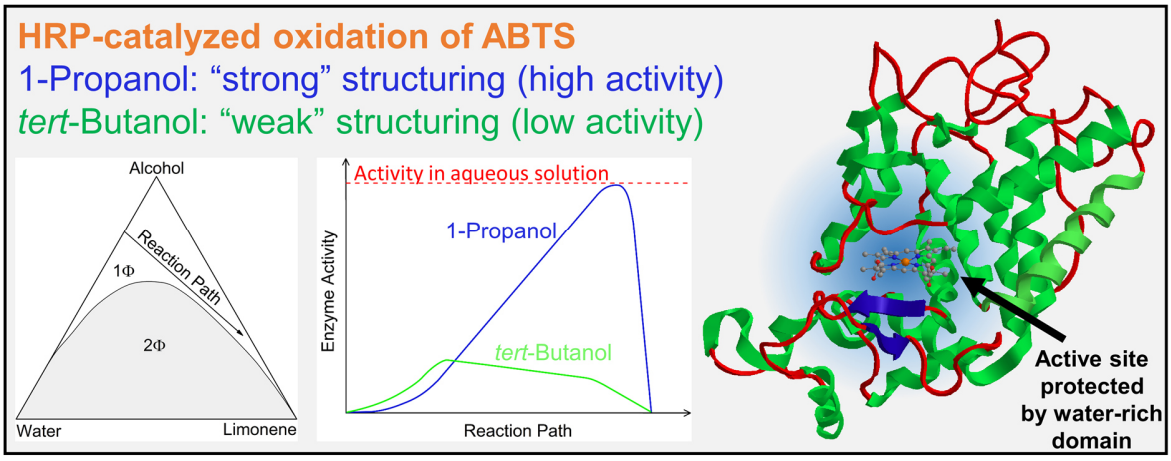

Figure 9.1: Graphical abstract schematically illustrating different enzyme activity of HRP in NPA-based and TBA-based SFME.

In the present contribution, we investigated the influence of the structuring of surfactant-free microemulsions (SFME) (water/1-propanol/limonene and water/*tert*-butanol/limonene) on the enzyme activity of horseradish peroxidase (HRP). To this purpose, the oxidation of 2,2’-azino-bis(3-ethylbenzo thiazoline-6-sulphonic acid) diammonium salt (ABTS) with hydrogen peroxide was chosen as a model reaction. Enzymatic activities in SFME of varying compositions were investigated by UV-Vis spectroscopy and compared to the enzyme activity in pure buffer solution. Dynamic light, small-angle X-ray scattering and conductivity measurements were performed in order to obtain structural information on the used SFME. Findings presented in this study revealed that the ability of short-chain alcohols to form mesostructures (aqueous aggregates in oil) has a crucial effect on the enzyme activity in SFME (see Figure 9.1). Mesoscale structuring with 1-propanol (NPA) was found to be more pronounced than with the more hydrophobic *tert*-butanol (TBA). It was concluded that the most pronounced mesoscale-structured SFME lead to the highest enzymatic activities.

This chapter has been published in *Journal of Colloid and Interface Science* (S. Krickl, D. Touraud, P. Bauduin, T. Zinn and W. Kunz, *J. Colloid Interface Sci.*, **2018**, *516*, 466–475.)

Contributions to the experimental work:

- Ternary phase diagram: S. Krickl
- Measurements of enzyme activity: S. Krickl
- Dynamic light scattering: S. Krickl
- Conductivity measurements: S. Krickl
- Small-angle X-ray scattering: S. Krickl, P. Bauduin and T. Zinn

9.2. Introduction

In the last few years, significant advance was made in the structural investigation and understanding of surfactant-free microemulsions (SFME).[1-13] It was observed that such mesoscale structured liquids show distinct compartmentation phenomena of aliphatic-rich and water-rich domains on the nm-scale. Such mixtures are easy to prepare, homogeneous, transparent and thermodynamically stable, which makes them attractive for many kinds of applications. Thus, their development was accompanied by evolving applications in the fields of extraction, solubilisation, separation techniques as well as product formulation.[13-22] Furthermore, the unique structure of SFME was also found to have a serious impact on the kinetics and outcome of chemical reactions when used as solvents.[23-25] This effect was mainly attributed to the fact that reacting starting materials are dissolved within different pseudo-phases of such compartmented systems. Depending on the chemical nature and the resulting mesoscale solubilisation of the reactants, the use of SFME and mesoscale structured liquids can be advantageous, but also in some cases obstructive for the outcome of a chemical reaction.[24-25] Accordingly, for chemical sensitive components like enzymes, SFME can provide a solvent system with a relatively low amount of water that is still able to protect the enzyme from unwanted solvent contact and thus from denaturation.[26-33] First studies of Khmelnitsky *et al.* involving SFME (water/2-propanol/*n*-hexane) as reaction media for enzymatic reactions were already carried out in the 1980s.[29-33] Unfortunately, techniques to investigate such types of solvent structuring were rather rare and thus structural investigations rather poor.[34] In order to get more in-depth structural information, modern and more sophisticated techniques like dynamic light scattering (DLS) or small-angle X-ray scattering (SAXS) can be helpful.

Thus, in the present contribution we investigated these systems more thoroughly in order to (i) extend the pioneering work on enzyme activity in SFME.[28-30] What is even more important is the question (ii): where are the limits of existence of mesoscale structuring and thus the

applicability as reaction media for enzymatic reactions? Furthermore (iii), we want to compare and correlate the structure-activity relationship of enzymes in SFME to that of enzymes in classical and well-structured surfactant-based microemulsions.

To this purpose, we chose the horseradish peroxidase (HRP) catalysed oxidation of 2,2'-azino-bis(3-ethylbenzothiazoline-6-sulphonic acid) diammonium salt (ABTS) using H_2O_2 as sacrificial oxidising agent (see Figure 9.2). The reaction is easy to follow via UV-Vis spectroscopy.[35] Further, detailed studies exist on this reaction performed in sodium dodecyl sulphate (SDS) based microemulsions.[36-39] It is important to stress that both the enzyme and the substrates are highly water soluble. To ensure a high reaction rate and to prevent enzyme denaturation, all three components (HRP, ABTS and H_2O_2) should be ideally surrounded by an aqueous environment.

Most important and delicate is the choice of suitable SFME as reaction media, in order to find the limits of mesoscale structuring necessary to obtain enzyme activity. In this study we used the ternary systems water(buffer)/alcohol/limonene as reaction media. Limonene, representing a natural, bio-sourced oil available in large amounts, was used as the hydrophobic component. 1-Propanol (NPA) and *tert*-butanol (TBA) were used as alcohols, because both alcohols show already good pre-structuring in the binary water/alcohol mixtures for certain compositions and allow sufficient solubility of limonene in the corresponding ternary mixture.[10,24] In order to investigate the structures of the SFME, DLS, SAXS and conductivity measurements were used. Results were finally correlated with the enzyme activities found in the SFME and compared to those obtained in classical microemulsions.[39]

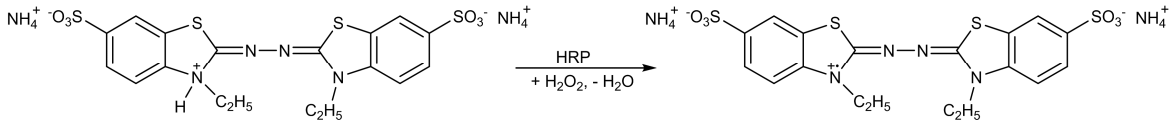

Figure 9.2: HRP catalysed oxidation of ABTS using H_2O_2 as sacrificial oxidizing agent.

9.3. Materials and methods

9.3.1. Materials

Ethanol (EtOH, purity ≥ 99.8%), 2-propanol (IPA, ≥ 99.8%), (*R*)-(+)-limonene (97%, *ee*: 98%) and ABTS (≥ 98%) were purchased from Sigma-Aldrich (Steinheim, Germany). 1-Propanol (NPA, ≥ 99.5%), *n*-hexane (≥ 95%), citric acid monohydrate (p.a. grade), H_2O_2 (aq, 30 wt% in

H_2O) were purchased from Merck (Darmstadt, Germany). *tert*-Butanol (TBA, ≥ 99%) and HRP (≥ 250 U mg^{-1} substrate) were obtained from Carl Roth (Karlsruhe, Germany). Citric acid trisodium salt dihydrate (≥ 99%) was purchased from Acros Organics (Geel, Belgium). All chemicals were used without further purification. Aqueous solutions were prepared using deionised water with a resistivity of 18 MΩ cm. Aqueous citrate buffer solutions contained 2 mmol L^{-1} citric acid trisodium salt dihydrate and 1.125 mmol L^{-1} citric acid monohydrate (pH = 5.00). The resulting pH was controlled using a commercial glass electrode and adjusted to 5.00 ± 0.02 using a diluted aqueous solution of citric acid monohydrate.

9.3.2. Ternary phase diagrams

Phase diagrams were recorded at 25 °C using a dynamic and static process according to Clausse *et al*. (see Section 2.3.2.1).[40]

9.3.3. Measurement of enzyme activity

The main procedure used for kinetic measurements of the enzyme activity of HRP was described by Bauduin *et al*.[39] Reaction mixtures consisted of 2.9 mL pure buffer or SFME. The reaction was initiated directly in the quartz measurement cells (Hellma Analytics, light path 10 mm) by addition of 10 mL of a solution containing 0.012 mol L^{-1} ABTS, followed by 10 mL of a solution containing 0.0262 mol L^{-1} H_2O_2. Final initiation of the reaction was induced by the addition of 10 mL HRP solution (31.25 mg L^{-1}). The whole reaction mixture was immediately stirred with a neoLab cuvette stirrer. Special care was taken that the time between the final addition (HRP solution), stirring and start of the measurement was always (10 ± 1) s. The reaction was monitored via UV-Vis spectroscopy (λ = 414 nm) at a constant temperature of (25 ± 0.1) °C using a Varian Cary 3E spectrometer. It can be assumed in good approximation that the measured absorption at this wavelength is proportional to the concentration of the product formed in the reaction medium (see Figure 9.2). The reactivity (activity of the enzyme) was measured relative to the pure buffer solution due to variable reproducibility of the mother enzyme solutions. To this purpose, the approximately linear increase of the absorbance of the first minute (monitored with UV-Vis) was fitted and the enzymatic activities were expressed as V/V_0, where V and V_0 are the slopes of the straight fit lines (initial velocity) for the enzymatic activities in the microemulsions (V) and the buffer (V_0), respectively. For each sample, at least three measurements were performed. Reproducibility of the results was evaluated using the standard deviation of the determined slopes, which was always below 10%, mostly in the range between 3 and 8%. To exclude unwanted effects caused by pH changes of the buffer solution, all measurements of a distinct SFME system

were performed at the same day (within 6 h) using freshly prepared buffer solution for each day. pH and enzyme activity in pure citrate buffer were controlled by the end of each day. Values for pH did not differ by more than 0.05 and enzymatic activities by not more than 3% (compared to measurements in pure buffer at the beginning of the day) with no preferred direction of the deviation. This is inside of the range of the usual standard deviation of the measurements.

9.3.4. Dynamic light scattering

DLS experiments were performed as described in Section 2.3.2.2. Data were analysed by a single exponential data fitting of the normalised autocorrelation function of intensity (see Section 1.2.1).[41,42] However, droplet sizes inferred from this method have to be considered carefully as possible aggregates, which might be formed in such solutions, are usually highly fluctuating systems and of no well-defined shapes. Hence, we renounced calculations of hydrodynamic radii and solely used this relation for size estimations of the formed mesoscale inhomogeneities. Instead, the DLS spectra were evaluated more qualitatively with regard to their decay rate and decay time. (As a rule of thumb, it was assumed that the higher the correlation function is at short correlation times and the later it drops down, the more time-stable and more pronounced is the mesoscale structuring of the solution).

9.3.5. Small-angle X-ray scattering

Synchrotron small-angle X-ray scattering (SAXS) data were collected at the European Synchrotron Radiation Facility (ESRF, Grenoble, France) on the beam-line ID02, with a wavelength of 0.995 Å (12.46 keV) at a samples-to-detector distance of 1.2 m giving an observed q-range of 0.1 nm^{-1} ≤ q ≤ 6.5 nm^{-1}. 2D data were radially averaged and standard reduction procedures (subtraction of empty capillary and solvent contribution) were applied. Background correction for the individual components i was done using following equation: $I = I_{\mathrm{exp}} - \sum_i I_i \phi_i$ with ϕ_i the volume fraction of the individual components ($\sum_i \phi_i = 1$).The scattering intensity I in mm^{-1} is plotted against the magnitude of the scattering vector q in nm^{-1}. The curves were fitted with an Ornstein–Zernike (OZ) formalism (see section 1.2.2).[8]

9.3.6. Conductivity measurements

Conductivity measurements were carried out in a thermostatted measurement cell (25 ± 0.2 °C) under permanent stirring using a low-frequency WTW inoLab Cond 730 conductivity meter connected with a WTW TetraCon 325 electrode (Weilheim, Germany).

20 g of each sample was filled in the measurement cell and successively diluted with water/alcohol mixtures (for measurements along the reaction path) or pure water (for measurements crossing the reaction path, see Appendix A.7). Each sample contained in addition 0.1 wt% sodium bromide to ensure a sufficient amount of charge carriers, as described previously.[4,10]

9.4. Results

9.4.1. Influence of aliphatic, fully water-miscible alcohols on the enzyme activity in binary water(buffer)/alcohol mixtures

In order to evaluate the influence of different, fully water-miscible aliphatic alcohols (as mostly used in SFME) on the enzyme activity, several binary water(buffer)/alcohol mixtures were investigated with increasing amount of alcohol. Results are shown in Figure 9.3. The enzyme activity compared to pure buffer solution (V/V_0) decreases rapidly for all alcohols. At x(alcohol) = 0.05, the activity is already below 30% compared to the activity in pure aqueous buffer, and at x(alcohol) = 0.2, almost no enzymatic activity can be measured at all. Activity curves decrease in the following order: EtOH > IPA > NPA ≈ TBA.

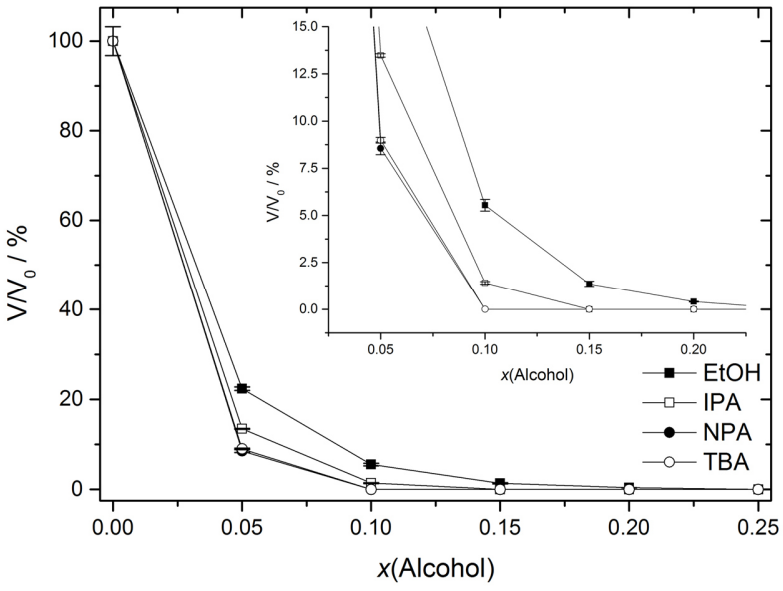

Figure 9.3: Relative enzymatic activities V/V_0 (V_0 corresponds to the activity in pure buffer solution) for the oxidation of ABTS with HRP and H_2O_2 in binary water(buffer)/alcohol mixtures at 25 °C as a function of the amount of alcohol given in mole fractions. Symbols denote the different alcohols used in the reaction medium. Inset: Zoom-in view at the region of interest (low amounts of alcohol). Error bars represent the standard deviations out of three measurements.

Consequently, the presence of EtOH has a less negative influence on the enzyme activity than the other three alcohols. The most hydrophobic alcohols, TBA and NPA, show an almost identic influence on the enzyme and exhibit the highest rates of inactivation. At *x*(alcohol) >0.15, no measurable reaction takes place anymore for reaction mixtures containing NPA and TBA. It has to be remarked that EtOH is too hydrophilic to sufficiently solubilise limonene in a ternary mixture with water to form suitable SFME compared to the other three alcohols. Due to this fact, and due to the almost identic effect of NPA and TBA on the enzyme activity in aqueous solution, NPA and TBA were chosen as alcohols for the following ternary reaction media.

9.4.2. Enzyme activity in water(buffer)/NPA/limonene and water(buffer)/TBA/ limonene ternary mixtures

The compositions of SFME investigated by enzyme activity measurements are shown by letters from *a* to *o* in the water/alcohol/limonene ternary phase diagrams, represented in mole (Figure 9.4a) and in weight fractions (Figure 9.4b). It is worth noting that both alcohols show an almost identical influence on the enzyme activity in the binary mixtures (see Figure 9.3). Thus, within each measurement series (*a*-*o*), a constant mole fraction of alcohol, *x*(alcohol) = 0.5, was chosen. This was done in order to exclude differing denaturation effects caused by a varying alcohol content.

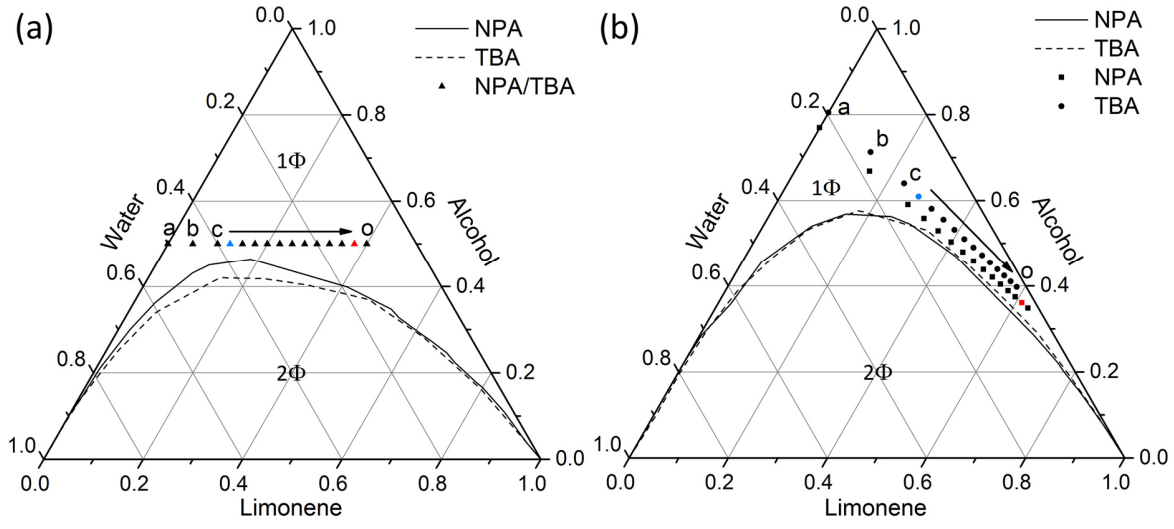

Figure 9.4: Ternary phase diagrams of water/NPA/limonene and water/TBA/limonene at 25 °C in (a) mole and (b) weight fractions. The mono- and two-phasic areas are represented as 1Φ and 2 Φ, respectively. Symbols denote the different compositions used as reaction media (*a*-*o*). Points with maximum enzymatic activity measured for NPA and TBA are denoted with red and blue symbols, respectively.

Results obtained by kinetic measurements as a function of the mole fraction of water for a constant amount of alcohol of *x*(alcohol) = 0.5 are shown in Figure 9.5 (see points *a*-*o*). For NPA as well as for TBA, no enzyme activity is observable for *x*(water) = 0.1 (point *o*).

The enzyme activity for NPA increases tremendously for *x*(water) > 0.1 and reaches a value comparable to the enzyme activity in pure buffer solution (point *n*, *x*(water) = 0.125, maximum enzymatic activity). For *x*(water) > 0.125 a continuous decrease of the activity is observed until reaching the binary buffer/alcohol mixture at *x*(water) = 0.5 (point *a*), where no enzyme activity is detectable. A much less pronounced trend can be found for TBA. Here, a rather moderate increase in activity can be observed than the formation of a distinct maximum and highest enzyme activity was found for *x*(water) = 0.375 (composition *d*). However, going to higher water contents (*x*(water) ≥ 0.375), both curves almost overlap meaning that both systems show a similar effect on the enzyme activity for higher water contents. It is worth noting that enzymatic activities in TBA-based SFME were found to be much lower than for NPA (factor four to five, comparing the two maximum activities). Although both alcohols showed a similar inhibition effect on the enzyme in binary aqueous solutions, significant differences were observed in ternary mixtures.

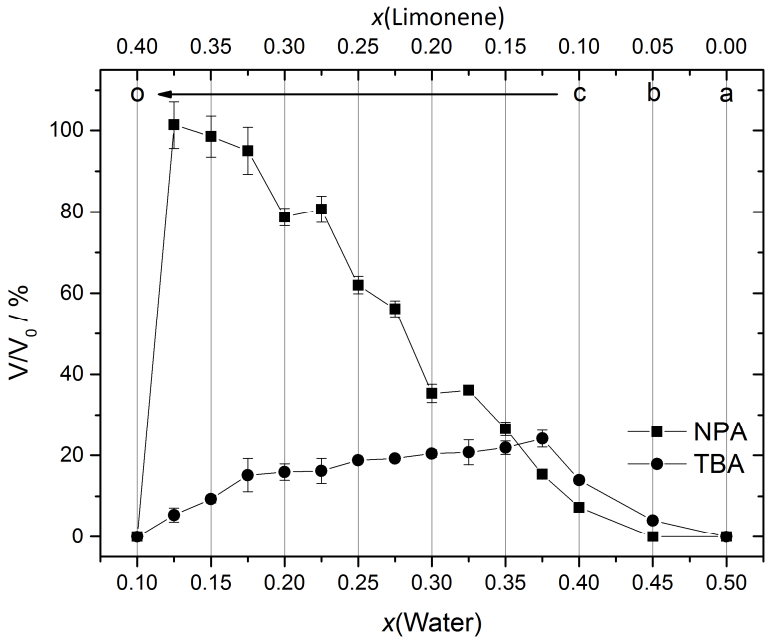

Figure 9.5: Relative enzymatic activities V/V_0 (V_0 corresponds to the activity in pure buffer solution) for the oxidation of ABTS with HRP and H_2O_2 in ternary water(buffer)/alcohol/limonene mixtures at 25 °C as a function of the water and limonene content given in mole fractions. Symbols denote the enzyme activity for different alcohols used in the reaction medium. Specific compositions of the reaction media (*a*-*o*) can be taken from Figure 9.4. Note that points *a* correspond to the binary buffer/alcohol mixtures. Error bars represent the standard deviations out of three measurements.

9.4.3. Structural investigations of ternary systems water/NPA/limonene and water/TBA/ limonene

9.4.3.1. Dynamic light scattering

To investigate the origin of the very different behaviour of HRP observed between SFME containing NPA or TBA, light scattering experiments were performed on the pure SFME (see Figure 9.6). It can be found for both systems that well-defined correlation functions first appear, once a certain amount of limonene is present (composition *c*). In the system water/NPA/limonene, well-defined correlation functions with a single exponential decay could be obtained by DLS measurements indicating the presence of structured solutions in the range of several nm (see compositions (*c*-*n*) in Figure 9.6a/c and Table A7.1 and Figure A7.1, Appendix A.7).

Note that only for these compositions a measurable enzyme activity could be obtained. Correlation functions increase steadily and are shifted to higher decay times from points (*a*) to (*g*). At composition (*g*) the most pronounced correlation can be found. From point (*g*) to (*n*) an almost gradual decrease of the correlation function and shift to lower decay times is discernible, except between compositions (*j*) and (*k*). There, an unsteady, jump-like decrease can be observed. Going further to point (*o*), a sudden breakdown of the correlation occurs. For TBA, a similar trend is visible (see Figure 9.6b/d) and correlation functions could also be described well using a mono-exponential fitting procedure (Table A7.1 and Figure A7.1, Appendix A.7). However, it has to be remarked that correlation functions are less pronounced, always remaining below a value of 0.6. In addition, decay times are always lower than in the case of water/NPA/limonene. Furthermore, there is a steady decrease between compositions (*g*) and (*o*). Nevertheless, reaction mixtures *a* and *o* again show very low correlation, which is in line with an extremely low (not measurable) enzyme activity.

Overall, correlation functions obtained by DLS show a similar trend as observed for the enzyme activity measurements. Exclusively, reaction mixtures that showed a measurable enzymatic activity also showed defined correlation functions that indicate the presence of mesoscale structures in the ternary reaction mixture.

In addition, light scattering experiments were also performed to investigate the influence of citrate buffer, substrates (H_2O_2/ABTS) and HRP on the SFME (see Figure A7.2a and b, Appendix A.7). To this purpose, sample *g* was prepared (i) with water and (ii) with buffer solution, which did not lead to a significantly altered correlation function.

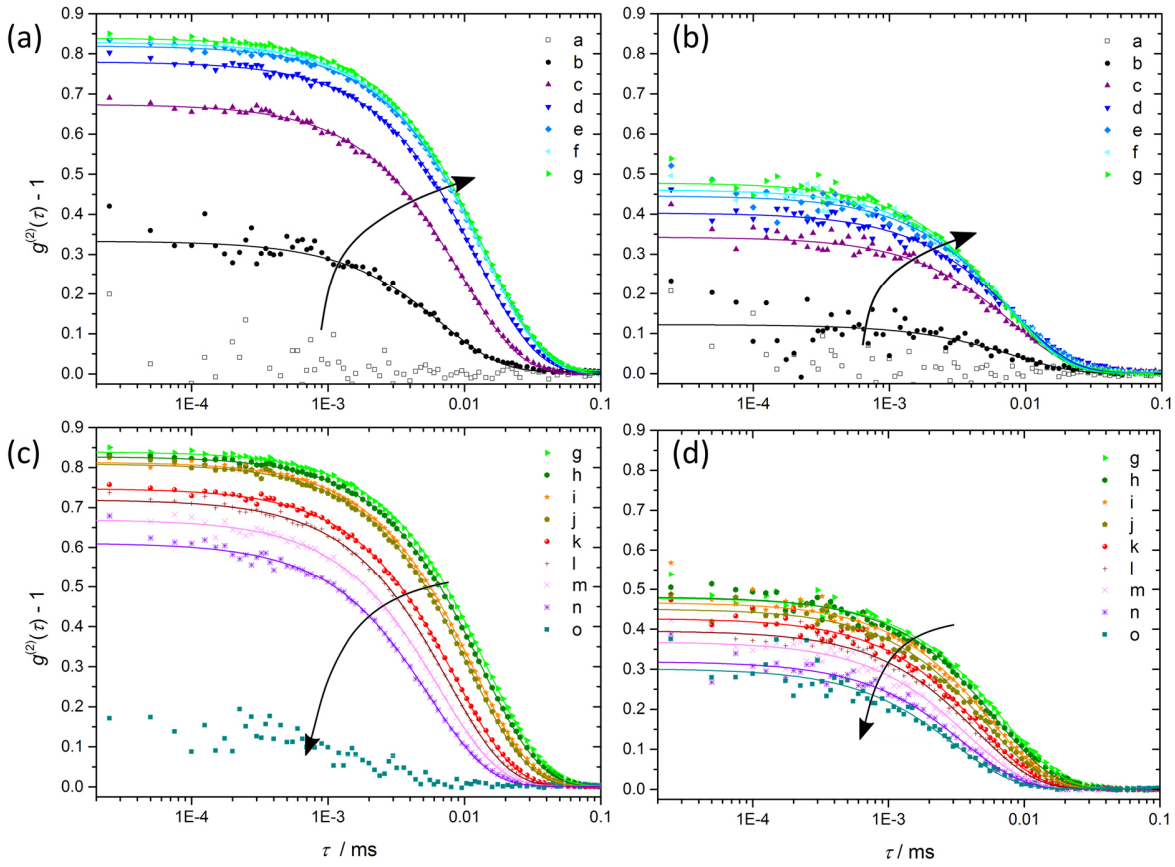

Figure 9.6: Normalised autocorrelation functions of intensity obtained by DLS measurements at 25 °C for the ternary systems (*a*,*c*) water/NPA/limonene and (*b*,*d*) water/TBA/limonene. The symbols refer to the specific compositions of the reaction media (*a*-*o*), which can be taken from Figure 9.4. Straight lines represent the corresponding fit using a mono-exponential fit model.

Addition of 10 mL of H_2O_2, ABTS or HRP solutions (same concentrations as used for the enzyme activity measurements) did not noticeably affect the correlation function either. Yet, with increasing enzyme concentration the formation of a bimodal exponential decay could be observed (second mode at higher decay times). Simultaneously, the first mode was found to slightly shift to higher decay times (see, Figure A7.2b, Appendix A.7).

9.4.3.2. Small-angle X-ray scattering

SAXS measurements were performed complementary to light scattering experiments (see Figure 9.7 and Figure A7.3, Appendix A.7). Spectra of samples (*c*-*i*) of the ternary system water/NPA/limonene show an excess scattering in the low *q*-range, $q < 2$ nm^{-1}. Such a scattering behaviour is typically found for SFME and indicates the presence of a mesoscale structured solution.

Spectra for (*c*-*i*) with the corresponding OZ-fits (q = 0.1–2 nm^{-1}) are shown in Figure 9.7. The characteristic correlation length ξ ranges from 1.0 to 2.1 nm, with a nearly linear increase from (*c*) to (*i*), see also Table A7.2, Appendix A.7. It is worth noting that no OZ-like scattering behaviour can be found going to compositions (*k*, *m* and *o*). Keep in mind that between samples (*j*) and (*k*) a more pronounced change of the correlation functions was also observed with DLS measurements.

In addition, the overall intensity is very low, indicating a low scattering contrast. Thus, a powerful X-ray radiation source was essential to obtain spectra with good statistics, *i.e.* low noise, and to resolve the OZ scattering pattern. SAXS spectra of the system water/TBA/limonene (not background corrected) on the other hand do not show a visible OZ-like scattering behaviour in the low-q-range (see Figure A7.3, Appendix A.7). It has to be remarked that background subtraction for spectra of ternary mixtures containing TBA could not be performed as in the case for water/NPA/limonene, since TBA is solid at 23 °C. For this reason, no spectrum of pure TBA could be obtained with the experimental setup used in this study.

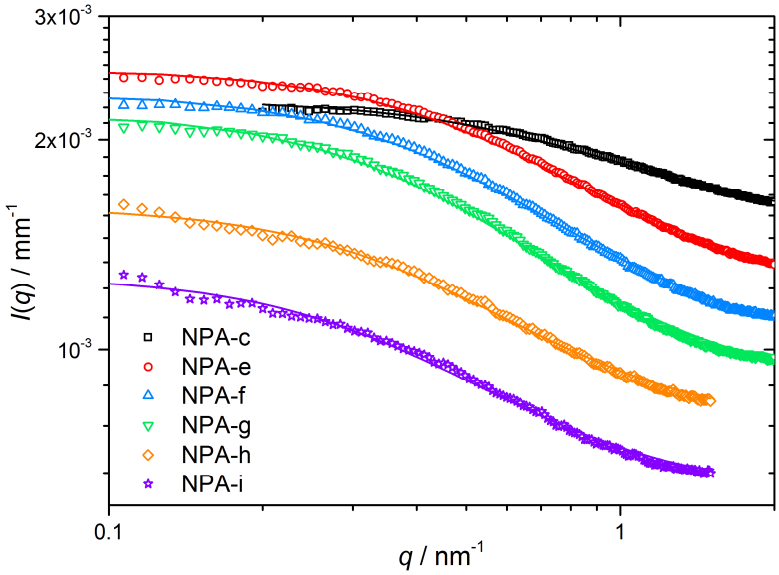

Figure 9.7: SAXS spectra of the ternary mixtures water/NPA/limonene for the q-range of 0.1–2 nm^{-1} (for full spectra see Figure A7.3, Appendix A.7). The symbols refer to the specific compositions of the reaction media (*c*-*i*), which can be taken from Figure 9.4. Straight lines represent the corresponding fits using an OZ formalism.

9.4.3.3. Conductivity measurements

To get additional insight into the structuring of the investigated reaction media, conductivity measurements were performed (see Figure 9.8). For low amounts of water, measurements

done along the reaction path (*o*-*a* in Figure 9.4) show a more or less flat rise of the conductivity. The slope of the conductivity curve is gradually increasing with increasing water content passing through a maximum before the conductivity decreases again due to excessive dilution. This curve shape is comparable to typical measurements of SDS-based microemulsions.[10] Accordingly, there are several typical points to mark probable transitions between the different mesoscale structures (T1-T4).[10] Unfortunately, the low amount of sodium bromide added for measurable conductivities already caused the system water/TBA/limonene to form a biphasic turbid mixture. Hence, values for the biphasic system (see Figure 9.8b, marked in grey) are less reliable. Although the shape of the curves changes only marginally, the absolute values for TBA containing mixtures are significantly lower comparing both systems.

Since a macroscopic change in the phase behaviour was observed for SFME containing TBA, additional conductivity measurements were performed (see Figure A7.4 and A7.5, Appendix A.7). Results confirm the overall relatively low conductivity in SFME composed of water/TBA/limonene compared to the system water/NPA/limonene (especially in the region where enzyme activities were investigated). Thus, one may conclude that in NPA containing SFME, significant changes of the mesoscale structuring can be expected, whereas results obtained for TBA containing SFME indicate only little changes of the solution structure and/or the presence of much less defined mesoscale structures.

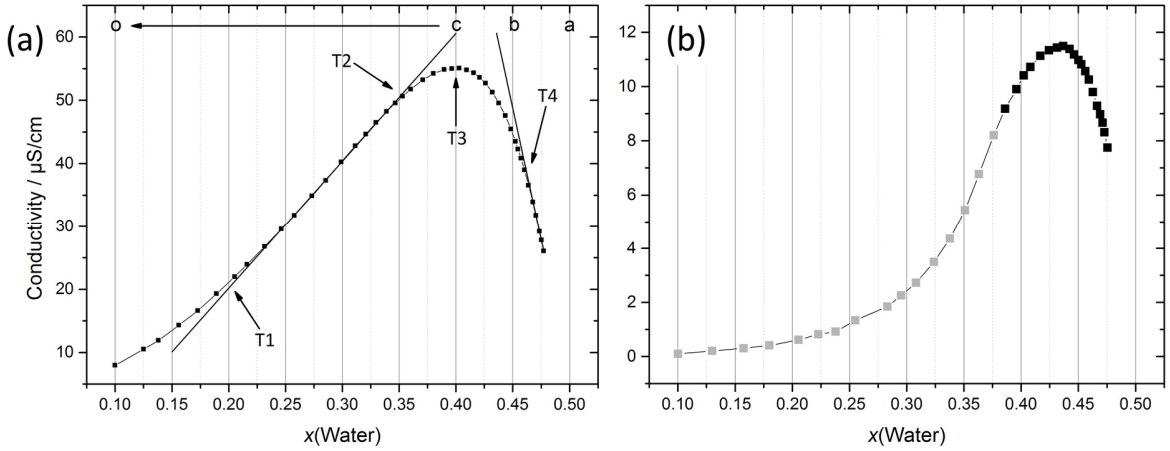

Figure 9.8: Conductivity measurements at 25 °C along the reaction path (see Figure 9.4) of water/NPA/limonene (a) and water /TBA/limonene (b). In order to ensure measurable conductivities, 0.1 wt% NaBr were dissolved in the starting mixtures (composition *o*). In (b) points, where the system was found to be biphasic, are marked in grey.

9.5. Discussion

9.5.1. Relationship between mesoscale solvent structuring of SFME and enzyme activity

As clearly discernible from scattering and kinetic experiments, enzymatic activity unambiguously coheres with the structure of the reaction medium. Adding more and more limonene to the unstructured binary mixtures H_2O/alcohol, successively induces a structuring of the reaction mixtures. We assume that during this progressive structuring, more and more alcohol is pushed in the oil-rich pseudo-phase and to the interface between the oil- and water-rich domains and therefore pulled out of the aqueous pseudo-phase. Hence, the enzyme gets less in contact with the alcohol, meaning that enzyme denaturation by the alcohol is less pronounced. Consequently, the enzyme activity rises until the water content is too low leading to a breakdown of the structures and activity (composition *o*).

Our results also show that in the case of water/NPA/limonene, structures were found to be more defined than it is the case for water/TBA/limonene, since correlation functions are more pronounced and drop down at higher decay times, which indicates the presence of a more defined compartmentation and larger aggregates within the solutions. These results are corroborated by SAXS measurements, showing an OZ-like scattering behaviour, which can be typically found for SFME, proving the presence of a mesoscale structured solution. In addition, our findings are supported by the fact that in the system water/NPA/limonene, enzyme activity is significantly higher compared to the system water/TBA/limonene. For some compositions, enzyme activities comparable to that in the pure aqueous buffer medium are measured. This suggests that a strong compartmentation between water- and limonene-rich domains is present in the ternary mixture, creating an almost alcohol-free and limonene-free environment for the enzyme, which is comparable to a small domain of bulk-water. It is worth noting that the overall intensity of the OZ-like scattering is very low. This finding can be attributed to the fact that all samples contain a relatively high amount of alcohol. The alcohol can be assumed to distribute over both pseudo-phases (water- and oil-rich, with a preference to accumulate at the interface) and thus lowers the difference in the scattering length density. We assume that this is also the reason, why samples *k* and *m* do not show excess scattering in the SAXS low-*q* region, although DLS experiments lead to well-defined correlation functions. Furthermore, the number density and the average volume of water clusters, which might be formed in samples *k* and *m*, are supposedly too low to be detectable (w(water) < 5 wt%). For SFME containing TBA, an OZ-like spectrum is not observable

anymore, which was expected, since results obtained by DLS already revealed this system to be weakly structured. Consequently, the remaining excess scattering in the low-*q* range is presumably too low to be detectable even with a high-performance X-ray source.

If the structuring within the SFME is assumed to be comparable to the one in classical surfactant-based microemulsions, four different regions of structuring can be expected and discriminated, regarding the results of conductivity measurements. First, for low water contents, there is a random, molecularly distributed mixture. With increasing water content, the formation of water clusters can be expected (w/o microemulsion), which (at point T1, see Figure 9.8a) starts to form a percolating system. Remember that in this region a pronounced change was discernible in DLS (compositions *k* and *j*), which also indicates a significant change in structure. After a linear increase of the conductivity, the slope decreases (point T2) and the conductivity passes through a maximum (point T3). At point T2, there still exists an oil-rich bicontinuous phase, changing into a water-rich bicontinuous microemulsion (point T3). At point T4, one would finally expect a transition to an o/w microemulsion system. However, due to the very high alcohol content in this region, such a behaviour is questionable, as results of DLS and SAXS measurements could not confirm the presence of a structured solution anymore.

Assuming this model, conductivity measurements as shown in Figure 9.8a explain well the activity of HRP in water/NPA/limonene mixtures. Below *x*(water) = 0.125, there are almost exclusively molecular dispersed water molecules. Consequently, there is no measurable activity due to a frequent contact of the enzyme with NPA and limonene and a lack of sufficient enzyme hydration. This is also supported by the fact that there is no defined correlation function obtainable for sample *o* (*x*(water) = 0.1). Increasing amounts of water lead to water cluster formation, in which the water behaves almost like bulk-water, explaining the enzyme activity to rise to a value comparable to that of pure water. At point T1 (percolation threshold, *x*(water) = 0.2), the activity (after passing its maximum value) finally decreases again. Three effects can explain this observation:

(i) water channels formed at this point could cause the water pseudo-phase to ‘‘thin out”, which automatically brings the enzyme in closer contact to the alcohol-rich interface, leading to denaturation. In addition, collision and merging of water droplets can enhance the contact of enzyme and alcohol/limonene.

(ii) The formation of water channels is likely to lead to a change in concentrations of HRP and ABTS, since water aggregates are no longer isolated. Following this

argument, the concentration of enzyme and substrate is supposed to decrease, followed by a gradual breakdown of the activity.

(iii) Probably most important is the fact that a rising water content leads to an enhanced solubility of NPA in the water-rich domains, leading also to higher denaturation rates.

Especially the third effect is expected to prevail for higher water contents since at point T4 no enzyme activity is measurable again, meaning that NPA is mostly dissolved in the water-rich domain or even a molecular dispersed solution is formed. Further, in this region, a remarkable breakdown of the correlation function is observable, indicating only very weak structuring of the solutions, if any.

It is worth noting that a similar enzyme activity could also be found for SFME composed of water(buffer)/IPA/*n*-hexane comparing with water(buffer)/NPA/limonene (see Figure A7.6, Appendix A.7). These findings are in good accordance with the results described by Khmelnitsky *et al*.[30] Yet, the difference in refractive indices between water- and oil-rich domains in this ternary mixture and thus the contrast for light scattering was found to be too low for a proper structural investigation (see Appendix A.7).

9.5.2. Influence of citrate buffer, substrates and HRP on the structure of used SFME

It has to be remarked that DLS experiments made on SFME composed of citrate buffer solutions instead of pure water do not lead to a significantly altered correlation function. Thus, the influence of the low-concentrated citrate buffer solution on the mesoscale structuring of the SFME can be regarded as negligible (see Figure A7.2a, Appendix A.7). A very similar result was found when adding the substrates (H_2O_2 or ABTS) to the microemulsion. The effect of the enzyme on the other hand is hard to evaluate since the used concentration of the enzyme is very low. From light scattering experiments, no significant deviation is discernible using the same enzyme concentration as for the enzyme activity measurements (see Figure A7.2b, Appendix A.7). Gradually increasing the enzyme concentration leads to the formation of a bimodal exponential decay with a second mode, appearing at higher decay times. This mode can be easily attributed to the enzyme by comparing the autocorrelation function of HRP in pure buffer solution with the same enzyme concentration. In addition, a slight shift of the first mode to higher decay times can be observed. Regarding this slight shift of the first exponential decay, one may argue that the enzyme influences the mesoscale structuring of the used SFME. It can be expected that the enzyme strengthens the aggregation

of water within the SFME due to hydration forces, leading also to a swelling of the water-rich domains. Nevertheless, significant effects on the solvent structuring are supposed to occur only at relatively high amounts of enzyme as shown by Pileni and co-workers for surfactant-based microemulsions.[43,44] It has to be further remarked that a complete intercalation of the enzyme in present water aggregates is not very likely. This is easily discernible by having a glance at the double exponential decay of the autocorrelation function measured for higher HRP concentrations. A rough estimation on the size domains of aggregates formed in the ternary systems (water/NPA/limonene and water/TBA/limonene, calculated radius approximately < 1.5-2.5 nm) shows that the size of the water-rich aggregates should be always lower than the size of the enzyme (HRP: 4.0 x 6.8 x 11.7 nm^3 according to X-ray crystallography/Protein Data Bank ID code 1H5A). Nevertheless, we assume that at least the active site of the enzyme should have a certain affinity to the present water-rich pseudo-phases and should thus be covered and preserved by surrounding water. It has to be noted that the enzyme itself is apparently not able to induce significant solvent structuring and that the enzyme activity is indeed depending on the mesoscale structuring of the SFME. This is reflected by the fact that in TBA containing systems (more fluctuating with less defined compartmentation) the enzyme is less reactive, although the influence of NPA and TBA on the enzyme are almost identic (see Figure 9.3). Consequently, the enzyme is not able to induce structuring in TBA containing SFME.

9.5.3. Comparison to SDS containing microemulsions

In 2005, Bauduin *et al.* investigated the HRP activity in citric buffer/SDS with co-surfactant/dodecane.[39] The same reaction and method was used in these studies to test the enzyme activity for different *n*-alkyl-alcohols (C_4–C_8) used as co-surfactants. Several key parameters were found to influence the enzyme activity in such solutions. Results presented in their work showed that (i) the interfacial film rigidity has an important influence on the enzymatic activity. It was further found (ii) that the enzyme activity depends on the residual amount of alcohol, still dissolved in the aqueous pseudo-phase. Hence, the maximum activity of the enzyme is always related to an optimum hydration (which again is closely linked to the formation of mesoscale structures). In general, it can be stated that the lower the amount of alcohol within the aqueous phase and the more hydration water is available for the enzyme, the higher its activity is expected to be. (There is always a competition for free hydration water between the alcohol and the enzyme.) Transferring this fundamental insight to the SFME used in our study, many parallels can be found.

(i) Compartmentation phenomena in SFME are responsible for enhanced enzyme activity. This results in the formation of a water-rich pseudo-phase that lowers the amount of alcohol and limonene, compared to a true molecular solution.

Consequently, a sufficient amount of hydration water is available for the enzyme, protecting it from denaturation. Hence, the well-structured NPA containing SFME lead to a better enzyme activity than the weaker structured TBA containing microemulsions.

(ii) This effect is also related to the dynamics of formed aggregates in solution. Since SFME are usually highly fluctuating systems, the interface between water- and oil-rich pseudo-phases is much less defined compared to classical microemulsions. (For this reason, SFME are sometimes also called ultraflexible microemulsions.)

Hence, the dynamics of such highly fluctuating systems is rather a further key parameter for enzymatic activity than the rigidity of the interfacial film itself. TBA containing SFME showed faster dynamics than NPA containing microemulsions. One can expect the TBA stabilised aggregates to be much more fluctuating than NPA stabilised aggregates. Consequently, the enzyme gets more often in contact with TBA than NPA and is thus inactivated faster.

9.6. Conclusion

With this study, we presented an in-depth investigation of the correlation between mesoscale structuring of SFME and the enzymatic activity of a highly water-soluble enzyme in such systems. Taking account of recent progresses in the field of mesoscale structuring of SFME[8], it could be shown that the HRP-catalysed oxidation of ABTS strongly depends on the dynamics and type of the used SFME (water/NPA/limonene and water/TBA/limonene). Our findings (i) confirm and support results of previous studies on enzyme activity in SFME.[27,30] Analogue to these studies, a maximum in enzyme activity could be detected for water/NPA/limonene SFME at compositions, where w/o microemulsions are likely to be formed.

Moreover (ii), the limits of mesoscale structuring, still able to protect the enzyme from denaturation, could be identified. Light and X-ray scattering experiments (as performed in this study) demonstrated that SFME formed of less defined and/or more fluctuating aggregates significantly decrease the enzyme activity. Further, these findings reveal that enzyme hydration alone cannot be the driving force for the induction of an aqueous environment. Instead, the mesoscale solution structure of the SFME itself is the key parameter. In addition, we could (iii) identify several parallels between the enzyme activity in surfactant-based

microemulsions[39] and that in SFME. It can be stated that a certain compartmentation between water- and oil-rich domains has to be present. Formed aggregates have to be time-stable and defined enough (fluctuations not too fast) to protect the enzyme from denaturation. This effect is accompanied by two mechanisms: first, the alcohol is pushed more to the interface and into the limonene-rich domain. Second, the resulting water-rich aggregates provide enough free hydration water for the enzyme to protect it against denaturation (mainly caused by contact with the alcohol).

However, some findings must remain speculative in this study. We assume that the enzyme may not necessarily be incorporated in given water clusters, since rough size estimations could not support this. According to our hypothesis, protection of the enzyme is rather due to the affinity of the active site to given water clusters, which leads to a strengthening and swelling of the water-rich domains. Thus, the presence of relatively weak mesoscale structured reaction media, such as SFME, is sufficient to generate a water pool large enough to protect the enzyme from denaturation. In doing so, enzyme activities comparable to those in pure buffer solutions can be reached, using SFME with a water content of less than 5 wt%. Consequently, SFME could provide a serious alternative as reaction media for such type of reactions, using a minimum amount of water. In this context, terpene-based SFME (as investigated in our study) could be of particular interest for biocatalytic oxidations of such bio-sourced terpenes using non-specific water-soluble enzymes in order to gain valuable oxidation products for the flavour and fragrance industries.[45-47]

We think that such kind of studies can help to better understand high enzymatic activities in the presence of high contents of very hydrophobic solvents.[48]

9.7. References

1 M. L. Klossek, D. Touraud, T. Zemb and W. Kunz, *ChemPhysChem*, **2012**, *13*, 4116–4119.

2 O. Diat, M. L. Klossek, D. Touraud, B. Deme, I. Grillo, W. Kunz and T. Zemb, *J. Appl. Crystallogr.*, **2013**, *46*, 1665– 1669.

3 S. Schöttl, J. Marcus, O. Diat, D. Touraud, W. Kunz, T. Zemb and D. Horinek, *Chem. Sci.*, **2014**, *5*, 2949–2954.

4 P. Bošković, V. Sokol, T. Zemb, D. Touraud and W. Kunz, *J. Phys. Chem. B*, **2015**, *119*, 9933–9939.

5 J. Marcus, D. Touraud, S. Prevost, O. Diat, T. Zemb and W. Kunz, *Phys. Chem. Chem. Phys.*, **2015**, *17*, 32528–32538.

6 S. Prevost, T. Lopian, M. Pleines, O. Diat and T. Zemb, *J. Appl. Crystallogr.*, **2016**, *49*, 2063–2072.

7 T. Lopian, S. Schöttl, S. Prevost, S. Pellet-Rostaing, D. Horinek, W. Kunz and T. Zemb, *ACS Cent. Sci.*, **2016**, *2*, 467–475.

8 T. Zemb, M. L. Klossek, T. Lopian, J. Marcus, S. Schöttl, D. Horinek, S. Prevost, D. Touraud, O. Diat, S. Marčelja and W. Kunz, *Proc. Natl. Acad. Sci. U. S. A.*, **2016**, *113*, 4260–4265.

9 S. Schöttl and D. Horinek, *Curr. Opin. Colloid Interface Sci.*, **2016**, *22*, 8–13.

10 T. Buchecker, S. Krickl, R. Winkler, I. Grillo, P. Bauduin, D. Touraud, A. Pfitzner and W. Kunz, *Phys. Chem. Chem. Phys.*, **2017**, *19*, 1806–1816.

11 D. Subramanian and M. A. Anisimov, *Fluid Phase Equilib.*, **2014**, *362*, 170–176.

12 S. Prevost, M. Gradzielski, T. Zemb, *Adv. Colloid Interface Sci.*, **2017**, *247*, 374–396.

13 W. Hou, J. Xu, Curr. Opin. *Colloid Interface Sci.*, **2016**, *25*, 67–74.

14 M. L. Klossek, D. Touraud and W. Kunz, *Phys. Chem. Chem. Phys.*, **2013**, *15*, 10971–10977.

15 J. Marcus, M. L. Klossek, D. Touraud and W. Kunz, *Flavour Fragrance J.*, **2013**, *28*, 294–299.

16 V. Tchakalova, T. Zemb and D. Benczedi, *Colloids Surfaces A Physicochem. Eng. Asp.*, **2014**, *460*, 414–421.

17 J. Marcus, M. Müller, J. Nistler, D. Touraud and W. Kunz, *Colloids Surfaces A Physicochem. Eng. Asp.*, **2014**, *458*, 3–9.

18 R.F. Hankel, P. E. Rojas, M. Cano-Sarabia, S. Sala, J. Veciana, A. Braeuer and N. Ventosa, *Chem. Commun.*, **2014**, *50*, 8215–8218.

19 V. Fischer, J. Marcus, D. Touraud, O. Diat and W. Kunz, *J. Colloid Interface Sci.*, **2015**, *453*, 186–193.

20 D. Brock, T. Lopian, A. Khoshsima, P. Bauduin, O. Diat, D. Touraud and W. Kunz, *Colloids Interface Sci. Commun.*, **2014**, *14*, 1–3.

21 U. Mohorič, A. Beutner, S. Krickl, D. Touraud, W. Kunz and F.-M. Matysik, *Anal. Bioanl. Chem.*, 2016, **408**, 8681–8689.

22 N. Grimaldi, E. Rojas, S. Stehle, A. Cordoba, R. Schweins, S. Sala, S. Luelsdorf, D. Piña, J. Veciana, J. Faraudo, A. Triolo, S. Braeuer and N. Ventosa, *ACS Nano.*, **2017**, *11*, 10774–10784.

23 L. O. Kononov, *RSC Adv.*, **2015**, *5*, 46718–46734.

24 S. Krickl, T. Buchecker, A. U. Meyer, I. Grillo, D. Touraud, P. Bauduin, B. König, A. Pfitzner and W. Kunz, *Phys. Chem. Chem. Phys.*, **2017**, *19*, 23773–23780.

25 J. Xu, H. Deng, J. Song, J. Zhao, L. Zhang and W. Hou, *J. Colloid Interface Sci.*, **2017**, *505*, 816–823.

26 E. Mitsou, A. Xenakis and M. Zoumpanioti, *Catalysts.*, **2017**, *7*, 52.

27 A. Xenakis, M. Zoumpanioti and H. Stamatis, *Curr. Opin. Colloid Interface Sci.*, **2016** *22*, 41–45.

28 M. Zoumpanioti, H. Stamatis, V. Papadimitriou and A. Xenakis, *Colloids Surfaces B Biointerfaces.*, **2006**, *47*, 1–9.

29 Y. L. Khmelnitsky, R. Hilhorst and C. Veeger, *Eur. J. Biochem.*, **1988**, *176*, 265–271.

30 Y. L. Khmelnitsky, I. N. Zharinova, I. V. Berezin, A. V. Levashov and K. Martinek, *Ann. N. Y. Acad. Sci.*, **1987**, *501*, 161–164.

31 Y. L. Khmelnitsky, A. K. Gladilin, I. N. Neverova, A. V. Levashov and K. Martinek, *Collect. Czech. Chem. Commun.*, **1990**, *55*, 555–563.

32 Y. L. Khmelnitsky, A. V. Levashov, N. L. Klyachko and K. Martinek, *Enzyme Microb. Technol.*, **1988**, *10*, 710–724.

33 Y. L. Khmelnitsky, A. Van Hoek, C. Veeger and A. J. W. G. Visser, *J. Phys. Chem.*, **1989**, *93*, 872–878.

34 G. D. Smith, C. E. Donelan and R. E. Barden, *J. Colloid Interface Sci.*, **1977**, *60*, 488–496.

35 R. E. Childs and W. G. Bardsley, *Biochem. J.*, **1975**, *145*, 93–103.

36 M. C. Pinna, P. Bauduin, D. Touraud, M. Monduzzi, B. W. Ninham and W. Kunz, *J. Phys. Chem. B*, **2005**, *109*, 16511–16514.

37 P. Bauduin, A. Renoncourt, D. Touraud, W. Kunz and B. W. Ninham, *Curr. Opin. Colloid Interface Sci.*, **2004**, *9*, 43–47.

38 P. Bauduin, F. Nohmie, D. Touraud, R. Neueder, W. Kunz and B. W. Ninham, J. Mol. Liq., **2006**, *123*, 14–19.

39 P. Bauduin, D. Touraud, W. Kunz, M. P. Savelli, S. Pulvin and B. W. Ninham, *J. Colloid Interface Sci.*, **2005**, *292*, 244–254.

40 M. Clausse, L. Nicolas-Morgantini, A. Zradba and D. Touraud, in Surfactant Science Series (Vol. 24) Microemulsion Systems, eds. H. L. Rosano and M. Clausse, Dekker, New York, 1987, p. 15.

41 T. Nicolai, W. Brown and R. Johnsen, *Macromolecules.*, **1989**, *22*, 2795–2801.

42 R. Pecora, *J. Nanoparticle Res.*, **2000**, *2*, 123–131.

43 J. P. Huruguen and M. P. Pileni, *Eur. Biophys. J.*, **1991**, *19*, 103–107.

44 G. Cassin, S. Illy and M. P. Pileni, *Chem. Phys. Lett.*, **1994**, *221*, 205–212.

45 Z. Li, J. B. Van Beilen, W. A. Duetz, A. Schmid, A. De Raadt, H. Griengl and B. Witholt, *Curr. Opin. Chem. Biol.*, **2002**, *6*, 136–144.

46 M. Trytek and J. Fiedurek, *Acta Microbiol. Pol.*, **2002**, *51*, 57–62.

47 S. Águila, R. Vazquez-Duhalt, R. Tinoco, M. Rivera, G. Pecchi and J. B. Alderete, *Green Chem.*, **2008**, *10*, 647–653.

48 A. M. Klibanov, *Nature*, **2001**, *409*, 241–246.

Chapter 10 Surfactant-free microemulsion polymerisation of methyl methacrylate

10.1. Abstract

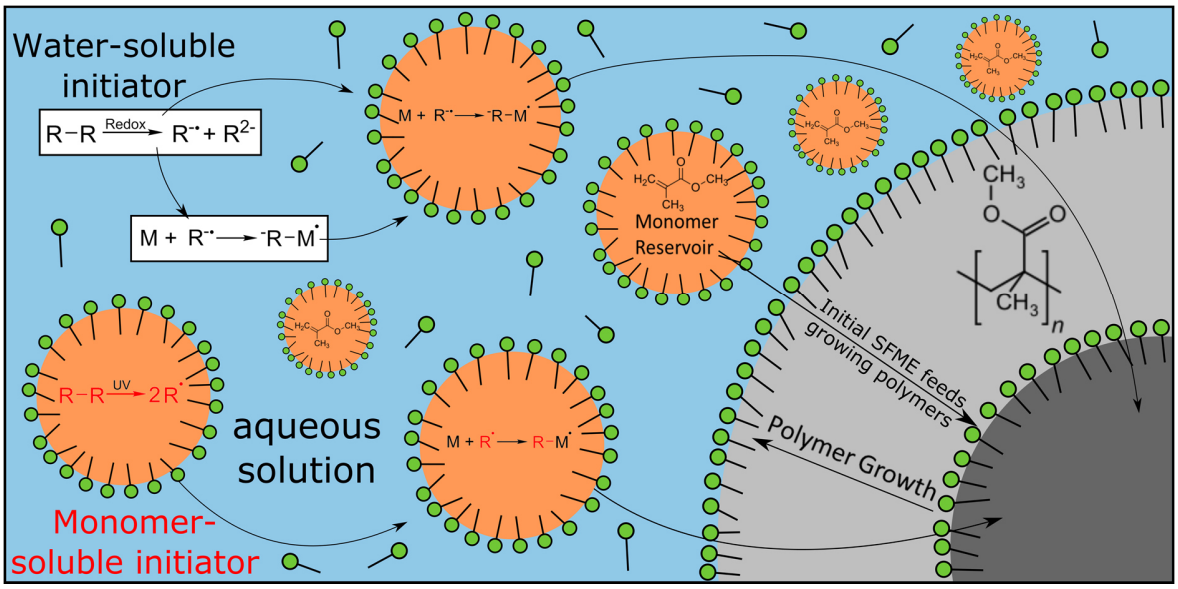

Figure 10.1: Graphical abstract schematically illustrating the concept of surfactant-free microemulsion polymerisation of methyl methacrylate. For the sake of clarity, SFME structuring shown in this figure is oversimplified.

Polymer growth of methyl methacrylate (MMA) to poly(methyl methacrylate) (PMMA) was investigated in different surfactant-free microemulsions (SFME). Various alcohols (ethanol and *n*-propanol) and mixtures of two alcohols (ethanol/*n*-butanol and *n*-propanol/*n*-butanol) were used in order to form SFME with water and MMA (hydrophobic compound). Dynamic light scattering (DLS) was used in order to investigate the presence and size of formed o/w SFME. Polymerisations were performed at 25 °C using two different initiators: potassium persulphate (PS, water-soluble initiator) activated by reduction with sodium sulphite and azobisisobutyronitrile (AIBN, oil-soluble initiator) activated by UV-irradiation. Polymer growth was measured using DLS. It was found that compartmentation of water-rich and MMA-rich domains within the SFME leads to a significant reduction of formed polymers compared to solution polymerisation, and size control can be obtained leading to polymers in the size range of 100-150 nm (hydrodynamic radius), see Figure 10.1.

This work is part of an invention disclosure that is submitted to the *Bayerische Patentallianz*. Title: *Polymerisation in tensidfreien Mikroemulsionen zur kontrollierten Herstellung von Polymersuspensionen/-dispersionen /-latizes* (ID: B78162).
Co-inventors: Prof. Dr. Werner Kunz and Dr. Klaus Schmid. K. Wolos contributed to the experimental work.

10.2. Introduction

Since the discovery and industrial use of natural rubber more than 200 years ago, natural and especially synthetic polymers gained huge importance as advanced materials for manifold applications.[1] Meanwhile, polymers and plastics are indispensable for daily life and can be found in almost all commercial products on the market, *e.g.* in packaging, personal care products, medicine, pharmaceutics and construction materials (just to name a few).[2–6] However, since the invention and industrial production of the first synthetic mass plastic, Bakelite, more than 100 years ago, the way of polymer synthesis has changed tremendously.[6] Aside of simple bulk polymerisation, several other techniques like suspension, (micro)emulsion or solution polymerisation have been developed.[6–13]
Especially, emulsion and also microemulsion polymerisation techniques are an attractive possibility for the targeted synthesis of polymer solutions and suspensions (also called polymer latices). In both cases, the formation of an o/w microemulsion is used for the controlled polymerisation of monomers within micelle-like aggregates. By doing so, well-defined particles can be obtained with a narrow size distribution. Furthermore, polymer sizes can be often adjusted by changing the composition/constituents of the microemulsion/emulsion or by the addition of different chain-regulating reagents, *e.g.* mercaptans.[7] Unfortunately, these techniques suffer from a major drawback. The recovery of surfactants (needed to form the microemulsion/emulsion) is often extremely complicated and quantitative recovery is virtually impossible. Furthermore, foaming can negatively affect the polymerisation process and surfactants can be released into the environment, which are often (eco)toxic and poorly biodegradable.[14,15]
In this context, surfactant-free emulsions and microemulsions (SFE/SFME) gain more and more importance for the replacement of conventional microemulsions and emulsions. Such systems usually contain a hydrotrope taking the role of the surfactant.[16,17] Depending on the composition (water/hydrotrope/oil), SFME can be obtained with different types of mesoscale structuring (direct, bicontinuous, inverse).[18–20] By doing so, processes can be often improved,

since hydrotropes are generally better biodegradable and often less foaming than conventional surfactants. Regarding in particular applications for polymerisation reactions, hydrotropes usually show a lower tendency to adsorb at the polymer surface and are often more volatile compared to conventional surfactants, which significantly facilitates recycling processes.

While there already exist several studies on polymerisations using SFE,[21–24] relatively little is known about polymerisations in SFME. In principle, SFME polymerisation is superior to SFE polymerisation techniques due to several advantages: the used mixtures are transparent, thermodynamically stable, homogenous solutions making intensive and energy-consuming stirring for emulsification unnecessary. However, only one rare example of SFME polymerisation exists, worth to be mentioned, describing the polymerisation of methyl methacrylate (MMA) in SFME composed of water, acrylic acid and MMA.[23] Yet, the use of acrylic acid used as the hydrotrope in this study always leads to the formation of porous polymeric structures. This is due to co-polymerisation of MMA and acrylic acid. Consequently, extended networks are formed instead of polymer latices independent of the mesoscale structure of the SFME (o/w, bicontinuous, w/o).

For this reason, the polymerisation of MMA was chosen as a model system and investigated in SFME composed of water, short-chain alcohols (non-reactive hydrotropes) and MMA (hydrophobic monomer). By doing so, o/w SFME can be obtained with MMA-rich droplets being the sole reactive species for polymerisation. Ethanol (EtOH), *n*-propanol (NPA) and *n*-butanol (NBA) were used as hydrotropes. Two different initiation methods were investigated: Potassium persulphate (PS) was used as water-soluble, charged initiator, redox-activated with sodium sulphite. Azobisisobutyronitrile (AIBN) was used as monomer-soluble initiator activated by UV-irradiation.[25] SFME formation and polymerisations were investigated using dynamic light scattering (DLS). Finally, the polymer growth was correlated with the existence and size of the compartmented monomer-rich droplets dispersed in the outer aqueous pseudo-phase.

10.3. Experimental

10.3.1. Chemicals

Methyl methacrylate (MMA, ≥ 99%, stabiliser: hydroquinone monomethyl ether), ethanol (EtOH, ≥ 99.9%), *n*-propanol (NPA, ≥ 99.5%), *n*-butanol (NBA, ≥ 99.5%) and potassium peroxodisulphate (PS, for analysis) were obtained from Merck (Darmstadt, Germany). Sodium

sulphite (for analysis) was purchased from Radiometer (Copenhagen, Denmark), *tert*-butanol (TBA, ≥ 99.7%) was purchased from Sigma- Aldrich (Steinheim, Germany). 2,2'-Azodiisobutyronitrile (AIBN, Peroxan AZDN, 99.4%) was a gift from Pergan (Bocholt, Germany). Prior to use, MMA was distilled at 40 °C and 60 mbar using a rotary evaporator in order to remove the stabiliser. All other chemicals were used without further purification. Aqueous solutions were prepared using deionised water with a resistivity of 18 MΩ cm.

10.3.2. Methods and techniques

10.3.2.1. Ternary phase diagrams

Phase diagrams were recorded at 25 °C using a dynamic and static process according to Clausse *et al*. (see Section 2.3.2.1).[26]

10.3.2.2. Polymerisation of methyl methacrylate

For PS initiated polymerisations, aqueous solutions of PS and sodium sulphite were used to prepare SFME with additional water, MMA and alcohol (EtOH, NPA, NBA). Final concentrations of PS of 10, 1 and 0.1 wt% were obtained with respect to the monomer (equal to 4, 0.4 and 0.04 mol% PS with respect to the monomer). The sodium sulphite concentration was kept constant at 4 mol% for all experiments. After addition, solutions were thoroughly mixed and the resulting homogeneous solution was immediately filtered into dust-free cylindrical light scattering cells (10 mm outer diameter) using 0.2 µm PTFE membrane filters. AIBN initiated polymerisations were performed dissolving AIBN within the pure monomer (AIBN concentration 3, 0.3 and 0.03 wt% with respect to the monomer, equal to 4, 0.4 and 0.04 mol% of free radicals with respect to the monomer). Subsequently, SFME were prepared, thoroughly mixed and filtered using 0.2 µm PTFE membrane filters. The homogeneous samples were irradiated for 4 min with UV-LEDs (λ = 365 nm, 0.92 W) for initiation[25] and subsequently transferred into dust-free cylindrical light scattering cells without additional filtration.

10.3.2.3. Dynamic light scattering

DLS experiments were performed as described in Section 2.3.2.2. Polymer radii were obtained by cumulant analysis.[27] In cases of correlation functions showing a double-exponential decay, functions were analysed by a constrained regularisation method based on the so-called CONTIN algorithm using ALV correlator software (see Section 1.2.1).

10.4. Results and discussion

10.4.1. Structural investigations

Ternary phase diagrams of water/EtOH/MMA and water/NPA/MMA are depicted in Figure 10.2. It can be seen that EtOH is more efficient than NPA in solubilising MMA in aqueous solution and full miscibility of water, EtOH and MMA can be obtained for *w*(EtOH) > 0.32 (see Figure 10.2a). For NPA, a more extended biphasic region can be observed and the miscibility gap closes at *w*(NPA) > 0.42 (see Figure 10.2b). In principle, the observed phase behaviour allows the formation of SFME with preferably high water-contents in the so-called pre-Ouzo region (oil-in water SFME).

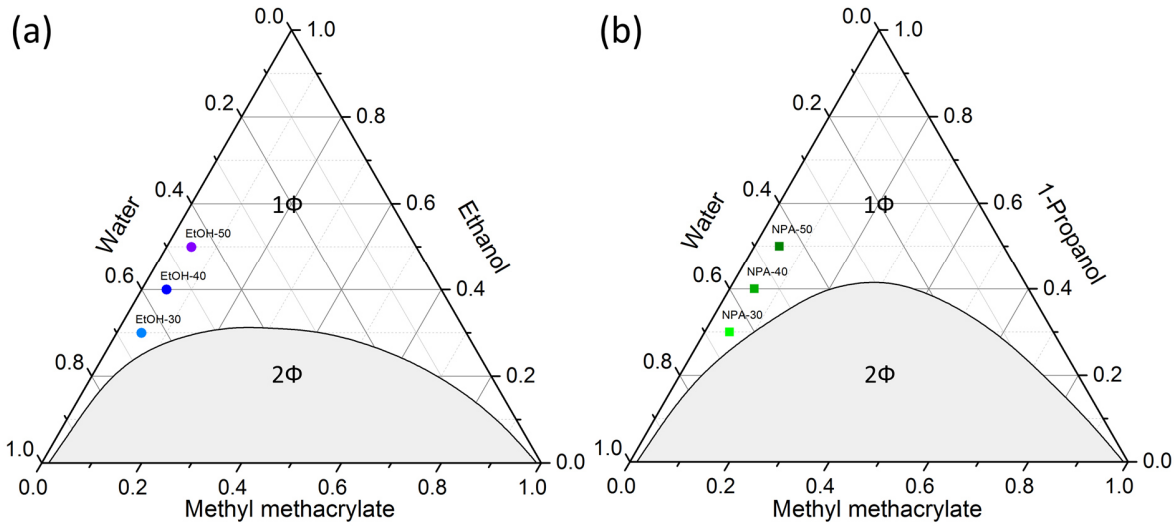

Figure 10.2: Ternary phase diagrams for the systems (a) water/EtOH/MMA and (b) water/NPA/MMA at 25 °C provided in weight fractions. The mono- and two-phasic areas are represented as white and grey areas, respectively. Symbols denote the different compositions measured with DLS and used for polymerisations.

Consequently, DLS measurements were performed in this concentration range for samples EtOH-50/30 and NPA-50/30 (see Figure 10.3a). The obtained correlation functions get successively more pronounced going from EtOH-50 to EtOH-30 and increase further for NPA-50 and NPA-30 with a shift to larger decay times. This indicates the gradual formation of mesoscopic compartmentation between water- and MMA-rich domains, most pronounced in the vicinity to the biphasic region. Furthermore, results show that NPA acts as the better structure-forming hydrotrope compared to EtOH, leading to a hydrodynamic radius of MMA aggregates of approximately 1.5 nm for sample NPA-30. This fact can be attributed to the more amphiphilic character of NPA compared to EtOH. Due to these findings, DLS

measurements were made for samples EtOH-30 and NPA-30 with mixtures of EtOH/NBA and NPA/NBA instead of using pure EtOH or NPA. In Figure 10.3b, hydrodynamic radii are plotted as a function of the NBA content within the alcohol mixture. It can be seen that replacement of EtOH/NPA by NBA leads to a reinforcement of the mesoscopic structure resulting in hydrodynamic radii of MMA aggregates up to 5 nm/13 nm, before phase separation occurs. Consequently, the compartmentation of MMA and water can be further enhanced by addition of NBA.

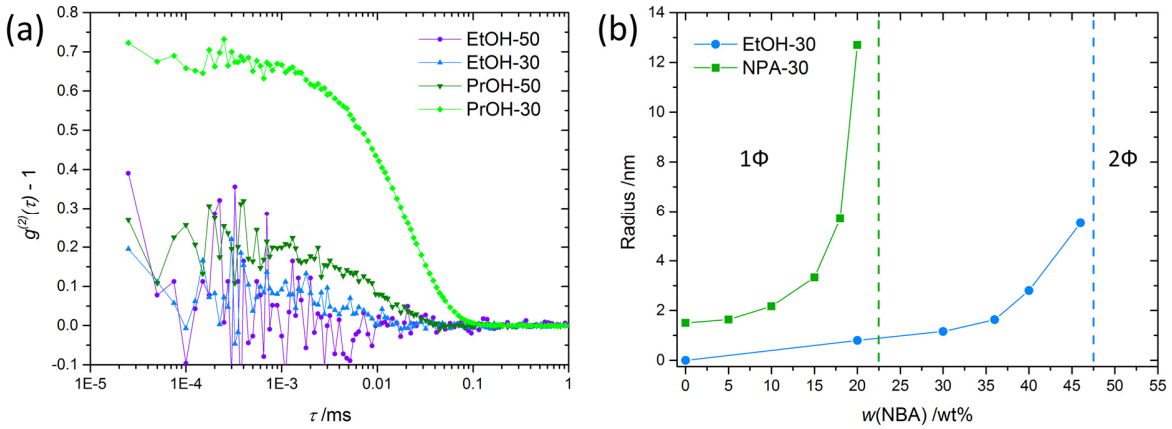

Figure 10.3: (a) Normalised autocorrelation functions of intensity obtained by DLS measurements at 25 °C for ternary mixtures water/EtOH/MMA and water/NPA/MMA. The symbols refer to the specific compositions, which can be taken from Figure 10.2. (b) Hydrodynamic radii calculated from DLS measurements for mixtures water, EtOH/NBA, MMA (EtOH-30) and water, EtOH/NBA, MMA (NPA-30) as a function of the weight fraction of NBA *w*(NBA) within the alcohol mixtures EtOH/NBA and NPA/NBA.

10.4.2. Influence of SFME composition on the polymer growth of PMMA

In order to gain information on the impact of SFME structuring on the polymerisation of MMA, polymer growth of PMMA was investigated for several SFME composed of water/EtOH/MMA and water/NPA/MMA (see Figure 10.2) with PS as initiator (*w*(PS)= 4 mol% with respect to the monomer). Polymer radii derived from DLS measurements as a function of time (corrected for initiation period) are shown in Figure 10.4. Polymers growing rapidly for ternary mixtures consisting of water/EtOH/MMA, decreasing with decreasing EtOH content: EtOH-50 > EtOH-40 > EtOH-30 (see Figure 10.4a). Overall, relatively large polymers were obtained with radii exceeding 1000 nm after only 10 min reaction time. Using NPA instead of EtOH leads to a tremendous decrease of the polymer sizes. Again, the decreasing NPA content results in decreasing polymer radii, reaching an almost linear correlation with increasing reaction time

for NPA-30. Regarding the chain-regulating effect of the alcohol, one would intuitively expect a reverse trend in polymer growth, meaning the observation of increasing radii with decreasing alcohol content.

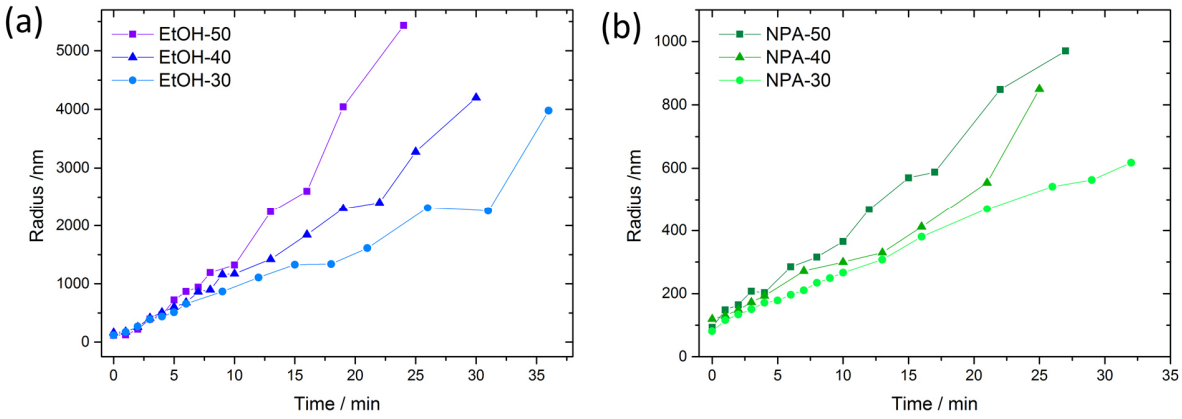

Figure 10.4: Polymer radii derived from DLS measurements as a function of time (corrected for initiation period) for ternary mixtures composed of (a) water/EtOH/MMA and water/NPA/MMA at 25 °C. Symbols denote different compositions used for polymerisation (see Figure 10.2).

Instead, it was observed that polymer growth obviously correlates with the successive formation of SFME going from EtOH-50 to EtOH-30 and NPA-50 to NPA-30. In other words, compartmentation between hydrophilic water-rich and hydrophobic monomer-rich pseudo-phases was found to be beneficial in order to retard the polymerisation. Consequently, control over polymer growth can be obtained using well-structured SFME. This observation may be attributed to the fact that the aqueous pseudo-phase creates a barrier between growing polymers and residual monomer droplets, which can act as a reservoir for a more controlled polymer growth.

10.4.3. Impact of initiator concentration and NBA addition

Measurements presented in Section 10.4.2 were carried out in the presence of relatively high amounts of initiator. Thus, the ratio of initiator to monomer was gradually reduced in order to investigate the influence of the initiator concentration on the polymer growth (see Figure 10.5a). By reducing the PS concentration, polymers start to grow more rapidly at the beginning, leading to polymer radii of 150-200 nm. However, the further polymerisation progress shows a relatively moderate polymer growth ending in particle radii of approximately 300 nm after 40 min reaction time. These significant differences upon decreasing the initiator concentration can be explained by a dilution effect of the growing polymers. For high initiator concentrations, there is a struggle for available monomers at the beginning of the

polymerisation, since many nucleation centres start to grow simultaneously. Following this argument, it is evident that polymer growth of solutions containing less growing polymers is less disturbed and polymer radii increase rapidly. Yet, after this induction period, further polymer growth is retarded. This finding may be attributed to a lower probability of radical recombination/agglomeration of two polymer chains.

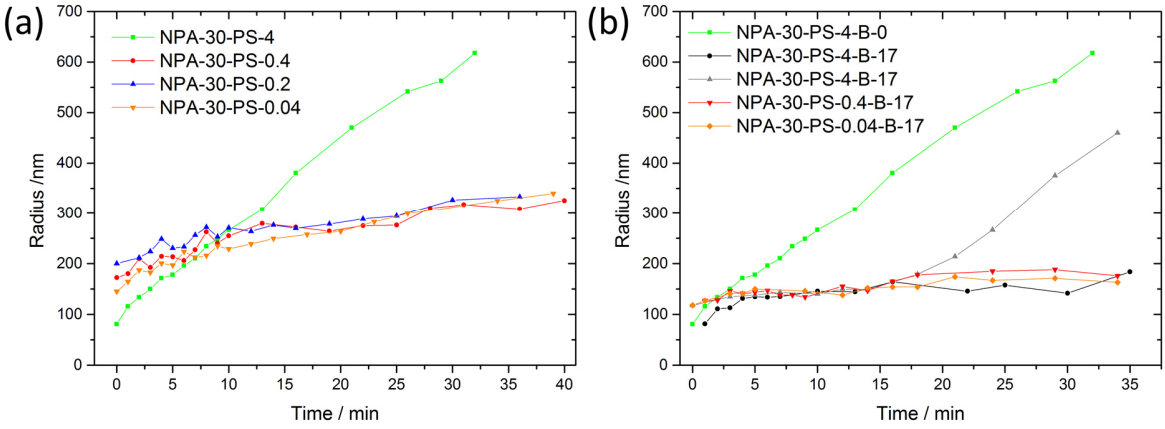

Figure 10.5: Polymer radii derived from DLS measurements as a function of time (corrected for initiation period) for ternary mixtures composed of (a) water/NPA/MMA (mixture NPA-30) and (b) pseudo-ternary mixtures water/alcohol/MMA (mixture NPA-30 with 17 wt% NBA in NPA) at 25 °C. Symbols denote different SFME compositions (NPA-30, see Figure 10.2) with varying PS concentrations used for polymerisation given in mol% (with respect to the monomer). In addition, the NBA content (B) within the alcohol mixture used for SFME formation is given in wt%.

Measurements of polymer growth in mixtures containing NBA are shown in Figure 10.5b. Polymerisations were performed in pseudo-ternary mixtures containing 5 wt% MMA, 65 wt% water and 30 wt% of a mixture containing 17 wt% of NBA in NPA. Furthermore, the PS concentration was varied as before. It can be seen that addition of NBA has a significant influence on the polymer growth, leading to a tremendous decrease of the polymer size (radius below 200 nm even after 35 min reaction time). Two effects can explain these findings:

(i) NBA has a stronger chain regulating effect, due to the longer alkyl chain compared to NPA. This leads to shorter mean polymer sizes.

(ii) Replacement of NPA by NBA leads to a strengthening and swelling of MMA-rich aggregates (as shown in Figure 10.3b), accompanied by a kinetic stabilisation of these aggregates resulting in more time stable monomer droplets and growing polymers.

Consequently, an enhanced compartmentation between water- and MMA-rich domains over a longer time period can be expected resulting in a slower and more controlled polymer

growth. These findings can be further supported by having a closer look at NBA-containing mixtures with the highest initiator concentration. Two measurements were performed for this mixture, resulting in a very different behaviour of polymer growth. Both mixtures lead to similar polymer sizes for up to 18 min reaction time. For one mixture, controlled polymer growth was found after this point leading to polymers with radii below 200 nm. On the other hand, a change of the slope was observed for the other mixture resulting in a rapid polymer growth, similar to the mixture without NBA addition. This behaviour reflects well the kinetic stabilisation mechanism due to compartmentation of water- and MMA-rich domains, which is sometimes not pronounced enough to avoid rapid polymer growth. It has to be noted that these findings are not expected regarding solely the chain regulating effect of butanol. Thus, mesoscale structuring of the SFME has to be the key parameter for the observed growth behaviour.

10.4.4. Water-soluble versus monomer-soluble initiator

Since the initiator itself can often have a significant influence on polymerisations, AIBN was chosen as a second, monomer-soluble, initiator in order to compare with polymerisation initiated by the charged, water-soluble PS. Polymer growth of AIBN initiated polymerisations for various initiator concentrations in ternary mixtures of water/NPA/MMA (mixture NPA-30) and pseudo-ternary mixtures containing 5 wt% MMA, 65 wt% water and 30 wt% of a mixture containing 17 wt% of NBA in NPA are shown in Figure 10.6. It has to be mentioned that the concentrations of AIBN were adapted in order to have the same ratio of free radicals to monomers as also used for polymerisations using PS as initiator.

Regarding AIBN initiated polymerisations in ternary mixtures of water/NPA/MMA, a similar trend compared to PS initiated reactions can be observed. Lowering the initiator concentrations again leads to lower particle sizes. Whereas for the lowest AIBN concentration similar radii (below 200 nm) are obtained as for the PS initiated reactions, higher concentrations lead to larger polymers as it was found for PS (r > 2000 nm for AIBN and r > 500 nm for PS). These results show that polymer radii for polymerisations started with AIBN can be less controlled for increasing concentrations of the initiator compared to PS initiated reactions. Furthermore, results indicate that an additional stabilisation mechanism has to be taken into consideration when high amounts of initiators are used: Since PS leaves a charge at one end of the growing polymer, electrostatic repulsion may help to stabilise formed polymers, which is not possible using AIBN as initiator. Consequently, chain recombination is less probable when a charged initiator is involved leading to smaller polymers. These findings are further supported by the fact that differences of the polymer size

are more visible for high initiator concentrations than for lower ones. Hence, when a sufficiently low number of growing polymers is reached, the choice of the initiator does no longer play a major role and similar polymer sizes are obtained.

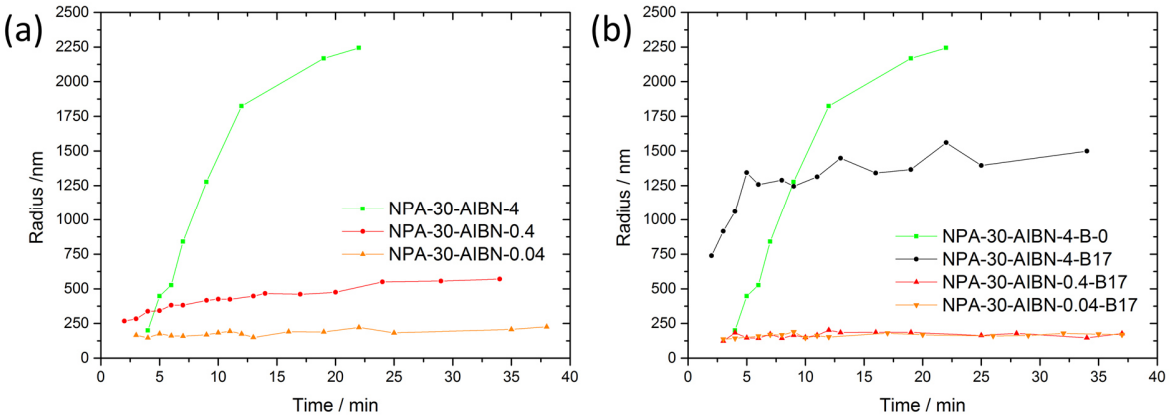

Figure 10.6: Polymer radii derived from DLS measurements as a function of time (corrected for initiation period) for ternary mixtures composed of (a) water/NPA/MMA (mixture NPA-30) and (b) pseudo-ternary mixtures water/alcohol/MMA (mixture NPA-30 with 17 wt% NBA in NPA) at 25 °C. Symbols denote different SFME compositions (NPA-30, see Figure 10.2) with varying AIBN concentrations used for polymerisation given in mol% (with respect to the monomer). In addition, the NBA content (B) within the alcohol mixture used for SFME formation is given in wt%.

Furthermore, results indicate that the location at which the polymer chain is started (aqueous versus monomer-rich pseudo-phase) has no influence on the polymer growth. Due to fluctuations of the aggregates, there is always enough monomer in the aqueous pseudo-phase which can react with the water-soluble initiator and subsequently diffuse in MMA-rich aggregates for chain propagation. In the case of AIBN initiated polymerisations, one may expect that initiation occurs directly within the monomer droplets.

In addition, the influence of partial NPA replacement by NBA was investigated analogous to PS initiated polymerisations (see Figure 10.6b). It was found that the usage of NBA to form the SFME can help to lower the polymer size depending on the AIBN concentration used for polymerisation. For high initiator concentrations, only a marginal decrease of the polymer sizes could be obtained compared to polymerisation without NBA. However, going to lower AIBN concentrations, it was found that addition of NBA can help to kinetically stabilise growing particles leading to polymers below 200 nm in radius, which are in the same size range as also observed for PS initiated polymerisations.

10.5. Conclusion and outlook

Results obtained for the polymerisation of MMA in SFME composed of water, alcohol and MMA lead to the conclusion that mesoscale compartmentation of monomer- and water-rich domains (o/w SFME) has a significant influence on the polymer growth of PMMA. DLS experiments showed that kinetic control over the particle growth can be obtained and tuned by the use of different alcohols (EtOH/NPA/NBA) and compositions of water/alcohol/monomer (pseudo-)ternary mixtures resulting in more or less pronounced structuring of the SFME. Gradual formation of SFME leads to a kinetic control mechanism of the polymer growth. In other words, compartmentation of monomer- and water-rich domains helps to retard the polymer growth. EtOH was found to form weakly to non-structured solutions leading to rapidly growing polymers (hydrodynamic radii > 2000 nm after 30 mins). On the other hand, PMMA growth was found to be retarded in NPA containing SFME, due to an enhanced compartmentation of MMA droplets in the outer aqueous pseudo-phase. It has to be noted that chain-regulating effects of the alcohol were found to play a minor role compared to the compartmentation effect of the solution.

Furthermore, it was found that partial replacement of NPA by NBA enhances the compartmentation between monomer- and water-rich domains, leading to polymer radii below 150 nm even after 30 min of reaction time. Moreover, it was found that polymer growth depends significantly on the initiator concentration. Lowering the concentration of AIBN/PS leads to faster polymer growth at the beginning of the reaction, compared to higher concentrations. This effect may be attributed to a struggle for monomers at the beginning of the reaction. However, the further progress of the reaction shows a decrease of the polymer growth for low initiator concentrations, due to a lower probability of chain recombination and agglomeration. In addition, the choice of the initiator was found to be important when it comes to high initiator concentrations. Using PS as water-soluble, charged initiator leads to smaller polymers compared to the hydrophobic, monomer-soluble AIBN. This fact may be explained by a further stabilisation mechanism, which is based on electrostatic repulsion resulting in lower probability of chain recombination and agglomeration.

All in all, it was found that compartmentation of MMA- and water-rich domains can help control the polymer growth, and particle radii below 150 nm can be obtained depending on the SFME composition. It is likely that the initial SFME serves as a monomer-reservoir feeding growing particles. Consequently, the principle of SFME polymerisation may be closely related to classical emulsion and microemulsion polymerisations. Thus, SFME can provide a serious alternative for polymer synthesis compared to classical microemulsions.

However, many things are left to be clarified and investigated. Other hydrotropes like TBA could even have an even stronger effect on the polymerisation due to enhanced chain-regulating effects (tertiary alcohol vs primary alcohol). First results seem promising for this assumption to be justified (see Appendix A.8, Figure A8.1). Effects of oxygen in the solutions have to be investigated. Furthermore, the use of retardants and inhibitors (*e.g.* mercaptans and hydroquinone) could help to obtain even smaller polymer chains. Especially short-chain thiols could act as both, structure-enhancing and chain-regulating agent. In addition, other investigation techniques like cryo-electron microscopy, size exclusion chromatography and NMR can be helpful in order to determine other important characteristic properties of the formed polymers, like the polydispersity, the molecular weight distribution or the reaction yield. Finally, having a look at long-term developments, the monomer should be replaced by industrially more relevant monomers like isoprene, styrene or vinyl chloride. By doing so, SFME polymerisation may be entrenched as a green polymerisation technique, widely replacing current polymerisation processes for the future production of a great variety of polymer latices.

10.6. References

1 D. C. Blackley, Polymer Latices, Volume 1, Chapman & Hall, London, 2nd edn., 1997.

2 V. Zargar, M. Asghari and A. Dashti, *ChemBioEng Rev.*, **2015**, *2*, 204–226.

3 K. Hamad, M. Kaseem, H. W. Yang, F. Deri and Y. G. Ko, *Express Polym. Lett.*, **2015**, *9*, 435–455.

4 K. S. Ngai, S. Ramesh, K. Ramesh and J. C. Juan, *Ionics (Kiel).*, **2016**, *22*, 1259–1279.

5 V. K. Thakur, M. K. Thakur, P. Raghavan and M. R. Kessler, *ACS Sustain. Chem. Eng.*, **2014**, *2*, 1072–1092.

6 J. Brydson, Brydson's Plastics Materials, Butterworth-Heinemann, Oxford, 8th edn., 2016.

7 D. C. Blackley, Polymer Latices, Volume 2, Chaoman & Hall, London, 2nd edn., 1997.

8 E. Vivaldo-Lima, P. E. Wood, A. E. Hamielec and A. Penlidis, *Ind. Eng. Chem. Res.*, **1997**, *36*, 939–965.

9 N. K. Pokhriyal and S. Devi, *Eur. Polym. J.*, **2000**, *36*, 333–343.

10 C. Norakankorn, O. Pan, G. L. Rempel and S. Kiatkamjornwong, *Macromol. Rapid Commun.*, **2007**, *28*, 1029–1033.

11 W. Ming, F. N. Jones and S. Fu, *Polym. Bull.*, **1998**, *40*, 749–756.

12 J. Ausa, *J. Polym. Sci. Part A Polym. Chem.*, **2004**, *42*, 1025–1041.

13 A. M. van Herk, Ed., Chemistry and Technology of Emulsion Polymerisation, John Wiley & Sons, Oxford, 2nd edn., 2013.

14 K. Jardak, P. Drogui and R. Daghrir, *Environ. Sci. Pollut. Res.*, **2016**, *23*, 3195–3216.

15 M. J. Scott and M. N. Jones, *Biochim. Biophys. Acta - Biomembr.*, **2000**, *1508*, 235–251.

16 T. Zemb, M. L. Klossek, T. Lopian, J. Marcus, S. Schöttl, D. Horinek, S. Prevost, D. Touraud, O. Diat, S. Marčelja and W. Kunz, *Proc. Natl. Acad. Sci. U. S. A.*, **2016**, *113*, 4260–4265.

17 W. Kunz, K. Holmberg and T. Zemb, *Curr. Opin. Colloid Interface Sci.*, **2016**, *22*, 99–107.

18 S. Prevost, T. Lopian, M. Pleines, O. Diat and T. Zemb, *J. Appl. Crystallogr.*, **2016**, *49*, 2063–2072.

19 T. Lopian, S. Schöttl, S. Prevost, S. Pellet-Rostaing, D. Horinek, W. Kunz and T. Zemb, *ACS Cent. Sci.*, **2016**, *2*, 467–475.

20 T. Buchecker, S. Krickl, R. Winkler, I. Grillo, P. Bauduin, D. Touraud, A. Pfitzner and W. Kunz, *Phys. Chem. Chem. Phys.*, **2017**, *19*, 1806–1816.

21 S. T. Camli, F. Buyukserin, O. Balci and G. G. Budak, *J. Colloid Interface Sci.*, **2010**, *344*, 528–532.

22 C. G. Dobie and K. V. K. Boodhoo, *Chem. Eng. Process. Process Intensif.*, **2010**, *49*, 901–911.

23 W. R. Palani Raj, M. Sasthav and H. Michael Cheung, *Langmuir*, **1991**, *7*, 2586–2591.

24 K. Tauer, R. Deckwer, I. Kühn and C. Schellenberg, *Colloid Polym. Sci.*, **1999**, *277*, 607–626.

25 Z. Liu, G. Zhang, W. Lu, Y. Huang, J. Zhang and T. Chen, *Polym. Chem*., **2015**, *6*, 6129–6132.

26 M. Clausse, L. Nicolas-Morgantini, A. Zradba and D. Touraud, in Surfactant Science Series (Vol. 24) Microemulsion Systems, eds. H. L. Rosano and M. Clausse, Dekker, New York, 1987, p. 15.

27 R. Pecora, *J. Nanoparticle Res.*, **2000**, *2*, 123–131.

Chapter 11 Summary and outlook

Within this work several potential fields of application of SFME were investigated. In the first part, general rules were provided for the formulation of aqueous SFME regarding the choice of hydrotropes and the hydrophobic component (oil). First, the influence on structure and solubility of SFME was systematically investigated with regard to the aliphatic moiety of the hydrotrope (short-chain alcohols). Subsequently, an analogue study was presented considering in particular the functional group of the hydrotrope. Both studies took also into account the chemical nature of the used oil. In summary, it was found that for hydrophobic components able to interact via hydrogen-bonding, SFME formation is facilitated and less specific demands have to be made on the hydrotrope. For purely aliphatic oils, more stringent requirements to the hydrotrope exist.

These findings were discussed in terms of pre-structuring of hydrotropes in aqueous solution and structure formation induced by the oil component. It was found that different solubilisation mechanisms are involved in SFME. Oil components, which have no functional groups, can be intercalated in given pre-structures of hydrotropes in water leading to a swelling and strengthening of such aggregates. However, a hydrotrope is needed with a pronounced amphiphilic character able to interact with both, water and oil. Typical representatives for such kind of hydrotropes are for example NPA and TBA, which can both interact well with water via hydrogen bonding and the oil via van der Waals interactions. This is usually accompanied by an enhanced solubility compared to more co-solvent-like hydrotropes like EtOH. Yet, the situation is different regarding hydrophobic components with functional groups that allow other ways of interactions (*e.g.* OH-groups). In such a case, pre-structuring is not pivotal for SFME formation and may be even obstructive. In fact, the addition of such oils itself to unstructured water/hydrotrope mixtures even induces the formation of the SFME. Thus, the requirements on the hydrotrope are lower, meaning that hydrotropes can be used which one may rather classify as a co-solvent (*e.g.* EtOH). Furthermore, the functional group of the hydrotrope may not necessarily act as both H-Bond donor and acceptor in order to obtain a structured ternary mixture. Even H-bond-free microemulsions can be formed, when other interactions like strong dipole-dipole interactions are involved. Nevertheless, the use of hydrotropes possessing both, acceptor and donor, was found to be beneficial for SFME formation. Besides, more complex solubilisation mechanisms may occur involving for instance the interface between

compartmented domains. In any case, the formation of SFME was found to be always beneficial for an enhanced miscibility of water and the oil.

Based on the general principles and guidelines for SFME formulation presented in the first part, the focus of the rest of this thesis was put on potential applications of SFME. The investigated fields of application can be further divided in two subparts: application of SFME for separation and extraction processes and their use as reaction media.

Within this context, a new method was developed in order to couple microemulsion electrokinetic chromatography (MEEKC) with UV and MS detection. The used SFME consisted of water, EtOH, 1-octanol and ammonium acetate in order to form charged octanol aggregates. By doing so, all components can be injected in an ESI-MS setup enabling successful detection of the analytes. The resulting method called surfactant-free microemulsion electrokinetic chromatography (SF-MEEKC) is an alternative method to classical surfactant-based MEEKC, coupling this analytical separation method to UV and MS detection. It could be shown that both, charged and neutral analytes can be successfully separated using SF-MEEKC. Within a proof of concept, the method was successfully applied determining the content of vitamin D_3 in a commercial drug.

In addition, two further concepts were presented which are focused on extraction processes and the subsequent separation of potential extracted compounds. For both concepts, advantages of SFME extraction can be exploited, meaning enhanced solubility of potential hydrophobic compounds within a mesoscale structured aqueous solution.

The first concept makes use of SFME with cleavable constituents. Solketal and triethyl citrate were used as cleavable hydrotrope/hydrophobic component. Analogue to the well-established concept using cleavable surfactants, phase separation is induced by hydrolysis of the labile compounds. As a proof of concept, surrogate solutes were used resulting in quantitative separation as expected. Thus, such mixtures are interesting media for green extraction processes but also as reaction media facilitating separation and recovery of solutes and reagents.

Another concept comprised the use of centrifugation techniques in order to separate SFME into oil-rich and water-rich mixtures. In principal, two separation procedures can be applied to do so. First, analytical ultracentrifugation of an o/w SFME can be performed leading to a concentration gradient within the centrifuged sample. Another approach is based on macroscopic phase separation of an o/w SFME and subsequent conventional centrifugation of the biphasic mixture. Phase separation can be easily induced by a change of temperature or the addition of water. Both methods may be relevant in practice and can be applied for

extractions using SFME. Yet, precise data on density and molar volumes had to be determined in order to apply these concepts. For this reason, hypersurfaces of density and molar volumes of different SFME were calculated based on precise density measurements, for a great number of samples. By doing so, highly precise data on densities and molar volumes for every monophasic composition of the investigated SFME can be easily calculated now.

In the last part of this dissertation, several reactions were performed in SFME used as reaction media. To this purpose, a systematic study was presented concerning the impact of mesoscale structuring on the kinetics of a chemical reaction. It could be demonstrated that mesoscale structuring can have significant influences on the outcome of a chemical reaction. However, the reaction investigated in this chapter was affected negatively due to compartmentation of the reactive species within water- and oil-rich domains. This study represents one of the first dealing with this topic by an in-depth analysis of the structure-reactivity relationship and provides basic strategies for a thorough approach to such an issue.

In addition, three types of reactions were investigated using SFME as reaction media. The first one are so-called “on water” reactions. To this purpose, kinetics of a typical Diels–Alder cycloaddition were measured in different SFME, SFE and on water. It could be shown that SFME as used in this study are not able to yield a similar reaction rate acceleration than obtained for systems where a macroscopic interface is present between water and the reagents. Results presented in this thesis revealed fundamental aspects on chemical reactivity of on water reactions. It was concluded that dynamics of SFME may play a major role for such kind of reactions. It is likely that dynamics of water molecules (*e.g.* reorientation and relaxation processes) at the interface of water- and reagent-rich compartments are much faster in SFME than for SFE. Furthermore, the interface may get blocked by the hydrotrope reducing the effective contact area to free water molecules. Consequently, SFME could not yield the same rate acceleration as found for SFE. Nevertheless, comparable reactivity could be obtained in monophasic aqueous SFME as observed for the reaction of pure components.

Another class of reactions investigated within this work were enzyme catalysed reactions performed in SFME. Based on pioneering studies of Khmelnitsky *et al.* and the working group of Xenakis, enzyme activity was investigated in different SFME and compared to those observed in SBME performed by Bauduin *et al.* in 2005 (see Chapter 9). Findings presented in this study revealed that the ability of short-chain alcohols to form mesostructures (aqueous aggregates in oil) has a crucial effect on the enzyme activity in SFME. It was concluded that the most pronounced mesoscale-structured SFME lead to the highest enzymatic activities,

resulting in comparable enzyme activities as observed for pure buffer solution, yet, with water contents below 5 wt%. Many parallels could be drawn to enzyme activity in SBME leading to a significant contribution for the understanding of enzyme activity in such systems.

In the last chapter of this dissertation, a more industrially relevant example for the use of SFME as reaction media was given. It could be successfully demonstrated that with the aid of SFME, polymerisation reactions can be conducted with a kinetic control of the polymer size. Overall, a reduction of the polymer size could be reached by approximately a factor of 50 compared to solution polymerisation (unstructured solutions). Thus, particle radii below 150 nm could be obtained, depending on the SFME composition. Unlike to classical polymerisation techniques like emulsion polymerisation, no surfactant or suspension agents had to be added, which significantly facilitates subsequent recovery of the solvent and polymer purification. Furthermore, this polymerisation technique avoids intense stirring of the solution (as needed for emulsion and suspension polymerisation) due to the use of a monophasic SFME. For all these reasons, SFME polymerisation represents a green alternative to conventional polymerisation techniques for the industrial production of polymer latices from many kinds of monomers like styrene, isoprene or vinyl chloride.

Studies performed within this dissertation show the great potential of SFME for various applications. However, the targeted use of SFME is still an emerging field and research has to be intensively continued for the market-ready use of such systems in industry. Beginning with the basic understanding of SFME, there are many things which have to be clarified. In this study, mostly simple aliphatic alcohols were used as hydrotropes. However, also other classes of hydrotropes may be of particular interest for a more targeted SFME formation. For instance, the use of charged and multifunctional hydrotropes could provide new opportunities and insights in SFME formulation. Overall, SFME were shown to be useful for the solubilisation of hydrophobic compounds making them attractive media for separation and extraction processes. In this context, well-established extraction processes using for example surfactant-based extraction media may be questioned regarding process optimisation.

In addition, reactivity in SFME could play an important role for future tailor-made reaction media. It is of great importance to investigate such phenomena, since such sort of supramolecular structures are often neglected when the influence of a solvent on the chemical reactivity is discussed. Ill-defined solution structuring may be the key for manifold types of reactions, including basic organic reactions, catalysis, enzymatic reactions, polymerisations or the template synthesis of nanoparticles. The targeted usage of a subtle mesoscale structured solution can help conducting a reaction in different ways and unlike more rigid

structures formed in surfactant-based mixtures, such aggregates can be easily broken after the desired application without much energy and effort. Especially biological processes often profit from such a concept. It is likely that many reactions performed in such mixtures unknowingly form mesoscale structured solutions with serious impact on the reaction kinetics. Such effects may have been overlooked in the past for a great variety of reactions showing extraordinary solvent sensitivity.

Regarding all these aspects it is evident that the investigation of SFME should be an important subject of future research. Thus, this thesis was one of the first to thoroughly investigate the capability of SFME for different potential fields of application, which are by far not exhausted.

Appendix

A.1 The impact of the structuring of hydrotropes in water on the mesoscale solubilisation of a third hydrophobic component

SANS-Measurements

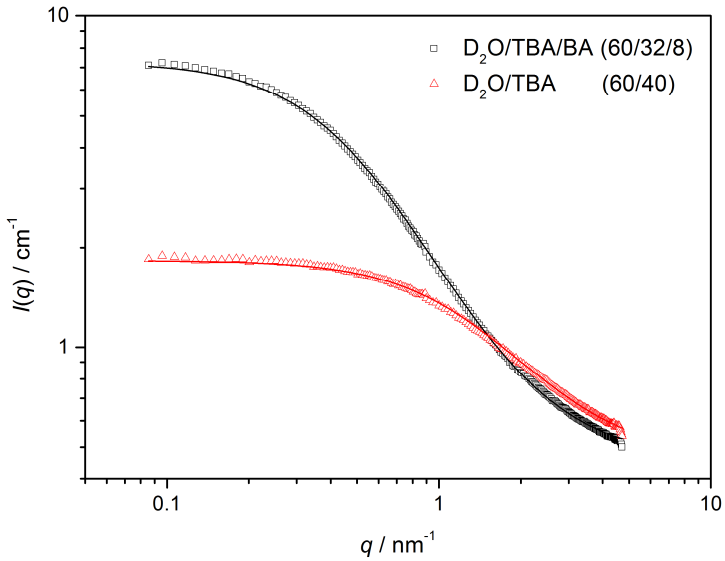

Figure A1.1: SANS spectra of the binary D_2O/TBA mixture and the ternary D_2O/TBA/benzyl alcohol (BA) mixture. Symbols indicate the different mass ratios of D_2O, TBA and BA in weight percentage.

Second-order derivative of Figure 2.5c

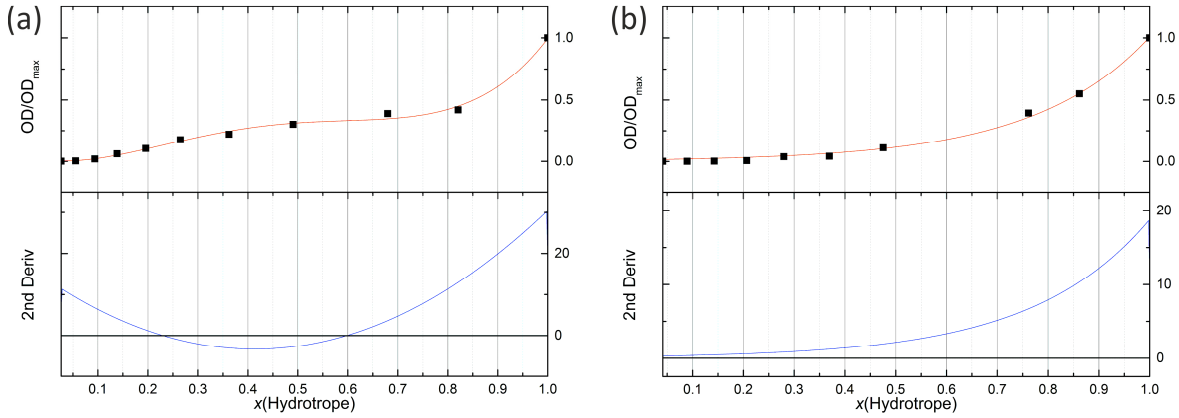

Figure A1.2: Fourth order polynomial/exponential fit function (Eq. A1.1 and A1.2) of data gained from OD measurements of DR-13 in (a) TBA/H_2O and (b) EtOH/H_2O mixtures with water (red curve) and their corresponding second derivative (blue curve). Black squares denote the experimentally determined data.

Functions used for data fitting:

Values for OD/OD_{max} of TBA were fitted according to a fourth order polynomial function as follows:

$$y = A_0 + A_1 x + A_2 x^2 + A_3 x^3 + A_4 x^4 \quad \text{(A1.1)}$$

Values for OD/OD_{max} of EtOH were fitted according to an exponential function as follows:

$$y = B_0 + B_1 \cdot \exp(B_2 \cdot x) \quad \text{(A1.2)}$$

All fit parameters are summarised in Table A1.1.

Table A.1.1: Fit parameters used for the fourth order polynomial/exponential fit function (Eq. A1.1 and A1.2) of data gained from OD measurements of EtOH/TBA mixtures with water.

Parameter	
A_0	0.00984
A_1	-0.40876
A_2	6.76631
A_3	-13.56793
A_4	8.19464
B_0	0
B_1	0.01339
B_2	4.32016

A.2 The role of hydrogen bond donor and acceptor functionalities on the formation surfactant-free microemulsions

Sample compositions

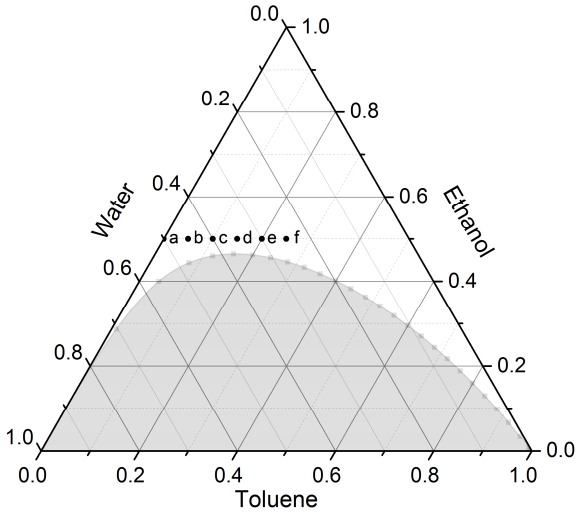

Figure A2.1: Sample compositions of water/ethanol/toluene given in mole fraction for points *a* to *f*: *a* - (50/50/0), *b* - (45/50/5), *c* - (40/50/10), *d* - (35/50/15), *e* - (30/50/20), *f* - (25/50/25).

H-bond-free SFME (Acetonitrile/Acetone/Limonene)

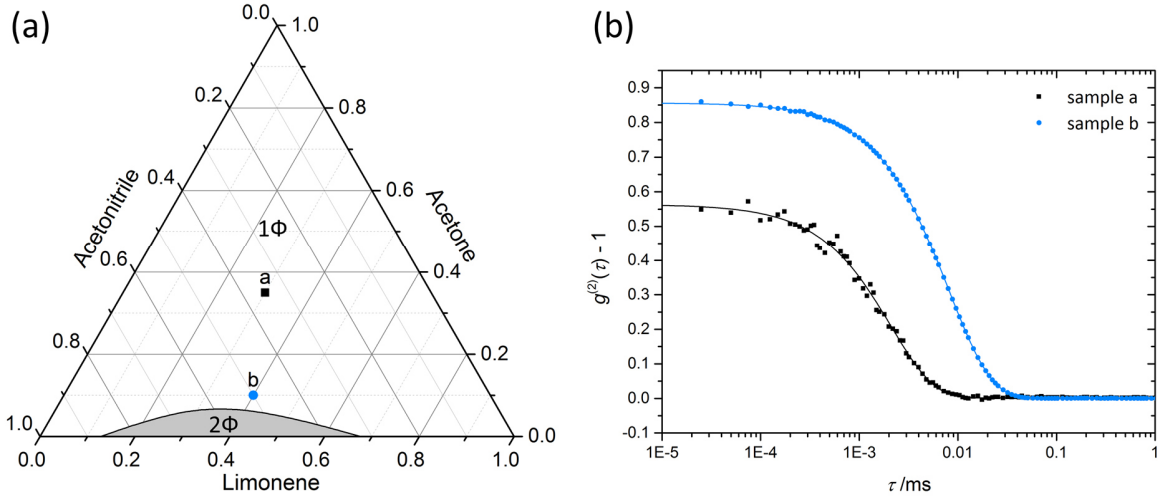

Figure A2.2: Ternary phase diagrams of acetonitrile/acetone/limonene at 25 °C provided in weight fractions. The mono- and two-phasic areas are represented as white and grey areas, respectively. Symbols denote the different compositions of acetonitrile/acetone/limonene measured with DLS (b).

A.3 Surfactant-free microemulsion electrokinetic chromatography (SF-MEEKC) with UV and MS detection – a novel approach for the separation and ESI-MS detection of neutral compounds

SAXS measurements, fit parameter and calculated aggregate radii

SAXS data were analysed using Table Curve 2D v5.01 software. Following Ornstein–Zernike (OZ) equation was used for data fitting in the low-*q*-range (0.275 - 4 nm^{-1}) with a constant background value (bkg) of 0.017 cm^{-1}:

$$I(q) = \frac{I_0}{1 + \xi^2 q^2} + \mathrm{bkg} \qquad \text{(A3.1)}$$

SAXS measurements with the corresponding fit functions are shown in Figure A3.1. Parameters of the applied fit functions and calculated aggregate radii are summarised in Table A3.1.

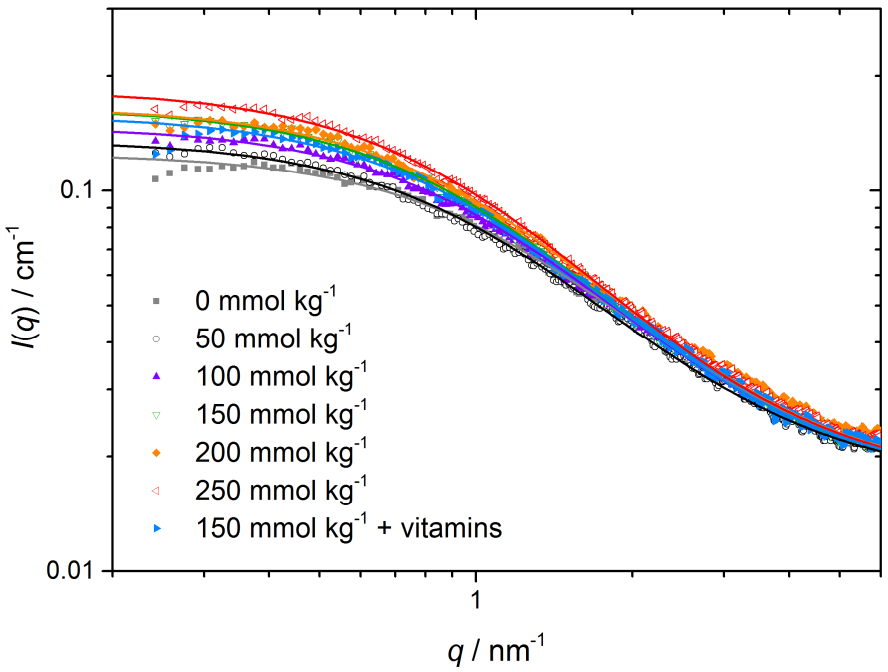

Figure A3.1: SAXS measurements and corresponding OZ fit functions for different molalities of ammonium acetate of surfactant-free microemulsions consisting of 37.5% water, 43.75% ethanol, and 18.75% 1-octanol (*w*/*w*/*w*).

Table A3.1: Parameters of the OZ fits and calculated aggregate radii R_G for different molalities of ammonium acetate of surfactant-free microemulsions consisting of 37.5% water, 43.75% ethanol, and 18.75% 1-octanol (*w*/*w*/*w*).

Ammonium acetate	I_0	ξ	R_G
mmol kg^{-1}	cm^{-1}	nm	nm
0	0.1085	0.838	1.873
50	0.1190	0.939	2.099
100	0.1307	0.943	2.108
150	0.1483	1.008	2.254
200	0.1488	0.969	2.168
250	0.1673	1.039	2.324
150 (+vitamins[a])	0.1412	0.981	2.193

[a] vitamins B_1, B_2 and D_3 added as described in Section 4.3.1.2

A.4 Surfactant-free microemulsions with cleavable constituents

Dynamic light scattering

Hydrodynamic radii were calculated using cumulant analysis according to Section 1.2.1.

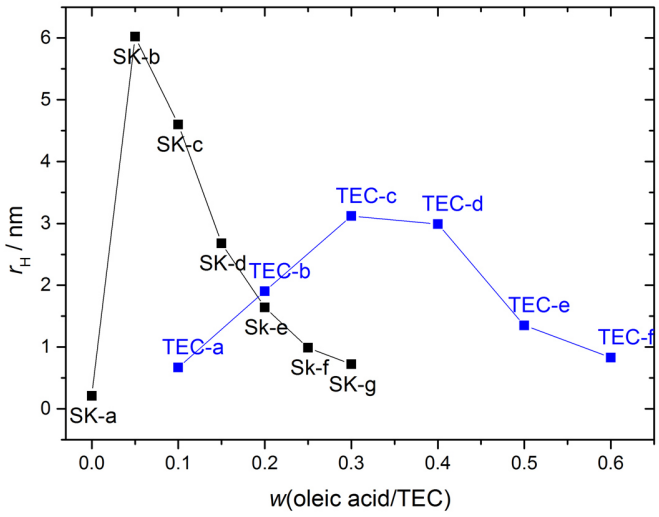

Figure A4.1: Hydrodynamic radii r_H obtained from DLS measurements for ternary mixtures composed of water/Solketal/oleic acid (samples SK-a to SK-g) and water/ethanol/TEC (samples TEC-a to TEC-f) as a function of the weight fraction of oleic acid and TEC, respectively.

Ternary system: water/acetone/oleic acid

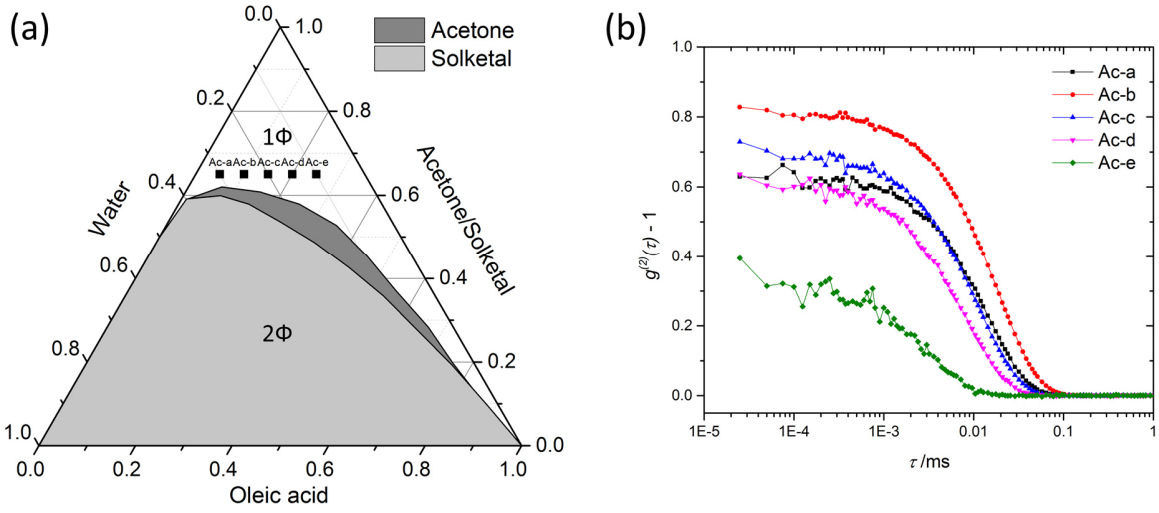

Figure A4.2: Ternary phase diagrams of water/acetone/oleic acid and water/Solketal/oleic acid at 25°C provided in weight fractions. The mono- and two-phasic areas are represented as white and grey areas, respectively. Symbols denote the different compositions of water/acetone/oleic acid measured with DLS (b).

pH-Measurements for the system water/Solketal/oleic acid

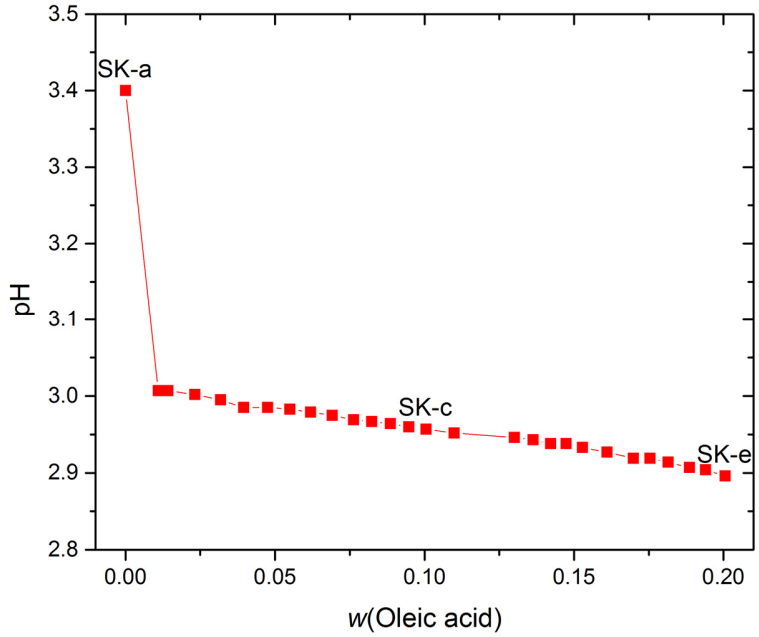

Figure A4.3: pH-Value as a function of the weight fraction of oleic acid for ternary mixtures water/Solketal/oleic acid (Samples SK-a to SK-e).

HPLC measurements

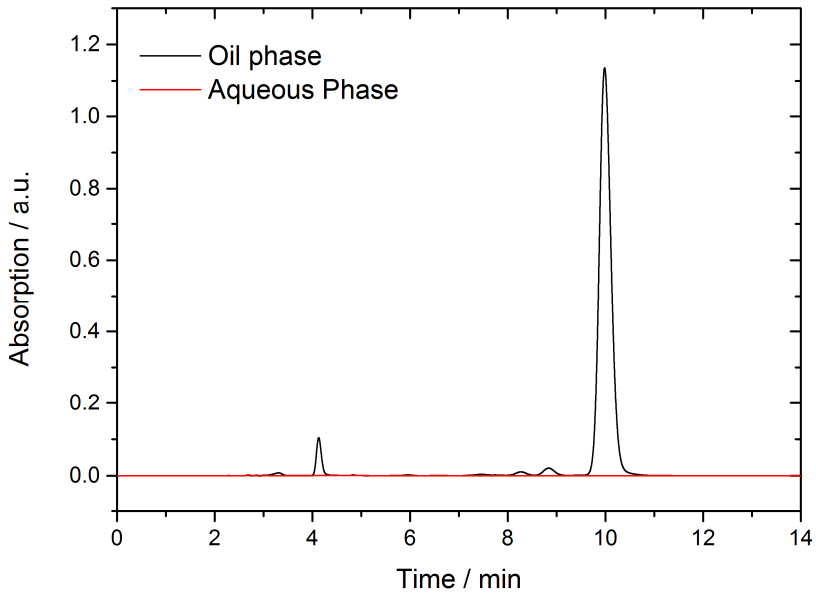

Figure A4.4: Chromatograms of the oil (black) and the water phase (red). The corresponding peak of Toc can be found at a retention time of 10 min.

^{1}H-NMR measurements

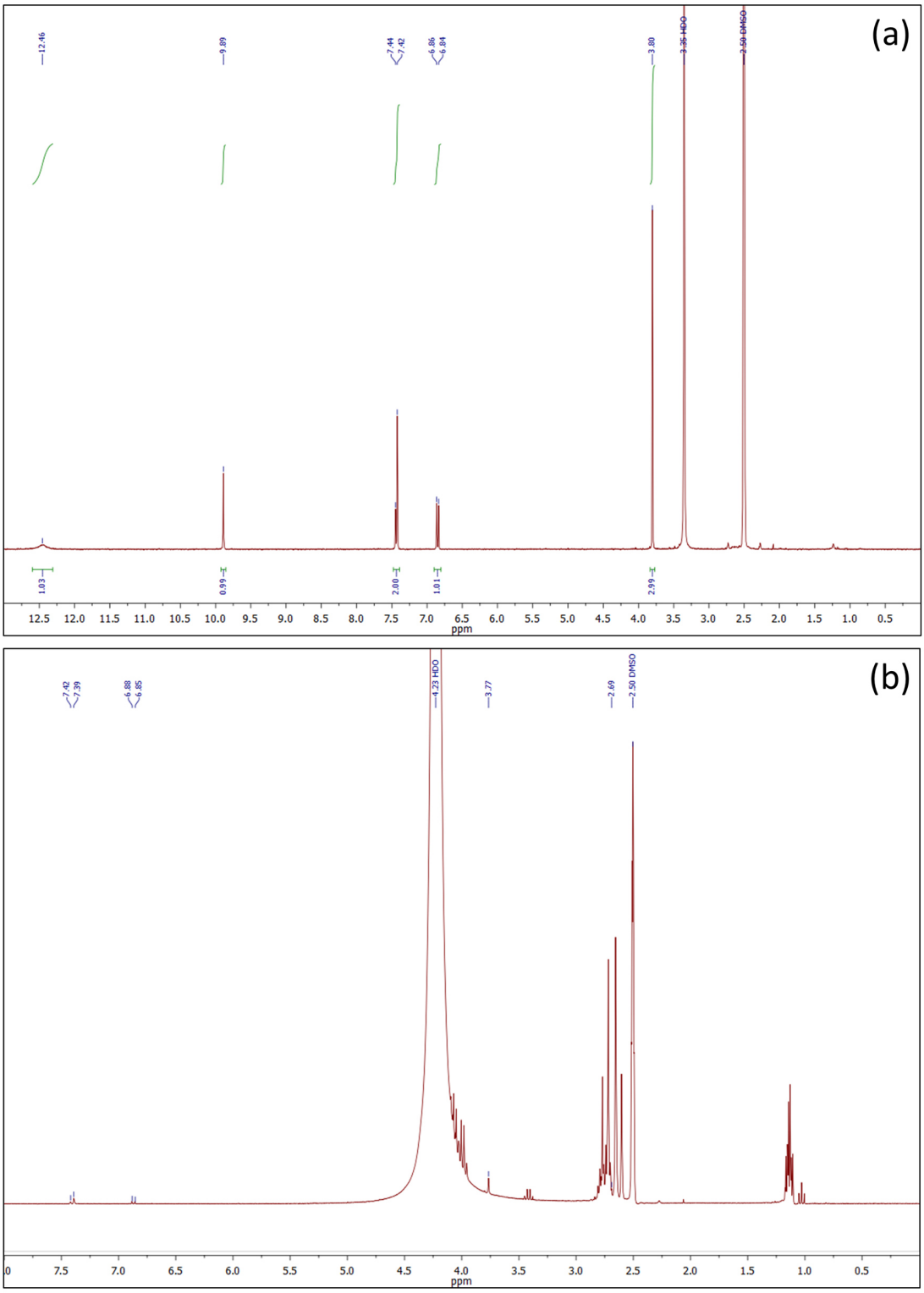

Figure A4.5: ^{1}H-NMR spectra (300 MHz) of filtered VA (a) and washing solution (b) in DMSO-d6.

Ternary system: water/ethanol/Triacetin

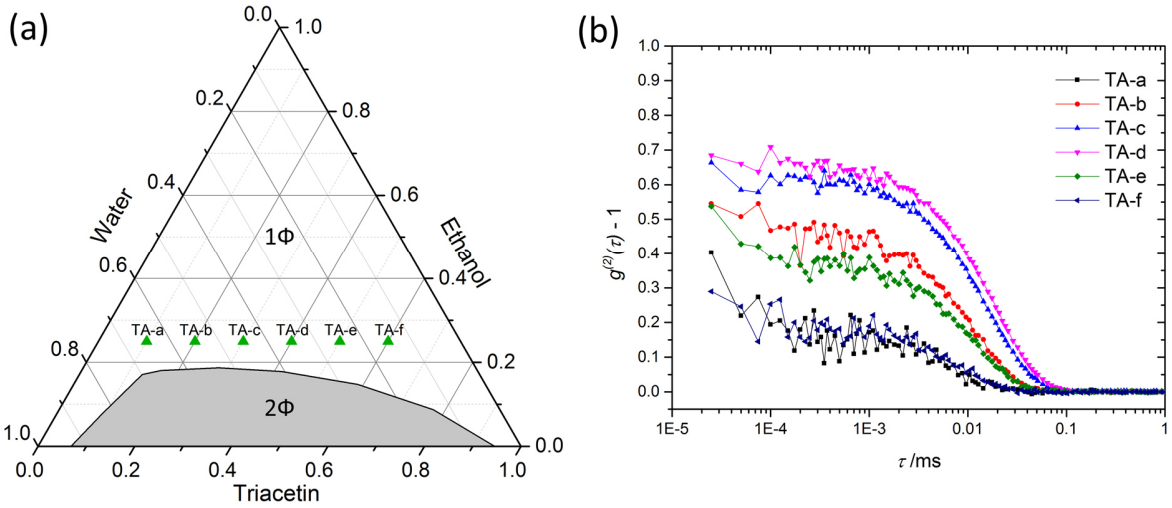

Figure A4.6: a) Ternary phase diagrams of water/ethanol/Triacetin at 25 °C provided in weight fractions. The mono- and two-phasic areas are represented as white and grey areas, respectively. Symbols denote the different compositions of water/ethanol/Triacetin measured with DLS (b).

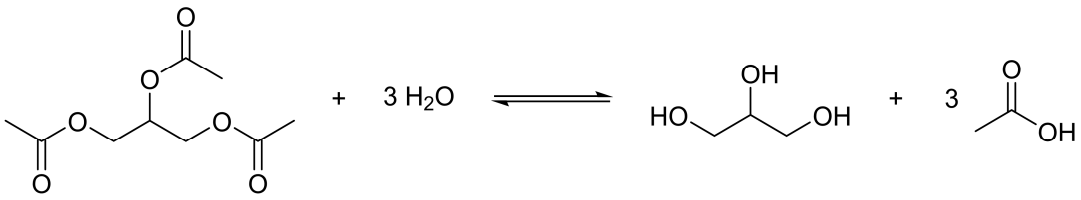

Figure A4.7: Chemical equilibria of Triacetin hydrolysis (formation) to glycerol and acetic acid.

A.5 Surfactant-free microemulsion supported extraction and separation – precise density data for (pseudo-)phase separation using (ultra)centrifugation techniques

Density and molar volume hypersurfaces

Table A5.1: Empirical fit functions of density data of water/ethanol/1-octanol, water/ethanol-d6/1-octanol and water/PnP/EA mixtures, 1-3, for different choices of X- and Y-axis (criteria, see Chapter 6) with corresponding fit-parameters, a-k, given in g cm^{-3} and correlation coefficients r^2.

Function	X-axis	Y-axis	Fit-function
1	*x*(water)	*x*(1-octanol)	$\rho(X,Y)=(a+bX+cX^2+dY+eY^2+fY^3)/(1+gX+hX^2+iX^3+jY)$
2	*x*(ethanol-d6)	*x*(water)	$\rho(X,Y)=(a+clnX+eY+g(lnX)^2+iX^2+kYlnX)/(1+blnX+dY+f(lnX)^2+hY^2+jYlnX)$
3	*x*(EA)	*x*(PnP)	$\rho(X,Y)=(a+cX+elnY+gX^2+i(lnY)^2+kXlnY)/(1+bX+dlnY+fX^2+h(lnY)^2+jXlnY)$

Table A5.1 (continued)

Function	Parameter / g cm^{-3}					
	a	b	c	d	e	f
1	0.792765	-1.08005	0.568175	1.582118	0.058635	-0.03956
2	0.896295	-2.2441	-1.81025	-3.22623	-2.60163	-0.04522
3	0.885895	0.207667	0.149025	0.176816	0.119712	-0.62686

Table A5.1 (continued)

Function	Parameter / g cm^{-3}					
	g	h	i	j	k	r^2
1	-1.49039	0.849548	-0.0767	1.918635	-	0.999941
2	-0.03199	0.822344	0.6034	1.452377	1.14142	0.999934
3	-0.56934	0.024667	0.01733	-0.58117	-0.51468	0.999976

Table A5.2: Empirical fit functions of molar volumes of water/ethanol/1-octanol mixtures, 1-3, for different choices of X- and Y-axis with corresponding fit-parameters, a-c, given in $cm^3\ mol^{-1}$ and correlation coefficients r^2.

Function	X-axis	Y-axis	Fit function	Parameter / $cm^3\ mol^{-1}$			
				a	b	c	r^2
1	*x*(1-octanol)	*x(*ethanol)	V_m=a+bX+cY	17.181	141.240	40.482	0.999937
2	*x(*ethanol)	*x*(water)	V_m=a+bX+cY	158.421	-100.758	-141.240	0.999937
3	*x*(water)	*x*(1-octanol)	V_m=a+bX+cY	57.663	-40.482	-100.758	0.999937

Table A5.3: Empirical fit functions of molar volumes of water/ethanol-d6/1-octanol mixtures, 1-3, for different choices of X- and Y-axis with corresponding fit-parameters, a-c, given in $cm^3\ mol^{-1}$ and correlation coefficients r^2.

Function	X-axis	Y-axis	Fit function	Parameter / $cm^3\ mol^{-1}$			
				a	b	c	r^2
1	*x*(1-octanol)	*x(*ethanol-d6)	V_m=a+bX+cY	17.115	141.365	40.404	0.999948
2	*x(*ethanol-d6)	*x*(water)	V_m=a+bX+cY	158.481	-100.962	-141.365	0.999948
3	*x*(water)	*x*(1-octanol)	V_m=a+bX+cY	57.519	-40.404	-100.961	0.999948

Table A5.4: Empirical fit functions of molar volumes of water/PnP/EA mixtures, 1-3, for different choices of X- and Y-axis with corresponding fit-parameters, a-c, given in $cm^3\ mol^{-1}$ and correlation coefficients r^2.

Function	X-axis	Y-axis	Fit function	Parameter / $cm^3\ mol^{-1}$			
				a	b	c	r^2
1	*x*(EA)	*x(*PnP)	V_m=a+bX+cY	17.186	80.671	115.214	0.999918
2	*x(*PnP)	*x*(water)	V_m=a+bX+cY	97.857	34.543	-80.671	0.999918
3	*x*(water)	*x*(EA)	V_m=a+bX+cY	132.400	-115.214	-34.543	0.999918

A.6 A systematic study of the influence of mesoscale structuring on the kinetics of a chemical reaction

SANS-Measurements

Table A6.1: Molar volumes and scattering length densities (SLD) of all components in the binary mixture P (D_2O/TBA 0.86/0.14), the ternary mixture Q (D_2O/TBA/BA 0.87/0.11/0.02) and the ternary mixture Q in the presence of the catalyst (D_2O/TBA/BA 0.87/0.11/0.02 and 2 mM $H_5PMo_{10}V_2O_{40}$). The correlation length ξ obtained from OZ fits of the scattering curves for ξ(P) = 0.8 nm, ξ(Q) = 2.1 nm and ξ(Q+2 mM $H_5PMo_{10}V_2O_{40}$) = 1.9 nm.

	Molar Volume	**Scattering length density (SLD)**
	$cm^3\,mol^{-1}$	$Å^2$
D_2O	18.1	$6.34 \cdot 10^{-6}$
tert-butanol	93.8	$-3.15 \cdot 10^{-7}$
benzyl alcohol	104.0	$1.30 \cdot 10^{-6}$
$H_5PMo_{10}V_2O_{40}$	566.0	$3.36 \cdot 10^{-6}$

Adsorption of $H_5PMo_{10}V_2O_{40}$ on the surface of BrijL23 micelles

SAXS experiments were performed on the system Brij L23 (tricosaethylene glycol dodecyl ether) - $H_5PMo_{10}V_2O_{40}$ in order to confirm the affinity of $H_5PMo_{10}V_2O_{40}$ to adsorb on surfaces covered with polar functional groups.

The concentration of $C_{12}E_{23}$ (c = 50 mM) is above the critical micellar concentration (CMC = 0.09 mM). Therefore, micelles of $C_{12}E_{23}$ are present in aqueous solution indicated by the black curve in Figure A6.1. 10 mM $PMo_{10}V_2O_{40}^{5-}$ provide a scattering pattern typical for spherical objects in pure water. The mixture of $C_{12}E_{23}$ and $PMo_{10}V_2O_{40}^{5-}$, respectively, at 50 and 10 mM revealed a completely different scattering pattern, showing large and intense oscillations typical for a core-shell system with an increased electron density in the shell. Consequently, these SAXS pattern indicate an adsorption of $PMo_{10}V_2O_{40}^{5-}$ to the surface of $C_{12}E_{23}$ micelles. Hence, this measurement also confirms the conclusions drawn from SANS measurements that $PMo_{10}V_2O_{40}^{5-}$ has the tendency to adsorb on neutral soft interfaces covered with functional groups.

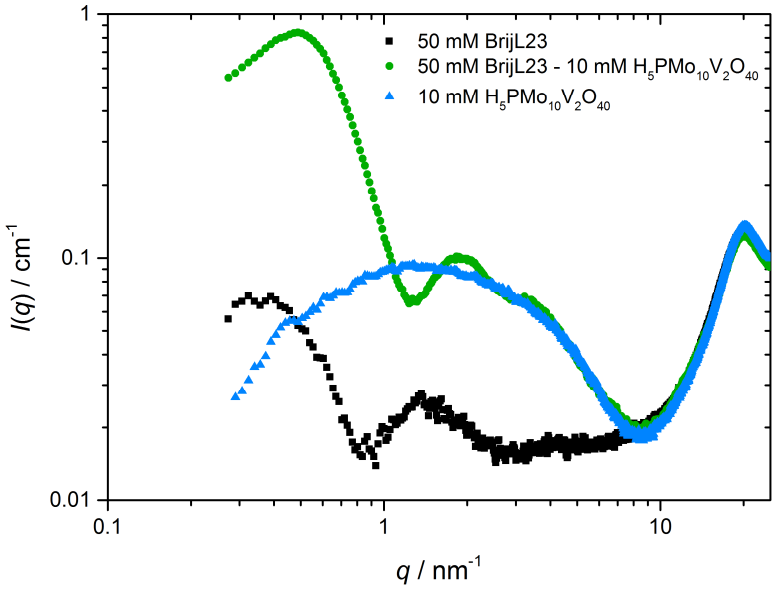

Figure A6.1: SAXS spectra of (black) $C_{12}EO_{23}$, (red) $PMo_{10}V_2O_{40}^{5-}$, and their mixture in aqueous medium. The Y-axis is the absolute scattered X-ray intensity. All experiments were performed at 23 °C.

Oxygen solubility measurements in binary mixtures H_2O/TBA and H_2O/EtOH

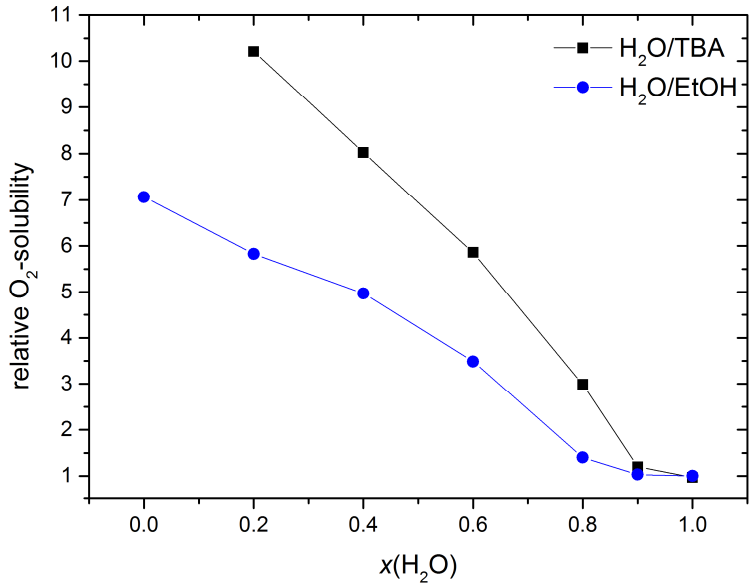

Figure A6.2: Oxygen solubility for binary mixtures H_2O/TBA and H_2O/EtOH at room temperature (23 ± 0.2) °C relative to water for binary mixtures H_2O/TBA and H_2O/EtOH. The amount of water of the binary H_2O/alcohol mixture is given in mole fractions $x(H_2O)$.

Yields of benzyl aldehyde in H_2O/TBA mixtures after 72 h

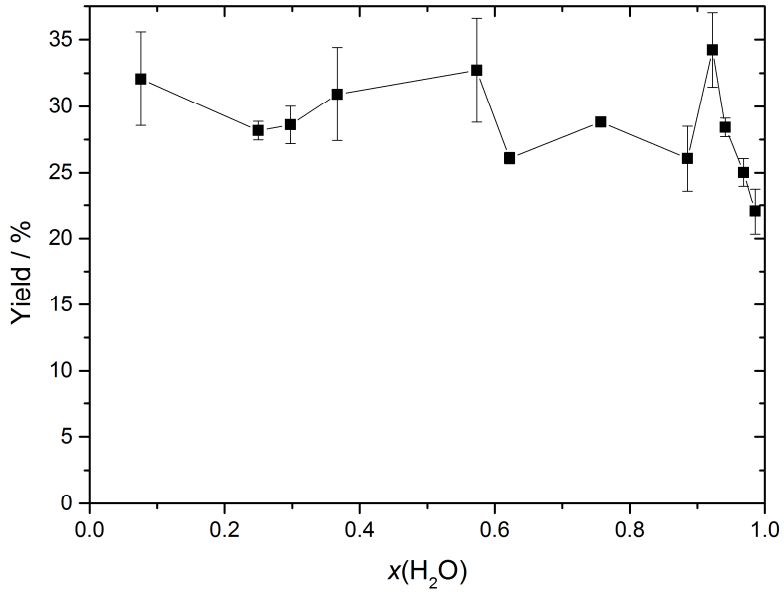

Figure A6.3: Yields of the reaction product, benzyl aldehyde, with the corresponding standard deviations for the binary system H_2O/TBA at 25 °C after 72 h determined with GC-FID.

Dynamic light scattering experiments

Light scattering experiments were performed in order to investigate the influence of benzyl aldehyde (produced during benzyl alcohol oxidation) on the solvent structure (see Figure A6.4). Point P (H_2O/TBA, molar fractions 0.86/0.14) was chosen, since SANS experiments were also carried out for this composition (see Section 7.4.1, Figure 7.3). Light scattering experiments show that correlation functions get more pronounced with a shift to higher lag times when adding benzyl alcohol (100 mM), benzyl aldehyde (100 mM) or a mixture of both (each 50 mM). These concentrations are equivalent to 0, 50 and 100% conversion regarding the reactivity measurements. The results indicate a strengthening of the structuring and swelling of the aliphatic (or TBA/BA) rich pseudo-phase, as already concluded from SANS measurements. Furthermore, no distinct differences of the correlation functions are visible when adding benzyl alcohol, benzyl aldehyde or a mixture of both. Thus, we conclude that there is no significant effect on the mesoscopic structuring during the reaction. Accordingly, a successive breakdown of the structuring of the reaction mixture with increasing reaction time can be excluded.

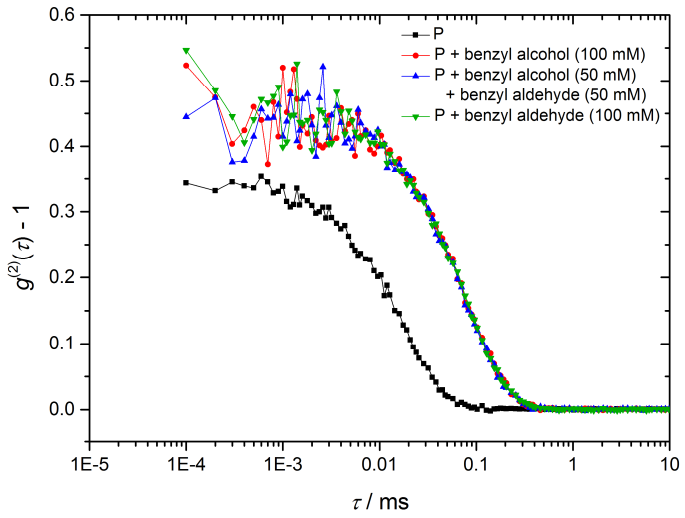

Figure A6.4: Self-correlation functions obtained by DLS measurements at 25 °C.

Yields of benzyl aldehyde in H_2O/EtOH mixtures after 16 h

In case of the unstructured binary solvent H_2O/EtOH, 6-10% of benzyl aldehyde are obtained, see Figure A6.5. The yields can be regarded as almost constant over the investigated H_2O/EtOH compositions. As no (or at least very weak) mesoscopic structuring is present in H_2O/EtOH mixtures, structure induced reactivity changes can be neglected in this case and no steep changes in the yields of benzyl aldehyde are observed by changing the solvent composition.

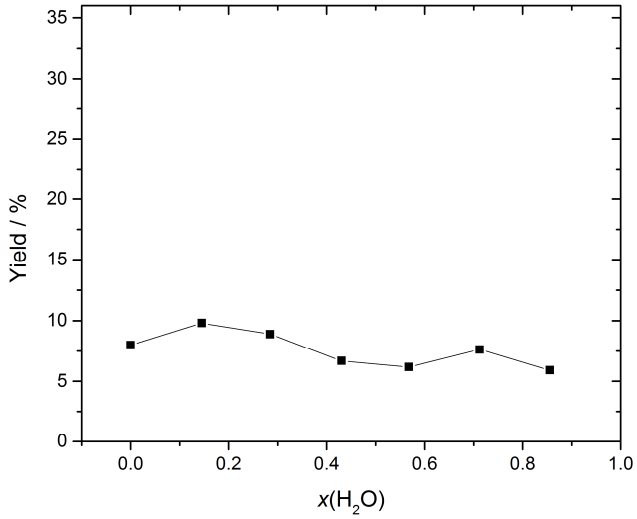

Figure A6.5: Yields of the reaction product, benzyl aldehyde, for the binary system H_2O/EtOH at 25 °C after 16 h determined with GC-FID.

Viscosities of binary mixtures H_2O/TBA and H_2O/EtOH

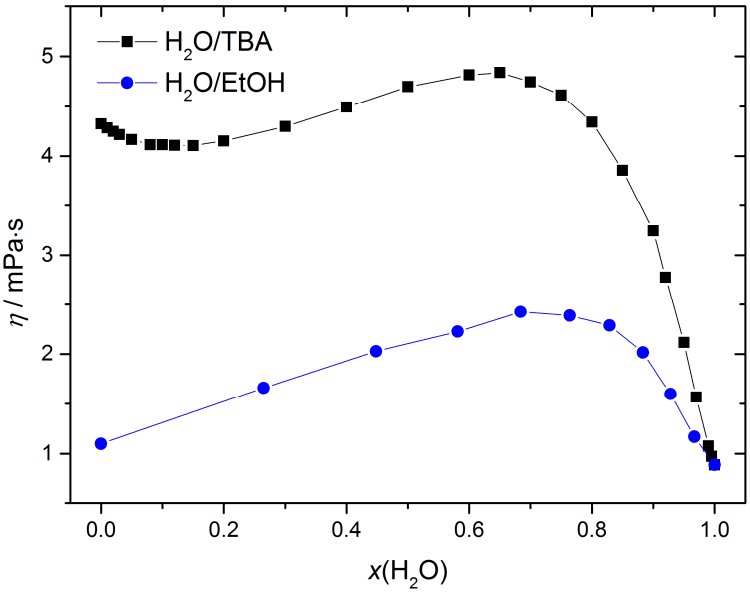

Figure A6.6: Dynamic viscosities η for binary mixtures H_2O/TBA and H_2O/EtOH at 25 °C. Data were taken from literature. The amount of water of the binary H_2O/alcohol mixture is given in mole fractions $x(H_2O)$.

A.7 Enzyme activity of horseradish peroxidase in surfactant-free microemulsions

Dynamic light scattering: Single exponential fit parameters

Table A7.1: Fit parameter for the single exponential fits of samples *a*-*o* for the ternary systems water/NPA/limonene and water/TBA/limonene. Specific compositions of the reaction media (*a*-*o*) can be taken from Figure 9.4.

Sample	water/NPA/limonene			water/TBA/limonene		
	β	Γ	C	β	Γ	C
		10^{-4} s			10^{-4} s	
a	-	-	-	-	-	-
b	0.5727	7.333	0.0054	0.3490	6.095	0.0004
c	0.8209	5.285	0.0003	0.5840	6.263	0.0018
d	0.8819	4.026	0.0023	0.6336	6.043	0.0016
e	0.9052	3.578	0.0006	0.6669	6.566	0.0013
f	0.9099	3.617	0.0008	0.6783	6.830	0.0008
g	0.9158	3.526	0.0008	0.6913	7.200	0.0005
h	0.9093	3.796	0.0006	0.6931	8.123	0.0006
i	0.9018	4.348	0.0003	0.6829	8.845	0.0005
j	0.8992	4.638	0.0008	0.6709	9.605	0.0008
k	0.8646	5.888	0.0002	0.6532	10.656	0.0005
l	0.8473	6.618	0.0016	0.6289	11.270	0.0007
m	0.8169	7.708	0.0027	0.6068	13.069	0.0007
n	0.7806	9.015	0.0019	0.5648	14.060	0.0006
o	-	-	-	0.5480	16.258	0.0015

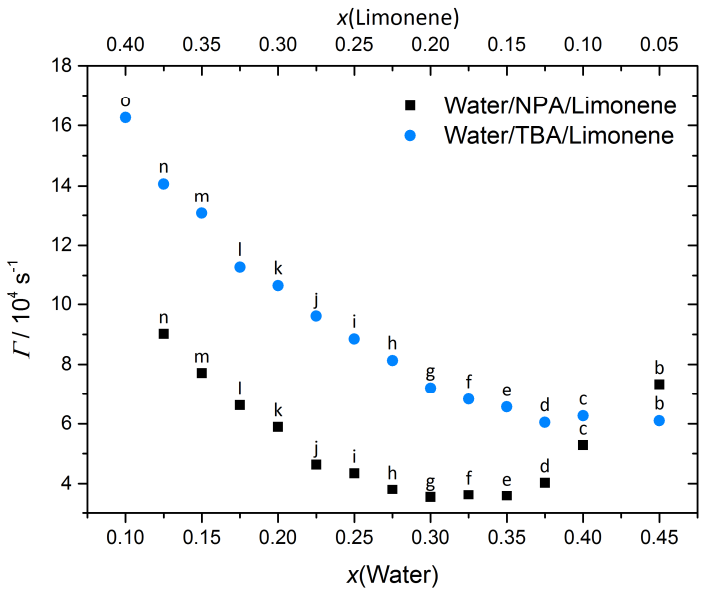

Figure A7.1: Decay rates obtained from single exponential data fitting of normalised autocorrelation function of intensity as a function of the water and limonene content given in mole fractions.

Influence of buffer, substrates (H_2O_2/ABTS) and HRP on the mesoscale structuring of water/buffer, NPA, limonene (sample *g*)

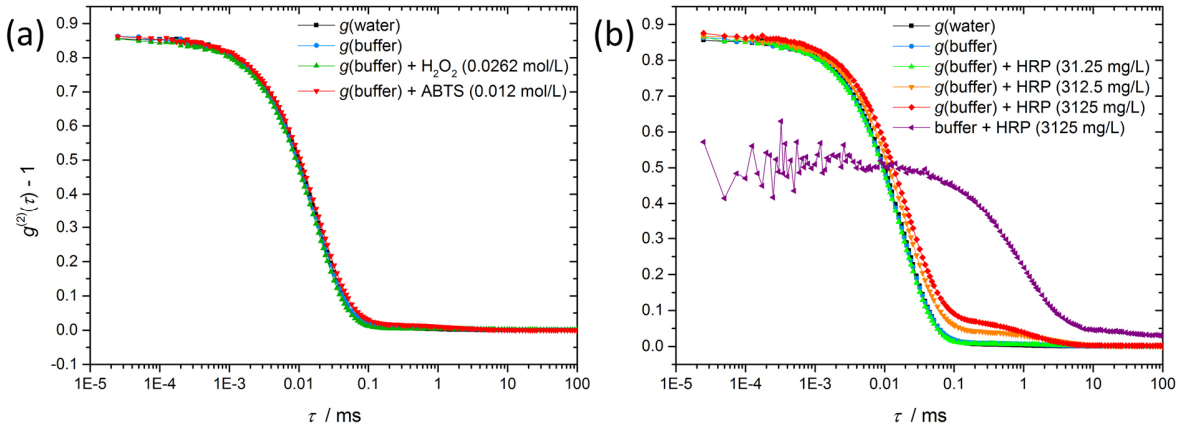

Figure A7.2: Normalised autocorrelation functions of intensity obtained by DLS measurements at 25 °C of the ternary system water(buffer)/NPA/limonene (sample *g*, V = 2.9 mL) with and without addition of (a) substrates (H_2O_2/ABTS, 10 µL) and (b) HRP (10 µL). Concentrations of the substrates and HRP in the added solutions (10 µL) are given in the figure legend.

Small-angle X-ray scattering measurements of the ternary systems water/NPA/limonene and water/TBA/limonene

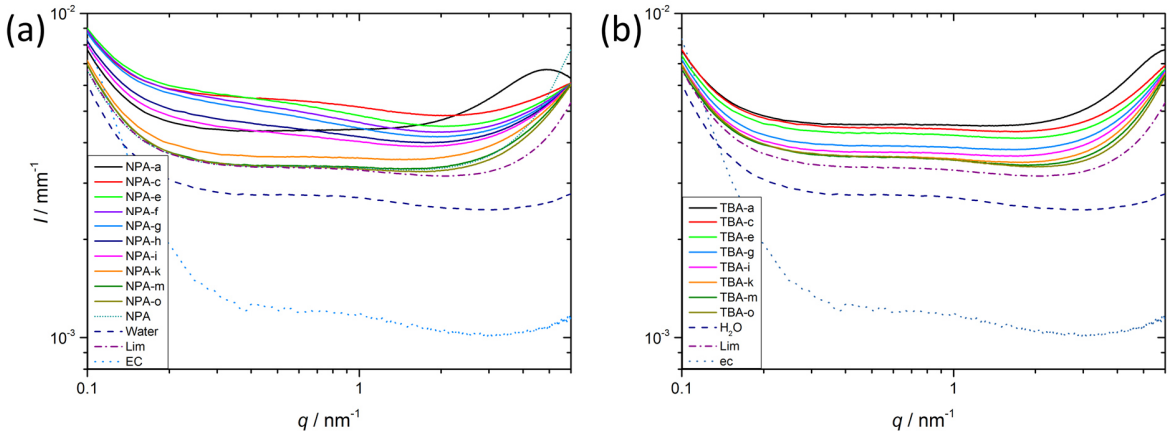

Figure A7.3: SAXS spectra of the ternary mixtures (a) water/NPA/limonene and (b) water/TBA/limonene. Spectra are not corrected for background.

Table A7.2: Fit parameter for the OZ-fit.

Sample	I_0 mm^{-1}	ξ nm	bkg mm^{-1}
NPA-c	0.00079	1.01	0.00147
NPA-e	0.00133	1.43	0.00118
NPA-f	0.00134	1.61	0.00098
NPA-g	0.00132	1.78	0.00085
NPA-h	0.00084	1.90	0.00075
NPA-i	0.00066	2.11	0.00060

Conductivity measurements crossing the reaction pass

Since a macroscopic change in the phase behaviour was observed for TBA SFME, additional conductivity measurements were performed. To this purpose, different binary mixtures of alcohol/limonene (containing 0.1 wt% sodium bromide) were successively diluted with pure water. For NPA, binary starting solutions with a weight fraction of *w*(NPA) = 1, 0.8, 0.6 and 0.4 (equal to *x*(NPA) = 1, 0.90, 0.77, 0.60) were used. For TBA, three solutions with *w*(TBA) =1, 0.8, 0.6 (equal to *x*(TBA) = 1, 0.88, 0.73) were measured, see Figure A7.4 and A7.5.

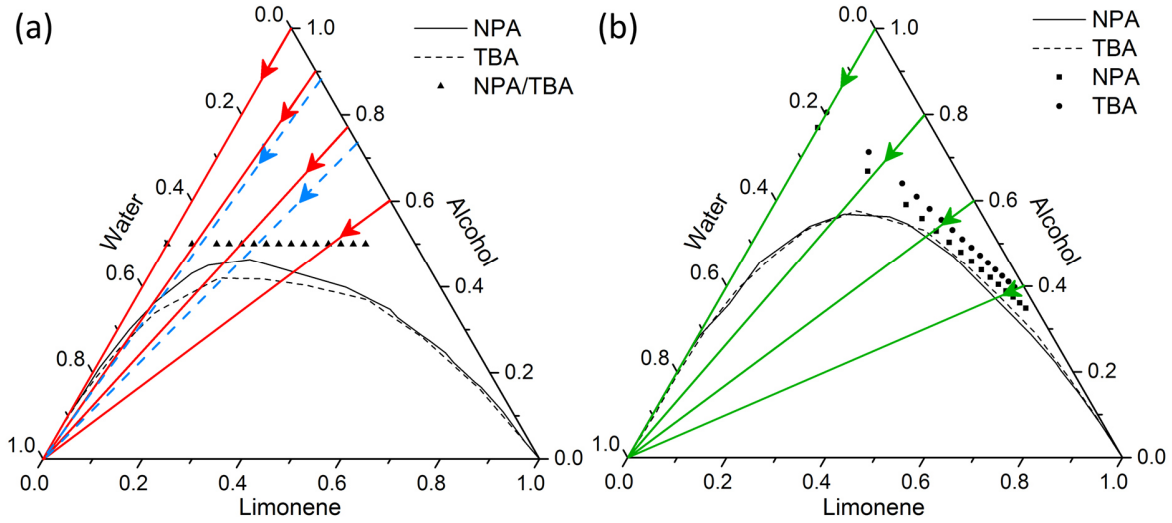

Figure A7.4: Ternary phase diagrams of water/NPA/limonene and water/TBA/limonene at 25 °C in (a) mole and (b) weight fractions. Symbols denote the different compositions used as reaction media. Coloured lines represent the paths along which conductivities were measured: red (water/NPA/limonene, mole fractions), blue dashed (water/TBA/limonene, mole fractions) and green (water/alcohol/limonene, weight fractions). Arrows indicate the way of dilution with pure water, starting from the binary mixtures alcohol/limonene.

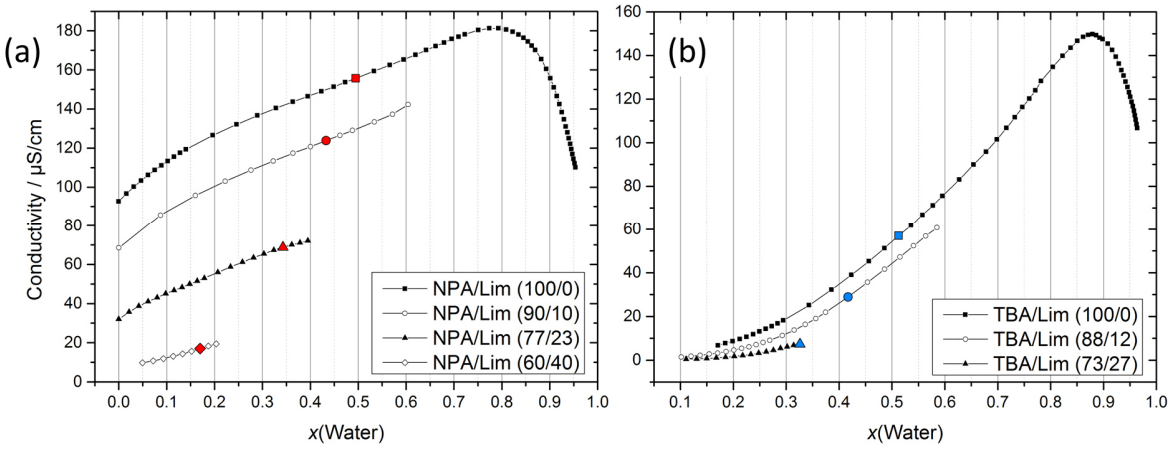

Figure A7.5: Conductivity measurements at 25 °C for ternary mixtures of water/NPA/limonene (a) and water/TBA/limonene (b) as a function of the mole fraction of water *x*(Water). Measurements were performed by diluting a binary mixture alcohol/limonene with water. The symbols refer to different molar ratios of alcohol to limonene (Lim) in the binary starting mixture alcohol/limonene before diluting with water. Red and blue symbols denote compositions with *x*(Alcohol) ≈ 0.5, as also used for enzyme activity measurements.

Reaction kinetics in water(buffer)/IPA/*n*-hexane

Analogue to the pioneering work of Khmelnitsky *et al*., reactions were also performed in ternary mixtures consisting of water(buffer)/2-propanol(IPA)/*n*-hexane. The results of the kinetic experiments are shown in Figure A7.6. Obviously, very poor enzyme activity is observed near the binary water/alcohol axis, increasing with increasing amount of *n*-hexane. After passing a maximum, the activity goes down again and no activity can be detected very near to the binary alcohol/*n*-hexane axis (not shown in Figure A7.6), due to the low water content in this region. These findings are in good accordance with the results described by Khmelnitsky *et al.* Analogue to their work, three zones of different enzymatic activity can be identified (see regions A, B, C in Figure A7.6). In region A, a very low, in region B, a moderate, and in region C, a maximum activity is observable. Furthermore, the position of the maximum point was found to be in the same region as for trypsin catalysed hydrolysis of *N*-α-benzoyl-L-arginine ethyl ester[1]. Considering the postulated models of structuring for these regions based on conductivity results by Barden and co-workers, the results obtained by kinetic measurements are in good accordance to the postulated mesoscale structures. In region A, the assumption of an unstructured solution explains well the low enzyme activity.

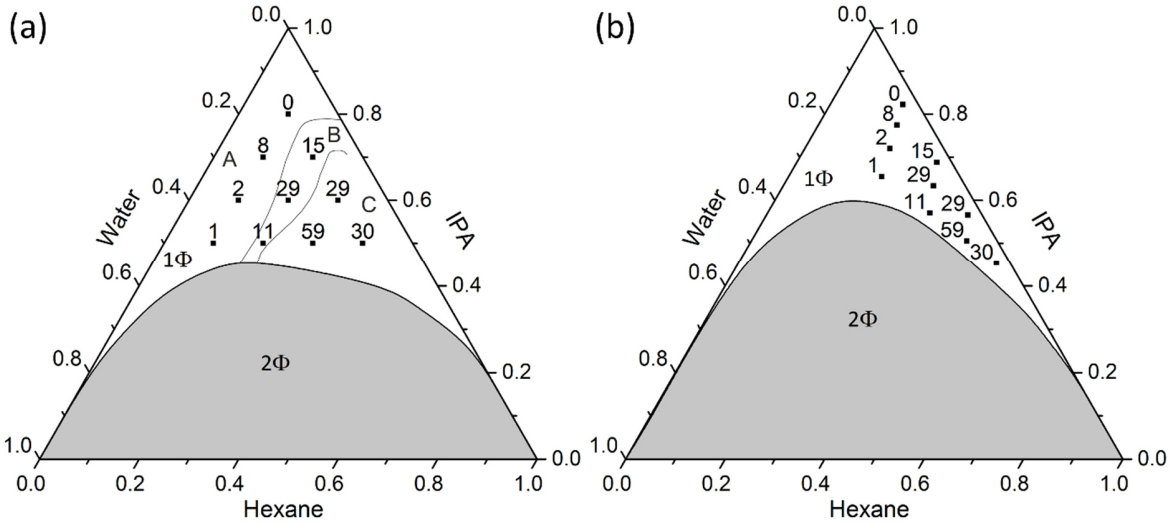

Figure A7.6: Ternary phase diagrams of water/IPA/*n*-hexane and relative enzymatic activities for the oxidation of ABTS with HRP and H_2O_2 at 25 °C in (a) mole and (b) weight fractions. The mono-(1Φ) and two-phasic (2Φ) areas are represented in white and grey, respectively. Symbols (black squares) denote the different compositions used as reaction media with the corresponding measured relative enzymatic activities V/V_0 in percentage (V_0 corresponds to the enzyme activity in pure buffer solution). Borders dividing the monophasic area into the different structural regions A,B and C were redrawn with reference to data published by Khmelnitsky *et al*.

Water, IPA and *n*-hexane are dispersed on a molecular level, and therefore the enzyme gets very often in contact with the alcohol (and *n*-hexane). Hence, denaturation takes place rapidly and the reaction stops immediately. Adding more *n*-hexane successively leads to the formation of a more rigid H-bond network (region B). A more bicontinuous structure is formed, where the denaturising alcohol accumulates at the interface. Simultaneously, the enzyme activity increases. The subsequent formation of a w/o microemulsion in region C enhances this effect. In these regions, water droplets are assumed to form an outer oil-rich domain, with IPA accumulating at the interface. However, IPA also partitions between both pseudo-phases, which is reflected by the fact that the activity at the maximum point does not reach the value of 100% (obtainable in pure buffer solution). Finally, the enzyme activity decreases again mainly due to poor solubility of ABTS (and the enzyme) in hexane and an insufficient amount of free hydration water, which leads to denaturation of the enzyme. Yet, DLS experiments carried out for the reaction media (buffer/alcohol/*n*-hexane) did not lead to well-defined correlation functions. At first glance, this seems to be contradictory to the results obtained by enzyme activity measurements, as light scattering experiments do not indicate the presence of a structured reaction medium preventing the enzyme from denaturation. Two possible explanations can be proposed for this apparent disagreement: (i) Possible structures might be too fluctuating to be detectable by light scattering experiments. And (ii), more likely, the difference of refractive indices between oil-rich and water-rich domains is too low in this special case. As already mentioned above and considering a similar model of structuring in the system water/IPA/*n*-hexane as in the well-investigated system water/EtOH/1-octanol, it can be assumed that IPA is partitioned between two distinct pseudo-phases (oil- and water-rich) with a preference to the interface. Regarding the refractive indices of water, IPA and *n*-hexane (n_D(water) = 1.333, n_D(IPA) = 1.377, n_D(*n*-hexane) = 1.375, for 20 °C) and assuming an equal distribution of IPA over both pseudo-phases as well as equal amounts of water and *n*-hexane with an additive behaviour of the refractive indices, the difference of the refractive indices of both pseudo-phases can be expected to be $\Delta n_D \approx 0.02$. This difference is supposedly too low to provide a sufficient contrast for light scattering of such small and highly fluctuating aggregates, which are usually present in SFME. Hence, results obtained by light scattering could not support the presence of the postulated regions of structuring. However, all results obtained by activity measurements are in good accordance with the postulated structures described in literature. Since DLS results did not further clarify the findings, we decided to change the reaction medium.

A.8 Surfactant-free microemulsion polymerisation of methyl methacrylate

SFME polymerisation of MMA in ternary mixtures composed of water/TBA/MMA

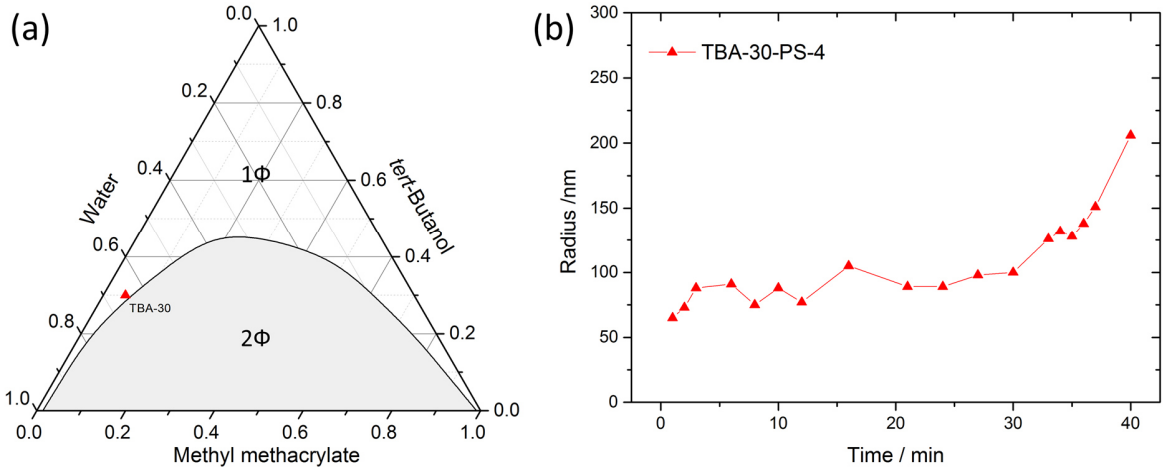

Figure A8.1: (a) Ternary phase diagram for the system water/TBA/MMA at 25 °C provided in weight fractions. The mono- and two-phasic areas are represented as white and grey areas, respectively. Symbols denote the composition used for polymerisation of MMA (b).

List of publications

1 U. Mohorič, A. Beutner, S. Krickl, D. Touraud, W. Kunz and F.-M. Matysik, *Anal. Bioanal. Chem.*, **2016**, *408*, 8681–8689.

2 T. Buchecker, S. Krickl, R. Winkler, I. Grillo, P. Bauduin, D. Touraud, A. Pfitzner and W. Kunz, *Phys. Chem. Chem. Phys.*, **2017**, *19*, 1806–1816.

3 S. Krickl, D. Touraud and W. Kunz, *Ind. Crops Prod.*, **2017**, *103*, 169–174.

4 S. Krickl, T. Buchecker, A. U. Meyer, I. Grillo, D. Touraud, P. Bauduin, B. König, A. Pfitzner and W. Kunz, *Phys. Chem. Chem. Phys.*, **2017**, *19*, 23773–23780.

5 S. Krickl, D. Touraud, P. Bauduin, T. Zinn and W. Kunz, *J. Colloid Interface Sci.*, **2018**, *516*, 466–475.

6 S. Friesen, S. Krickl, M. Luger, A. Nazet, G. Hefter and R. Buchner, *Phys. Chem. Chem. Phys.*, **2018**, *20*, 8812–8821.

7 S. Krickl, L. Jurko, K. Wolos, D. Touraud and W. Kunz, *J. Mol. Liq.*, **2018**, *271*, 112–117.

8 M. Hahn, S. Krickl, T. Buchecker, G. Jost, D. Touraud, P. Bauduin, A. Pfitzner, A. Klamt and W. Kunz, *ACS Nano*, **2018**, manuscript in preparation.

Eidesstattliche Erklärung

Ich erkläre hiermit an Eides statt, dass ich die vorliegende Arbeit ohne unzulässige Hilfe Dritter und ohne Benutzung anderer als der angegebenen Hilfsmittel angefertigt habe; die aus anderen Quellen direkt oder indirekt übernommenen Daten und Konzepte sind unter Angabe des Literaturzitats gekennzeichnet. Die Arbeit wurde bisher weder im In- noch im Ausland in gleicher, oder ähnlicher Form einer anderen Prüfungsbehörde vorgelegt. Ich versichere an Eides statt, dass ich nach bestem Wissen die reine Wahrheit gesagt und nichts verschwiegen habe.

Regensburg, 28. September 2018	
Ort, Datum	Unterschrift, Sebastian Krickl